KU LEUVEN

ARENBERG DOCTORAL SCHOOL
Faculty of Science

Present and future impact of the African Great Lakes on the regional climate

Wim Thiery

Supervisor:
Prof. dr. N. van Lipzig

Dissertation presented in partial fulfillment of the requirements for the degree of Doctor in Science

September 2015

Present and future impact of the African Great Lakes on the regional climate

Wim THIERY

Examination committee:
Prof. dr. G. Verstraeten, chair
Prof. dr. N. van Lipzig, supervisor
Prof. dr. ir. S. Bouillon
Prof. dr. ir. P. Willems
Prof. dr. ir. H. Goosse (UC Louvain)
Dr. E. Davin (ETH Zurich)

Dissertation presented in partial fulfillment of the requirements for the degree of Doctor in Science

September 2015

Uitgegeven in eigen beheer, Wim Thiery, Celestijnenlaan 200E, B-3001 Leuven (Belgium)

Preface

This PhD thesis was established with the support of many people. First of all I would like to thank my promoter, Nicole van Lipzig. Nicole, thank you for the opportunity to start a PhD under your supervision. One could not wish for a better mentor. Your corrections and suggestions regarding analyses and manuscripts were always highly valuable, and whenever important choices had to be made, the advice was well-directed. And then there were the words of motivation to get me back on track when the model was - again - demonstrating unexpected behaviour. I also very much enjoy the way in which we are encouraged to come up with new ideas to push our research forward, as well as to improve the functioning of the group. Your scientific rigour, integrity in academia and people management skills (patience and diplomacy!) will continue to be a source of inspiration for me.

The collaboration with scientists at the Land-Climate dynamics group at the Swiss Federal Institute of Technology Zurich (ETH Zurich) has been of great significance for the fulfilment of this thesis. I would like to thank all members of Landclim, in particular prof. Sonia Seneviratne for her continued support and the numerous useful suggestions, and dr. Edouard Davin for the excellent scientific guidance and the friendship developed last summer during my stay in Zurich.

Impossible to forget are the field campaigns to Lake Kivu conducted together with François, Alberto, Jean-Pierre, Cédric, Fleur, Marc, Bruno and many others collaborators within the EAGLES project. Together we faced the challenges of working under explosive political conditions, shared the frustrations of witnessing extreme poverty and experienced the joy of conducting research in an incredibly beautiful landscape. Equally memorable is the warm welcome and expert advice that I received from Andrey Martynov and Laxmi Sushama during my stay at UQAM in Montreal, as well as the great time spend with Georgiy Kirillin while improving FLake at IGB-Berlin. During my PhD, I also had the opportunity to collaborate with many other scientists worldwide. Of great significance in

this respect has been the CLM-Community, an open international network of scientists voluntarily providing training and sharing expertise on regional climate modelling with COSMO-CLM. I also explicitly want to thank Victor Stepanenko, Klaus Jöhnk, Dmitrii Mironov, Kris Bedka, Hans-Jürgen Panitz, Zack Subin, Pierre-Denis Plisnier, Lies Jacobs, Elise Monsieurs, Olivier Dewitte, Tom Shatwell, Pieter Hawinkel, Xing Fang, Zhongshun Li and Marjorie Perroud. This work benefited a lot from their willingness to share ideas, model results and data.

I would also like to acknowledge the members of my examination committee, prof. Hugues Goosse, dr. Edouard Davin, prof. Patrick Willems, prof. Steven Bouillon and prof. Gert Verstraeten. Thanks to their input provided over the past years and during the preliminary defence, the quality of this PhD thesis has significantly improved.

The support of the Flemisch Supercomputer Centre (VSC), and in particular of Martijn Oldenhof, has been key for the fulfilment of this PhD. Martijn, without your help I would probably still be debugging COSMO-CLM^2 on ThinKing at this time rather than honouring you in my preface. Many thanks also to Hilde, Johan, Greet, Marie-Rose, Ludo, Sofie, Petra, Ria, Annemie and Rik, the administrative and technical staff at the institute who sustain a great working environment. And a special acknowledgment to Valentijn and Jos for your great aid with designing the weather station, a fruitful collaboration of which I cherish good memories.

The colleagues of the KU Leuven Geography division, and in particular the Regional Climate Studies group, deserve a special recognition for the pleasant working atmosphere and the many great moments spend together. Annemarie, David, Erwan, Fabien, Hendrik, Irina, Jan, Jochem, Kristof, Maffie, Sajjad, Sam, Stef, Tom: our lunches, group drinks and discussions on scientific and other important matters are countless and they transform the RCS group into the stimulating environment we all seek. A special thank you also to Niels Souverijns and Stijn Bruggen; I really enjoyed working with you on your exciting master thesis projects and wish you all the luck on your future endeavours.

Finally, I would very much like to thank all my friends and family who supported me while I was engaged in this project. I especially mention my parents and my brother, whose support has been frequent and unconditional. Mom and Dad, the opportunities you gave me have led me to the point where I stand today. Thanks also to the Dehaspe family, always ready to jump in in case of an emergency. And of course thanks to Esben, Harry and David, who really can make you get the best out of yourself, and are friends for life. A big shout out finally to my friends from OLV, chiro Sjoen Linkebeek and geography (that includes you Laurens) for all the good times we had and continue to have.

But most of all I want to thank my wife and sons. Thank you Kats, once more for your loving support, from the early beginnings of my explorative encoding all the way up to the final slog. I do believe that all the stressful aspects of academic research have made us only more aware of how much we need each other. Thank you Loïc, for the immense joy you brought into our lives. I hope you will continue to share as you do now, and that you and your brother will grow up witnessing a low RCP world. Thank you "broer", for the excitement triggered by your small kicks in your mom's belly. We look forward to welcome you in our family.

To the three of you I dedicate this work.

Wim

Leuven, 1 September 2015.

This work was financially supported by a PhD fellowship and travel grant from the Research Foundation Flanders (FWO). In addition, field campaigns and computing infrastructure were funded by the Belgian Science Policy Office (BELSPO) through the research project "East African Great Lake Ecosystem Sensitivity to changes" (EAGLES, SD/AR/02A).

Abstract

Weather hazards in East Africa have a detrimental impact on local societies. The African Great Lakes, a collection of vast inland waters in equatorial East Africa, exert a major influence on the hydrological cycle and frequently trigger hazardous thunderstorms. Yet the mechanisms behind their climatic influence are poorly understood. And while global simulations of future climate project an intensification of rainfall extremes, little is known about future scenarios of extreme precipitation for this region and about the role of lakes therein. This dissertation therefore aims at an improved understanding of tropical lake-climate interactions and at the development of a future projection assessing the consequences of increased greenhouse gas concentrations on extreme rainfall in the African Great Lakes region.

In this thesis, we use the COSMO-CLM^2 regional climate model coupled to a one-dimensional lake model, FLake, to generate the first high-resolution assessment of the present and future imprint of the African Great Lakes on the regional climate system. Model integrations are performed at a horizontal resolution of 0.0625° (∼7 km), unprecedented for climate-scale simulations in this region. The choice and configuration of the coupled lake-land-atmosphere climate model are informed by two detailed studies of the behaviour of one-dimensional lake models over the African Great Lakes.

To start, the one-dimensional lake model FLake is extensively evaluated and tested over two African Great Lakes. Careful forcing data correction and model configuration allowed for the correct representation of mixed layer depths and water temperatures at three multiyear monitoring sites in equatorial East Africa. However, while lake surface temperature predictions are robust, bottom temperatures appear very sensitive to perturbations in the external parameters and meteorological driving data. Constraints on the applicability of the model are therefore identified: while this model is a suitable tool for lake surface temperature parameterizations in climate models, it cannot be used to study climate change influences on lake stratification and hydrodynamics. Finally, a

process study established the primary control of dry-season evaporative-driven cooling on seasonal mixed layer dynamics.

The skill of the FLake model is additionally benchmarked against six other lake models. FLake is the fastest model and demonstrates good predictive skill relative to the other models in terms of water column temperatures and lake enthalpy change, but its limitations in terms of representing stratification and hydrodynamics are confirmed by sensitivity experiments. In the multi-model framework, differences in model skill are explained by variations in the treatment of stratification and the role of salinity, radiative forcing and turbulent heat fluxes.

Evaluation of the COSMO-CLM^2 simulation with optimized configuration reveals good performance compared to both in situ and satellite observations, notably for lake surface temperatures and precipitation. This procedure also demonstrates the added value of this COSMO-CLM^2 integration relative to the parent simulation and a state-of-the-art reanalysis product. Comparison to a no-lakes simulation indicates that the four major African Great Lakes nearly double the annual precipitation amounts over their surface, but hardly exert any influence on precipitation beyond their shores. Most of the lakes also cool the annual mean near-surface air, this time with pronounced downwind influence. The lake-induced cooling happens during daytime, when the lakes absorb incoming solar radiation and inhibit upward turbulent heat transport. At night, when this heat is released, the lakes warm the near-surface air. The comparison also reveals the profound lake influence on atmospheric dynamics and stability: the example of Lake Victoria shows how lakes induce circular airflow with over-lake convective inhibition during daytime, and the reversed pattern at night.

The first high-resolution, coupled lake-land-atmosphere future climate projection for the African Great Lakes underlines the major role for Lake Victoria in modulating precipitation changes. Our results indicate that, under a high-emission scenario, the future increase of precipitation extremes is amplified over Lake Victoria relative to the surrounding land. After isolating changes in the distribution from the mean change, the 1% most extreme precipitation may intensify about three times faster over the lake compared to the surrounding land towards the end of the century. Interestingly, the increase in extremes contrasts to the change in average over-lake precipitation, which is projected to decrease for the same period. Further analysis enables attribution of the increase in extremes to thermodynamic processes, that is, an increased water-holding capacity of over-lake and advected air masses. These findings highlight a new major hazard associated with climate change over East Africa with potentially severe human impacts.

Beknopte samenvatting

Extreme weersfenomenen hebben een nadelige invloed op plaatselijke gemeenschappen in Oost-Africa. De Afrikaanse Grote Meren, een verzameling grote watermassa's in Oost-Afrika, oefenen een belangrijke invloed uit op de hydrologische cyclus en veroorzaken vele schadelijke stormen. De processen verantwoordelijk voor deze invloed op het klimaat zijn echter onvoldoende onderzocht, en terwijl globale klimaatmodellen een intensifiëring van extreme neerslag voorspellen, is er slechts weinig bekend over mogelijke veranderingen van extreme neerslag in dit gebied en over de mogelijke rol die de meren daarin zouden kunnen spelen. Dit proefschrift tracht daarom een verbeterd begrip op te bouwen van tropische meer-klimaatinteracties, alsook een voorspelling te ontwikkelen die de gevolgen van toenemende broeikasgassen op extreme neerslag in het gebied nagaat.

In deze thesis wordt het regionaal klimaatmodel COSMO-CLM^2, gekoppeld aan het meer-model FLake, aangewend om de huidige en toekomstige invloed van de Afrikaanse Grote Meren op het regionaal klimaat na te gaan. Modelsimulaties werden uitgevoerd met een horizontale resolutie van 0.0625° (∼7 km), hetgeen ongezien is voor klimaatstudies in dit gebied. De modelkeuze en -configuratie werden ingegeven door twee detailstudies naar het gedrag van één-dimensionale meer-modellen over de Afrikaanse Grote Meren.

Ten eerste werd het meer-model FLake uitgebreid geëvalueerd en getest voor de Afrikaanse Grote Meren. Mede dankzij een correctie van meteorologische variabelen en een zorgvuldige modelconfiguratie slaagt FLake erin de diepte van de menglaag, alsook de watertemperaturen correct weer te geven. Hoewel oppervlaktetemperaturen robust voorspeld worden, blijken gemodelleerde bodemtemperaturen tegelijk uiterst gevoelig voor veranderingen in inputdata. Daardoor legt deze studie ook de beperkingen van dit model bloot: terwijl FLake geschikt is om oppervlaktetemperaturen te voorspellen in klimaatmodellen, kan het niet aangewend worden om de invloed van klimaatfluctuaties op stratificatie en hydrodynamische processen in meren te bestuderen. Een processtudie

wijst tenslotte de toenemende evaporatie tijdens het droge seizoen aan als de dominante oorzaak voor seizoenale veranderingen in de diepte van de menglaag.

De kwaliteit van FLake werd vervolgens vergeleken met zes andere meermodellen. FLake is het snelste model en legt een goede voorspellende waarde aan de dag in vergelijking met de andere modellen wat betreft watertemperaturen en enthalpieverschillen. Tegelijk echter worden de eerder ontdekte beperkingen met betrekking tot de weergave van stratificatie en hydrodynamica bevestigd door middel van een aantal gevoeligheidstests.

Vergelijking van in situ- en satellietwaarnemingen enerzijds en de optimaal geconfigureerde COSMO-CLM^2 simulatie anderzijds, toont de kwaliteit van laatstgenoemde aan, in het bijzonder wat betreft neerslag en oppervlaktetemperatuur van de meren. Deze evaluatie bevestigt tevens de toegevoegde waarde van de COSMO-CLM^2 simulatie ten opzichte van een recente continentale klimaatsimulatie en een moderne globale reanalyse. Vergelijking met een simulatie waarbij alle meren door land vervangen werden, geeft vervolgens aan dat vier belangrijke Afrikaanse Grote Meren de neerslag boven hun gebied nagenoeg verdubbelen, maar dat ze amper een invloed hebben op neerslag buiten hun eigen oppervlak. Daarnaast vertonen ze meestal ook een verkoelend effect, ditmaal met duidelijke invloed windafwaarts. De verkoeling vindt plaatst gedurende de dag, wanneer inkomende zonnestraling geabsorbeerd wordt en turbulente opwarming beperkt wordt. 's Nachts wordt deze warmte opnieuw vrijgegeven en warmen de meren de onderste lagen van de atmosfeer op. Tenslotte maakt deze vergelijking de diepgaande invloed van de meren op atmosfeercirculatie en -stabiliteit duidelijk: het voorbeeld van het Victoriameer toont aan hoe de meren overdag celvormige circulatie teweeg brengen met onderdrukking van convectie boven de meren tot gevolg, en het omgekeerde patroon 's nachts.

De eerste hoge resolutie klimaatprojectie voor het gebied van de Grote Meren benadrukt de centrale rol van het Victoriameer op het vlak van toekomstige neerslagveranderingen. Onze resultaten geven meer bepaald aan dat, voor een hoog-emissiescenario, de toekomstige toename van neerslagextremen versterkt wordt boven het Victoriameer in vergelijking met het omliggende land. Nadat veranderingen in de neerslagdistributie geïsoleerd zijn van de gemiddelde verandering, zal volgens ons model de 1% meest intense neerslag ongeveer drie maal sneller stijgen boven dit meer dan boven het omringende land. Verdere analyse laat toe om de toename in extremen te verklaren aan de hand van thermodynamische processen, meer bepaald door het toegenomen potentieel vochtgehalte van aangevoerde en lokale luchtmassa's. Deze resultaten benadrukken een nieuw gevaar van klimaatverandering in Oost-Africa, met mogelijk ernstige gevolgen voor lokale gemeenschappen.

Abbreviations and symbols

α_{LW}	Surface longwave albedo (reflectivity) [0-1]
α_{SW} (α)	Surface shortwave albedo (reflectivity) [0-1]
AGL	African Great Lakes*
AR5	Fifth Assessment Report of the IPCC
ARC-Lake	Along-track scanning radiometers Reprocessing for Climate-Lake
AUC	Area-Under-the-Curve
AVHRR	Advanced Very High Resolution Radiometer
AWS	Automatic Weather Station
β	Solar radiation partitioning coefficient [0 1]
BSS	Brier Skill Score [$-\infty$ 1]
C	Conductivity [mS cm^{-1}]
CCF	cloud cover fraction [%]
CES	Same as control, but excluding spin-up
CLM	Community Land Model*
CMIP3/5	Coupled Model Intercomparison Project phase 3/5
CMORPH	Climate Prediction Center Morphing Technique
control	FLake simulation with u and k corrected
CORDEX	Coordinated Regional Climate Downscaling Experiment*
COSMO	Consortium for Small-scale Modelling*
COSMO-CLM	COSMO model in Climate Mode*
COSMO-CLM^2	COSMO-CLM coupled to CLM*
c_p	Specific heat capacity at constant pressure [J kg^{-1} K^{-1}]
C_T	Shape factor for the thermocline temperature profile [0.5 0.8]
CTL	COSMO-CLM^2 control simulation (ERA-Interim downscaling)
CTD	Conductivity-Temperature-Depth cast
DEE	Same as control, but with lake depth set to 120 m
D_{turb}	Turbulent diffusivity [m^2 s^{-1}]
ENSO	El Niño-Southern Oscillation
ESM	Earth system model
ϵ	Longwave emissivity [0-1]
ECMWF	European Centre for Medium-Range Weather Forecasts
ET	Evapotranspiration [mm yr^{-1}]
ff	See u
FLake	Freshwater Lake model*
Fluxnet-MTE	Flux tower data upscaling using model tree ensembles

Note: entries marked by an asterisk (*) are further described in the Glossary.

FUT	COSMO-CLM^2 scenario simulation (GCM downscaling)
G	Subsurface storage and conductive heat fluxes [W m^{-2}]
GCM	Global climate model(also: general circulation model)*
GEWEX-SRB	Global Energy & Water cycle Experiment Surface Radiation Budget
GPCC	Global Precipitation Climatology Centre
GPCP	Global Precipitation Climatology Project
H	Enthalpy change [W m^{-2}]
h_{BOT} (h)	Lake depth [m]
HIS	COSMO-CLM^2 historical simulation (GCM downscaling)
h_{ML}	Mixed layer depth [m]
IFS	Integrated Forecast System
IOD	Indian Ocean Dipole
IPCC	Intergovernmental Panel on Climate Change
ISCCP	International Satellite Cloud Climatology Project
ITCZ	Intertropical Convergence Zone
JJA	June-July-August
k	Downward light attenuation coefficient [m^{-1}]
KHI	Same as control, but with k set to 0.46 m^{-1}
KLO	Same as control, but with k set to 0.15 m^{-1}
LakeMIP	Lake Model Intercomparison Project
LandFlux-EVAL	diagnostic evapotranspiration estimates
LHF	Latent heat flux [W m^{-2}]
LNB	Level of neutral buoyancy
LISSS	Lake, Ice, Snow and Sediment Simulator within CLM4
LSM	Land surface model
LSWT (LST)	Lake surface water temperatures
L_v	Latent heat of evaporation [J kg^{-1}]
LW_{in}	Incoming longwave radiation at the surface [W m^{-2}]
LW_{out}	Outgoing longwave radiation at the surface [W m^{-2}]
LW_{net}	Net long-wave radiation [W m^{-2}]
MAM	March-April-May
MCS	Mesoscale convective system
MES	Same as control, but initially fully mixed and excluding spin-up
MERRA	Modern Era Retrospective analysis for Research and Applications
MFC	Moisture flux convergence
MIS	Same as control, but initially fully mixed
MODIS	Moderate Resolution Imaging Spectroradiometer
MSG	Meteosat Second Generation
n	Number of observations
NWP	Numerical weather prediction
NOL	COSMO-CLM^2 no-lakes simulation (ERA-Interim downscaling)
OND	October-November-December
OT	Overshooting top
OTDA	Overshooting top detection algorithm
p	Air pressure [Pa]
p_0	Standard reference pressure [Pa]
P	precipitation [mm yr^{-1}]
PFT	Plant functional type
Φ_T	Dimensionless function for the thermocline shape [0 1]
POM	Princeton Ocean Model

Q_V (q)	Specific humidity [kg kg^{-1}]
r	Pearson correlation coefficient [0 1]
ρ	Density [kg m^{-3}]
raw	FLake simulation with observed meteorology and k
RCM	Regional climate model*
RCP	Radiative concentration pathway
RH	Relative humidity [%]
$RMSE$	Root mean square error [variable]
$RMSE_c$	Centred root mean square error [variable]
R_{net}	Net radiation [W m^{-2}]
ROC	Receiver Operating Characteristic
S	Salinity [g l^{-1}]
σ	Standard deviation [variable]
σ_{norm}	Normalised standard deviation [variable]
SEB	surface energy balance
SES	Same as control, but initially stratified and no spin-up
SEVIRI	Spinning Enhanced Visible and Infrared Imager
SHA	Same as control, but with lake depth set to 30 m
SHF	Sensible heat flux [W m^{-2}]
SRTM	Shuttle Radar Topography Mission
SST	Sea surface temperature [K]
SW_{in}	Incoming shortwave radiation at the surface [W m^{-2}]
SW_{out}	Outgoing shortwave radiation at the surface (reflected) [W m^{-2}]
SW_{net}	Net shortwave radiation at the surface (absorbed) [W m^{-2}]
θ_e	Equivalent potential temperature [K]
T	Air temperature [K]
T_{2m}	2-meter air temperature [K]
T_s	Surface temperature [K]
T_{BOT}	Lake bottom temperature [K]
T_{ML}	Mixed layer temperature [K]
T_{MW}	Water column average temperature [K]
t_{rc}	Relaxation time scale for the thermocline shape [s]
TRMM	Tropical Rainfall Measuring Mission
u (ff)	Wind velocity [m s^{-1}]
UDEL	University of Delaware precipitation product
WD (dd)	Wind direction [°]
WMO	World Meteorological Organization
WS	Weather station (manned)
ζ	Dimensionless function for thermocline depth [0 1]
z_{sd}	Disappearance depth of the Secchi disk [m]

Glossary

African Great Lakes	Collection of large lakes in Equatorial East Africa. Among other, they comprise Lake Victoria, Lake Tanganyika and Lake Kivu.
CMIP	International framework to coordinate global, coupled ocean-atmosphere general circulation model projection for the assessment reports of the Intergovernmental Panel on Climate Change (IPCC).
Community Land Model	State-of-the-art land surface model, developed and maintained at the National Center for Atmospheric Research (NCAR).
CORDEX	International framework to coordinate and advance regional climate change projections for all land regions of the world.
COSMO	Non-hydrostatic limited-area atmospheric model, used for numerical weather prediction. Developed and maintained at the German Weather Service.
COSMO-CLM	Regional climate model, based on the COSMO* model. Developed and maintained by the open and international CLM-Community.
COSMO-CLM^2	COSMO-CLM* coupled to Community Land Model* and FLake*. Developed and maintained at the Swiss Federal Institute of Technology Zurich (ETHZ).
Dimictic lake	Lake mixing from top to bottom twice a year.
Global climate model	Atmospheric model designed for global, multiyear simulations. The most recent generation of GCMs are also referred to as earth system models (ESMs).
ERA-Interim	Global reanalysis* product of the ECMWF from January 1979 onward. Can be used as lateral boundary conditions* of regional climate models*.
FLake	Two-layer, one-dimensional lake model.
Indian Ocean Dipole	Prominent mode of coupled ocean-atmosphere variability with relatively cold (warm) sea surface temperatures in the eastern (western) tropical Indian Ocean during a positive phase, and vice versa. Positive phases, and associated more intense Short Rains in East Africa, are projected to increase in frequency with with future climate change.
Meromictic lake	Lake containing layers that never intermix.

Mixed layer (in lake)	Upper stratum in a lake with homogeneous characteristics. The mixing is induced by the interaction with the overlying atmosphere (e.g. wind stress or evaporative cooling)
Mixolimnion	Upper stratum in a meromictic lake that is subject to (seasonal) mixing.
Monimolimnion	Lower stratum in a meromictic lake that is never subject to mixing.
Monomictic lake	Lake mixing from top to bottom exactly once a year.
MPI-ESM-LR	Global climate model, developed and maintained at the Max-Planck-Institut für Meteorologie (MPI-M). Can be used as lateral boundary conditions* of regional climate models*.
Radiative concentration pathway	Greenhouse gas concentration trajectories developed for the Fifth Assessment Report (AR5) of the Intergovernmental Panel on Climate Change (IPCC). Pathways are labelled after their possible radiative forcing by the year 2100 relative to pre-industrial values.
Reanalysis (Meteorological)	Three-dimensional global dataset of historical climate, derived by blending computer simulations with available observations ("assimilation"). It is considered as "best estimate" for many variables and has the advantage of providing spatially-continuous information, also in vertical direction.
Lateral boundary conditions	Coarse-scale data providing atmospheric variables at the domain borders of a regional climate model. May consist of meteorological reanalyses* (e.g. ERA-Interim*), global climate model output (e.g. MPI-ESM-LR*) or coarser-scale regional climate model output (e.g. CORDEX*).
Regional climate model	Limited-area atmospheric model specifically adapted for and applied on climate time scales. Often based on models for short-range numerical weather prediction.
Thermocline	Thin but distinct layer within a lake (or other large body of fluid such as an ocean or atmosphere) characterised by a rapid temperature decrease with depth.

Contents

Abstract v

Abbreviations and symbols ix

Contents xv

List of Figures xix

List of Tables xxiii

1 African lakes in a changing climate 1

1.1 Importance of the African Great Lakes 2

1.2 Climate of East Africa 4

1.3 Climate change in East Africa 8

1.4 Lake-atmosphere interactions 11

1.4.1 Surface energy balance 11

1.4.2 Modelling interactions between the African Great Lakes and the regional climate 13

1.4.3 Research aims 16

1.5 This thesis 17

2 Methods 19

2.1 Lake models 20
2.1.1 FLake 20
2.1.2 Other lake models 23
2.2 Regional atmospheric climate model 23
2.3 Coupled climate models 24

3 Understanding the performance of the FLake model over two African Great Lakes 29

3.1 Introduction 31
3.2 Data and methods 33
3.2.1 AWS data 33
3.2.2 FLake model 35
3.2.3 Water transparency and temperature profiles 36
3.2.4 Model configuration, evaluation and sensitivity 38
3.3 Results 42
3.3.1 Ishungu 42
3.3.2 Kigoma 45
3.3.3 Mpulungu 46
3.3.4 Comparison between sites 48
3.3.5 Sensitivity study 51
3.3.6 Mixing physics at Lake Kivu 57
3.4 Discussion and conclusions 59
3.5 Code availability 61
3.6 Acknowledgements 61

4 LakeMIP Kivu: evaluating the representation of a large, deep tropical lake by a set of one-dimensional lake models 63

4.1 Introduction 65

4.2 Data and methods 67
4.2.1 Lake models 67
4.2.2 Observations 68
4.2.3 Experimental setup 72
4.3 Results 75
4.3.1 Model performance over the mixolimnion 75
4.3.2 Lake energy balance 81
4.3.3 Deep water stratification 84
4.4 Discussion 88
4.4.1 Model improvement 88
4.4.2 Validity of the horizontal homogeneity assumption . . . 89
4.5 Conclusion 89
4.6 Acknowledgements 91

5 The impact of the African Great Lakes on the regional climate 93

5.1 Introduction 95
5.2 Model, data and methodology 97
5.2.1 COSMO-CLM^2 97
5.2.2 FLake 98
5.2.3 Model set-up 99
5.2.4 Evaluation datasets 102
5.2.5 Surface energy balance decomposition 104
5.3 Results 105
5.3.1 Model evaluation 105
5.3.2 Impact of the African Great Lakes on the regional climate 114
5.3.3 Decomposing the lake-induced surface temperature change 119
5.3.4 Dynamical response to lake presence 122

5.4 Conclusions 126
5.5 Acknowledgments 128

6 Lake Victoria, hotspot of future hazardous thunderstorm intensification 129

6.1 Methods 137
6.1.1 Overshooting top detections 137
6.1.2 Climate simulations 137
6.1.3 CORDEX ensemble analysis 138
6.2 Acknowledgements 139
6.3 Supplementary Information 140
6.3.1 Evaluation of COSMO-CLM^2 for extremes 140
6.3.2 Projected climate change for the African Great Lakes region 143
6.3.3 Clausius-Clapeyron scaling 145

7 Conclusions 151

7.1 Concluding summary 151
7.2 Ongoing work 156
7.2.1 Measuring lake-atmosphere interactions 156
7.2.2 Towards an early warning system for hazardous thunderstorms over Lake Victoria 158
7.2.3 Improving the stratification treatment in FLake 159
7.3 Recommendations for further research 160
7.3.1 Climate modelling over the African Great Lakes 161
7.3.2 Regional climate assessments 164

Bibliography 165

List of publications 197

List of Figures

1.1 TRMM precipitation over the African Great Lakes 3
1.2 Traditional fishing on Lake Kivu 4
1.3 TRMM precipitation over East Africa 6
1.4 Projected temperature and precipitation change for East Africa 9
1.5 Lake-atmosphere interactions schematic 12
1.6 General outline of this PhD thesis 18

2.1 Schematic temperature profile representation in FLake 21
2.2 Finding the optimal model configuration 26

3.1 Overview map of East Africa 33
3.2 Ishungu water temperature profile 34
3.3 Comparative histogram of the light attenuation coefficient . . . 39
3.4 Modelled and observed 5 m/60 m temperature at Ishungu . . . 43
3.5 Modelled and observed temperature at Ishungu 44
3.6 Modelled and observed 5 m/60 m temperature at Kigoma . . . 45
3.7 Modelled and observed temperature at Kigoma 47
3.8 Modelled and observed 5 m/60 m temperature at Mpulungu . . 48
3.9 Modelled and observed temperature at Mpulungu 49

3.10 FLake sensitivity to external parameters 52
3.11 FLake sensitivity to forcing fields 54
3.12 FLake sensitivity to radiation forcing fields 55
3.13 FLake sensitivity to initial conditions 56
3.14 Meteorological controls on mixing dynamics 58
3.15 monthly mean surface energy balance components at Ishungu . 59

4.1 Overview map of Lake Kivu 69
4.2 Modelled and observed lake temperatures at Ishungu 77
4.3 Modelled and observed 5m/30m/60m lake temperatures at Ishungu 78
4.4 Brier Skill Score vertical profiles at Ishungu 79
4.5 Taylor diagram indicating model performance 80
4.6 Monthly mean lake energy balance components 82
4.7 7-days running mean lake energy balance components 85
4.8 Deepwater temperatures at Ishungu 86
4.9 Overview map of Lake Kivu 87
4.10 Simstrat (modified) lake temperatures at Ishungu 88
4.11 Temperature profiles collected at 14 locations in Lake Kivu . . 89

5.1 Topography and model domain 101
5.2 Observed and modeled annual precipitation 107
5.3 Observed and modeled seasonal precipitation 108
5.4 In-situ observed versus modeled precipitation 109
5.5 Observed and modeled lake surface water temperatures 110
5.6 In-situ observed versus modeled lake surface water temperatures 111
5.7 Observed and modeled surface energy balance 112
5.8 Impact of the AGL on 2 m air temperature 115
5.9 Impact of the AGL on precipitation 117

5.10 Domain-averaged seasonal and diurnal cycles 118
5.11 Lake-induced change in the surface energy balance components 119
5.12 Lake-induced change in the diurnal surface energy balance components 121
5.13 Daytime vertical cross sections 123
5.14 Nighttime vertical cross sections 125
5.15 Impact of the AGL on convective mass flux density 126

6.1 Lake imprint on hazardous thunderstorm occurrence 130
6.2 Afternoon controls on nighttime extreme precipitation 131
6.3 Projected changes in extreme precipitation over Lake Victoria . 133
S1 COSMO-CLM^2 domain description 141
S2 Evaluating COSMO-CLM^2 and CORDEX for OT occurrence . 142
S3 Projected climate change for the African Great Lakes region . . 144
S4 CORDEX Projected precipitation change in East Africa 145
S5 Projected precipitation percentile changes over Lake Victoria . 145
S6 CORDEX member dependence on lateral boundary conditions 146
S7 Clausius-Clapeyron scaling 147
S8 Cross sections for extremes 148
S9 Illustration of lake breeze calculation 149

7.1 Automatic weather station on Lake Kivu 157
7.2 Lake-atmosphere interactions at AWS Kivu 158
7.3 Potential of an observation-based early warning system 159
7.4 Empirical evidence in favour of an new formulation of dC_T/dt . . 161

List of Tables

2.1 FLake forcing fields and external parameters 22
2.2 Description of the sensitivity experiments 25

3.1 AWS topographic and meteorological characteristics 35
3.2 Evaluation sites characteristics 38

4.1 Participating one-dimensional lake models and numerical settings 67
4.2 WS Kamembe meteorological characteristics 70
4.3 Net radiation used by the different lake models 83

5.1 Data products used for model evaluation 103
5.2 Bias and RMSE of COSMO-CLM^2, ERA-Interim and CORDEX 114
5.3 Impact of the African Great Lakes on climatological values . . 115

Chapter 1

African lakes in a changing climate

This introductory chapter presents an overview of the role of lakes in the climate of East Africa. Particular focus is put on the key importance of the African Great Lakes for local communities in East Africa, notably through their regulative role in the hydrological cycle. Then, a review of the present-day climate of East Africa and the projected impacts of anthropogenic climate change for the region are presented. In the next part, important processes determining lake-atmosphere interactions are introduced, followed by a description of recent scientific efforts that have increased our understanding of the role of some of the African Great Lakes within the regional climate system. Finally, we identify four main research goals along with the pathways to achieve them.

1.1 Importance of the African Great Lakes

The African Great Lakes are of utmost importance for regional economies, as well as being essential to the survival of the local population. As the largest reservoir of freshwater lakes in the tropics, they provide numerous ecosystem services to local communities, such as fishing grounds, drinking water and electricity. Lake Victoria alone directly supports 200 000 fishermen operating from its shores and sustains the livelihood of more than 30 million people living at its coasts (Semazzi, 2011). During the last decades, however, the African Great Lakes experienced fast changes in ecosystem structure and functioning, and their future evolution is a major concern (O'Reilly et al., 2003; Verburg et al., 2003; Verburg and Hecky, 2009).

Most enumerations of the African Great Lakes include, in order of size from largest to smallest, Lake Victoria, Lake Tanganyika, Lake Malawi, Lake Turkana, Lake Albert, Lake Kivu, and Lake Edward. Overall, lakes cover about 9% of the surface of the African Great Lakes region (defined here as the region 10°S to 3°N, 26°E to 36°E). While Lake Victoria, Albert and Edward empty into the white Nile, Lake Tanganyika and Lake Kivu are drained by the Congo River system. Lake Tanganyika, Lake Kivu, Lake Edward and Lake Albert are located in the graben of the Albertine rift. Consequently, these lakes are usually deep (e.g. up to 1470 m in Lake Tanganyika, Verburg and Hecky (2009)). Lake Victoria, in contrast, formed in the depression between the Western (Albertine) and Eastern branches of the East African rift and is therefore less deep (maximum depth of about 80 m, MacIntyre (2012)). The lakes deeper than 100 m are permanently stratified (meromictic lakes), whereas the more shallow lakes mix once a year (monomictic lakes, MacIntyre (2012)). Given their location close to the equator, and associated limited fluctuations in air temperature and incoming shortwave radiation, vertical and temporal variations in the water column are small (MacIntyre, 2012).

Apart from their key role in sustaining local livelihoods, the African Great Lakes are also important regulators of the East African climate. Observed precipitation patterns (Kummerow et al., 2000) in particular suggest an important impact of the African Great Lakes on the diurnal precipitation cycle, especially over Lake Victoria and Lake Tanganyika (Fig. 1.1). In the afternoon, the typical tropical convective precipitation falls over land, but hardly any rainfall is observed over the lakes (Fig. 1.1a). At night, in contrast, very little precipitation is produced over land, while strong convection develops over the lakes, leading to high precipitation amounts (Fig. 1.1b). The basic principle behind this phenomenon is relatively straightforward: due to the thermal inertia of the water surface, at night land breezes build up across the lakes borders, causing surface winds to converge over the lake surface. When these air masses, moistened by the lake,

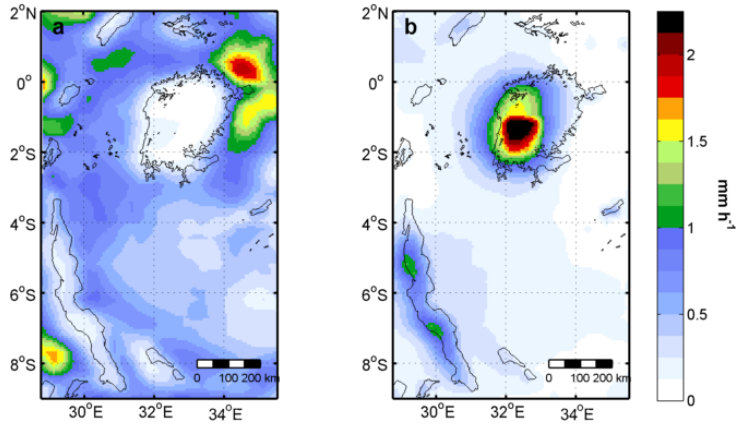

Figure 1.1: **Hourly mean precipitation over the African Great Lakes as observed by the Tropical Rainfall Measuring Mission (TRMM) satellite from 1998 to 2013: (a) 9-15 UTC, (b) 0-9 UTC.**

lift up into the atmosphere, they generate convective precipitation and often thunderstorms.

This effect would normally not be a major problem, were it not that every night, most of the 200 000 fishermen living on the shores of Lake Victoria ascend the lake to fish. Accurate estimates are lacking, but it is assumed that up to 5000 fishermen die every year on Lake Victoria only, most of them related to severe weather (Semazzi, 2011). Lake Victoria is therefore arguably the most dangerous stretch of water on Earth. The large number of weather related fatalities has a number of reasons. First, fishing is still mostly done in a traditional way, in wooden pirogues (Fig. 1.2), which renders the vessels more prone to destruction by wind gusts and high waves. Moreover, fishermen usually cannot swim, while life jackets are rarely used as they are often too costly for the local population. A final reason is the current absence of a well-functioning early warning system preventing fishermen from sailing off when a severe thunderstorm is forecast, although steps in this direction are made (Semazzi, 2011; Chamberlain et al., 2014; Eagle et al., 2015).

The significance of the African Great Lakes for local societies and their manifest imprint on the climate of the region together call for an in-depth understanding of East African lake-atmosphere interactions under present and future climate conditions. Special attention should thereby be paid to the controlling factors on the occurrence of extremes, in particular hazardous thunderstorms over Lake Victoria, as well as on the projection of their future change. In turn, this requires the development of a model framework able to relate large-scale

Figure 1.2: **Traditional fishing on Lake Kivu (©Wim Thiery).**

dynamical processes to local responses, since the interactions between tropical lakes and the overlying atmosphere (and therewith ultimately the occurrence of lake-induced climate extremes) have been identified as strongly dependent on atmospheric variability (Anyah et al., 2006; Verburg and Antenucci, 2010; Verburg et al., 2011). While Global Climate Models (GCMs) are widely used to analyse the present-day climate and project its future change (Christensen et al., 2013), they are limited in capturing local effects on regional scales due to their coarse resolution (Nyeko-Ogiramoi et al., 2010). In that respect, Regional Climate Models (RCMs) emerge as a powerful tool to downscale large-scale processes to higher resolution and perform dedicated process studies as well as climate assessments for a particular region (Laprise et al., 2008). Consequently, RCMs are increasingly applied to study climate processes over East Africa (e.g. Sun et al., 1999a; Indeje et al., 2001; Lauwaet, 2009; Segele et al., 2009b; Sylla et al., 2009; Davis et al., 2009; Vizy and Cook, 2012; Krähenmann et al., 2013; Saeed et al., 2013; Crétat et al., 2014; Kothe et al., 2014; Moufouma-Okia and Jones, 2014).

1.2 Climate of East Africa

The interplay between large-scale and local processes highlights the need to consider the climatic influence of the African Great Lakes against the background climate. In this section, we therefore review the current understanding of the present-day climate of East Africa.

While most of the tropical land is characterized by a wet climate, Large proportions of East Africa are semiarid to arid, with precipitation less than 2

mm day^{-1} (Yang et al., 2015). The complex orography of East Africa, with its coastal lowlands and the Turkana depression separating the Ethiopian highlands to the north from the East African highlands in the south, has an important influence on the climate of East Africa through its modulation of low-level atmospheric circulation and moisture transport.

Seasonal rainfall variability in East Africa is dominated by the Inter Tropical Convergence Zone (ITCZ) sweeping over the region (Anyah and Semazzi, 2006, 2007). The ITCZ is a narrow tropical belt of deep convective clouds and associated high precipitation (Schneider et al., 2014). Its seasonal migration towards the relatively warming hemisphere (Schneider et al., 2014) translates into a strong seasonal cycle of precipitation amounts over East Africa and important spatial differences (Fig. 1.3). Over the horn of Africa and the Lake Victoria Basin, a bimodal annual precipitation cycle is observed with two wet seasons associated with the ITCZ overpass and two dry periods associated with the descending branch of the Hadley circulation cell from June to September (JJAS) and January to February (JF; Fig. 1.3a,c; Yang et al., 2015). The wet period during March to May (MAM) is usually referred to as the Long Rains, whereas the Short Rains denote the wet period from October to December (OND; Fig. 1.3b,d; Anyah and Semazzi, 2006; Philippon et al., 2015). The Long Rains generate higher seasonal precipitation amounts since they generally count more, longer and more intense wet spells compared to the Short Rains owing to higher Sea Surface Temperatures (SSTs; Philippon et al., 2015; Yang et al., 2015). The eastern Sahel and southern half of the African Great Lakes region, in contrast, are characterised by a unimodal annual precipitation cycle with maximum during boreal and austral summer, respectively (Fig. 1.3a,c; Yang et al., 2015).

A strong relation exists between convective activity and surface rainfall amounts (Ba and Nicholson, 1998), indicating that most of the precipitation produced in East Africa is generated through convective activity. The land surface plays a key role in modulating convective intensity in tropical Africa, in particular (i) by supplying moisture through evapotranspiration from vegetation (Spracklen et al., 2012; Akkermans et al., 2014), (ii) by the soil moisture induced partitioning of radiative energy between sensible and latent heat fluxes (Taylor et al., 2012a; Guillod et al., 2015), (iiii) by causing orographic lifting (Laing et al., 2011; Anyah and Semazzi, 2007) and (iv) by initiating mesoscale circulation induced by land-water contrasts, for instance (e.g. Ba and Nicholson, 1998; Anyah et al., 2006; Laing et al., 2011; Lauwaet et al., 2012). Moreover, these semi-permanent convection generators may trigger the organisation of convection into structures larger than individual thunderstorms, referred to as Mesoscale Convective Systems (MCSs; Lauwaet et al., 2009, 2010; Goyens et al., 2011). The regeneration of convection through multiple diurnal cycles produces coherent

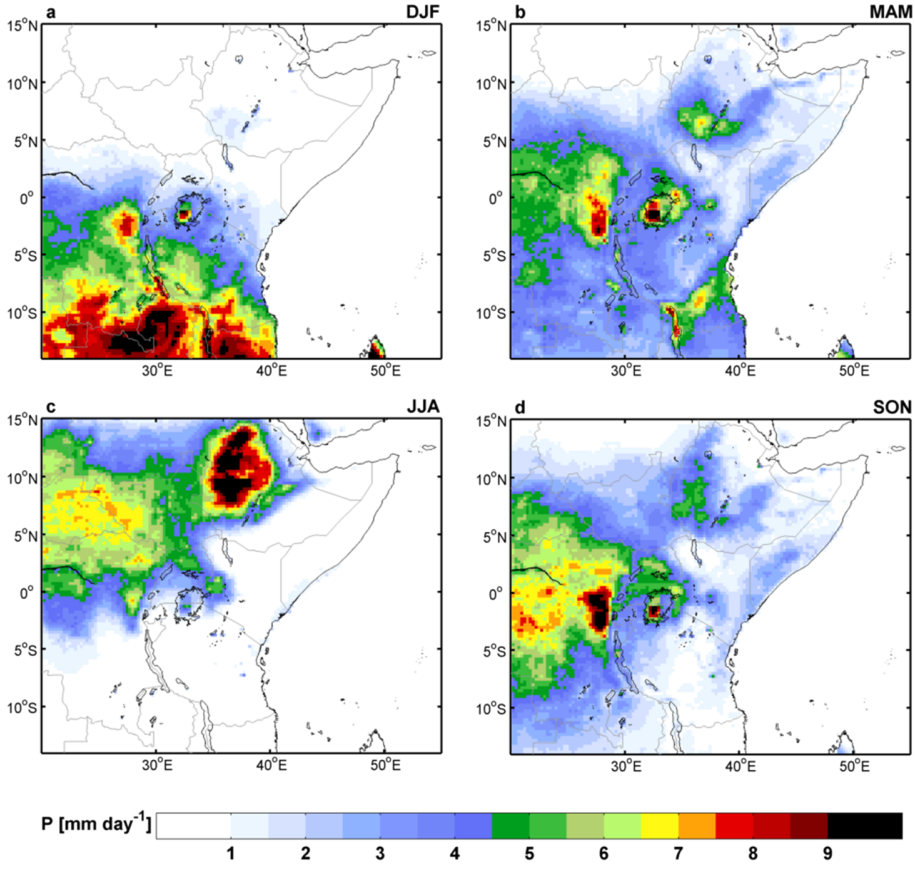

Figure 1.3: **Seasonal land precipitation cycle over East Africa as observed by the Tropical Rainfall Measuring Mission (TRMM) satellite from 1998 to 2013: (a) December-February, (b) March-May, (c) June-August, (d) September-November.**

episodes of convection propagating westward along with the trade winds (Laing et al., 2011).

Inter-annual precipitation variability over East Africa is large, in terms of magnitude as well as timing (Kizza et al., 2009). In addition, the variability depends on the season, with, for instance, the Short Rains displaying stronger inter-annual variability compared to the Long Rains (Behera et al., 2005). Long-term precipitation measurements around Lake Victoria mostly indicate a wetting trend (Kizza et al., 2009), more recently also for extremes (Mbungu et al., 2012). The important role of low frequency variability is also apparent in paleoclimatic records available for East Africa (Verschuren et al., 2000; Hastenrath, 2001; Scholz et al., 2007; Burnett et al., 2011) and highlights the impact of long-term precipitation variation on historic societal development (Verschuren et al., 2000) and even the human evolution and expansion from East Africa (Scholz et al., 2007).

Inter-annual precipitation variability in East Africa is generally attributed to annual-to-decadal oscillations of SSTs, which influence the climate over vast distances through teleconnections. In particular, most of the interannual variability during the Short Rains as well as other seasons has been linked to the Indian Ocean Dipole (IOD; Black et al., 2003; Behera et al., 2005; Conway et al., 2007; Marchant et al., 2007; Williams and Funk, 2011; Omondi et al., 2013; Zaroug et al., 2014; Lanckriet et al., 2014), an aperiodic SST oscillation with a warm anomaly in the Western Indian Ocean and cold anomaly in the Eastern part during a positive phase, and vice versa (Saji et al., 1999). A positive IOD phase is induced by upwelling of cold waters off the Sumatra and Java coasts, leading to anomalous easterlies along the equatorial Indian Ocean and warm SSTs in the western Indian Ocean (Cai et al., 2014). Extreme East African Short Rains have been associated with persistent positive IOD modes (Black et al., 2003; Behera et al., 2005), and explained by the anomalous low-level easterly flow of moist air during a positive IOD phase (Shongwe et al., 2011). Several studies have also found the imprint of El-Niño-Southern Oscillation (ENSO) on Short Rains variability over parts of East Africa (Sun et al., 1999b; Indeje et al., 2000; Plisnier et al., 2000; Schreck and Semazzi, 2004; Giannini et al., 2008; Segele et al., 2009a; Smith and Semazzi, 2014), which can be ascribed to the strong linkages between the IOD and the Southern Oscillation (Black et al., 2003; Behera et al., 2005). State-of-the-art GCMs generally succeed in reproducing the IOD influence on the East African Short Rains (Conway et al., 2007; Rowell, 2013), but face difficulties when it comes to representing the ENSO influence on the regional climate due to substantial errors in the SST representation in the GCMs (Rowell, 2013).

Climate extremes generated by this interannual variability have been the dominant trigger of natural disasters in East Africa, particularly in Kenya,

Ethiopia and Somalia (Otieno and Anyah, 2012). On the one hand, East Africa was recently hit by excessive rainfall triggering devastating floods (e.g. in 1961, 1996 and 2006; Behera et al., 2005; Anyah and Semazzi, 2006; Segele et al., 2009b; Kijazi and Reason, 2009). On the other hand, during this same period deficient rainfall led to severe droughts (e.g. in 1984, 2005 and 2011; Black et al., 2003; Behera et al., 2005; Hastenrath et al., 2007; Segele et al., 2009b; Zeleke et al., 2012). The extreme and oppressive climate under natural circumstances stands in sharp contrast to the vulnerability of societies in East Africa. The most notorious example is the 1983-1985 famine hitting North-Ethiopia, but also more recently, the failure of consecutive rainy seasons caused a major humanitarian crisis in 2011 across Somalia, Djibouti, Ethiopia and Kenya, and threatened the livelihood of millions of people (Lyon and DeWitt, 2012). In the absence of dedicated detection-attribution studies for potential changes in climate extremes in East-Africa, it is not yet known whether the occurrence of these events is to be attributed to anthropogenic drivers.

1.3 Climate change in East Africa

The devastating impacts of natural climate variability in East Africa has raised the question to what might be expected for the region under future anthropogenic climate change. According to the Intergovernmental Panel on Climate Change (IPCC) Fifth Assessment Report (AR5), a warming by 2.0 °C (1.0 - 3.1 °C) is projected by the end of the century under radiative concentration pathway (RCP) 4.5 and a warming up to 4.0 °C (2.4 - 5.6 °C) under RCP8.5 over East Africa (Fig. 1.4a; Christensen et al., 2013; van Oldenbrogh et al., 2013). The GCMs participating in the Coupled Model Intercomparison Project phase 3 (CMIP3) and phase 5 (CMIP5) - and thus forming the base of the AR4 and AR5 projections - are in consensus regarding the projected widespread warming (Anyah and Qiu, 2012; Otieno and Anyah, 2013). Note that the total uncertainty of the CMIP ensemble projections has three sources: (i) internal variability of the climate system, (ii) choice and structure of the RCP scenario (i.e. the greenhouse concentration trajectory) and (iii) differences and uncertainties in the GCMs utilized. Only the latter can potentially be eliminated (Knutti and Sedláček, 2012).

Future annual precipitation projections are less clear, with CMIP5 models showing a larger spread (Fig. 1.4b-d). By 2100, a multimodel median precipitation increase by 2% (11%) is projected under RCP4.5 (RCP8.5), but the multimodel spread (-7% to 21% and -11% to +34% under RCP4.5 and RCP8.5, respectively) indicates that for the annual mean most models do not even agree upon the sign of change over East Africa (Fig. 1.4b-d; Christensen

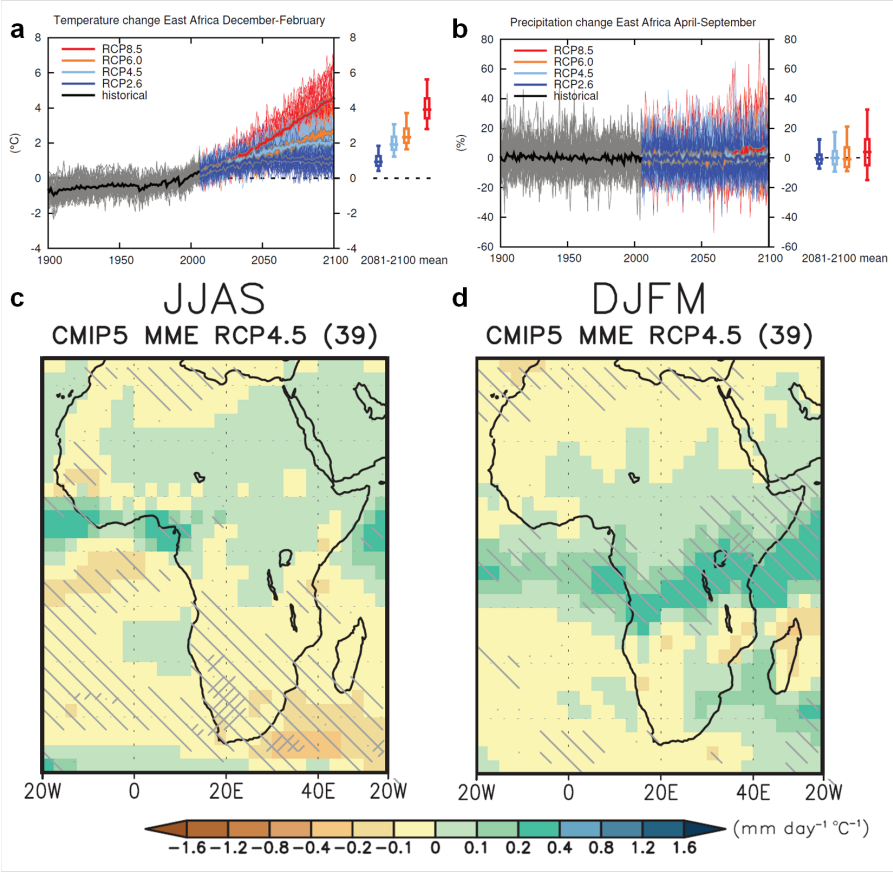

Figure 1.4: **Time series of (a) December to February temperature and (b) April to September precipitation change relative to 1986–2005 averaged over land grid points in East Africa (11.3°S to 15°N, 25°E to 52°E). Thin lines denote one ensemble member per model, thick lines the CMIP5 multimodel mean. On the right-hand side the 5th, 25th, 50th (median), 75th and 95th percentiles of the distribution of 20-year mean changes are given for 2081–2100 in the four RCP scenarios.**
Maps of precipitation changes for Africa in 2080–2099 with respect to 1986–2005 in (c) June to September and (d) December to March in the RCP4.5 scenario with 39 CMIP5 models. Precipitation changes are normalized by the global annual mean surface air temperature changes in each scenario. Light hatching denotes where more than 66% of models (or members) have the same sign with the ensemble mean changes, while dense hatching denotes where more than 90% of models (or members) have the same sign with the ensemble mean changes (Adapted from Christensen et al. (2013); van Oldenbrogh et al. (2013)).

et al., 2013; van Oldenbrogh et al., 2013), and no clear multimodel trends can be revealed for the whole region (Conway et al., 2007; Otieno and Anyah, 2013) despite several subregional scale patterns (Cook and Vizy, 2013; Akurut et al., 2014). In contrast, merging precipitation and evapotranspiration changes, Otieno and Anyah (2013) reveal a high likelihood of an increased deficit in local moisture supply. And in contrast to the annual mean precipitation change, a clear increase is projected during the Short Rains (Fig. 1.4d), consistent with a differential warming of 21st century Indian Ocean SSTs leading to more frequent positive IOD phases (Shongwe et al., 2011; Christensen et al., 2013; Cai et al., 2014).

A decreasing dryness is projected in a large part of East Africa (Shongwe et al., 2011; Seneviratne et al., 2012), although some regional climate projections suggest an increase in the number of dry days by 5%-10% over East Africa associated with a weakening of the boreal spring long rains (Vizy and Cook, 2012). At the same time, there is *high confidence* for a *likely* (66-100%) increase in wet extremes over East Africa, especially during the Short Rains (Seneviratne et al., 2012; Tebaldi et al., 2006; Paeth and Thamm, 2007; Shongwe et al., 2011; Vizy and Cook, 2012; Akurut et al., 2014, the confidence assessment is an expert-based evaluation of the confidence in the tools and data basis for the projected change; the likelihood assessment indicates the likelihood for a direction of change).

The anticipated impacts of projected climate change on human societies as well as terrestrial ecosystems in East Africa are numerous. Potential consequences include, but are not limited to: (i) changes in growing season length (Cook and Vizy, 2012) and food security, (ii) a potential increase in groundwater availability associated with the increase in intense rainfall (Taylor et al., 2012b), (iii) increased risk of natural hazards such as precipitation triggered landslides and flash floods (Jacobs et al., 2015b). Aquatic ecosystems, and lakes in particular, are early sentinels of climate change and already experience the first impacts of anthropogenic climate change. Following the atmospheric temperature increase throughout the 20th century, the African Great Lakes have experienced steady warming (Verburg et al., 2003; Vollmer and Bootsma, 2005; Verburg and Hecky, 2009; Tierney et al., 2010; Katsev et al., 2014; Saulnier-Talbot et al., 2014) at historically exceptional rates (Tierney et al., 2010). The most notable ecological consequences of this warming are reduced ecosystem productivity and associated declining fish catches (O'Reilly et al., 2003; Verburg et al., 2003; Verschuren, 2003; Hecky et al., 2010; Naithani et al., 2011; MacIntyre, 2012; Saulnier-Talbot et al., 2014). A comprehensive overview of the potential impacts of projected future climate change for East Africa is provided in Niang et al. (2014).

1.4 Lake-atmosphere interactions

1.4.1 Surface energy balance

This thesis mainly focuses on the climatic influences of lake-atmosphere exchanges of energy, water and momentum. The energy exchange is described through the surface energy balance (SEB). In mathematical form, the SEB at the water-air interface and for a particular point in the lake is expressed as:

$$SW_{in} - SW_{out} + LW_{in} - LW_{out} - LHF - SHF - G = 0 \qquad (1.1)$$

In equation 1.1, SW_{in} represents the incoming shortwave radiation, SW_{out} equals the reflected shortwave radiation, LW_{in} is the incoming longwave radiation, LW_{out} expresses the longwave radiation emitted by the lake surface, LHF and SHF are the turbulent fluxes of latent heat and sensible heat, respectively, and G finally describes the subsurface energy flux (Fig. 1.5). SEB components are described in units of W m^{-2} and are usually larger than the energy exchange between the water and the bottom sediments Q_{bot}. Note that next to the water-air interface, the energy budget may also be computed for a lake layer or the entire water column (see e.g. sect. 4.3.2 and Rouse et al. (2003))

Differences between lakes and adjacent land in terms of SEB components are the primary cause of the impact of lakes on the climate system. For instance, the net solar radiation available at the surface ($SW_{net} = SW_{in} - SW_{out}$) for a given incoming flux SW_{in} depends on the surface reflectivity (shortwave albedo). Since the shortwave albedo over open water is typically lower compared to land (Mironov et al., 2010; Balsamo et al., 2012; Davin et al., 2014; Balsamo et al., 2015), a higher fraction of the incoming solar radiation will be absorbed by lakes. In addition, this net shortwave radiation also penetrates through the water surface, heating up the part of the water column where it is absorbed (Potes et al., 2012, 2013; Le Moigne et al., 2013) rather than the surface itself. Different heat capacities of water and land further influence the temperature response to a change in the heat content (Subin et al., 2012b), whereas horizontal water currents on the one hand and vertical mixing and stratification processes on the other hand redistribute the heat stored in the lake (Fig. 1.5; Song et al., 2004; Martynov et al., 2010). Finally, for similar atmospheric conditions, the LHF from a lake surface will typically be higher compared to land, as lakes are not limited in their ability to supply moisture to the atmosphere and therefore evaporate at the potential evaporation rate. A higher LHF also implies a higher moisture supply to atmosphere, therewith coupling the SEB to the lake's water balance (Seneviratne et al., 2010). On average, the diurnal cycle of the turbulent fluxes is also low compared to the surrounding land, with latent heat fluxes

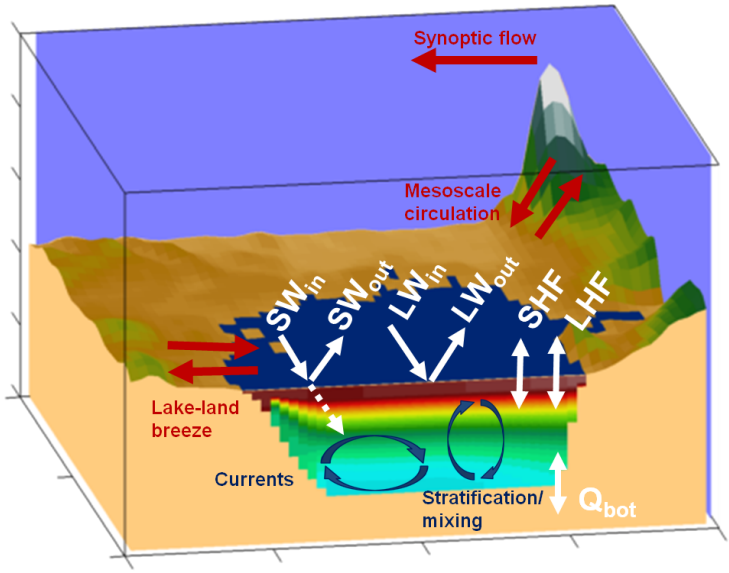

Figure 1.5: **Schematic overview of the processes that determine lake-atmosphere interactions (see text).**

ranging typically between ∼120-130 W m^{-2}. Sensible heat fluxes are much lower and typically vary between ∼5-15 W m^{-2} during the day. Evaporation-induced cooling is therefore the main source of turbulent energy loss at the surface.

All these effect add up to a significant influence of lakes on near-surface air temperatures. Notably, lakes tend to dampen the diurnal and seasonal cycle of near-surface temperature across the globe (Martynov et al., 2010; Samuelsson et al., 2010; Subin et al., 2012a). Depending on the lake size and geographical setting, modification of the surface energy and water balances as well as the lower surface roughness over open water may induce further impacts, such as changes in mesoscale atmospheric circulation, atmospheric convection, cloud cover and ultimately precipitation generation (Fig. 1.5).

Many studies have developed and applied an RCM to investigate the influence of lakes on the regional climate (e.g. Hostetler et al., 1994; Hostetler and Giorgi, 1995; Bates et al., 1995; Goyette et al., 2000; Samuelsson et al., 2010; Gula and Peltier, 2012; Lauwaet et al., 2012; Martynov et al., 2012; Gu et al., 2013; Notaro et al., 2013; Bennington et al., 2014; Mallard et al., 2014, 2015). These studies mostly focused on midlatitude or boreal regions where lakes are abundant. However, the influence exerted by midlatitude or boreal lakes can be expected to greatly differ from the climatic impact of the African Great Lakes. To start,

the climate of East-Africa is very different from these other regions (Sect. 1.2), excluding certain influences such as lake-effect snow (Mallard et al., 2015) or anticyclone weakening (Notaro et al., 2013), for instance. In addition, the limnological characteristics of the African Great Lakes are unique: often they are deep, meromictic lakes characterised by a limited seasonal temperature cycle and a weak stratification in their surface layers. They are also permanently ice-free and their mixing dynamics are not governed by seasonal temperature fluctuations. This unique setting indicates that findings from other regions cannot be readily transferred to the African Great Lakes and calls for dedicated model studies investigating the climatic influence of these lakes.

1.4.2 Modelling interactions between the African Great Lakes and the regional climate

> *I was in a camp on the north end of Bugalla, the largest island of the Sese Archipelago. The camp lay about 300 yards from the shore of a small bay. At daybreak on June 30 there were very lowering black clouds and every indication of an immediate heavy storm. While looking out from the tent I suddenly saw that a waterspout was travelling obliquely towards us, and as it eventually came to within about 100 yards of the shore a very good view was obtained for about five minutes before it came to an end. [...] The pedicle was extremely narrow at its lower end, and not quite straight, being sinuous in outline. It broadened out gradually into a column which went up into the low cloud; the core of this column was much less dense than the periphery, and the violent upward spiral ascent of the water could be clearly seen. [...] Its cessation was followed by violent rain and thunder.*
>
> G. D. Hale Carpenter, Waterspouts on Lake Victoria (Nature, 1922)

The first modelling activities explicitly examining African lake-atmosphere interactions have mostly focused on Lake Victoria and suggested that the lake plays an important role in regional precipitation production (Song et al., 2004; Anyah and Semazzi, 2004; Anyah et al., 2006; Anyah and Semazzi, 2009; Argent et al., 2014; Sun et al., 2014, 2015; Chamberlain et al., 2014; Williams et al., 2014). Atmospheric stability and associated precipitation production over this lake is to a large extend dominated by mesoscale circulation, in contrast to the land surface where precipitation is moisture limited (Yang et al., 2015). The main reason for the enhanced precipitation observed at night over Lake Victoria

(Fig. 1.1) is the development of a mesoscale lake-land breeze system, with the nighttime land breeze leading to moisture convergence and an associated precipitation maximum during late night and early morning (Song et al., 2004; Anyah et al., 2006). During daytime, convection is suppressed due to near-surface moisture divergence along the lake breeze. Additional experiments for a 5-day up to 4-month period revealed an important sensitivity of basin-wide spatial precipitation distribution to lake surface temperatures, confirming the key importance of surface triggered convection over the Lake Victoria basin (Anyah and Semazzi, 2004; Anyah et al., 2006; Sun et al., 2014, 2015).

The asymmetrical precipitation pattern over Lake Victoria, noted both in model results (Song et al., 2004; Anyah et al., 2006; Anyah and Semazzi, 2009) and satellite-based observations (Fig. 1.1; Argent et al., 2014), also highlights the role of the surrounding orography, large-scale moisture convergence and the unidirectional nature of prevailing trade winds on which the lake-land breeze is superimposed. During daytime, moisture advected along the prevailing easterly trade winds hits the westerly lake breeze, triggering convection and an associated precipitation maximum on the eastern shore (Fig. 1.1a; Anyah et al., 2006). At night, the trade winds and a katabatic (downslope) wind from the steep orography east of Lake Victoria reinforce the land breeze across the eastern shore, favouring convection and precipitation generation over the western lake sector (Fig. 1.1b; Anyah et al., 2006). Accumulated over 24h, the interplay of meso- and synoptic-scale circulation results in a dry-wet-dry-wet quadrupole over the Lake Victoria basin, with a dry western shore, a wet western and dry eastern lake sector, and a wet eastern shore (Fig. 1.1; Argent et al., 2014).

The above description of a waterspout by Dr. Hale Carpenter is just one example of a weather hazard triggered in this part of the world by the complex interplay of lakes, mountains and monsoons. Both the timing and location of the observed event matches with the expected maximum thunderstorm intensity in the western sector of the lake around daybreak, and according to Dr. Carpenter, this feature is very commonly observed over this part of the lake.

It is clear that in this unique setting, obtaining a regional climate simulation of acceptable skill may turn out to be quite challenging. Argent et al. (2014) and Williams et al. (2014) discuss some of the challenges when configuring a regional, coupled lake-land-atmosphere model for the Lake Victoria Basin. Sufficiently high resolution, choice of the convection parameterization scheme and especially the inclusion of a lake model are identified as key ingredients to a successful reproduction of the observed precipitation climatology for the region. Preliminary results show that accounting for some of these aspects may enable numerical storm prediction over the lake to some extent (Chamberlain et al., 2014; Eagle et al., 2015).

Fewer model studies have explicitly examined the diurnal variability of atmospheric circulation around Lake Tanganyika. Here, the steep mountain chains on both sides of the lake may either block or channel atmospheric flow (Savijärvi and Järvenoja, 2000), and slope winds account for more than half of the diurnal circulation variability compared to only a quarter by the lake/land breeze effect and synoptic flow, respectively (Savijärvi, 1997; Podsetchine et al., 1999; Savijärvi and Järvenoja, 2000). These findings are confirmed by the rare over-lake observations available for the African Great Lakes (Verburg and Hecky, 2003; Verburg and Antenucci, 2010; Verburg et al., 2011) and are consistent with cruise data obtained for Lake Malawi (Hamblin et al., 2003).

Overall, the first regional climate model studies of African lake-atmosphere interactions clearly demonstrate the importance of lakes for the climate of East Africa and have increased the understanding of the processes responsible for their influence. At the same time, however, these studies are also marked by a number of limitations.

(i) First, while most studies focus on the effect of an African Great Lake on the climate, little is known about the influence of climate variability on the lake temperatures. Yet spatio-temporal variability of the heat budgets of the African Great Lakes constitutes an important aspect of the two-way interaction with the overlying atmosphere. (ii) Second, the lack of reliable observational data for the region has so far impeded a thorough evaluation of the climate models applied to the region. (iii) In addition, most studies focus on one particular lake and were based on short integration periods ranging from less than one to a few months. This has important implications regarding the influence of model spin-up and inter-annual variability on the simulation quality. Given their thermal inertia, lake temperatures require considerably longer spin-up times than the atmosphere or the land surface. The strong interannual variability of the East African climate (Sect. 1.2) moreover highlights the need to consider long time series when studying this region. Considering a 30-year time series for precipitation yields an inherent uncertainty of 15% for East Africa attributable to internal variability, and even 37% when considering only 10 years (Brisson et al., 2014). (iv) The unique characteristics of the African Great Lakes region finally require dedicated climate change projections. However, high-resolution, coupled lake-land-atmosphere simulations projecting the impacts of future climate change for this region are currently still absent. The Coordinated Regional Climate Downscaling Experiment (CORDEX; Giorgi et al., 2009), a major international effort to produce continental-scale RCM ensemble simulations of present and future climate, presents an important step forward in this respect; however these simulations are generally characterised by relatively low spatial resolution ($\sim$50 km) and crude parameterizations of lake surface temperatures (Nikulin and Jones, 2011; Hernández-Díaz et al., 2012;

Panitz et al., 2014; Dosio et al., 2014; Endris et al., 2013; Laprise et al., 2013; Williams et al., 2014).

1.4.3 Research aims

In this thesis, we use a regional atmospheric climate model, COSMO-CLM^2, coupled to a one-dimensional lake model, FLake, to assess the interactions between the African Great Lakes and the overlying atmosphere at high resolution, now and in the future. With this model, we set out to address the challenges of current research on the lake-climate interactions in East Africa (identified in sect. 1.4.2). In particular, we advance four main research goals, along with four pathways to achieve them:

i **Assess whether standalone lake models are able to reproduce the effect of climate on the thermal structure of the African Great Lakes and identify the climatic controls on their mixing dynamics and heat budget.** Thanks to the roll out of several in-situ lake monitoring programs (Plisnier et al., 2009; Darchambeau et al., 2014), it becomes possible to test FLake over the African Great Lakes and compare its skill to other state-of-the-art lake models [Chapters 3 and 4].

ii **Test the ability of a climate model to reproduce the climatic conditions of the African Great Lakes region.** A thorough model evaluation is enabled by efforts to collect in-situ measurements and the recent advent of satellite-derived observational products, in particular for precipitation (e.g. Legates and Willmott, 1990; Kummerow et al., 2000; Huffman and Adler, 2001; Joyce and Janowiak, 2004; Rudolf et al., 2011), lake surface temperature (e.g. MacCallum and Merchant, 2012) and SEB components (e.g. Jung et al., 2010; Stackhouse et al., 2011; Mueller et al., 2013) [Chapter 5].

iii **Quantify the imprint of the African Great Lakes on present-day regional atmospheric dynamics and the hydrological cycle.** Recent enormous advances in computing power and data storage capacities now allow to extend model domains to larger areas and simulation periods to climate time scales while maintaining - or even increasing - the horizontal grid resolution. More robust assessments of climatic responses to lake presence are therewith enabled. The model framework also allows for the isolation of the lake forcing from all other drivers of climate variability and for the application of the SEB framework(sect. 1.4.1) [Chapter 5].

iv **Construct climate projections for hazardous storm intensity over Lake Victoria and understand the role of the lake therein.** Having

tailored a climate model for the African Great Lakes region, it becomes possible to conduct the first dedicated high-resolution, coupled lake-land-atmosphere climate change projection to investigate the role of anthropogenic greenhouse gas emissions on future precipitation patterns [Chapter 6].

1.5 This thesis

In Chapter 2, we briefly describe the lake and climate models used in this thesis and their coupling. Then, in Chapters 3 and 4, results of applying lake models in standalone mode are presented, followed by results obtained with the coupled lake-land-atmosphere model in Chapters 5 and 6 (Fig. 1.6).

In Chapter 3, FLake is used in standalone mode to simulate lake temperatures of Lake Kivu and Lake Tanganyika. We start by evaluating the model's ability to reproduce water column temperatures, followed by an extensive model sensitivity study. In addition, we uncover the meteorological controls on mixed layer dynamics of the African Great Lakes.

Chapter 4 describes the results of applying seven one-dimensional lake models to Lake Kivu. The unique limnology of this permanently stratified lake presents a worthy challenge to the models currently involved in the Lake Model Intercomparison Project (LakeMIP). We compare the model skill for both surface and deep water temperatures, and identify differences in the ability to represent the lake's heat budget. We then attribute these differences to variations in the treatment of radiation and turbulence in the models.

In Chapter 5, COSMO-CLM^2 is applied to East Africa to assess the influence of the African Great Lakes on the present-day regional climate. To this end, we use COSMO-CLM^2 coupled to FLake at a horizontal resolution of $\sim$7 km for a period of 10 years (1999-2008). We first provide an in-depth evaluation of the optimal COSMO-CLM^2 configuration (defined in Chapter 2) using multiple available in-situ and remotely sensed observations. The good agreement between COSMO-CLM^2 and observations supports the presentation of the imprint of the African Great Lakes on the regional climate, achieved through the comparison of the optimal simulation with a second simulation where all lakes are replaced by representative land. We present the spatial and temporal variability of the lake influence on precipitation and temperature, and decompose the latter impact into contributions from the different surface energy balance components. We also show how the lake presence influences atmospheric circulation and stability.

Chapter 6 discusses the projected influence of anthropogenic climate change on hazardous thunderstorm intensity over Lake Victoria. We start by presenting

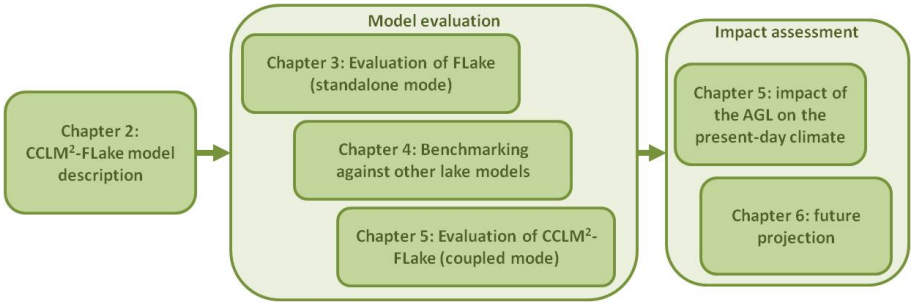

Figure 1.6: **General outline of this PhD thesis.**

a new satellite-based detection of severe thunderstorms and demonstrate the marked imprint of the lake on their occurrence. After that we apply COSMO-CLM^2 to project robust changes in average and extreme precipitation over and around Lake Victoria by the end of the 21^{st} century under a high emission scenario. We cross-check our findings with an ensemble of coarser-scale regional climate projections for East Africa and use it to assess the sensitivity of precipitation extremes to global warming. Further analysis of the high-resolution output finally allows to attribute the projected changes to dynamic and thermodynamic drivers. We summarize this thesis in Chapter 7, and conclude with an overview of ongoing efforts and recommendations for future research.

Chapter 2

Methods

This chapter briefly describes the various one-dimensional lake models used in this research, the limited-area atmospheric climate model COSMO-CLM, and the coupling between COSMO-CLM, the lake model FLake and the land surface model Community Land Model.

2.1 Lake models

2.1.1 FLake

The Freshwater Lake model (FLake) is a one-dimensional lake model which computes the evolution of a lake column temperature profile and the integral energy budgets of its different layers (Mironov et al., 2010). The following brief overview of the model physics is based on the comprehensive FLake documentation (Mironov, 2008).

The model considers two layers in the water column: a mixed layer of constant temperature (T_{ML}) at the top and a thermocline down to the lake bottom (Fig. 2.1). Instead of solving partial differential equations (varying both with time and depth) for the temperature and turbulence quantities, it solves ordinary differential equations for time-dependent variables from which the temperature profile is diagnosed. The prognostic variables therewith reduce to the mixed layer depth (h_{ML}), the mixed layer, bottom and mean water column temperatures (T_{ML}, T_{BOT} and T_{MW}, respectively) and the shape factor with respect to the temperature profile in the thermocline (C_T, Fig. 2.1).

Within the thermocline, the temperature-depth curve is parameterized through the concept of self-similarity, an idea suggesting that the characteristic *shape* of the thermocline temperature-depth curve is conserved irrespective the depth of that layer (Munk and Anderson, 1948). A first mathematical formulation for this "assumed-shape" was proposed by Kitaigorodskii and Miropolskii (1970) to describe the vertical structure of the seasonal thermocline in the ocean. According to the self-similarity concept, the water temperature $T(z,t)$ in the thermocline at a certain time t and depth z can be computed from

$$\frac{T_{ML}(t) - T(z,t)}{T_{ML}(t) - T_{BOT}(t)} = \Phi_T(\zeta) \tag{2.1}$$

with $\Phi_T(\zeta)$ a dimensionless function ($0 < \Phi_T(\zeta) < 1$) depending on dimensionless depth ζ (i.e. $\zeta = 0$ at depth h_{ML} and $\zeta = 1$ at depth h_{BOT}) which satisfies the boundary conditions $\Phi_T(0) = 0$ and $\Phi_T(1) = 1$. In particular, FLake implements the following empirical fourth-order polynomial approximation of the shape function $\Phi_T(\zeta)$ with respect to the temperature profile in the thermocline:

$$\Phi_T = \left(\frac{40}{3}C_T - \frac{20}{3}\right)\zeta + (18 - 30C_T)\zeta^2 + (20C_T - 12)\zeta^3 + \left(\frac{5}{3} - \frac{10}{3}C_T\right)\zeta^4 \tag{2.2}$$

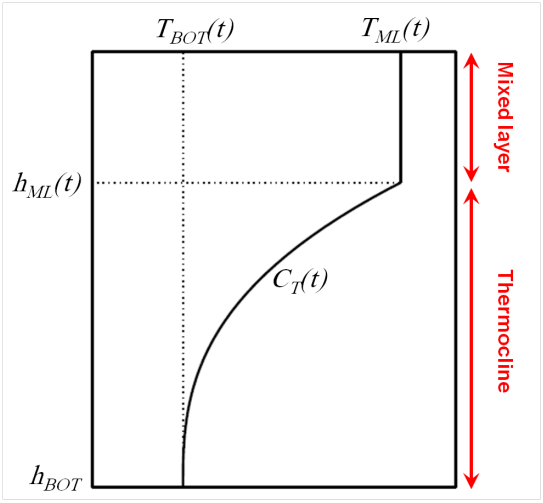

Figure 2.1: **In FLake, the evolving temperature profile in a lake of depth h_{BOT} is characterised by several time-dependent variables, namely, the temperature $T_{ML}(t)$ of the mixed layer, its depth $h_{ML}(t)$, the bottom temperature $T_{BOT}(t)$, and the temperature-profile shape factor $C_T(t)$ for the thermocline. Computation of the temperature profile within lake ice/snow and bottom sediments is optional and not shown here (adapted from Mironov, 2008).**

and computes the temporal change in the shape factor C_T from:

$$\frac{dC_T}{dt} = sign(dh_{ML}/dt)\frac{C_T^{max} - C_T^{min}}{t_{rc}} \tag{2.3}$$

where t_{rc} is the relaxation time scale and C_T^{min} and C_T^{max} the minimum and maximum values of the shape factor, respectively (with $C_T^{min} = 0.5$ and $C_T^{max} = 0.8$, defined theoretically). In turn, t_{rc} depends on the thermocline depth, the average buoyancy frequency and a mixing velocity scaling parameter. The proposed relationship for the shape function Φ_T was derived from lake temperature observations and theoretical considerations. It should however be emphasized that the definition of an exact form of Φ_T is not required, as not the shape function Φ_T but the shape factor C_T enters the model equations computing the integral heat budget for the thermocline, thus removing the dependency on the empirically derived eq. 2.2.

Furthermore, given their control on turbulence in the surface mixed layer (Read et al., 2012), temporal changes in h_{ML} are calculated taking both convective and

Table 2.1: **FLake forcing fields and external parameters.**

	Symbol	unit
Forcing variable		
Incoming shortwave radiation	SW_{in}	W m^{-2}
Incoming longwave radiation	LW_{in}	W m^{-2}
Air temperature	T	K
Relative humidity	RH	%
Wind velocity	u	m s^{-1}
Air pressure	p	Pa
External parameter		
Lake depth	h_{BOT}	m
Downward light attenuation coefficient	k	m^{-1}

mechanical mixing into account, whereas volumetric heating is computed from the net short-wave radiation penetration through the lake surface and absorption at depth according to the Beer-Lambert law. Through the computation of the integral energy budgets of the mixed layer and thermocline, the model is expected to conserve energy within the water column. FLake assumes a constant surface shortwave albedo α_{SW} of 0.07 and a surface longwave emissivity of the water surface of 0.97, the latter serving as input to the Stefan-Boltzmann law calculating the longwave radiation emitted by the lake surface. Additional routines describing the temperature profiles within the bottom sediments and lake ice/snow as well as their interaction with the water column are available, but are not relevant for the present study. Besides meteorological forcing fields, the model also requires input for two fixed external parameters, i.e. the lake depth and the vertical light attenuation coefficient, a measure for the water transparency (Table 2.1). The model can be initialised using an observed temperature profile or any other profile of choice (The default initialisation assumes $T_{BOT} = 4$ °C). The time is 60 s by default in standalone mode but set to the atmospheric time step in coupled mode. Finally, along with the standalone FLake model comes a set of surface flux subroutines originating from the limited-area atmospheric model COSMO (Consortium for Small-scale Modeling; Doms, 2011), hence the components of the surface energy balance are computed following the method described by Raschendorfer (2001, see also Doms et al. (2011); Akkermans et al. (2012)).

Besides being computationally cheap, FLake has the prime advantage of containing only two free external parameters (Lake depth and water transparency; Table 2.1), which can moreover be provided from observations. In fact, the model was originally developed with the goal of being universally applicable, that is, without further necessity of tuning internal model parameters. Due to these two advantages, FLake has become a landmark for parametrising lakes in atmospheric model systems. Details regarding the configuration of

FLake in this thesis are provided in sections 3.2.2, 4.2.1 and 5.2.2.

2.1.2 Other lake models

Besides FLake, a large number of one-dimensional lake models have been developed in the past decades. Notable examples are the models from the Hostetler-family, i.e. the Hostetler model (Hostetler et al., 1993) and CLM4-LISSS (Subin et al., 2012b). Like the FLake model, Hostetler-type models are computationally cheap, and they have therefore been used to represent lake-climate interactions in many global and regional studies (e.g. Hostetler et al., 1994; Hostetler and Giorgi, 1995; Bates et al., 1995; Song et al., 2004; Martynov et al., 2012; Subin et al., 2012a; Gu et al., 2013; Notaro et al., 2013; Bennington et al., 2014; Wen et al., 2014).

Examples of other, more complex one-dimensional lake models are LAKEoneD, SimStrat, LAKE, MINLAKE2012. Belonging to the family of $k - \epsilon$ models, LAKEoneD, SimStrat, LAKE all solve the turbulence parameterization problem by using the one-dimensional transport equations for turbulent kinetic energy and turbulent dissipation (Stepanenko et al., 2013). However, these models contain a number of parameters requiring re-tuning for every case study. As a consequence they have only rarely been coupled to GCMs or RCMs. A further description of the one-dimensional lake models applied in this thesis is provided in section 4.2.1.

2.2 Regional atmospheric climate model

In this study, we employ the COSMO model in CLimate Mode (COSMO-CLM), a three-dimensional, non-hydrostatic regional climate model. COSMO-CLM is maintained by the CLM-Community, an open international network of more than 50 research institutions, and was applied in over 140 international peer-reviewed publications over the last five years (www.clm-community.eu). The model is a spin-off from the COnsortium for Small-scale MOdelling (COSMO) model, originally developed at the German Weather Service and nowadays used for operational weather predictions by an increasing number of national weather services, notably from Germany, Switzerland, Italy, Greece, Poland, Romania and Russia. The CLM-community and COSMO consortium work closely together to develop the source code, therewith simultaneously achieving better weather forecasts and an improved understanding of the climate system.

The dynamical core of the model solves the primitive thermo-hydrodynamical equations for compressible flow in a moist atmosphere on rotated geographical coordinates and terrain-following coordinates in the vertical (Doms, 2011). A significant fraction of the physical processes is however not accounted for by this explicit solution, and therefore needs to be parameterized. Examples of parameterized processes are grid-scale clouds and precipitation, subgrid-scale clouds and turbulence, and shallow and moist convection (Doms et al., 2011, see also section 5.2.1). A complete and detailed description of the model system dynamics, numerics and physical parameterizations can be found in the model documentation (e.g. Doms, 2011; Doms et al., 2011, http://www.cosmo-model.org). Climatologically constant data (external parameters) such as topographic and vegetation characteristics are prepared using the EXTPAR software (Smiatek et al., 2008), whereas initial lateral boundary conditions are interpolated from a coarser resolution model using the INT2LM software (Schaettler, 2014).

Although COSMO-CLM is designed to be applicable to every region of the world, default parameter values were, for obvious historical reasons, derived and fine-tuned for one particular region, viz. Central Europe. In this study, where COSMO-CLM is applied to equatorial East Africa, the default parameter settings were therefore replaced by the tropical configuration developed by Panitz et al. (2014) for the model's contribution to the African Coordinated Regional Climate Downscaling Experiment (CORDEX). The tropical configuration includes the following modifications with respect to the standard set-up: (i) the artificial model top is enhanced from the default value of 22 km to 30 km, this to account for the higher tropopause height in the tropics and to accommodate tropical meteorological features such as deep convection. (ii) Second, the height above which Rayleigh damping is applied is enhanced from the default 11 km to 18 km. Rayleigh damping is a numerical smoothing applied in the top levels of the model to suppress non-physical wave reflections from the rigid top boundary (Doms, 2011). (iii) The third aspect of the tropical configuration, i.e. improving the surface albedo representation, was addressed by replacing the default land surface model of COSMO-CLM by the Community Land Model (sect. 2.3). Further grid specifications and model settings implemented to facilitate simulations at a horizontal resolution of 0.0625° (∼7 km) are described in detail in section 5.2.3.

2.3 Coupled climate models

The optimal model configuration for the coupled lake-land-atmosphere regional climate model simulations over the African Great Lakes region was defined

Table 2.2: **Description of the sensitivity experiments shown in Fig. 2.2**

Sensitivity experiment	Change with respect to the "FLake" simulation
FLake	None (COSMO-CLM coupled to FLake)
FLake_IFS	Integrated Forecast System (IFS) convection parameterization replaces default Tiedtke Convection scheme
FLake_bigdom_14km	Domain enlarged by 3.125 ° in every direction, 14 km horizontal resolution instead of 7 km
FLake_bigdom_14km_IFS	Larger domain, 14 km horizontal resolution, IFS convection
FLake_bigdom	Larger domain
FLake_nincconv	Convection parameterisation called every time step instead of every 4 time steps
FLake_sea10	Ocean evaporation tuning parameter "rat_sea" = 10 (default value: 20) to increase evaporation
FLake_sea40	Ocean evaporation tuning parameter "rat_sea" = 40 (default value: 20) to decrease evaporation
CCLMsq	COSMO-CLM coupled to CLM and Hostetler lake model
CCLMsq_bigdom	CCLMsq with enlarged domain
CCLMsq_IFS	CCLMsq with IFS convection scheme
CCLMsq_nincconv	CCLMsq, convection parameterisation called every time step
CCLMsq_FLake	CCLMsq, Hostetler replaced by FLake

through a comprehensive sensitivity study. Over 15 different configurations were launched and evaluated over a period of one year (Table 2.2; Fig. 2.2). For instance, four of the sensitivity experiments involved testing the model for a larger domain, i.e. the domain displayed in Fig. 5.1 enlarged by 3.125° in each direction("FLake_bigdom", "FLake_bigdom_14km", "FLake_bigdom_14km_IFS" and "cclmsq_bigdom"; Table 2.2). In none of the cases a consistent improvement in the model skill was found. When simply enlarging the domain (FLake_bigdom), model skill even decreased for nearly all considered evaluation products, whereas in other cases gridded precipitation reproduction improves but at the expense of lake surface temperature and in-situ precipitation predictions. Likewise, other sensitivity experiments, such as replacing the Tietdke shallow and moist convection parameterization by the Integrated Forecast System scheme ("FLake_IFS"), calling the Tietdke scheme every model time step rather than every four model time steps ("FLake_nincconv"), or tuning an ocean evaporation parameter ("FLake_sea10"; "FLake_sea40"), usually yielded enhanced skill for some model variables while deteriorating the predictive skill for others.

Interestingly, these compensating effects are also obtained when COSMO-CLM's native land surface model (TERRA-ML, Grasselt et al., 2008) is replaced by the more comprehensive Community Land Model (CLM, Oleson et al., 2004, 2008) version 3.5 ("CCLMsq"). In this case, the improved skill of CLM3.5 over land is offset by the Hostetler model, which displays a cold bias relative to remotely sensed lake surface temperature observations. In fact, only treating the land

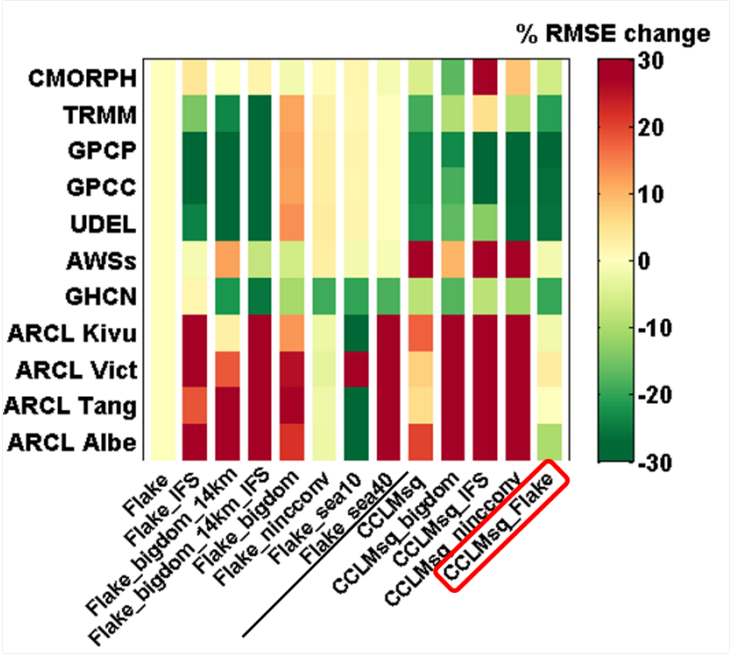

Figure 2.2: **Percentage change in spatial root mean square error (RMSE) of annual means for 13 sensitivity experiments (x-axis) relative to one reference simulation ("FLake": COSMO-CLM for the domain displayed in Fig. 5.1 and FLake switched on) with respect to eight different observational products (y-axis). Sensitivity experiments are described in Table 2.2. Observational products are for precipitation (CMORPH, TRMM 3B42, GPCP, GPCC, UDEL and AWSs), near-surface air temperature (GHCN) and lake surface temperature (ARCL; see sect. 5.2.4 for a detailed description of these datasets). All simulations were run for a period of one year (2002) and spatial RMSEs are computed for the whole model domain. The black line separates COSMO-CLM (with default land surface model) from COSMO-CLM^2 simulations (with alternative, more complex land surface model), whereas the red square denotes the chosen configuration for the final multi-year experiments.**

pixels by CLM3.5 while using FLake for the lake pixels ("CCLMsq_FLake") yields a consistent and significant improvement in model skill for all considered variables. Consequently, this model configuration was selected for producing the climate simulations described in this thesis.

The coupling between COSMO-CLM and the Community Land Model, hereafter referred to as COSMO-CLM^2, was developed at the Swiss Federal Institute of Technology Zurich (ETHZ), where Community Land Model version 3.5 was included in COSMO-CLM version 4.0 by Davin et al. (2011). More recently, COSMO-CLM was updated to version 4.8 (Davin and Seneviratne, 2012); this version is used in the thesis. Here, the lake and atmospheric model are coupled in the following way. The lake surface temperatures and other prognostic variables are updated every time step by FLake using the forcing variables (Table 2.1) provided by COSMO-CLM as input. The outgoing radiative and turbulent fluxes are subsequently computed using a dedicated surface flux routine and passed on to the atmosphere. The added value of COSMO-CLM^2 compared to the standard COSMO-CLM set-up has been demonstrated both over Europe (Davin et al., 2011; Davin and Seneviratne, 2012; Lorenz et al., 2012) and central Africa (Akkermans, 2013, see also sect. 5.2.1), and is confirmed by the above sensitivity study over East Africa. Since its first release, COSMO-CLM^2 has been applied in a number of studies, predominantly for studying biogeophysical impacts of altered land surface characteristics (e.g. Lorenz et al., 2012, 2013; Akkermans et al., 2014; Davin et al., 2014; Lejeune et al., 2014; Jacobs et al., 2015a,b; Thiery et al., 2015; Vanden Broucke et al., 2015).

Chapter 3

Understanding the performance of the FLake model over two African Great Lakes

This chapter is published as: Thiery, W., Martynov, A., Darchambeau, F., Descy, J.-P., Plisnier, P.-D., Sushama, L., and Van Lipzig, N., 2014. Understanding the performance of the FLake model over two African Great Lakes. *Geoscientific Model Development* 7, 317-337. doi:10.5194/gmd-7-317-2014

The ability of the one-dimensional lake model FLake to represent the mixolimnion temperatures for tropical conditions was tested for three locations in East Africa: Lake Kivu, Lake Tanganyika's northern and southern basins. Meteorological observations from surrounding automatic weather stations were corrected and used to drive FLake, whereas a comprehensive set of water temperature profiles served to evaluate the model at each site. Careful forcing data correction and model configuration made it possible to reproduce the observed mixed layer seasonality at Lake Kivu and Lake Tanganyika (northern and southern basins), with correct representation of both the mixed layer depth and water temperatures. At Lake Kivu, mixolimnion temperatures predicted by FLake were found to be sensitive both to minimal variations in the external parameters and to small changes in the meteorological driving data, in particular wind velocity. In each case, small modifications may lead to a regime switch from the correctly represented seasonal mixed layer deepening to either completely mixed or permanently stratified conditions from ∼10 m downwards. In contrast,

model temperatures were found to be robust close to the surface, with acceptable predictions of near-surface water temperatures even when the seasonal mixing regime is not reproduced. FLake can thus be a suitable tool to parameterize tropical lake water surface temperatures within atmospheric prediction models. Finally, FLake was used to attribute the seasonal mixing cycle at Lake Kivu to variations in the near-surface meteorological conditions. It was found that the annual mixing down to 60 m during the main dry season is primarily due to enhanced lake evaporation and secondarily due to the decreased incoming long wave radiation, both causing a significant heat loss from the lake surface and associated mixolimnion cooling.

3.1 Introduction

Owing to the strong contrast in albedo, roughness and heat capacity between land and water, lakes significantly influence the surface-atmosphere exchange of moisture, heat and momentum (Bonan, 1995; Mironov et al., 2010). Some effects of this modified exchange are (i) the dampening of the diurnal temperature cycle and lagged temperature response over lakes compared to adjacent land, (ii) enhanced winds due to the lower surface roughness, (iii) higher moisture input into the atmosphere as lakes evaporate at the potential evaporation rate, and (iv) the formation of local winds, such as the lake/land breezes (Savijärvi and Järvenoja, 2000; Samuelsson et al., 2010; Lauwaet et al., 2012).

One such region where lakes are a key component of the climate system is the African Great Lakes region. During the last decades, the African Great Lakes experienced fast changes in ecosystem structure and functioning, and their future evolution is a major concern (O'Reilly et al., 2003; Verburg et al., 2003; Verburg and Hecky, 2009). To better understand the present lake hydrodynamics and their relation to aquatic chemistry and biology, several comprehensive one-, two- or three-dimensional hydrodynamic models have been developed and applied in standalone mode to lakes in this region (Schmid et al., 2005; Naithani et al., 2007a; Gourgue et al., 2011; Verburg et al., 2011). However, to investigate the two-way interactions between climate and lake processes over East Africa, a correct representation of lakes within Regional Climate Models (RCMs) and General Circulation Models (GCMs) is essential (Stepanenko et al., 2013, see appendix for a list of all acronyms, variables and simulation names). For now, the high computational expense of complex hydrodynamic lake models limits the applicability of coupled lake-atmosphere model systems to process studies (Anyah et al., 2006; Thiery et al., 2014b). To overcome this issue, the Freshwater Lake model (FLake) was recently developed (Mironov, 2008; Mironov et al., 2010). It offers a very good compromise between physical realism and computational efficiency.

As a one-dimensional lake parameterisation scheme, FLake has already been coupled to a large number of Numerical Weather Prediction (NWP) systems, RCMs and GCMs (Kourzeneva et al., 2008; Dutra et al., 2010; Mironov et al., 2010; Salgado and Le Moigne, 2010; Samuelsson et al., 2010; Martynov et al., 2012). However, even though it has become a landmark in this respect, FLake has never been thoroughly tested for tropical conditions (see sect. 4.1 for an overview of previous test experiments). Moreover, as several joint efforts to provide society with climate change information, such as the COordinated Regional climate Downscaling EXperiment (CORDEX), explicitly focus on the African continent (Giorgi et al., 2009), a correct representation of the African Great Lakes within NWP, RCMs and GCMs becomes of particular importance.

Hence, the main goal of this study is to test - for the first time - the ability of FLake to reproduce the temperature regimes of two tropical lakes in East Africa. Lake Kivu and Lake Tanganyika are selected as they are the only rift lakes for which both local weather conditions and lake water temperatures have been monitored for several years. Lake Kivu (Fig. 3.1b) is a deep meromictic lake, with an oxic mixolimnion seasonally extending down to 60-70 m, below which the monimolimnion is found rich in nutrients and dissolved gases, in particular carbon dioxide and methane (Fig. 3.2; Degens et al., 1973; Borges et al., 2011; Descy et al., 2012). Due to the input of heat and salts from deep geothermal springs, temperature and salinity in the monimolimnion increase with depth (Degens et al., 1973; Spigel and Coulter, 1996; Schmid et al., 2005). Moreover, in the deeper layers, vertical diffusive transport is dominated by double diffusive convection (Schmid et al., 2010). Lake Tanganyika (Fig. 3.1c), the first Albertine rift lake south of Lake Kivu, stretches 670 km southwards and, with its 60 km mean width and maximum depth of 1470 m, represents the second largest surface freshwater reservoir on earth (18 880 km^3; Savijärvi, 1997; Alleman et al., 2005; Verburg and Hecky, 2009). Lake Tanganyika is also meromictic (Naithani et al., 2007b), but its salt content is lower compared to Lake Kivu (Spigel and Coulter, 1996). Lake Kivu and Lake Tanganyika are both characterised by long lake water retention times (∼100 years and ∼800 years, respectively; Schmid and Wüest, 2012; Coulter, 1991), hence the impact of riverine in- and outflow is of little importance to the circulation within these lakes.

In this study, lake temperatures were calculated for three sites, one at Lake Kivu and two at Lake Tanganyika, by forcing FLake with observations from surrounding Automatic Weather Stations (AWSs) and subsequently comparing them to observed time series. Besides integrating with the raw meteorological observations, wind speed measurements and water transparency were also refined within their uncertainty range (defined here as two standard deviations around the multiyear mean) to yield a control simulation representing the correct mixing regime. At each location, FLake was also driven by the re-analysis product ERA-Interim (Simmons et al., 2007). Furthermore, a systematic analysis of FLake's sensitivity to variations in external parameters, meteorological forcing data, and temperature initialisation was conducted. Finally, a study of the surface energy balance allowed attributing the mixing regime at Lake Kivu to changes in near-surface meteorological conditions.

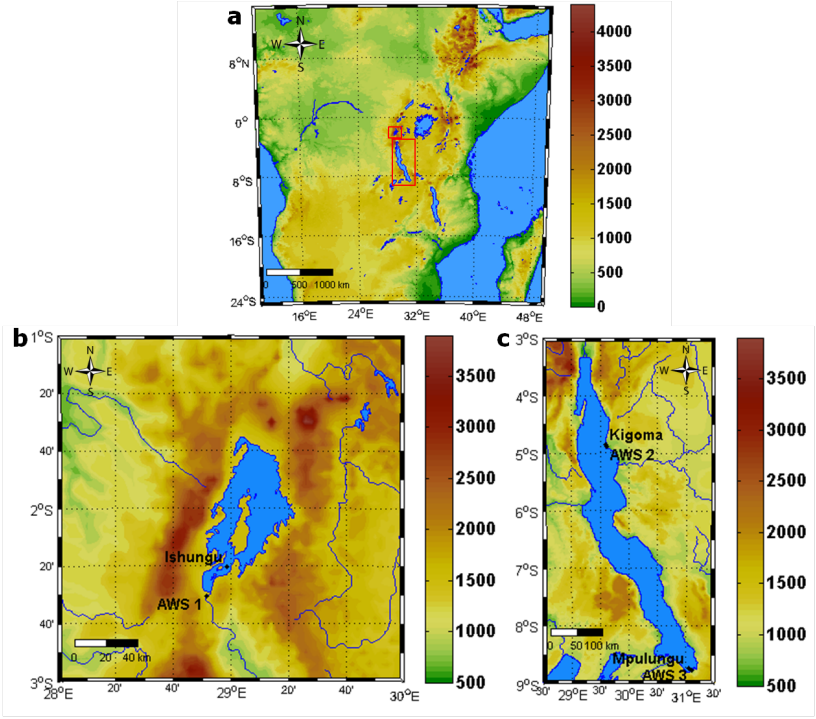

Figure 3.1: **(a) Overview map of East Africa with rectangles around Lake Kivu (upper) and Lake Tanganyika (lower), (b) Lake Kivu, (c) Lake Tanganyika. Surface altitude is shown in m a.s.l.**

3.2 Data and methods

3.2.1 AWS data

The Lake Kivu region is characterised by a long dry season extending from June to September, and a wet season from October to May, interrupted by a short dry season around January (Beadle, 1981). Further south in Lake Tanganyika, the dry season sets in one month earlier (Spigel and Coulter, 1996; Verburg and Hecky, 2003). Over both lakes, predominantly southeasterly winds reach a maximum during the dry season (Nicholson, 1996; Verburg and Hecky, 2003; Sarmento et al., 2006).

AWS 1 is located on the roof of the Institut Supérieur Pédagogique in Bukavu, Democratic Republic of the Congo, approximately 1 km from the southern

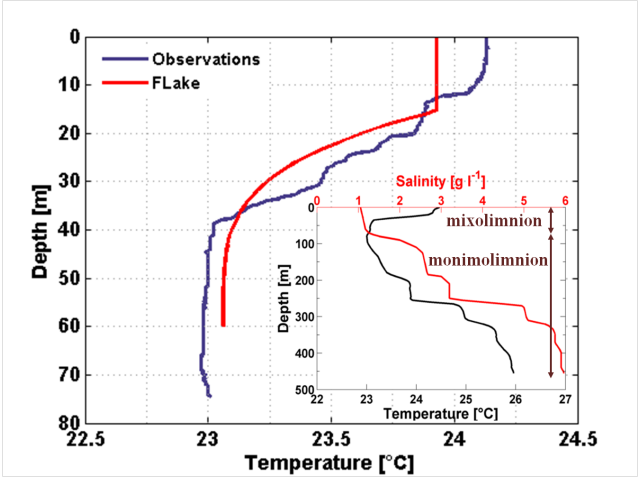

Figure 3.2: **Water temperature recorded at Ishungu on 21 April 2009 and corresponding FLake midday temperature profile, the latter with its distinct two-layer structure (mixed layer and thermocline). Inset: temperature (black) and salinity (red) profile representative for the main basin during February 2004, as reported by Schmid et al. (2005). For Lake Kivu, the artificial lake depth set in FLake corresponds to the mixolimnion depth, hence the monimolimnion has no counterpart in FLake. Note the strong increase in salinity from 60-70 m downwards, i.e. below the mixolimnion.**

border of Lake Kivu and 27 km southwest from the monitoring site in the Ishungu Basin (Fig. 3.1b). For this study, meteorological observations covering a period of 9 years (2003-2011) were used. AWS 2 is situated at the Tanzania Fisheries Research Institute in Kigoma, Tanzania, 50 m from the lake shore and 4 km southeast from the evaluation site in Kigoma (Fig. 3.1c). As such, this station recorded meteorological conditions representative for the northern Tanganyika basin from 2002 to 2006. Finally, considered as representative for the southern Tanganyika basin, AWS 3 is located at Mpulungu Department of Fisheries, on the lake shore and 8.5 km south of the monitoring site of Mpulungu (Fig. 3.1c). Unfortunately, for this station only 13 months of data (Feb. 2002 – Apr. 2003) were available. With all three AWSs located on land, one can expect some differences between the measured values and actual meteorological conditions at the sites they aim to represent. However, given the lack of meteorological observations at these locations, it is difficult to assess the degree to which these stations represent their respective evaluation site, except probably for wind speed measurements (Sect. 3.2.4). Possibly AWS 3, the most exposed station and located on the lake shore, succeeds best at representing the meteorological conditions of the evaluation site. AWS

Table 3.1: **Automatic Weather Station (AWS) topographic and meteorological characteristics.**

	AWS 1	**AWS 2**	**AWS 3**
Location			
Corresponding evaluation site	Ishungu	Kigoma	Mpulungu
Latitude	2° 30' 27" S	4° 53' 15" S	8° 45' 59" S
Longitude	28° 51' 27" E	29° 37' 11" E	31° 6' 25" E
Altitude (m a.s.l.)	1570	777	782
Setup of this study			
Start of observation	1 Jan. 2003	1 Jan. 2002	2 Feb. 2002
End of observation	31 Dec. 2011	31 Dec. 2006	4 Apr. 2003
Meteorological averages, after corrections			
T (°C)	19.4	24.5	24.1
R (%)	76	70	58
ff (m s^{-1})	1.9	0.3	2.6

topographic characteristics and meteorological averages are listed in Table 3.1.

Each AWS records air temperature (T), pressure (p), wind speed (ff) and direction (dd), relative humidity (RH) and downward short-wave radiation (SW_{in}) at a single level above the surface, and at an estimated accuracy of ±0.5 °C, ±1 hPa, ±5%, ±3 °, ±3% and ±5%, respectively. The measurement frequency is 30 min at AWS 1 and 15 min at AWS 2 and 3, but for the integrations only hourly instantaneous values were retained. Three problems needed to be overcome to prepare the forcing data for the FLake simulations. First, all stations experience frequent data gaps (50%, 23% and 37% of the time at AWS 1, 2 and 3, respectively), and gaps are too long to be filled using simple interpolation techniques. This issue was solved by calculating for each hour of the year the climatological average from available observations and subsequently filling all data gaps with the corresponding climatological value. When no climatological value is available for SW_{in}, the value of the previous day was used. At AWS 3, where the time series is too short to obtain climatological values, data gaps were instead filled by the average daily cycle. Second, time series of downward long-wave radiation (LW_{in}), a necessary forcing variable to FLake, are not measured by the AWSs. Hence, they were retrieved from the ERA-Interim grid point closest to the evaluation site and subsequently converted from 6-hourly accumulated values to hourly instantaneous value.

3.2.2 FLake model

The one-dimensional FLake model is designed to represent the evolution of a lake column temperature profile and the integral energy budgets of its different layers (Mironov, 2008; Mironov et al., 2010). In particular, the model consists

of two vertical water layers: a mixed layer, which is assumed to have a uniform temperature (T_{ML}), and an underlying thermocline, extending down to the lake bottom (Fig. 3.2). The temperature-depth curve in the thermocline is parameterized through the concept of self-similarity, or assumed-shape (Kitaigorodskii and Miropolskii, 1970), meaning that the characteristic shape of the temperature profile is conserved irrespective of the depth of this layer (Munk and Anderson, 1948). Hence, within the thermocline, temperature at a relative (dimensionless) depth within the thermocline depends only on the shape of the thermocline curve. In turn, this shape is determined only by the temperature at the top and bottom of the thermocline and by a shape factor, describing the curve through a fourth-order polynomial (Mironov, 2008). Additionally, FLake includes the representation of the thermal structure of lake ice and snow cover and (optionally) also of the temperature of two layers in the bottom sediments, all using the concept of self-similarity. Without considering ice/snow cover and bottom sediments, the prognostic variables computed by the model reduce to: the mixed layer depth (h_{ML}), the bottom temperature (T_{BOT}), the water column average temperature (T_{MW}) and the shape factor with respect to the temperature profile in the thermocline (C_T). The mixed layer depth is calculated including effects of both convective and mechanical mixing, while volumetric heating is accounted for through the net short-wave radiation penetrating the water and becoming absorbed according to the Beer-Lambert law (Mironov, 2008; Mironov et al., 2010). Note that FLake is a thermodynamic model using lake depth as a constant external parameter, hence lake level changes are not considered in this model.

The approach adopted in this study is to test FLake version 1 as close as possible to its native configuration, i.e. how it is operationally used as a lake parameterisation scheme within most atmospheric prediction models. Consequently, modifications in the source code from which the predictions would potentially benefit, such as including time dependent water transparency, making the distinction between the visible and near-infrared fractions of SW_{in} (each with their own absorption characteristics), improving the parameterisation of the thermocline's shape factor, defining a geothermal heat flux, accounting for the effect of bottom sediments, and including an abyssal layer or diurnal stratification, were not taken into account in this study. Conversely, some of these effects were considered during the lake model intercomparison experiment for Lake Kivu (Thiery et al., 2014b).

3.2.3 Water transparency and temperature profiles

In oligotrophic environments such as Lake Tanganyika and Kivu, water transparency is predominantly related to phytoplankton development, which is

usually confirmed by a good correlation between the chlorophyll a concentrations and the downward light attenuation coefficient k (m^{-1}) or related quantity (Naithani et al., 2007b; Darchambeau et al., 2014). In FLake, however, k has to be ascribed a constant value. A large measurement set of disappearance depths of the Secchi disk z_{sd} (m) are available for each site (Table 3.2). z_{sd} were converted to k using the relationship

$$k = \frac{-\ln 0.25}{z_{sd}} \tag{3.1}$$

where 0.25 refers to the fraction of incident radiation penetrating to the depth at which the Secchi disk is no longer visible. This fraction, differing from one Secchi disk to another, was retrieved at Lake Kivu by means of 15 simultaneous measurements of z_{sd} and the vertical profile of light conditions using a LI-193SA Spherical Quantum Sensor, from which k was estimated. For each dataset of k, a gamma probability density function was fitted (Fig. 3.3), from which subsequently average $\bar{k}$ and standard deviation σ_k were calculated (Table 3.2). The higher $\bar{k}$ observed at Ishungu relative to Kigoma and Mpulungu is caused by the higher phytoplankton biomass (represented by Chlorophyll a concentrations) in Lake Kivu (2.02 $\pm$0.78 mg m^{-3}; Sarmento et al., 2012) compared to Lake Tanganyika (0.67 $\pm$0.25 mg m^{-3}; Stenuite et al., 2007). Note that, since a measurement uncertainty remains associated with the exact value of k, its value was allowed to vary within given bounds in the different simulations (see Sect. 3.2.4).

The evaluation of the FLake simulations was made by the use of 419 Conductivity-Temperature-Depth (CTD) casts collected at Ishungu (Lake Kivu), Kigoma (Lake Tanganyika's northern basin) and Mpulungu (Lake Tanganyika's southern basin; Table 3.2). At each of these locations, they provide a clear image of the surface lake's thermal structure and hence mixing regime. While it can be argued that temperature recordings at Ishungu are representative for the whole Lake Kivu, except Bukavu Bay and Kabuno Bay (Thiery et al., 2014b), the same cannot be claimed for Lake Tanganyika, where seasonal variations in wind velocity and internal wave motions cause spatially variant mixing dynamics (Plisnier and Chitamwebwa, 1999). This is also apparent from the comparison of the CTD casts of Kigoma and Mpulungu (Sect. 3.3.2, 3.3.3). Consequently, the results of the FLake simulations for Ishungu can be used to study the mixing physics of Lake Kivu (Sect. 3.3.6), whereas the mixing processes within the whole Lake Tanganyika cannot be captured by single-column simulations at two sites only.

To ease the intercomparison of the different CTD casts, first, each temperature

Table 3.2: **Characteristics of the model evaluation sites. Water transparency characteristics are the downward light attenuation coefficient k (m^{-1}) and its standard deviation σ_k (m^{-1}). Control run scores are standard deviation σ_T (°C), centred Root Mean Square Error $RMSE_c$ (°C), Pearson correlation coefficient r and Brier Skill Score BSS.**

	Ishungu	**Kigoma**	**Mpulungu**
General characteristics			
Lake	Kivu	Tanganyika (northern basin)	Tanganyika (southern basin)
Latitude	2° 20' 25" S	4° 51' 16" S	8° 43' 59" S
Longitude	28° 58' 36" E	29° 35' 32" E	31° 2' 26" E
Altitude (m a.s.l.)	1463	768	768
Depth (m)	120	600	120
Number of CTD casts	174	119	126
Water transparency			
Number of Secchi depths	163	114	124
Average k (m^{-1})	0.28	0.11	0.13
σ_k (m^{-1})	0.06	0.02	0.05
Minimun k (m^{-1})	0.15	0.07	0.06
Maximum k (m^{-1})	0.46	0.17	0.31
Vertically averaged scores for control run			
σ_T (°C)	0.30	0.70	0.67
($\sigma_{T,obs}$ (°C)	0.32	0.49	0.65)
$RMSE_c$ (°C)	0.22	0.59	0.89
r	0.71	0.51	0.05
BSS	-0.13	-9.63	-1.81

profile was spatially interpolated to a regular vertical grid with increment 0.1 m using the piecewise cubic Hermite interpolation technique (De Boor, 2001). Subsequently the depth of the mixed layer was determined for each cast as the depth with the maximum downward temperature change per meter lower than a predefined threshold (-0.03 °C m^{-1}). Whenever the thermal gradient did not exceed this threshold, the lake was assumed to be mixed down to the artificial model depth (see Sect. 3.2.4). Finally, both temperature profiles and mixed layer depths were also temporally interpolated to a grid with increment of one day using the same spline interpolation.

3.2.4 Model configuration, evaluation and sensitivity

Both in situ meteorological measurements and ERA-Interim data from the nearest grid cell were used to drive FLake in standalone mode (decoupled from an atmospheric model) for three different locations: Ishungu, Kigoma and Mpulungu (Fig. 3.1). One of FLake's main external parameters is the lake depth (Mironov, 2008; Kourzeneva et al., 2012b). However, for most of the deep African Great Lakes, their actual lake depth cannot be used, since FLake only

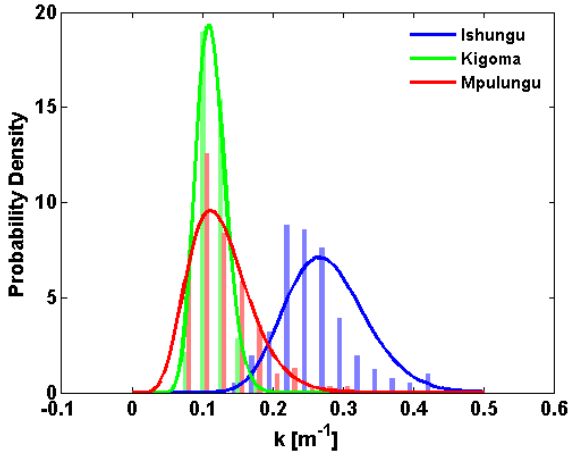

Figure 3.3: **Comparative histogram of the downward light attenuation coefficient k (m^{-1}) as observed at Ishungu Basin (Lake Kivu) and Kigoma and Mpulungu stations (Lake Tanganyika). Gamma distribution probability density functions are plotted to the data (R^2 = 0.82, 0.99 and 0.93 for Ishungu, Kigoma and Mpulungu, respectively).**

describes the mixed layer and thermocline, whereas in reality a monimolimnion is found below the thermocline of these meromictic lakes. Consequently, an artificial model lake depth was defined at the maximum depth for which the observed temperature range exceeds 1°C during the measurement period. When applying this criterion to the vertically interpolated temperature profiles, it was found that 60 m is an appropriate artificial depth for Lake Kivu, while for both basins of Lake Tanganyika the seasonal temperature cycle penetrates down to a depth of 100 m. Note that for Lake Kivu, this depth coincides with the onset of the salinity increase, which inhibits deeper mixing (Fig. 3.2). As a consequence of using an artificial lake depth, the bottom sediments module was switched off in all simulations. Therewith, a zero heat flux assumption was adopted at the bottom boundary.

At each location, three simulations were conducted. First, FLake was integrated with observed meteorological values and using the average observed value for k (hereafter referred to as "raw"). However, due to the location of AWS 1 and 2 – both surrounded by several buildings and large trees – especially the wind speed values are expected to be underestimated by these stations. Moreover, as the data gap filling technique averaged out high values for ff, unrecorded high wind speed events were not recreated. Consequently, wind speed recordings at these stations can be considered as a lower bound for the actual ff at the respective

evaluation sites. As a supplementary evidence, wind velocity measurements from a state-of-the-art AWS, newly installed over the lake surface on a floating platform in the main basin and 2 km off the shoreline (AWS Kivu: 1° 43' 30" S, 29° 14' 15" E), showed that wind speeds at AWS Kivu were on average 2.0 m s^{-1} higher compared to AWS 1 (from October to November 2012, $n = 892$, Root Mean Square Error $RMSE = 2.7$ m s^{-1}). By applying a constant increase of 2.0 m s^{-1} to the wind velocities observed at AWS 1, the $RMSE$ between wind velocities from both AWSs reduced to 1.8 m s^{-1}. Since the location of AWS Kivu is much more exposed than the Ishungu basin – especially given the predominance of southeasterlies over the lake – wind velocities measured by AWS Kivu provide a definite upper bound for wind velocities in the Ishungu Basin. Hence, a second AWS-driven simulation was conducted wherein wind velocities were allowed to vary within specific upper (from AWS Kivu) and lower (from AWS 1) bounds until the observed mixing regime is reproduced (0.1 m s^{-1} increment; see Sect. 3.3.5 for another important argument in support of this operation). It was found that at Ishungu, increasing all ff by 1.0 m s^{-1} resulted in a correct representation of the mixing regime (Sect. 3.3.1), whereas at Kigoma, ff had to be increased by 2.0 m s^{-1} (Sect. 3.3.2). At Mpulungu, where the driving AWS is located close by the evaluation site and on the lake shore, the correct mixing regime is already reproduced by the raw integration, and hence no wind speed correction needed to be applied (Sect. 3.3.3). After correcting for the wind speed, k was varied iteratively between bounds $\bar{k} - \sigma_k$ and $\bar{k} + \sigma_k$ until the best values for the set of model efficiency scores were obtained (see below; hereafter referred to as "control"). This operation led to values of 0.32 m^{-1}, 0.10 m^{-1} and 0.09 m^{-1} for k at Ishungu, Kigoma and Mpulungu, respectively. Note however that this second correction, restricted by σ_k (Table 3.2), had little to no impact upon the final model outcome (At Ishungu, for instance, mean mixed layer and water column temperatures differ less than 0.001 °C and 0.04 °C, respectively, after this second correction).

Finally, FLake was integrated using ERA-Interim data from the nearest grid cell as forcing. ERA-Interim is a global reanalysis product produced by the European Centre for Medium-Range Weather Forecasts (ECMWF; Simmons et al., 2007). It consists of a long-term atmospheric model simulation in which historical meteorological observations are consistently assimilated. Note however that the horizontal resolution of this product is T255 (0.703125° or about 80 km), hence a large fraction each nearest pixel represents land instead of lake. Moreover, only few observations are assimilated into ERA-Interim over tropical Africa, adding to the uncertainty of this product as a source of meteorological input to FLake. At Mpulungu, the only site where this integration led to a correct representation of the mixing regime (Sect. 3.3.3), k was again allowed to vary within bounds $\bar{k} - \sigma_k < k < \bar{k} + \sigma_k$, with $k = 0.09$ m^{-1} retained.

In each simulation, lake water temperatures were initialised by the average T_{ML}, T_{WM} and T_{BOT} calculated from the linearly interpolated observed January temperature profiles (n = 14, 8 and 10 at Ishungu, Kigoma and Mpulungu, respectively). Then, for each location the spin-up time was determined by repeatedly forcing the model with the atmospheric time series until the initial T_{BOT} remained constant. This approach was found to be preferable above a spin-up with a constant forcing or with a climatological year (Mironov et al., 2010), as the averaging of the wind speed observations removes extremes which may trigger the deep mixing in these lakes. It was found that, depending on the location and for the control model configuration, a spin-up time from 9 to 330 years is needed before convergence is reached.

The ability of FLake to reproduce the observed temperature structure was tested by comparing FLake's near-surface and bottom temperature to the corresponding observed values at each location. Note that surface fluxes cannot be evaluated in the absence of observational reference. A depth of 5 m was chosen representative for the surface waters, since (i) CTD casts were generally collected around noon and temperatures in the first meters are therefore positively biased relative to the daily averages, and (ii) FLake does not fully account for the daytime surface stratification because the mixed layer has a uniform temperature. Furthermore, a set of four model efficiency scores was computed: the standard deviation σ_T (°C), the centred Root Mean Square Error $RMSE_c$ (°C), the Pearson correlation coefficient r and the Brier Skill Score BSS (Nash and Sutcliffe, 1970; Taylor, 2001; Wilks, 2005). The former three calculated scores are visualised together in a Taylor diagram (Taylor, 2001), enabling the performance assessment of FLake. The $RMSE_c$ is given by:

$$RMSE_c = \sqrt{\frac{1}{n}\sum_{i=1}^{n}((m_i - \bar{m}) - (o_i - \bar{o}))^2} \tag{3.2}$$

while the BSS is computed according to:

$$BSS = 1 - \frac{\sum_{i=1}^{n}(o_i - m_i)^2}{\sum_{i=1}^{n}(o_i - \bar{o})^2} \tag{3.3}$$

with o_i the observed (interpolated) water temperature, $\bar{o}$ the average observed water temperature, and m_i and $\bar{m}$ the corresponding modelled values at time i.

Values for BSS range from $-\infty$ (no relation between observed and predicted value) to +1 (perfect prediction). Note that, compared to the variables displayed in a Taylor diagram, the BSS has the advantage of accounting for the model bias.

The sensitivity of the model was evaluated by conducting a number of simulations, each with an alternative configuration. In particular, the effects of variations in the external parameter values, the driving data and the initial conditions were investigated in this sensitivity study. Depending on the nature of each sensitivity experiment, different scores are applied to quantify the effect of a specific modification. Details of the different experiments are outlined in Sect. 3.3.5.

3.3 Results

3.3.1 Ishungu

Comparing modelled and observed water temperatures of Lake Kivu near the surface (5 m) shows that the timing of the near-surface seasonal cycle is well represented by the raw, control and ERA-Interim simulations (Fig. 3.4a). However, whereas it shows a small negative bias compared to the observations, only the control integration grasps the correct magnitude of the seasonal temperature range. The overestimation of the temperature seasonality in the raw and ERA-Interim simulations is reflected by 5 m BSS of -0.36 and -2.13, respectively, compared to only -0.26 for the control case. At a depth of 60 m, both the raw and ERA-Interim integration predict a year-round constant temperature of 3.98 °C, the temperature of maximum density, resulting in a cold bias of about 19 °C. At the bottom, the lake's thermal structure is reproduced only by the control simulation ($BSS = -0.17$; Fig. 3.4b).

Once a year, during the dry season (from June to August), the mixed layer depth at Ishungu extends down to approximately 60 m. At this depth, the upwelling of deep, saline waters (0.5 m yr^{-1}; Schmid and Wüest, 2012) equilibrates with mixing forces. The result is a strong salinity gradient from 60 m downwards (Fig. 3.2). During the remainder of the year, stratified conditions dominate, with the mixed layer depth varying between 10 and 30 m (Fig. 3.5a). The raw simulation does not reproduce this mixing seasonality, but instead predicts permanently stratified conditions and a complete cooling down to 3.98 °C from 30 m downwards. On the other hand, with ff corrected for the land effect and k tuned to 0.32 m^{-1}, the control simulation closely reproduces the mixing regime at Ishungu (Fig. 3.5b; Table 3.2). In this case, also the lower stability,

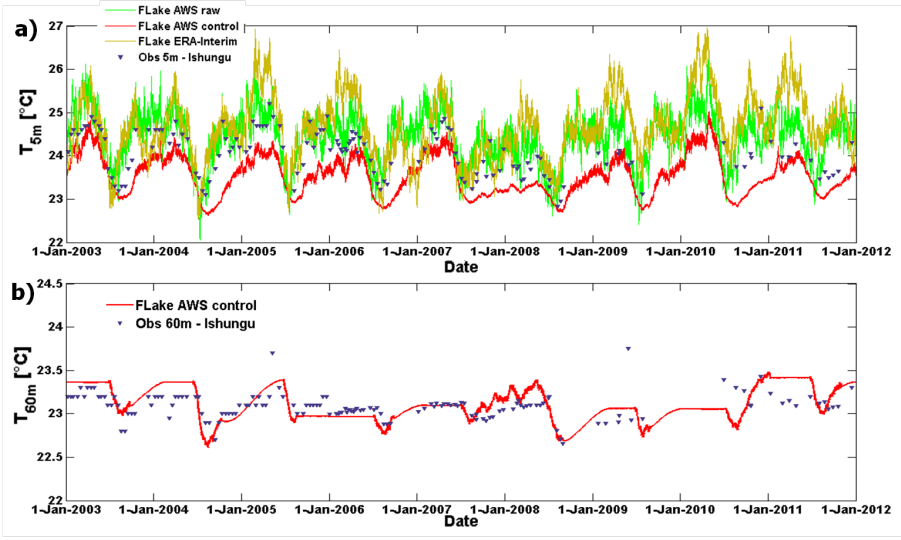

Figure 3.4: **Modelled and observed temperature evolution at Ishungu (Lake Kivu) at (a) 5 m, and (b) 60 m depth. FLake temperatures at 60 m predicted by the raw and ERA-Interim integration are omitted as they are constant at 3.98 °C.**

indicated by the observations near the end of 2006 and during 2008 and 2009, is captured by this control simulation, although it is somewhat overestimated in 2008 with a predicted year-round mixing down to ∼55 m. Note however that, due to the lower stability during these years, the effect on the near-surface water temperatures is limited. Furthermore, also the late onset of the stratification in early 2007 is represented by the model.

Finally, feeding FLake with ERA-Interim derived near-surface meteorology does not succeed in reproducing the mixing regime. Instead, this simulation predicts permanently stratified conditions and a complete cooling down to 3.98 °C, the temperature of maximum density, from 30 m downwards (Fig. 3.5c). The low and constant mixed layer depth generates near-surface temperature fluctuations found too strong on seasonal time scales (Fig. 3.4a). Similar to the raw integration, the inability of the ERA-Interim integration to produce deep mixing is primarily due to the predicted values for the wind velocity, which are 33% lower compared to the control run average wind velocity and 49% lower compared to wind speeds from AWS Kivu (measured over the lake surface during 59 days in October-November 2012). Underlying reasons for this deviation are (i) the fact that the lake surface covers only a fraction of the selected ERA-Interim grid box, and (ii) the higher uncertainty of this product

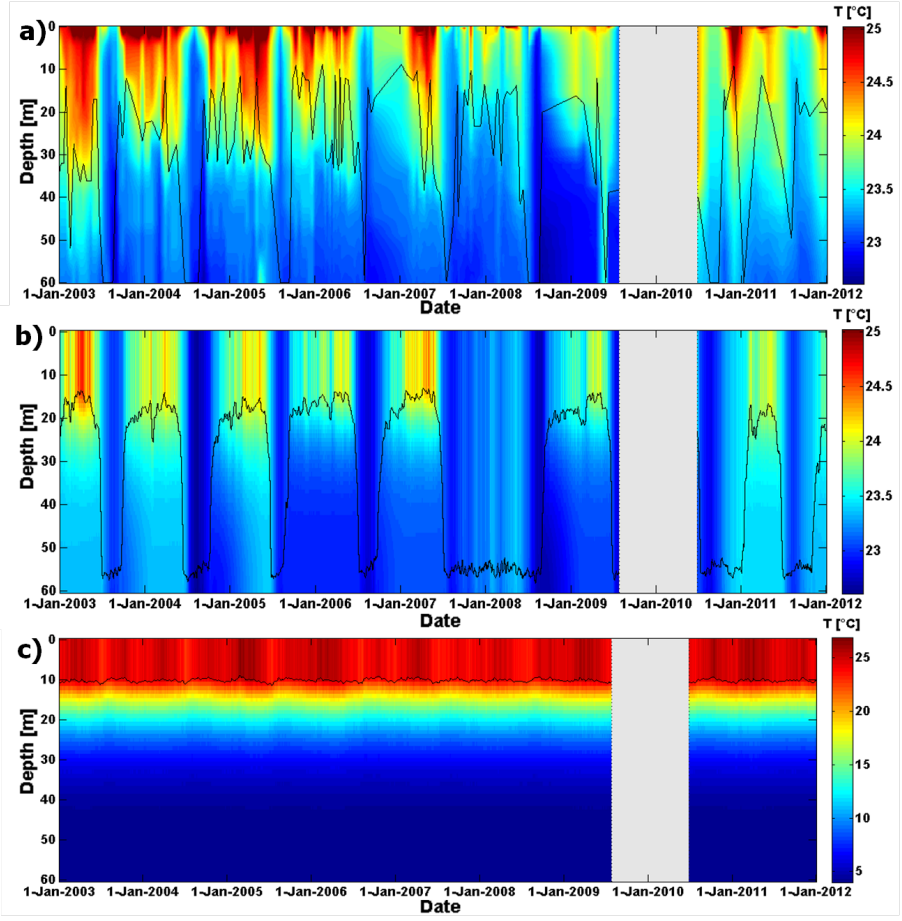

Figure 3.5: **Lake water temperatures (°C) at Ishungu (Lake Kivu) (a) from observations, (b) as predicted by the AWS-driven FLake-control, and (c) as predicted by FLake-ERA-Interim. The black line depicts the mixed layer depth (Sect. 3.2.3; weekly mean for the simulations). Note the different colour scaling in (c). The lake water temperatures for the raw simulation are not shown as they strongly resemble the predictions of the ERA-Interim simulation.**

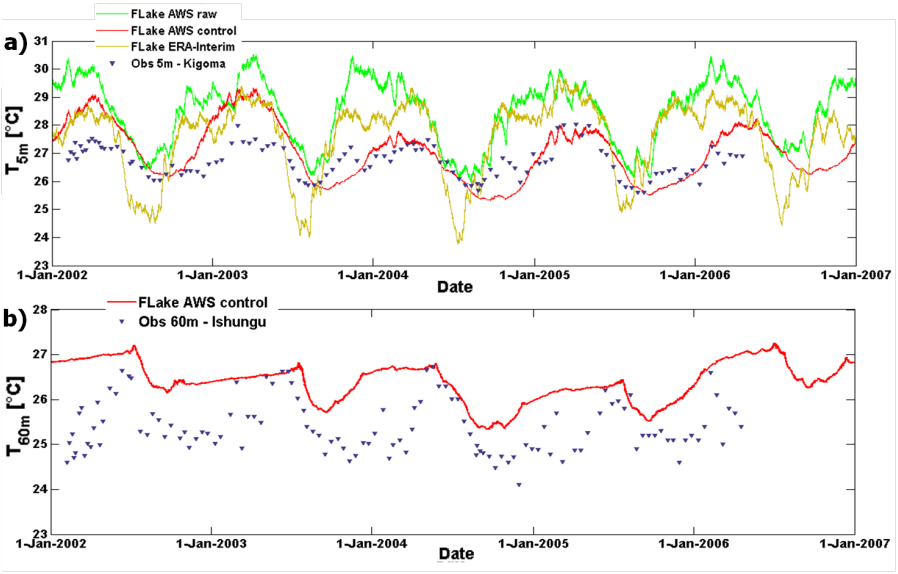

Figure 3.6: **Modelled and observed temperature evolution at Kigoma (northern basin of Lake Tanganyika) at (a) 5 m, and (b) 60 m depth. FLake temperatures at 60 m predicted by the raw and ERA-Interim integration are omitted as they are constant at 3.98 °C.**

in central Africa owing to the sparse observational data coverage in this region (Dee et al., 2011).

3.3.2 Kigoma

At Kigoma, the raw and ERA-Interim integrations both predict too high temperature seasonality in the near-surface water (Fig. 3.6a). On the other hand, the control experiment clearly displays improved skill at 5 m, especially during 2004 and 2005. At depth, both the raw and ERA-Interim integrations obtain a constant 3.98 °C and therewith strongly deviate from the observations (Fig. 3.6b). In return, the control simulation again captures the actual conditions much better, even though it slightly underestimates the seasonal temperature range and retains a positive bias between 0 and 2 °C.

Contrary to Lake Kivu, in Lake Tanganyika salinity-induced stratification below 60 m is negligible and seasonal variations in near-surface meteorology are more pronounced (Sect. 3.3.4). Consequently, the seasonal mixed layer extends further down both during the dry and wet season (Fig. 3.7a), with mixing

recorded down to even 150 m (Verburg and Hecky, 2003) and 300 m (Plisnier and Chitamwebwa, 1999). Similar to Ishungu, also at Kigoma the raw simulation does not result in a correct representation of the mixing regime, but predicts permanent stratified conditions and a complete cooling along the thermocline. Again, upward correction of ff by 2 m s^{-1} and reducing k to a value of 0.09 m^{-1} brings the model to the correct mixing regime at Kigoma (Fig. 3.7b; Table 3.2). The ERA-Interim simulation predicts permanent stratification due to too low wind velocities (Fig. 3.7c). Note that in both the ERA-Interim and the raw simulations, decreasing k from 0.11 m^{-1} to 0.09 m^{-1} leads to a regime switch from permanent stratification directly to fully mixed conditions (down to the model lake depth), the latter associated with a strong positive temperature bias both near the surface and at depth.

3.3.3 Mpulungu

At Mpulungu, all three experiments capture the magnitude of the seasonal cycle in near-surface temperature and show little to no bias compared to the observations (Fig. 3.8a). However, also in each simulation the onset of complete mixing lags by around one month and lasts too long compared to observations (Fig. 3.8a). At 60 m, a similar lag is found back (Fig 8b). Furthermore at this depth, the enhanced temperature seasonality of the control integration compared to the raw integration depicts its improved skill.

Although the FLake-AWS simulation at Mpulungu spans only 13 months, during this period two stratified periods and one fully mixed season are predicted by the model in both the raw ($k = 0.13$ m^{-1}) and control ($k = 0.09$ m^{-1}) setup, in agreement with observations (Fig. 3.9a, b; Table 3.2). With AWS 3 located on the lake shore (exposed) and relatively close to the evaluation site, no correction of ff was necessary, and the mixing regime is correctly represented within the range $0.09m^{-1} < k < 0.22m^{-1}$. Furthermore, also driving FLake with ERA-Interim at Mpulungu leads to a correct representation of the mixing regime (Fig. 3.9c).

From May to September, persistent southeasterly winds over Lake Tanganyika cause a tilting (downwards towards the north) of the mixolimnion-monimolimnion interface, and therewith generate the upwelling of deep, cold waters at the southern end of the lake (Plisnier and Chitamwebwa, 1999). The resulting breakdown of the stratification appears through the absence of the thermocline at Mpulungu during the dry season (Fig. 3.9a), whereas at Kigoma, even during this period a weak thermocline remains present (Fig. 3.7a). Due to its self-similar, one-dimensional nature, FLake does not account for complex hydrodynamic phenomena such as local upwelling and associated internal wave

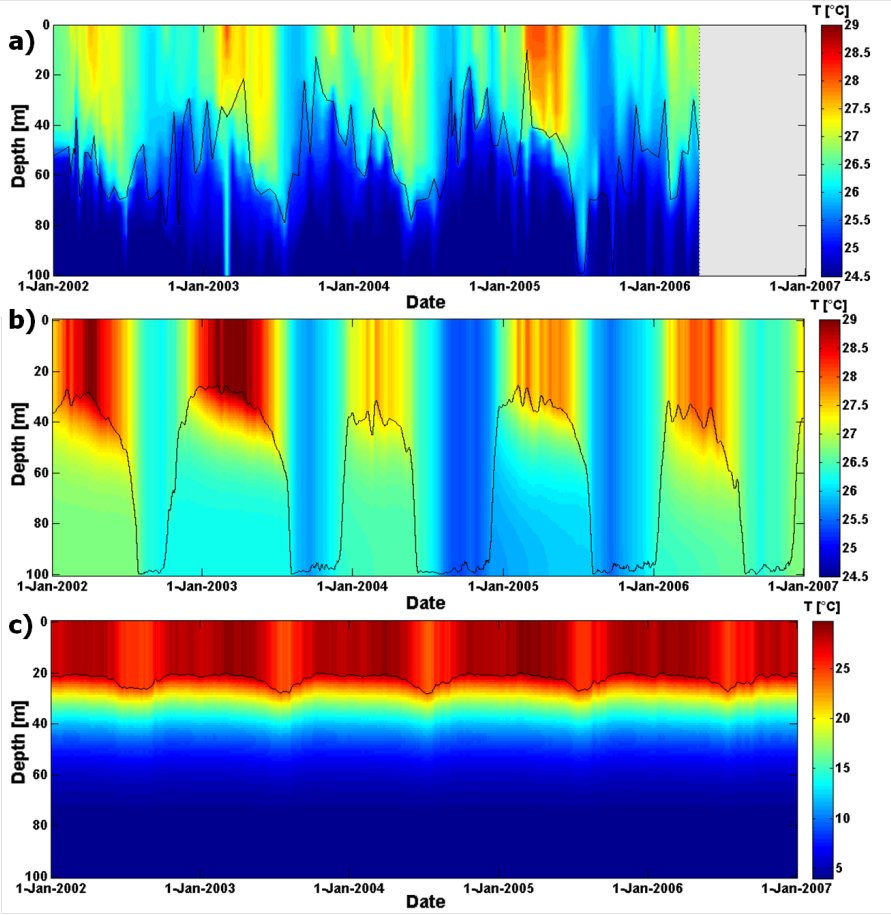

Figure 3.7: **Lake water temperatures (°C) at Kigoma (northern basin of Lake Tanganyika) (a) from observations, (b) as predicted by the AWS-driven FLake-control, and (c) as predicted by FLake-ERA-Interim. The black line depicts the mixed layer depth (Sect. 3.2.3; weekly mean for the simulations). Note the different colour scaling in (c).**

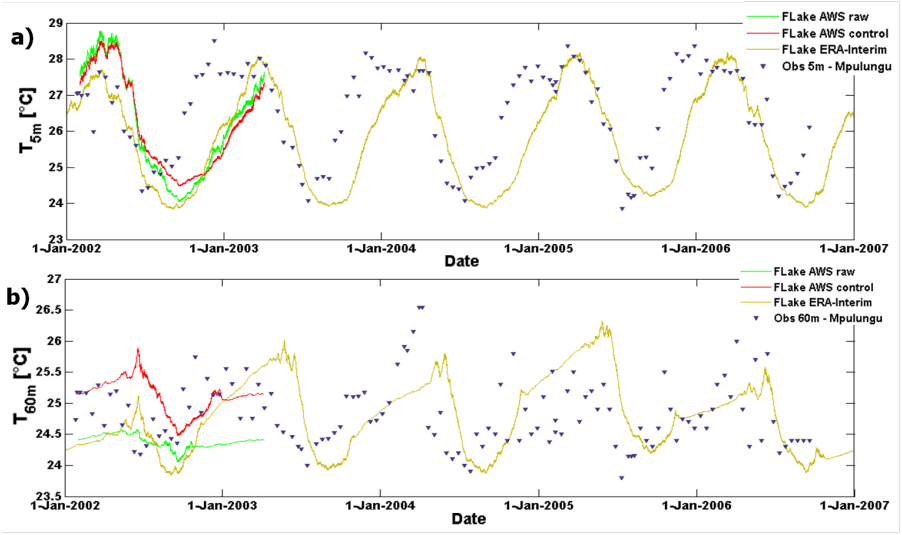

Figure 3.8: **Modelled and observed temperature evolution at Mpulungu (southern basin of lake Tanganyika) at (a) 5 m, and (b) 60 m depth.**

phenomena (Naithani et al., 2003), and therefore does not capture this difference between both sites (Fig. 3.7, 3.9). Probably, this phenomenon may also explain the time lag noticed from all Mpulungu simulations. The hydrodynamic response to the wind stress reinforces the seasonal cycle induced by lake-atmosphere interactions (Sect. 3.3.6): while the onset of the upwelling accelerates the cooling at the start of the dry season, a cessation of southeasterly winds in September generates the fast advection of warm mixolimnion waters from the north back towards Mpulungu, inducing a faster restoration of stratification than can be predicted by FLake from lake-atmosphere interactions alone.

3.3.4 Comparison between sites

A number of differences can be noted between the three locations. First, the average observed 5 m temperature is 2.6 °C and 2.4 °C lower in Ishungu (altitude 1463 m a.s.l.) compared to Kigoma and Mpulungu (altitude 768 m a.s.l.), respectively. Second, it can be observed that the water temperature seasonality increases with distance from the equator: at 5 m, the maximal observed temperature ranges are 2.4 °C, 2.5 °C and 5.4 °C in Ishungu, Kigoma and Mpulungu, respectively. This is related to differences in near-surface meteorology, since in the southern hemisphere at tropical latitudes, a higher

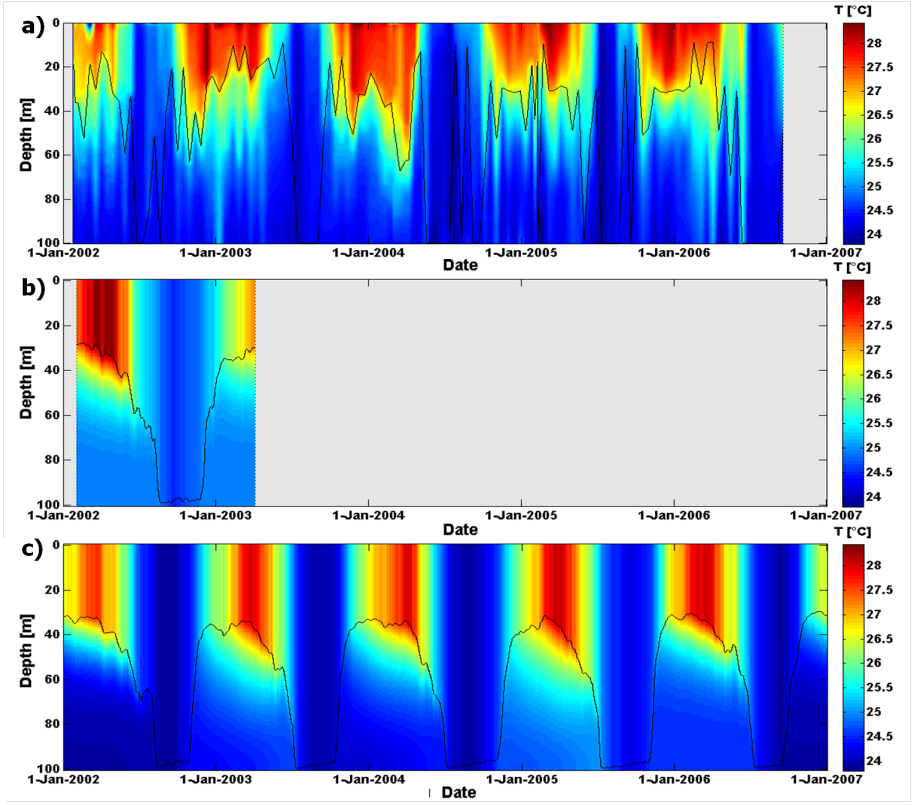

Figure 3.9: **Lake water temperatures (°C) at Mpulungu (southern basin of Lake Tanganyika) (a) from observations, (b) as predicted by the AWS-driven FLake-control, and (c) as predicted by FLake-ERA-Interim. The black line depicts the mixed layer depth (Sect. 3.2.3; weekly mean for the simulations). Results in (c) were obtained with $k = 0.09$ m^{-1}.**

distance from the equator coincides with a higher distance from the Intertropical Convergence Zone (ITCZ) during austral winter and thus a larger contrast between dry and wet season (Akkermans et al., 2014).

Third, although the average latent heat flux (LHF) is very similar at Ishungu (88 W m^{-2}) and Kigoma (86 W m^{-2}), it increases by 56% at Mpulungu (134 W m^{-2}) during the respective measurement periods. Extrapolating the average LHF at Ishungu to the entire Lake Kivu surface (estimated by the control simulation and using a surface area of 2370 km^2; Schmid and Wüest, 2012) leads to a preliminary estimate of the total annual evaporative flux of 2.6 km^3 yr^{-1} for the period 2003-2011. Note that, based on calculations from Bultot (1971), Schmid and Wüest (2012) estimate a total annual evaporation of 3.0-4.0 km^3 yr^{-1} for Lake Kivu. Analogous, extrapolating the average LHF computed for Kigoma to the Northern Tanganyika basin (17572 km^2; Plisnier, 2007) leads to a preliminary estimate of 18.8 km^3 yr^{-1} for the total annual evaporation from the Northern basin. At Mpulungu, where the control simulation predicts an average LHF of 133 W m^{-2} for the measurement period, extrapolation yields a total annual evaporation of 23.8 km^3 yr^{-1} from the Southern basin (14173 km^2; Plisnier, 2007). For the ERA-Interim simulations, the average LHF amounts up to 114 W m^{-2} (25.3 km^3 yr^{-1}) at Kigoma and 138 W m^{-2} (24.7 km^3 yr^{-1}) at Mpulungu. Note that Verburg and Antenucci (2010) computed a lake-wide evaporation amounting up to 63 km^3 yr^{-1}, when assuming a total surface area of 31745 km^2 for Lake Tanganyika. The annual lake-wide evaporation estimates from the control and ERA-Interim simulations are only 65% (42.6 km^3) and 80% (50.1 km^3) of this value, respectively. Possible explanations for this discrepancy are (i) the different method used to compute the latent heat flux, (ii) differences in the quality and length of the meteorological time series, and (iii) the period of observation (1994-1996 versus 2002-2003 and 2002-2006, respectively). Especially the latter effect is potentially relevant, given the influence of large-scale climate oscillations such as the El Niño-Southern Oscillation (ENSO) on the regional climate (Plisnier et al., 2000) and the contrasting ENSO indices found for both periods (La Niña years versus El Niño years). Further research will aim at quantifying uncertainties associated with lake-wide evaporation estimates for tropical lakes.

Results from the AWS control simulations show that FLake successfully incorporates these differences between the sites, since the model, through the differences in forcing and configuration, successfully represents the thermal structure of both Lake Kivu and Lake Tanganyika and discerns the differences between the two basins within Lake Tanganyika.

3.3.5 Sensitivity study

Originally designed for implementation within NWP systems or climate models, FLake requires information on lake depth and water transparency (downward light attenuation coefficient) for each lake within its domain. But despite recent efforts to gather and map lake depth on a global scale (Kourzeneva, 2010; Kourzeneva et al., 2012a), in East Africa information on lake depth and water transparency is only available for the largest lakes, adding uncertainty to FLake's outcome when it is applied to the entire region. Furthermore, the effect of the forcing data source – e.g. originating from an AWS, a reanalysis product or RCM output – and its associated quality might significantly affect the outcome of a simulation. As RCMs and standalone lake models are being applied to increasingly remote lakes, the need to consider this data quality issue grows (Martynov et al., 2010). Finally, in the absence of initialisation data, several approaches to lake temperature initialisation and spin-up have been applied in the past (Kourzeneva et al., 2008; Mironov et al., 2010; Balsamo et al., 2012; Hernández-Díaz et al., 2012; Rontu et al., 2012). Hence, a systematic study of the sensitivity of the model to different sources of error is appropriate. Hereafter, results of FLake's sensitivity to variations in (i) external parameters, (ii) meteorological forcing data, and (iii) temperature initialisation are presented. Note that each set of the following tests was conducted starting from the Lake Kivu control simulation (Sect. 3.3.1). However, the same experiments have been conducted for Kigoma and Mpulungu as well, and revealed very similar responses to the imposed changes.

External parameters

The first set of model sensitivity tests was conducted to investigate FLake's sensitivity to changes in the model's external parameters. Using a set of four model efficiency scores (Sect. 3.2.4), the impact of setting the model lake depth to a relatively shallow 30 m (SHA) or a relatively deep 120 m (DEE), and setting k to the highest (KHI) or lowest (KLO) observed value at Ishungu (Table 3.2) was quantified. σ_T, $RMSE_c$ and r calculated at three depths (5 m, 30 m and 60 m, respectively) are visualised in Taylor diagrams (Fig. 3.10). Furthermore, note that we also investigated the sensitivity of FLake to changes in the fetch, by conducting a set of simulations with the fetch varying between 1 and 100 km, respectively (the value in all other simulations is 10 km). It was however found that for Lake Kivu, FLake exhibits only little sensitivity to modifications in this parameter.

At 5 m depth, the different sensitivity experiments produce similar values for $RMSE_c$, r, and BSS (not shown). The only score for which the control

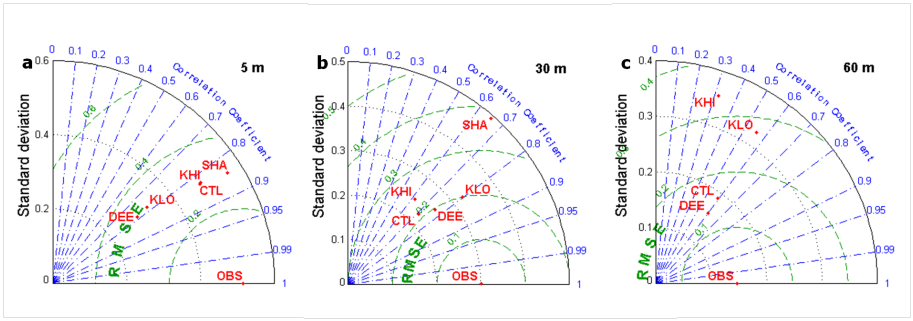

Figure 3.10: **Taylor diagram indicating model performance for water temperature at (a) 5 m, (b) 30 m and (c) 60 m depths for different external parameter values at Ishungu (January 2003 – December 2011). Standard deviation σ_T (°C; radial distance), centred Root Mean Square Error $RMSE_c$ (°C; distance apart) and Pearson correlation coefficient r (azimuthal position of the simulation field) were calculated from the observed T-profile interpolated to a regular grid (1 m increment) and corresponding midday FLake profile. OBS: observations, CTL: control, SHA (DEE): model lake depth set to and 30 m (120 m), KHI (KLO): downward light attenuation coefficient k set to the highest (lowest) observed value at Ishungu. Note that model performance indicators at 60 m cannot be calculated for the SHA integration.**

simulation outcompetes the other members is σ_T, suggesting that in this case seasonal temperature variability is closest to reality. At 30 m, already some changes to this pattern can be noticed (Fig. 3.10b). Most notably, for the SHA test case predictive skill significantly decreases. For this test, FLake predicts fully mixed conditions down to 30 m during most of the time, except during the 2005, 2007 and 2009 rainy seasons, when mixing down to 10 m is predicted. However, only at 60 m the differences fully emerge, with a clear reduction in predictive skill for the simulations with k decreased (increased) to the lowest (highest) observed values at Ishungu. Higher water transparency leads to deeper mixing, as solar radiation penetrates down to the interface between mixed layer and thermocline and therewith enhances h_{ML}. Note that for the more transparent Lake Tanganyika, FLake's sensitivity to changes in k is even more important (not shown). There, a change of less than 1 σ away from the average observed k already led to a switch from permanently mixed conditions to a continuously stratified regime.

Forcing data

In a second set of experiments, FLake's sensitivity to changes in forcing variables was investigated. Starting from the control simulation at Ishungu, values for

T, RH, ff and LW_{in} were varied in pairs between bounds $o_i - 2\sigma$ to $o_i + 2\sigma$, with o_i the actual observed value at time step i and σ the standard deviation of a given variable (see also Thiery et al., 2012). Standard deviations for T, RH, ff and LW_{in} are 2.4 °C, 14%, 1.7 m s^{-1} and 18 W m^{-2}, respectively. The perturbation increment was 0.4σ in each experiment. The vertically averaged BSS for water temperature calculated per meter depth for 2003-2011 after this pairwise perturbation (Fig. 3.11) allowed to select the main environmental variables controlling h_{ML} in tropical conditions. Sensitivity experiments for p and SW_{in} are not shown, the former since FLake was found to be not sensitive to this variable, the latter since its high standard deviation (252 W m^{-2}) led to unrealistic perturbations. To overcome this issue, an additional experiment was conducted wherein the SW_{in} and LW_{in} time series were perturbed by the respective standard deviations of their daily means (σ_{dm}, with values of 35 W m^{-2} and 12 W m^{-2}, respectively; Fig. 3.12).

For Lake Kivu, FLake results reveal a marked sensitivity to variations in wind speed (Fig. 3.11a-b). Generally, when wind velocities increase (decrease), mechanical mixing reaches deeper (less deep) into the lake, causing a cooling (warming) of the mixed layer for the same energy budget. For Lake Kivu, at some point the increased wind velocity however provokes a regime switch from seasonally mixed conditions to (almost) permanently mixed conditions. This switch, illustrated by the sharp decrease in BSS in Fig. 3.11a-b along the ff axis, is already reached before ff is enhanced by 0.4 σ. Similarly, only slightly decreasing ff already leads to a sharp switch to the permanently stratified regime. Increasing (decreasing) T and RH by their respective σ equally contributes to higher (lower) mixed layer temperatures, which in turn enhances (reduces) stratification (Fig. 3.11c). Again, the vertically averaged BSS depicts the switch to both other regimes: a sharp transition to permanent stratification for increased T and RH and a gradual transition to fully mixed conditions for lower T and RH. A similar sensitivity is found when testing for LW_{in}, although FLake seems less sensitive to variations in this variable (Fig. 3.11d). When comparing SW_{in} and LW_{in} for perturbations of the order of their respective σ_{dm} (Fig. 3.12), it can be noted that fairly large perturbations are needed to provoke a regime switch, and that such a switch is provoked more easily by modifying SW_{in} than LW_{in} by their respective σ_{dm}. Note that when combined in pairs, errors may compensate each other and still generate adequate model predictions, as is the case when e.g. simultaneously reducing ff and T by one respective σ, or increasing LW_{in} while decreasing RH by one respective σ.

Finally, for each variable in this experiment, one can also derive an uncertainty range for which FLake predicts the correct mixing regime. With a vertically averaged BSS threshold set to -20, the range width of wind velocities for which

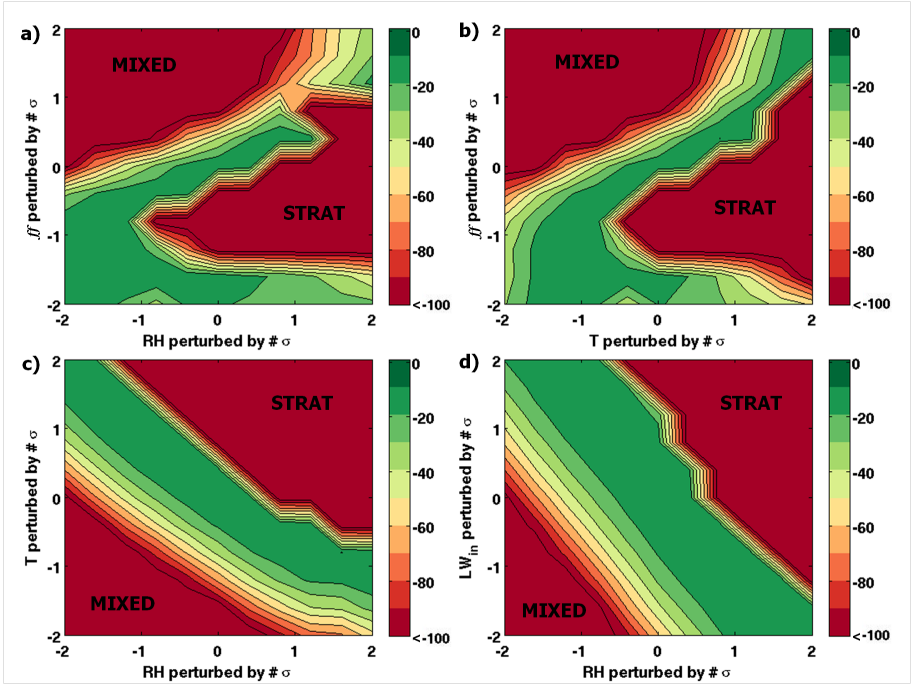

Figure 3.11: **Vertically averaged Brier Skill Scores (BSS) of water temperature profiles (0 – 60 m; 1 m vertical increment) at Ishungu from 4 sensitivity experiments, wherein pairs of forcing variables recorded at AWS 1 were perturbed by proportions of their respective standard deviations σ. Perturbed forcing variables are wind velocity (ff), Relative humidity (RH), air temperature (T) and incoming long-wave radiation (LW_{in}). Generally, values for BSS range from $+1$ (perfect prediction) to $-\infty$ (no relation between observation and prediction). Here, BSS below -100 are set to -100. Permanently stratified (STRAT) and fully mixed conditions down to 60 m (MIXED) are indicated.**

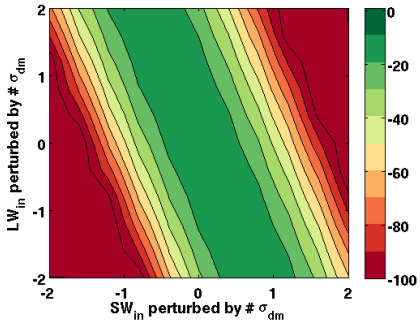

Figure 3.12: **Vertically averaged Brier Skill Scores (BSS) of water temperature profiles ($0-60$ m; 1 m vertical increment) at Ishungu from a set of simulations with SW_{in} and LW_{in} perturbed by proportions of their respective standard deviations of daily mean values (σ_{dm}).**

a correct mixing regime is predicted is 0.7 m s^{-1} around the actual observed values of the control run (Fig. 3.11a). For RH, T, LW_{in} and SW_{in}, this range is 17%, 2.0 °C, 50 W m^{-2} and 42 W m^{-2}, respectively. While for the latter four variables, collecting in situ measurements within these uncertainty bounds is feasible, clearly, the room for manoeuvre in case of wind velocity measurements is very small. Consequently, the need for reliable wind velocities is critical to have FLake predicting the right mixing conditions over deep tropical lakes. Note that this is also the reason why wind speed was selected as the forcing variable to correct (Sect. 3.2.4). In return, when the same computation is conducted for the 5 m BSS instead of the vertically averaged BSS, the narrow band widens to 3.4 m s^{-1} (even with a 5 m BSS threshold set to only -2, the acceptable uncertainty range is still 2.0 m s^{-1}). Thus, in cases where the primary interest of the FLake application is the correct representation of near-surface water temperatures, the need for very high accuracy wind velocity measurements becomes less pressing.

This has implications for the applicability of FLake to the study of tropical lake-climate interactions. When FLake is interactively coupled to an atmospheric model, it may very well be that e.g. the near-surface wind velocities serving as input to FLake will not fall within the narrow range for which it predicts a correct mixing regime. However, the only FLake variable which directly influences the atmospheric boundary layer is T_{ML}, the variable from which the exchange of water and energy between the lake and the atmosphere are computed. In this study, T_{ML} predictions were found to be robust, even when modelled T_{BOT} values are biased. We may therefore suppose that for tropical conditions, a coupled model system will not be much affected by the strong

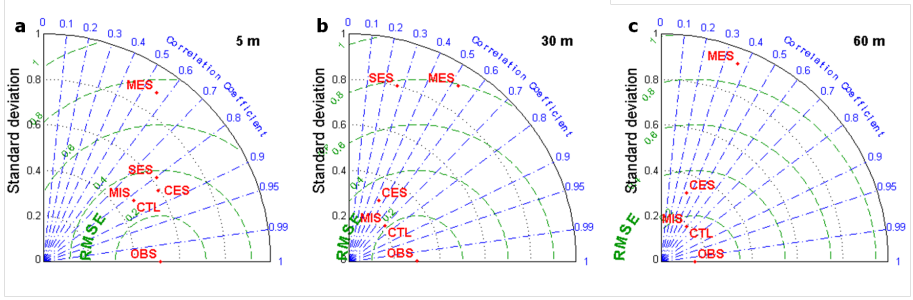

Figure 3.13: **Taylor diagram indicating model performance for water temperature at (a) 5 m, (b) 30 m and (c) 60 m depths for different initial conditions at Ishungu (January 2003 – December 2011). OBS: observations, CTL: control, CES: control excluding spin-up, SES: stratified excluding spin-up, MIS (MES): mixed warm initialisation including (excluding) spin-up. Note that SES is omitted at 60 m given its strong deviation from observations there.**

sensitivity of FLake's deepwater temperatures to, for instance, wind speed values.

Initial conditions

The third set of experiments at Lake Kivu was designed to test the model to different initial conditions. In the control simulation, FLake was initialised with the average mixed layer, total water column and bottom temperatures calculated from the January CTD profiles (n = 14), after which spin-up cycles were repeated until convergence is reached. Sensitivity experiments encompassed a simulation with the same initialisation but excluding spin-up (CES), a fully mixed (i.e. down to 60 m depth) water column initialisation including (MIS) or excluding spin-up (MES), and a stratified water column excluding spin-up (SES). By setting the initial mixed layer depth to 60 m and the lake water temperature to 28 °C, full mixing was imposed, whereas permanently stratified conditions were obtained by setting the initial mixed layer depth to 8 m, T_{ML} to 23.5 °C and T_{BOT} to 4 °C (comparable to Hernández-Díaz et al., 2012; Martynov et al., 2012). Note that a stratified initialisation including spin-up is omitted, since downward heat transport within the thermocline can only occur through molecular diffusion in this case, and hence would require millennia scale spin-up time. Again, σ_T, $RMSE_c$, and r were calculated and visualised for three depths (Fig. 3.13).

First, it can be noted that omitting spin-up in the optimal simulation (CES) has only limited, though negative, influence on the predictive skill. This shows

that when a reliable initial CTD profile is available, spin-up has some, but only little added value. More interestingly, however, is the fact that a fully mixed and artificially warm initialisation with spin-up (MIS) succeeds very well in reproducing the thermal structure of Lake Kivu. Within 9 spin-up years, the complete mixing allows for an efficient heat release until the regime switches to the expected pattern. Since the model is allowed to spin-up until convergence is reached, the selection of the initial water column temperature does not influence the model performance, as long as it is chosen artificially warm. However, without spin-up (MES), this advantage vanishes and results have limited skill, since the lake has been initialised too warm. Alternatively, when offline spin-up of lake temperatures is not feasible within the coupled model system, imposing permanently stratified conditions by means of a 4 °C lake bottom (SES) becomes an option, given the acceptable results near the lake surface even though the thermal structure is not reproduced. Note that this was the approach adopted for the CORDEX-Africa simulations conducted with the Canadian Regional Climate Model version 5 (Hernández-Díaz et al., 2012; Martynov et al., 2012). Hence, for coupled FLake-atmosphere simulations over regions with no initialisation information available, a fully mixed, artificially warm initialisation appears to be the best option, but only if offline lake temperature spin-up is applied; else an imposed permanently stratified regime is to be preferred.

3.3.6 Mixing physics at Lake Kivu

Studying the seasonal variations in the near-surface meteorological conditions and in the surface energy balance of the Ishungu control experiment, allows us to attribute the seasonal mixing cycle for Lake Kivu. On the one hand, even though ff depicts some seasonality (Fig. 3.14a), neither ff nor T influence the seasonality of the mixed layer depth at Ishungu. First, a comparative histogram of corrected ff binned per month (1 m s^{-1} bin width; not shown) reveals that the probability of occurrence of stronger winds ($ff > 5$ m s^{-1}) is lower from April to July, adding to the hypothesis that higher wind velocities are not responsible for the deepening mixed layer depth during the dry season. This is confirmed by FLake, who attributes the mixed layer deepening at the start of the dry season to convection rather than wind-driven mixing. Moreover, when conducting the Ishungu control simulation with the seasonality removed from ff, the predicted water temperatures are almost identical to the control simulation. This indicates that the ff seasonality also has no major influence on the convective driven mixing.

On the other hand, in contrast to ff and T, RH and LW_{in} both show a clear seasonality, with three-monthly averages 13% and 11 W m^{-2}, respectively, lower

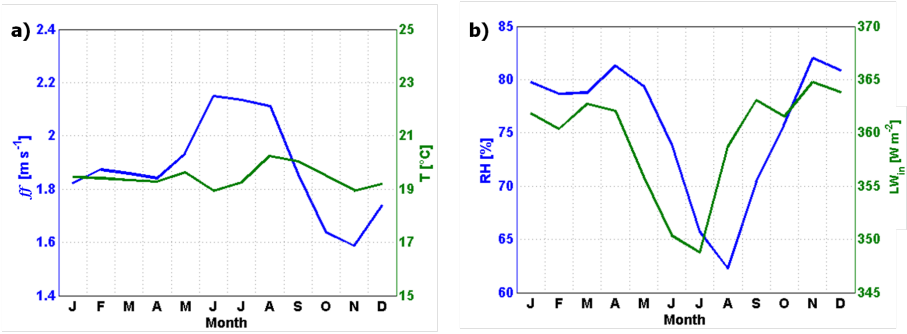

Figure 3.14: **Monthly averages for 2003-2011 of (a) wind velocity ff (m s^{-1}) and air temperature T (°C); (b) relative humidity RH (%) recorded at Automatic Weather Station (AWS) 1 and incoming long-wave radiation LW_{in} (W m^{-2}) from ERA-Interim. Note the different y-axes increments.**

for the June-August period compared to December-February period. Their monthly average values show that the seasonal RH cycle lags the LW_{in} cycle by about one month, but confirm the strong drop during the main dry season (Fig. 3.14b). Here, two effects enforce each other to reduce the amount of energy available to stratify the lake surface. First, as a consequence of reduced cloudiness during the dry season, less thermal radiation reaches the surface. This, in turn, causes a higher upward net long-wave radiation flux (LW_{net}) from May to July (Fig. 3.15). Second, more importantly, while a moisture climate close to saturation inhibits significant evaporation throughout most of the year, the RH drop during the dry season opens a larger potential to evaporation. This effect can be noted in the monthly average anomalies of the surface energy balance components, wherein the LHF shows a marked positive anomaly in months with low RH (Fig. 3.15). The energy consumed for evaporating is no longer available to heat the water surface. Thus, lower thermal radiation input and especially enhanced evaporation cause a significant reduction in the amount of energy available to heat near-surface waters. To compensate for this surface heat deficit, the upward subsurface conductive heat flux enhances, in turn generating a drop in the mixed layer temperature.

From mid-June onwards, near-surface water temperatures become low enough for the deep mixing to set in. Near the end of the dry season, from the mid-August onwards, evaporation rates dramatically drop, causing the warming of surface waters from mid-September forward. Note that whereas enhanced solar radiation penetration into the lake is absent during the first phase of the dry season, near the end it slightly contributes to the restoration of surface stratification (Fig. 3.15). Overall, monthly variations in downward short-wave

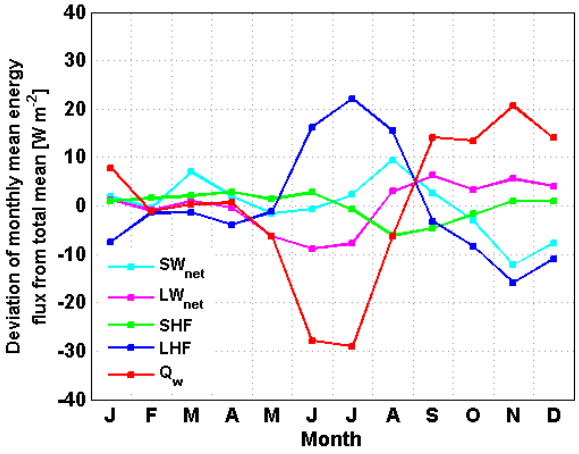

Figure 3.15: **Deviation of the monthly average of the surface energy balance components from its long-term mean (W m^{-2}) at Ishungu, 2003-2011, calculated by FLake's surface flux routines. Components are net short-wave radiation SW_{net}, net long-wave radiation LW_{net}, sensible heat flux SHF, latent heat flux LHF and subsurface conductive heat flux Q.**

radiation (SW_{in}) seem to have only little effect on the mixed layer seasonality. Possibly, the interplay of astronomic short-wave radiation variability (with less short-wave radiation reaching the top of the atmosphere during the dry seasons) and seasonally varying cloud properties (Capart, 1952) balances out the amount of short-wave radiation reaching the surface on monthly time scales.

3.4 Discussion and conclusions

In general, this study shows that the thermal structure of the mixed layer and thermocline of two African Great Lakes can be reproduced by the FLake model. In particular, the seasonality of the near-surface water temperatures of Lake Kivu and Lake Tanganyika is well captured by the AWS-driven simulations when choosing appropriate values for the wind speed correction factor and k within their uncertainty range. Moreover, FLake was found capable of reproducing the observed interannual variability, as well as the observed differences between the three sites. The spatial variability is accounted for through varying lake characteristics and meteorological conditions associated with different surface altitude and distance from the equator. At Ishungu, a study of the near-surface meteorology and surface heat balance was used to attribute seasonal

mixing cycle of Lake Kivu. Rather than seasonal variations in wind velocity or air temperature, the marked dry season decrease of the incoming long-wave radiation and, especially, relative humidity with an associated evaporation peak, reduce the amount of energy available to induce surface stratification.

The near-surface water temperatures were found to be quite robust to changes in the model configuration. If the observed mixing regime is not reproduced, 5 m temperature predictions deteriorate compared to the control integration, but are relatively little affected. Hence, FLake can be considered an appropriate tool to study the climatic impact of lakes in the region of the African Great Lakes. In contrast, an accurate representation of the thermal structure of the mixed layer and thermocline depends strongly on the reliability of meteorological forcing data and a correct choice of model lake depth and water transparency. Slight differences in external parameters, and uncertainties associated with the meteorological forcing data (for instance related to measurement or atmospheric model uncertainty, or to the representativeness of the data for over-lake conditions) may already lead to a switch from the observed regime of seasonal mixed layer deepening to either the permanently stratified or the fully mixed regime.

One important reason for this delicate balance found at Lake Kivu is the absence of an abyssal layer in FLake. In reality, the abyssal layer acts as a heat reservoir which buffers potential changes in bottom temperature. FLake, on the contrary, assumes a zero heat flux at the water-sediment interface (sediment routine switched off) or at the lower bound of the active sediment layer (sediment routine switched on). In cases where an artificial lake depth is set, this assumption can lead to unrealistic temperature fluctuations near the bottom. Hence, a future development could be to include an abyssal layer in FLake (Mironov et al., 2010).

A second issue is the reliability of water transparency values. Even in more studied areas, information on the spatial and temporal variability of water transparency is mostly lacking (Kirillin, 2010; Kourzeneva et al., 2012b; Rontu et al., 2012). Therefore, the first need is to collect more observations of k and to gain more insight in the relationship between water transparency and seasonal mixing cycles in deep tropical lakes. In the future, FLake could then also be adapted to account for these seasonal fluctuations in k.

When applying FLake over regions containing warm deep lakes, values for the external parameters thus need to be considered carefully. This is especially true when FLake is coupled to NWP, RCM or GCM models, since the meteorological forcing data are potentially biased in that case. When setting up a climate or NWP simulation with interactive lakes, moreover, no information on the lake's initial conditions is available. In that respect, this study clearly shows that it is

advisable to initialise all lakes with an artificially warm, uniform temperature and to allow for a considerable offline spin-up of the lake module. When such an offline lake spin up is not feasible, initialising FLake with stratified conditions and an artificially low bottom temperature of 4 °C is to be preferred.

To conclude, the goal of this study was to assess the quality of lake temperature predictions by FLake when applied to tropical lakes. This was done through a number of simulations for three locations in the African Great lakes region: Ishungu (Lake Kivu), Kigoma (northern basin of Lake Tanganyika) and Mpulungu (southern basin of Lake Tanganyika). Results show that FLake is able to well represent the mixing regime at these different locations, however only when the model was carefully configured and allowed to spin-up over a considerable period. When input data quality is an issue, or the model is poorly configured, model results tend to deviate from observations towards the deep in large tropical lakes.

3.5 Code availability

FLake is freely available under the terms of the GNU Lesser General Public License (http://www.gnu.org/licenses/lgpl.html). The model source code, external parameter datasets and a comprehensive model description can be obtained from the official FLake website (http://www.lakemodel.net), along with pre-processed meteorological forcing for several test cases.

3.6 Acknowledgements

We would like to thank Dmitrii Mironov for the helpful discussions on the modelling of tropical lakes and the Institut Supérieur Pédagogique in Bukavu for supplying data of AWS 1. This work was financially and logistically supported by the Research Foundation – Flanders (FWO) and the Belgian Science Policy Office (BELSPO), the latter through the research projects EAGLES and CHOLTIC.

Chapter 4

LakeMIP Kivu: evaluating the representation of a large, deep tropical lake by a set of one-dimensional lake models

This chapter is published as: Thiery, W., Stepanenko, V.M., Fang, X., Jöhnk, K.D., Li, Z., Martynov, A., Perroud, M., Subin, Z.M., Darchambeau, F., Mironov, D., and Van Lipzig, N., 2014. LakeMIP Kivu: Evaluating the representation of a large, deep tropical lake by a set of one-dimensional lake models. *Tellus A* 66, 21390. doi:10.3402/tellusa.v66.21390

The African great lakes are of utmost importance for the local economy (fishing), as well as being essential to the survival of the local people. During the last decades, these lakes experienced fast changes in ecosystem structure and functioning and their future evolution is a major concern. In this study, for the first time a set of one-dimensional lake models are evaluated for Lake Kivu (2.28 °S; 28.98 °E), East Africa. The unique limnology of this meromictic Lake, with the importance of salinity and subsurface springs in a tropical high-altitude climate, presents a worthy challenge to the seven models involved in the Lake Model Intercomparison Project (LakeMIP). Meteorological observations from two automatic weather stations are used to drive the models, whereas a unique dataset, containing over 150 temperature profiles recorded since 2002, is used to assess the model's performance. Simulations are performed over the freshwater layer only (60 m) and over the average lake depth (240 m), since salinity increases with depth below 60 m in Lake Kivu and some lake models do not account for the influence of salinity upon lake stratification. All models are

able to reproduce the mixing seasonality in Lake Kivu, as well as the magnitude and seasonal cycle of the lake enthalpy change. Differences between the models can be ascribed to variations in the treatment of the radiative forcing and the computation of the turbulent heat fluxes. Fluctuations in wind velocity and solar radiation explain inter-annual variability of observed water column temperatures. The good agreement between the deep simulations and the observed meromictic stratification also shows that a subset of models is able to account for the salinity- and geothermal-induced effects upon deep water stratification. Finally, based on the strengths and weaknesses discerned in this study, an informed choice of a one-dimensional lake model for a given research purpose becomes possible.

4.1 Introduction

In regions where lakes compose a large fraction of the earth surface, they form an important component of the climate system. The strong contrasts in albedo, surface roughness and heat capacity between land and water modify the surface-atmosphere exchanges of moisture, heat and momentum over lakes compared to adjacent land (Bonan, 1995). Some reported effects of this modified exchange are the dampened diurnal temperature range over lakes (Subin et al., 2012a), the enhanced evaporation or even a persistent unstable atmospheric boundary layer (Verburg and Antenucci, 2010), the resulting increased precipitation downwind of the lake (Lauwaet et al., 2012), the stronger winds due to higher wind fetch (Subin et al., 2012a), and the formation of local diurnal winds (Verburg and Hecky, 2003; Savijärvi, 1997).

Given the significant impact of lakes on surface-atmosphere interactions, the need for an accurate representation of lake surface temperatures in Numerical Weather Prediction systems (NWP), Regional Climate Models (RCM) and General Circulation Models (GCM) arises. Although a multitude of one-dimensional lake models developed in the past may candidate to represent lake-atmosphere exchanges, only a subset of these models has been interactively coupled to atmospheric prediction models so far (Hostetler et al., 1994; Bonan, 1995; Song et al., 2004; Kourzeneva et al., 2008; Mironov et al., 2010; Balsamo et al., 2012; Martynov et al., 2012; Goyette and Perroud, 2012; Akkermans et al., 2014). Computational efficiency of the lake parameterisation scheme is often decisive for the choice of the scheme. A comparative assessment of different one-dimensional lake models, with emphasis on the strengths and weaknesses with respect to specific research goals, could however favour an informed choice.

From this need, in 2008 the Lake Model Intercomparison Project (LakeMIP) emerged. In a first stage, this project aims at a comparison of the thermodynamic regime of a wide range of climatic conditions and mixing regimes by a number of one-dimensional lake models (Stepanenko et al., 2010). Inspired by a model intercomparison study for the deep lake Geneva (Perroud and Goyette, 2009), LakeMIP focused on a number of test cases such as, for mid-latitudes, the small Lake Sparkling (Stepanenko et al., 2010) and the shallow turbid Lake Kossenblatter (Stepanenko et al., 2013) whereas for a boreal climate, the small Lake Valkea-Kotinen was investigated (Stepanenko et al., 2014).

However, despite the abundance of lakes in tropical regions such as East Africa and Indonesia, up to now a lake model intercomparison study has never been conducted for an equatorial lake. In tropical climates, the limited seasonal cycle of both air temperature and incoming shortwave radiation makes way for other factors to control the mixing regime. With the meteorological controls on a

lake's mixing regime and its water temperatures varying between climate zones, the need arose to conduct a model intercomparison experiment for a tropical lake.

Consequently, in this study, for the first time a set of one-dimensional lake models is evaluated over an East African lake: Lake Kivu (2.28 °S; 28.98 °E). Lake Kivu's meromictic mixing regime clearly differs from lakes previously studied within the project, i.e. monomictic, dimictic or polymictic lakes with seasonal complete or partial ice cover. Furthermore, given the influence of salinity, dissolved gases and geothermal springs on the characteristics of the hypolimnion, the modelling of Lake Kivu presents a worthy challenge to the one-dimensional lake models currently involved in LakeMIP. Finally, as a consequence of its distinct characteristics, Lake Kivu is among the best studied lakes in the African Great Lakes region. Anthropogenic influences and recurrent natural hazards call for a close monitoring of the lake's physical and biological characteristics. For instance, when lava flowed into the lake after a major eruption of the near-shore Nyiragongo volcano, no significant impact on the water column stability was recorded (Lorke et al., 2004). In contrast, effects on density stratification of the emerging industrial methane extraction from lake Kivu are expected and will critically depend on the reinjection depth of the deep waters after the methane harvest (Descy et al., 2012; Wüest et al., 2012). To meet these and other challenges, a comprehensive dataset containing observed lake temperatures, Secchi depths and many other variables has been compiled over the last decade.

The two main goals of this study are (i) the evaluation of the seasonal and inter-annual variability of Lake Kivu's thermal structure as represented by a set of one-dimensional lake models, and (ii) the assessment of the ability of the different models to simulate the effects of salinity, chemical composition and geothermal energy sources upon deep water stratification. This was done by performing two sets of simulations, one including only the freshwater mixed layer and another one for the whole lake including salinity, chemical and geothermal effects in the equation of state.

In the next section, an overview of the participating one-dimensional lake models is provided, together with a description of the observational dataset and the experimental setup. Section 4.3 describes the results of the intercomparison, with emphasis on the ability of the different models to reproduce Lake Kivu's mixing cycle, the surface energy exchange and the deep water stratification. Finally, in section 4.4, different options to improve individual model performance are discussed, and the validity of the horizontal homogeneity assumption is investigated.

Table 4.1: **Participating one-dimensional lake models and numerical model settings used in this study for Kamembe meteorology runs on a 60 m and 240 m depth grid. Note that MINLAKE2012 includes fine layer spacing in the first 1 m to facilitate the ice formation prediction. * All CPU times were measured on an Intel Core i5 processor (2.27 GHz), except for CLM4-LISSS (2.1 GHz AMD Magny-Cours processor), a model tailored for a supercomputing environment and therefore not easily portable to a single-processor machine.**

Lake model	# layers	layer thickness	Time step	CPU time (Kamembe 60 m; 2557 days)
Hostetler	60	1 m	60 min	6.1 s
SimStrat	60 / 240	1 m	10 min	20.5 s
LAKEoneD	60 / 240	1 m	5 min	52.5 s
LAKE	40 / 40	1.5 / 6 m	20 min	226 s
FLake	2	/	60 min	1.7 s
MINLAKE2012	65 / 80	1 / 5 m	60 min	8.3 s
CLM4-LISSS	25	irregular	30 min	150 s

4.2 Data and methods

4.2.1 Lake models

Seven one-dimensional lake models participate in the LakeMIP-Kivu experiment (Table 4.1). Time step, number of horizontal layers and their interspacing used by the different models are listed in Table 4.1, including the Central Processing Unit (CPU) time needed to conduct a single simulation. All models compute lake water temperatures and heat, water and momentum exchange between the lake surface and the overlying atmosphere from basic meteorological quantities. Below a short description of the different models is given; for more extensive overviews one is referred to Perroud and Goyette (2009), (Stepanenko et al., 2014) and references herein.

- The Hostetler model (Hostetler et al., 1993) includes semi-empirical formulations for the buoyant convection and wind-driven eddy turbulence mixing, adding to the thermal conductivity and molecular diffusion in a multilayered water column. A second model, the Lake, Ice, Snow and Sediment Simulator within the Community Land Model 4 (CLM4-LISSS; Subin et al., 2012b) is originally based on the Hostetler model, but has undergone major improvements since its first inclusion in CLM2 (Bonan et al., 2002). The now comprehensive treatment of lake snow and -ice, bottom sediments, lake depth and surface-atmosphere exchange significantly improved the model's performance, for shallow to medium-depth small lakes as well as for large, deep lakes (Subin et al., 2012b).

- Three models belong to the class of $k-\epsilon$ turbulence closure models: LAKEoneD

(Jöhnk and Umlauf, 2001; Jöhnk, 2013), SimStrat (Goudsmit, 2002) and LAKE (Stepanenko and Lykosov, 2005). They encompass a more sophisticated representation of the turbulent diffusivity (D_{turb}) at a certain depth and time through the relation $D_{turb} = ck^2/\epsilon$, where k is the turbulent kinetic energy, ϵ the turbulent dissipation rate and c either a constant or a stability function, depending on the models (Stepanenko et al., 2013). Although $k - \epsilon$ models formally employ identical model equations, some differences in water temperature distribution are expected, given the variations in the coefficients used in the $k - \epsilon$ equations, and given the model-dependent treatment of the heat exchange with the overlying atmosphere and underlying bottom sediments.

- In contrast to other participating models, that are multilayered finite difference models, FLake (Mironov, 2008) is a two layer bulk model, employing the concept of self-similarity to parameterise the temperature-depth curve. FLake consists of a mixed layer of constant temperature and an underlying thermocline down to the lake bottom, the latter parameterised through a fourth-order polynomial depending on a shape coefficient. The mixed layer depth is computed depending on convective entrainment and wind-driven mixing. The inclusion of the mixed layer depth and its temporal change at the heart of FLake is very different from other lake models, where the mixed layer depth is often not even considered. FLake is therefore not more or less empirical than other lake models, but instead takes a very different approach to the problem of computing lake temperatures.

- Next, MINLAKE2012 presents an update of MINLAKE96 (Fang and Stefan, 1996), used in previous intercomparison experiments. The model solves the one-dimensional, unsteady heat transfer equation using empirical formulations for the variable vertical diffusion coefficient and the heat exchange between water and bottom sediments (Fang and Stefan, 1996). The most important upgrades compared to MINLAKE96 are the conversion to a user-friendly spreadsheet environment and the introduction of variable temporal resolution, allowing to run the model at hourly time step in contrast to the daily time step previously applicable.

4.2.2 Observations

Study area

Lake Kivu (01° 35' S - 02° 30' S 028° 50' E - 029° 23' E; 2370 km^2 surface area; 485 m maximum depth; 1463 m a.s.l.) is located on the border between Rwanda and the Democratic Republic of Congo, and is one of the seven African Great Lakes (Fig. 4.1). It drains into the Ruzizi river, which flows south towards lake Tanganyika. Below an oxic mixolimnion, which deepens to 60-70 m during the

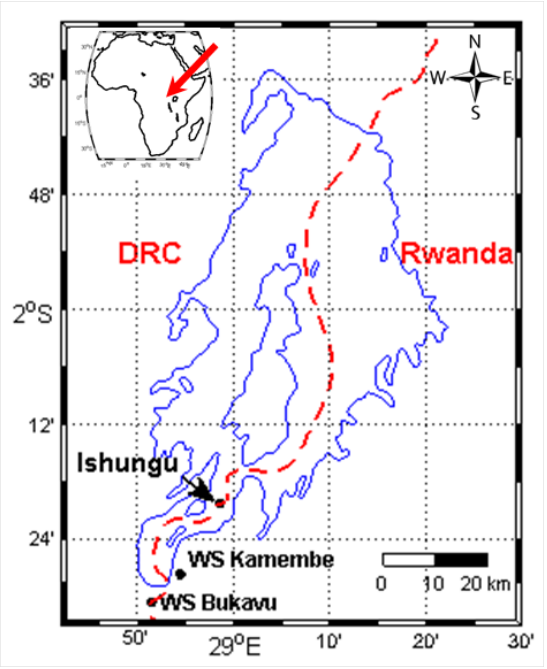

Figure 4.1: **Lake Kivu with situation of the Ishungu evaluation site and the Kamembe Weather Station (WS Kamembe) and Automatic Weather Station Bukavu (WS Bukavu).**

dry season, the monimolimnion is found rich in nutrients and dissolved gases, in particular carbon dioxide and methane (Degens et al., 1973; Borges et al., 2011; Descy et al., 2012). Due to the input of heat and salts from deep geothermal springs, temperature and salinity in the monimolimnion increase with depth (Degens et al., 1973; Spigel and Coulter, 1996; Schmid et al., 2005). Lake Kivu's surface water temperatures vary less compared to African Great Lakes located further away from the equator.

Model forcing data

The Kamembe airport Weather Station (WS Kamembe; 02° 27' 31" S – 028° 54' 30" E, 1591 m a.s.l.) is used to force the participating lake models. It is situated approximately 1.5 km from the lake shore and 15 km southwest of the lake monitoring site Ishungu, but is assumed representative for meteorological conditions over this sub basin. The station records air temperature T (K),

Table 4.2: **Average meteorological conditions at Kamembe Weather Station (WS Kamembe) during the model integration period excluding spin-up (2003-2008). Depicted meteorological averages are prior to any correction.**

	meteorological average	**measurement frequency**	**data gaps**	**source**
T	19.6 °C	3 h	3 %	WS Kamembe
RH	77 %	3 h	4 %	WS Kamembe
p	842 hPa	3 h	25 %	WS Kamembe
u	2.7 m s^{-1}	1 h, 6-18 UTC	47 %	WS Kamembe
WD	114 °	1 h, 6-18 UTC	47 %	WS Kamembe
P	3.8 mm d^{-1}	24 h, accumulated	2 %	WS Kamembe
SW_{in}	193 W m^{-2}	6 h, accumulated	0 %	ERA-Interim
LW_{in}	361 W m^{-2}	6 h, accumulated	0 %	ERA-Interim

relative humidity RH (%), air pressure p (Pa) at three-hourly resolution throughout the whole day, wind velocity u (m s^{-1}) and direction WD (°) at hourly resolution from 6 to 18 UTC (assumed at 4 m height), and precipitation P (mm d^{-1}) at daily resolution. Although it contains only small data gaps during the integration period (January 2002 – December 2008), it does not record incoming shortwave radiation SW_{in} (W m^{-2}) and incoming longwave radiation LW_{in} (W m^{-2}), input variables necessary to run the lake models. Hence, both SW_{in} and LW_{in} data were obtained from the ERA-Interim (Dee et al., 2011) grid point closest to the Ishungu evaluation site and converted from six-hourly accumulated values to hourly instantaneous values. After linearly interpolating T, RH and p from three-hourly to hourly resolutions, and assuming that the different meteorological variables show only little spatial variability over short distances, data gaps at WS Kamembe were filled with corresponding recordings from an Automatic Weather Station in Bukavu (WS Bukavu, 2° 30' 27" S - 28° 51' 27" E), located approximately 8 km southwest of WS Kamembe. After this operation, remaining data gaps were filled by the corresponding, climatological value which was calculated for each hour of the year from available observations. WS Kamembe characteristics and meteorological averages are listed in Table 4.2.

Furthermore, each simulation was also conducted using the time series of WS Bukavu as forcing (observation height assumed at 10 m). However, since data gaps occur more often at this station, an elaborate gap correction was conducted, whereas comparison to a newly installed, offshore automatic weather station led to an upward corrected by 1 m s^{-1} of all measured wind velocities at this station (Thiery et al., 2014a). Note that WS Kamembe was chosen as the reference time series since it required less invasive corrections.

Model evaluation data

Model integrations are evaluated using 125 Conductivity-Temperature-Depth (CTD) casts collected at Ishungu (2° 20' 25" S 28° – 58' 36" E; Fig. 4.1) from January 2003 to August 2008. The 125 CTD casts represent a slice of the longest time series of vertical water temperature observations available for a tropical lake (ongoing since 2003). Although the CTD casts are primarily representative for the Ishungu sub basin (101 km^2; 180 m maximum depth), the horizontal homogeneity across all sub basins – except Bukavu and Kabuno bay – allows to assume their representativeness for the whole lake (Sect. 4.4.2). Vertical piecewise cubic Hermite interpolation (increment 1 m; De Boor, 2001) was applied to each cast (original vertical resolution ranging from 0.01 m to 10 m), serving as reference in the evaluation procedure. Note that for visualisation purposes (Fig. 4.2), an increment of 0.1 m was employed, and the same technique was applied for temporal interpolation (increment 1 day). The model's ability to reproduce the observed temperature structure was tested using a set of four model efficiency scores: the normalised standard deviation, σ_{norm} (°C), the centred Root Mean Square Error $RMSE_c$ (°C), the Pearson correlation coefficient r and the Brier Skill Score BSS (see eq. 3.3; Nash and Sutcliffe, 1970; Wilks, 2005). σ_{norm} is computed according to:

$$\sigma_{norm} = \sqrt{\frac{\sum_{i=1}^{n}(m_i - \bar{m})^2}{\sum_{i=1}^{n}(o_i - \bar{o})^2}} \tag{4.1}$$

while the $RMSE_c$ is given by

$$RMSE_c = \sqrt{\frac{1}{n}\sum_{i=1}^{n}((m_i - \bar{m}) - (o_i - \bar{o}))^2} \tag{4.2}$$

with o_i the observed (interpolated) water temperature at time i, $\bar{o}$ the average observed water temperature, and m_i and $\bar{m}$ the corresponding modelled values. Together, σ_{norm}, $RMSE_c$ and r can be visualised in a Taylor diagram (Taylor, 2001). The BSS represents the ratio of the mean square error to the observed variance, and values for BSS range from $-\infty$, suggesting no relation between observed and predicted value, to $+1$, implying a perfect prediction. Furthermore, while the BSS quickly degrades in the presence of a systematic bias, σ_{norm},

$RMSE_c$ and r are bias-independent model skill scores of the degree of agreement of the variance, the centred pattern of variation and the linear dependence between modelled and observed values, respectively (Taylor, 2001).

4.2.3 Experimental setup

Parameter and model settings

To obtain a sensible comparison of the treatment of limnological processes within each model, parameter settings have been unified as far as possible in the control and sensitivity experiments. Besides the unifications described hereafter, no additional calibration step was included.

Optical parameters. The light attenuation coefficient of water (k) has a value of 0.27 m^{-1}, computed from the average Secchi depth in Lake Kivu ($z_{sd} = 5.21$ m; $n = 163$) according to (Poole and Atkins, 1929):

$$k = \frac{-\ln 0.25}{z_{sd}} \tag{4.3}$$

where the value 0.25 represents the fraction of the incident solar radiation remaining at the time of the visual disappearance of the Secchi disc used for the measurements. Note that this fraction was retrieved through 15 simultaneous measurements during 2007 and 2008 of z_{sd} (using the Secchi disc) and k (using a LI-193SA Spherical Quantum Sensor). Additional lake optical parameters had to be used in the experiments. These are the surface shortwave albedo α_{SW} (0.07), the surface longwave albedo α_{LW} (0.03) and the surface longwave emissivity of the water surface (0.97), the latter serving as input to the Stefan-Boltzmann law. Finally, 35% (β in Table 4.3) of the incoming solar radiation signal is partitioned to the near-infrared part of the electromagnetic spectrum, while the remainder is attributed to the visible/ultraviolet part. In most models (LAKE, CLM4-LISSS, LAKEoneD, MINLAKE2012 and optionally in FLake), the near-infrared radiation fraction is absorbed directly at the surface, whereas the remaining part (65%) penetrates through the lake water column and is gradually absorbed according to the Beer-Lambert law. The value of β was obtained through integration of the ASTM G-173-03 global reference spectrum (ASTM, 2012) from 280 to 750 nm, and from 750 to 1175 nm and served to determine the visible/ultraviolet and the near-infrared fraction arriving at the surface, respectively. The value is assumed constant.

Lake bathymetry. Although a detailed bottom topography of Lake Kivu exists (Lahmeyer and Osae, 1998), it can only be included in a subset of lake models (LAKEoneD, SimStrat, LAKE and MINLAKE2012). The influence of lake bathymetry was therefore neglected to avoid an additional source of discrepancy among participating models. Since the concerned one-dimensional lake models only implicitly account for the lake bathymetry through the distribution of the geothermal heat – and optionally the exchange with a bottom sediment layer – over the difference in area between two consecutive horizontal layers, this is achieved by equating the surface area of all layers ('bathtub morphometry').

Surface flux schemes. By unifying the surface flux routines, it would be possible to exclude discrepancies among the participating lake models caused by surface-atmosphere interactions. From the comparison of five stand-alone surface flux schemes over Lake Kossenblatter, Stepanenko et al. (2013) concluded that differences between these modules indeed impact the lake's heat budget (from May to November 2003, average LHF and SHF differ up to 19.0 W m^{-2} and 3.8 W m^{-2}, respectively). In this study, however, it was chosen to maintain the native surface flux scheme of each participating model. This way, variations in predicted lake water temperatures can be caused both by the representation of lake hydrodynamics and of surface-atmosphere interactions. It also makes the comparison more relevant for researchers employing the standard surface fluxes/lake hydrodynamics package available for each model.

Horizontal variability. Horizontal variability of all forcing quantities and external parameters, such as the treatment of the Coriolis effect in LAKEoneD, or the influence of riverine and subsurface groundwater inflows on the thermal structure, are neglected in all the experiments. Meteorological forcing fields of Bukavu and Kamembe are assumed valid at Ishungu. The validity of this assumption is investigated in Sect. 4.4.2.

Numerical settings. No stringent requirements are imposed with respect to numerical settings. In particular, the choice of the number of vertical layers, the layer spacing and the model time step was free; an overview is presented in Table 4.1. However, the evaluation of model output was performed using 5 m layer spacing up to 60 m, and with 20 m layer spacing there below (if applicable), all at a temporal resolution of one hour. For models using a shorter time step, surface energy balance components are integrated over this period to permit energy balance closure.

Initial conditions. Initial conditions for temperature and salinity in the top 100 m were set by the climatological vertical profile for January at Ishungu (i.e. the mean profile computed from the 14 CTD casts collected in January). Salinity (S) is calculated from measured conductivity (C) in mS cm^{-1} using the relationship $S = 0.4665C^{1.0878}$ derived by Williams (1986). The conditions

below this depth, and initial concentrations of dissolved CO_2 and CH_4 are estimated from Schmid et al. (2005).

Control and sensitivity experiments

To assess and understand the ability of different lake models to reproduce both the mixolimnion temperature variability and the deep water stratification, two control integrations were conducted with each model. In the first simulation, an artificial lake depth of 60 m was imposed to each model. Additionally, effects induced by salinity, aquatic chemistry and geothermal sources were neglected in this simulation, leaving the computation of the water column stability to the native equation of state of the respective models. The calculation of heat conduction through the bottom sediments was switched off in the models explicitly treating this process (FLake, CLM4-LISSS, LAKE and MINLAKE2012). This first experiment is hereafter referred to as the freshwater simulation. The freshwater simulation focuses on the depth range influenced by seasonal variability: given the relatively homogeneous salt content in this layer, water temperatures vary according to meteorological variability (Sect. 4.3.2), whereas below ∼65 m, the stabilizing salinity gradient causes a permanent stratification and therewith inhibits seasonal temperature variability (Schmid and Wüest, 2012).

In the second control integration, set up to investigate deep water stratification, a subset of models was run with the observed average depth of 240 m. Note that FLake, Hostetler and CLM4-LISSS cannot be applied in this case as they do not account for salinity. FLake, moreover, assumes the extension of the thermocline layer down to the lake bottom. Here, the bottom sediment routine was switched on in the models treating the exchange of the water body with the underlying sediments. Furthermore, following computations by Schmid et al. (2010), an upward bottom heat flux of 0.3 W m^{-2} is introduced in each model, either at the water bottom interface (SimStrat, MINLAKE2012 and LAKEoneD), or at the lowest layer of bottom sediments (LAKE). Finally, the effects of salinity and dissolved gas concentrations upon water column stratification are accounted for in LAKEoneD, LAKE and MINLAKE2012 through implementation of one and the same equation of state for the water density ρ (kg m^{-3}; Schmid et al., 2003):

$$\rho(T, S, CO_2, CH_4) = \rho(T)(1 + \beta_S S + \beta_{CO_2} CO_2 + \beta_{CH_4} CH_4) \tag{4.4}$$

with $\rho(T)$ water density (kg m^{-3}) depending on water temperature T (K) only, S salinity (g kg^{-1}), CO_2 and CH_4 carbon dioxide and methane mass concentrations, respectively (g kg^{-1}), β_S the coefficient of saline concentration (0.75 x 10^{-3} kg g^{-1}; Wüest et al., 1996), β_{CO_2} the coefficient of CO_2 concentration (0.284 x 10^{-3} kg g^{-1}; Ohsumi et al., 1992), and β_{CH_4} the coefficient of CH_4 concentration (-1.25 x 10^{-3} kg g^{-1}; Lekvam and Bishnoi, 1997). Note that profiles of S, CO_2 and CH_4 are kept constant throughout the simulation period. This second experiment is hereafter referred to as the deep simulation.

To compare the model's computational expense, CPU times needed to conduct the WS Kamembe driven simulation at 60 m depth (2557 days) were recorded for each model (Table 4.1). CPU times indicate that FLake is the fastest one-dimensional model, followed by Hostetler, which partly explains their success when it comes to coupling with climate and numerical weather prediction models (e.g. Martynov et al., 2012). The slowest model is LAKE: it requires, for instance, 133 times more computational resources compared to FLake. Although the differences in computation time between one-dimensional models (10^0 – 10^2) are smaller than typical differences between one- and three-dimensional models (10^3 – 10^4, Jöhnk and Umlauf, 2001) – this issue requires consideration in applications where computational efficiency is critical.

Besides the two control integrations from January 2002 to December 2008, 12 additional sensitivity experiments were designed. In particular, a subset of the models was run at both depths for the highest and lowest observed value of the light attenuation coefficient, while for the deep simulation additional experiments without geothermal heat flux and without bottom sediments were conducted. Additionally, each control and sensitivity integration was conducted using the WS Bukavu forcing fields from January 2003 to December 2011. Both in the control and sensitivity experiments, the first year was considered as spin-up and removed from the results. Subsequently, the output of the models was vertically interpolated (increment 1 m) using the piecewise cubic hermite interpolation technique (De Boor, 2001, see also Sect. 3.2.3).

4.3 Results

4.3.1 Model performance over the mixolimnion

While throughout most of the year, Lake Kivu is weakly stratified below 10 – 30 m, the mixed layer deepens during the dry season to approximately 60 m (Fig. 4.2a), driven primarily by the significantly reduced RH at that time,

which opens up the potential for evaporative-driven cooling of near-surface waters, and secondly by the reduced LW_{in} reaching the lake surface due to lower cloudiness (Thiery et al., 2014a). In general, all models succeed in reproducing the enhanced stratification during the rainy season relative to the dry season (Fig. 4.2). Hostetler, CLM4-LISSS and SimStrat however display clearly lower water temperatures, suggesting an underestimation of heat entering the lake (Fig. 4.2b, d). Since this affects the whole water column, it cannot be primarily due to differences in the mixing processes, but is likely due to a different surface energy exchange. In Sect. 4.3.2 this issue is further investigated. Furthermore, in the top 5 m of the water column, LAKE predicts a slightly unstable stratification (Fig. 4.2e). This can be ascribed to a numerical precision artefact of the fully implicit time stepping scheme employed in this model. For each iteration, the numerical procedure solves the temperature conductance equation including radiative heating, and using a Dirichlet top boundary condition. The temperature profile will therefore contain its temperature maximum close to the surface – instead of at the surface – with the abundance of this maximum depending on the eddy conductance at the top layers calculated by the $k - \epsilon$ scheme. Hence, in LAKE the top boundary conditions of the $k - \epsilon$ parameterisation might be inappropriate to successfully simulate the mixing at the top of water column.

From mid 2006 onwards, a sudden temperature decrease appears in all simulated time series, a change hardly visible in the measured data. This apparent cooling is related to a change in the meteorological forcing. During the 2006 dry season, wind velocities attain clearly higher values compared to other years (4.3 m s^{-1} versus 3.6 m s^{-1} for JJA), with the maximum wind velocity measured at this station since 1977 occurring during this period (35 m s^{-1} on June 19 2006). Especially in the models LAKEoneD, SimStrat and LAKE, but to a lesser extent also in FLake, MINLAKE2012 and CLM4-LISSS, the enhanced winds cause a more intense evaporative driven cooling at the start of the dry season relative to previous years. Comparing modelled to observed water temperatures at 5 m, 30 m and 60 m illustrates that this sudden cooling results in a negative bias in all models from mid 2006 onwards (Fig. 4.3). Before that time, however, nearly all models very closely reproduce observed near-surface water temperatures at Ishungu. Hence, either all models react too strongly to the enhanced wind speeds, or wind speeds are overestimated during this period.

Vertical profiles of the BSS (1 m vertical increment, BSS below -20 were set to -20) indicate that models skills decrease with depth in all models (Fig. 4.4a). Since the BSS accounts for the effect of a systematic bias, BSS for Hostetler, CLM4-LISS and SimStrat quickly reach low values. A Taylor diagram, in contrast, allows to assess model performance irrespective of a possible systematic bias, given its use of the normalised standard deviation σ_{norm} (°C), the centred

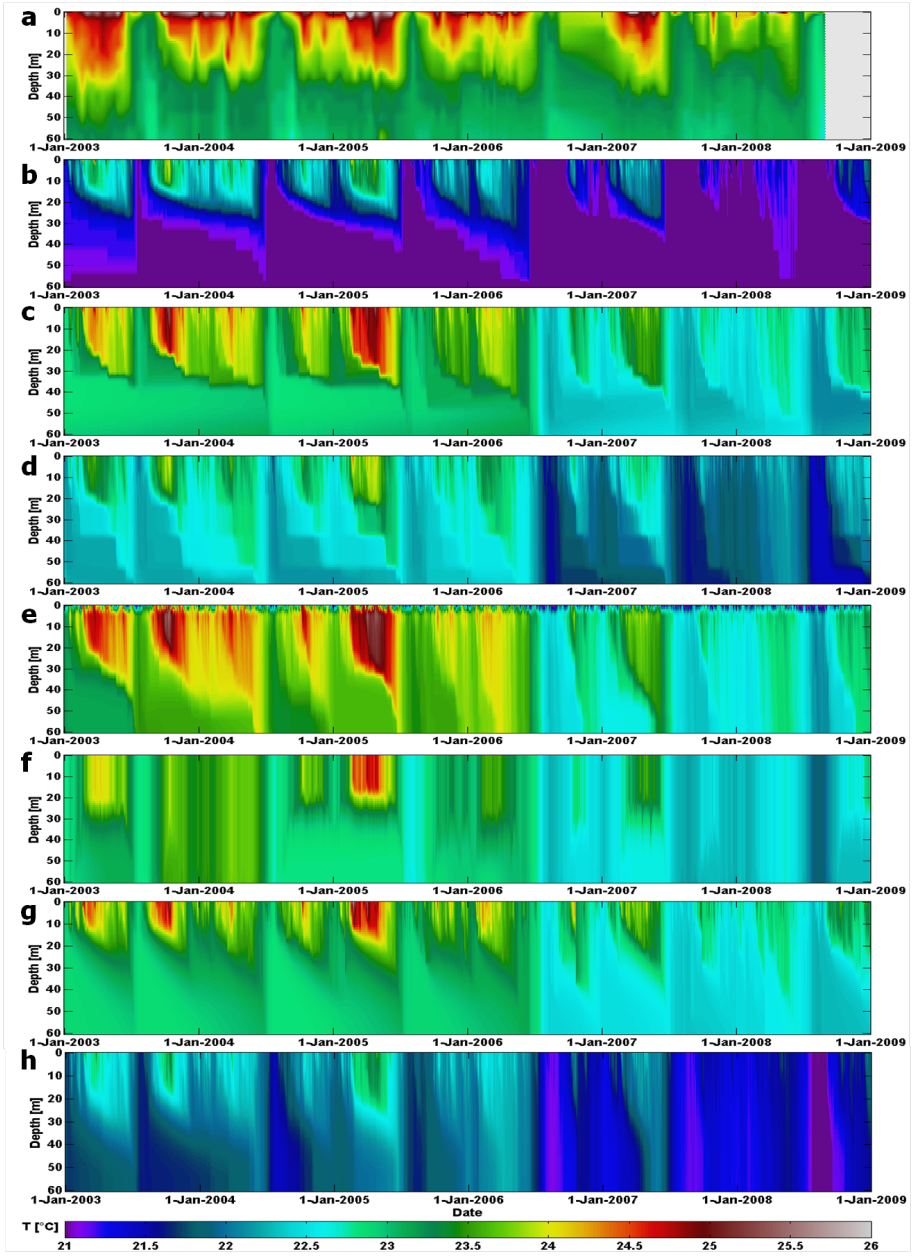

Figure 4.2: **Lake water temperatures (°C) at Ishungu (Lake Kivu), 2003 – 2008: (a) from observations, and as predicted by the models: (b) Hostetler, (c) LAKEoneD, (d) SimStrat, (e), LAKE, (f) FLake, (g) MINLAKE2012, (h) CLM4-LISSS.**

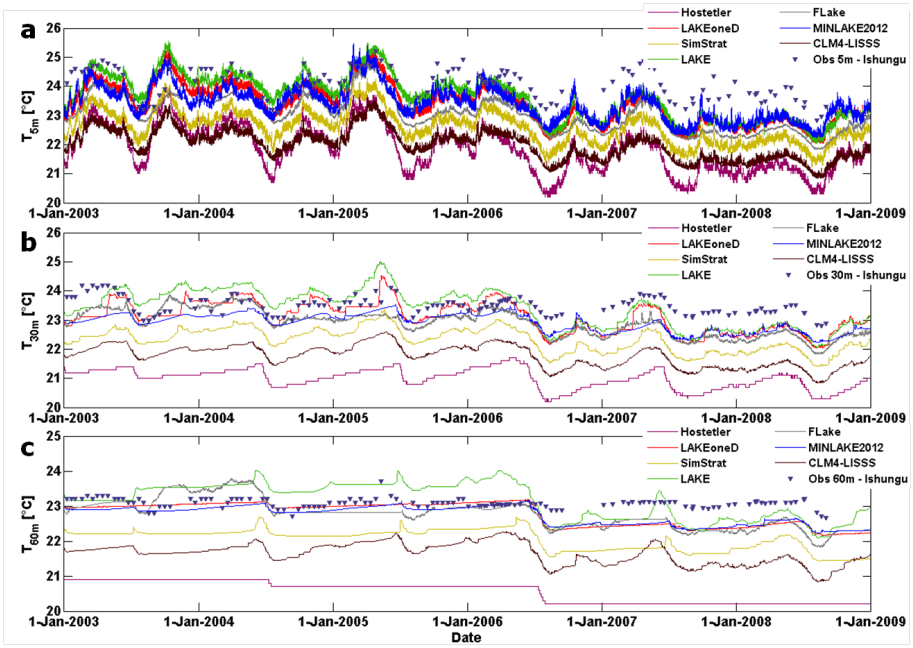

Figure 4.3: **Modelled and observed temperature evolution at Ishungu (Lake Kivu), 2003 – 2008, at (a) 5 m, (b) 30 m, and (c) 60 m depth.**

Root Mean Square Error $RMSE_c$ (°C) and the Pearson correlation coefficient r. Here, surprisingly, the best model scores at 5 m are attained by CLM4-LISSS ($\sigma_{norm} = 0.98$; $RMSE_c = 0.36$ °C; $r = 0.76$), SimStrat ($\sigma_{norm} = 1.11$; $RMSE_c = 0.39$ °C) and Hostetler ($r = 0.78$) (Fig. 4.5a). Also at 30 m and 60 m, all three models depict high skills: at these depths they are only outperformed by MINLAKE2012 in terms of σ_{norm} and $RMSE_c$ (Fig. 4.5b-c). Hence, although Hostetler and SimStrat both depict a cold bias, they most successfully reproduce seasonal and interannual lake water temperature variability. On the other hand, towards deeper layers both LAKE and, to a lesser extent, FLake depict reducing skill compared to other models (Fig. 4.5b-c). For LAKE, the overestimation of the observed variance can probably be explained by a higher sensitivity of LAKE to wind velocity relative to other models (Fig. 4.2), whereas for FLake, this might be ascribed to the fully mixed conditions predicted during the 2003-2004 wet season (Fig. 4.2f): in both cases this increases the deep water temperature variability during the integration period (Fig. 4.2c).

The different sensitivity experiments generally show only a small response from the models, except for FLake (not shown). This model exhibits a marked

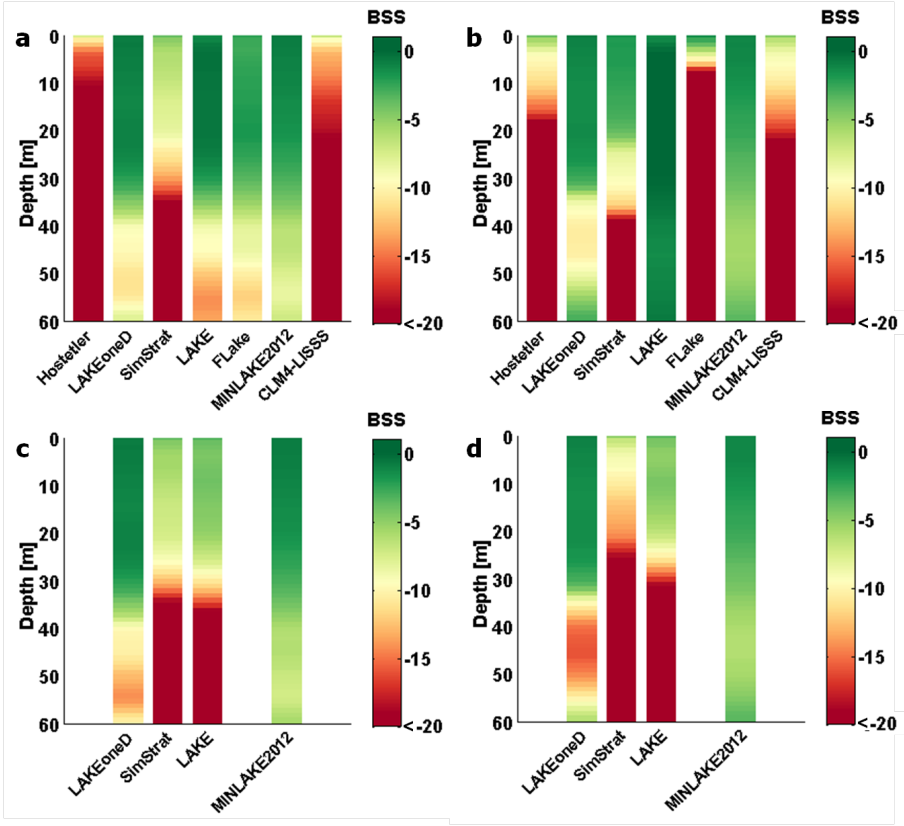

Figure 4.4: **Brier Skill Score (BSS) vertical profiles at Ishungu (Lake Kivu), calculated per 1 m vertical increment over the respective integration period, for (a) the WS Kamembe 60 m, (b) the WS Bukavu 60 m, (c) the WS Kamembe 240 m and (d) the WS Bukavu 240 m integrations. Note that Hostetler, FLake and CLM4-LISSS were not applied in the 240 m depth experiment.**

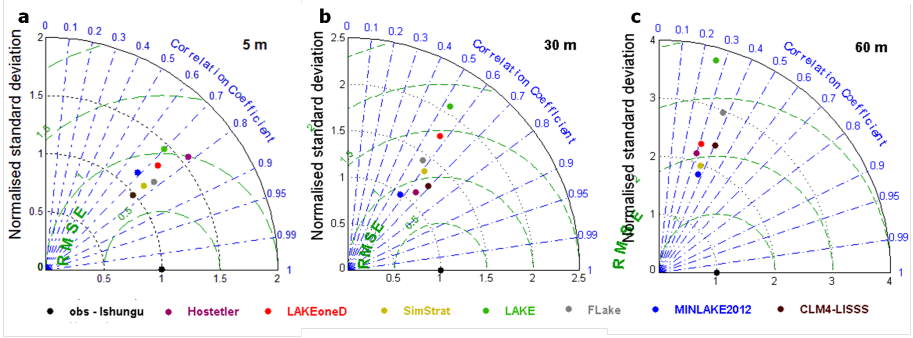

Figure 4.5: **Taylor diagram indicating model performance for water temperature at (a) 5 m, (b) 30 m and (c) 60 m depths at Ishungu (Lake Kivu), 2003 – 2008. Normalised standard deviation σ_{norm} (°C; radial distance), centred Root Mean Square Error $RMSE_c$ (°C; distance apart) and Pearson correlation coefficient r (azimuthal position of the simulation field) were calculated from the observed temperature profile interpolated to a regular grid (1 m increment) and the corresponding modelled midday profile.**

sensitivity to its configuration. Setting the light attenuation coefficient k to the highest and lowest value observed at Ishungu (WS Kamembe forcing), generally has little effect upon the different model's ability to represent water column temperatures. Vertically averaged BSS never change more than 20%, except for FLake in case of increasing k (BSS reduces by 60% as average water column temperature values cool by 0.15 °C) and MINLAKE2012 when decreasing k (BSS increases by 25%). Note that when k is reduced to 0.20 m^{-1}, BSS increases for Hostetler, LAKEoneD, FLake and MINLAKE2012.

Each control and sensitivity experiment was also conducted using meteorological measurements at Bukavu (Fig. 4.1) as forcing. Relative to the WS Kamembe driven control integration, vertically averaged BSS of Hostetler, LAKEoneD, SimStrat, MINLAKE2012 and CLM4-LISSS showed little to no change when forced by the alternative dataset (Fig. 4.4b). In contrast, LAKE enhances its predictive skill, whereas FLake's predictions deteriorate below ∼5 m. For LAKE, model predictions improve especially because the observed water temperature variability at depth is well captured when forced by WS Bukavu. When LAKE is forced by WS Kamembe, significant wind velocity increases during the dry season result in too strong mixing. For FLake, the WS Bukavu driven simulation decreases in predictive skill as from mid 2004 onwards, a strong cooling of the thermocline layer sets in, reaching down to the temperature of maximum density (4 °C) near the bottom. Note however that this effect does not influence the good skill of FLake near the surface (Fig. 4.4a, b).

This cooling of thermocline layer in FLake has been encountered in previous studies (Subin et al., 2012b; Thiery et al., 2014a) and during the development of its online version, FLake-Global (Kirillin et al., 2011). The thermal behaviour of dimictic and temperate polymictic lakes, where the average water column temperature approaches the temperature of maximum density twice or several times a year, respectively, can generally be reproduced very closely by FLake (e.g. Kirillin, 2010; Martynov et al., 2010). Lake Kivu's mixolimnion, in contrast, is characterised by a weak stratification, with a seasonally mixed layer deepening down to ∼60 m, so the model needs to be able to develop and maintain this weak stratification. Possibly, the observed transition to the shallow, permanent stratification and cold bottom is related to the self-similar representation of the shape factor of the thermocline and its time rate-of-change. When the mixed layer deepens, FLake will respond by changing its thermocline shape towards a more convex shape (Mironov, 2008). However, during aforementioned cooling, the thermocline's shape factor is permanently at its maximum value, 0.8 (maximum convexity), thus inhibiting any thermocline response to mixed layer deepening. As the small-scale fluctuations of the mixed layer depth are not mirrored by changes in the thermocline shape, they could cause an unphysical loss of heat from the thermocline layer. This effect might be responsible for the observed cooling near the lake bottom which can reach down to 4 °C and therewith trigger an irreversible switch to a permanently stratified mixing regime, but further research is necessary to investigate this issue.

4.3.2 Lake energy balance

Differences in column-integrated water temperatures between the one-dimensional lake models can be understood when comparing their lake energy budget. To this end, we first employ the relationship describing the enthalpy change H_{obs} of the lake's top 60 m (assuming constant pressure):

$$H_{obs} = h\rho c_p \frac{d\bar{T}}{dt} \tag{4.5}$$

with h the water column height (60 m), ρ the lake water density (1000 kg m^{-3}), c_p the specific heat capacity of water at constant pressure (4.1813 x 10^3 J kg^{-1} K^{-1}) and $d\bar{T}/dt$ the average water column temperature change computed per output time step based on the observed temperature profiles. Since all models switched off the bottom sediment routine and adopted a zero heat flux assumption at the artificial lake bottom, the predicted enthalpy change H_{mod} is given by:

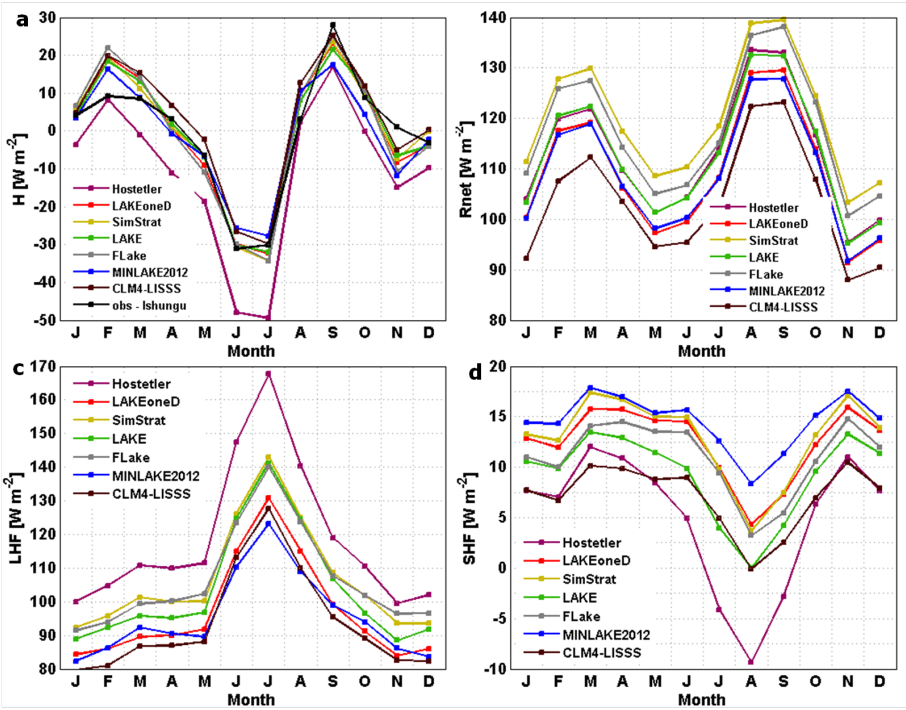

Figure 4.6: **Monthly average lake energy balance components (W m^{-2}) at Ishungu (Lake Kivu), 2003 – 2008, calculated by model's surface flux routines. Components are (a) lake enthalpy change H, (b) net radiation R_{net}, (c) latent heat flux LHF, and (d) sensible heat flux SHF.**

$$H_{mod} = R_{net} - LHF - SHF \tag{4.6}$$

with R_{net} the net radiation, and with LHF and SHF the turbulent fluxes of latent heat and sensible heat, respectively (all units W m^{-2}). Comparison of monthly average H_{obs} and H_{mod} shows that H_{mod} is well captured by the different models throughout most of the year (Fig. 4.6a). Although the observed variation is also subject to uncertainty, this given the CTD casts' low temporal resolution and variable collection hours, the good agreement between model and observation indirectly suggests that the seasonal cycles of the radiative inputs and turbulent fluxes are correctly reproduced.

Table 4.3: **Net radiation R_{net} (W m^{-2}) calculation used in this study by the different one-dimensional lake models to close the hourly lake energy balance. The terms are: shortwave (longwave) albedo α_{SW} (α_{LW}), incoming shortwave (longwave) radiation SW_{in} (LW_{in}), outgoing longwave radiation LW_{out}, SW_{in} fractioning coefficient $\beta = 0.35$ (35% to near-infrared, 65% to visible/ultraviolet radiation). Formulations are valid for each 1 h output time step (except LAKEoneD where this is for the last time step of each hour), with Δ denoting the change between the previous and current time step. Note that CLM4-LISSS does not account for SW_{in} when the computed zenith angle is at or below the horizon.**

Lake model	Net radiation calculation
Hostetler	$R_{net} = (1-\alpha_{SW})SW_{in} + (1-\alpha_{LW})LW_{in} - LW_{out}$
LAKEoneD	$R_{net} = (1-\beta)(1-\alpha_{SW})SW_{in} + \beta SW_{in} + (1-\alpha_{LW})LW_{in} - LW_{out}$
SimStrat	$R_{net} = (1-\alpha_{SW})(SW_{in,t-1} + 7/12\Delta SW_{in}) + (LW_{in,t-1} + 7/12\Delta LW_{in}) - LW_{out}$
LAKE	$R_{net} = (1-\beta)(1-\alpha_{SW})(SW_{in,t-1} + 2/3\Delta SW_{in}) + \beta(SW_{in,t-1} + 2/3\Delta SW_{in}) + (1-\alpha_{LW})(LW_{in,t-1} + 2/3\Delta LW_{in}) - LW_{out}$
FLake	$R_{net} = (1-\alpha_{SW})SW_{in} + LW_{in} - LW_{out}$
MINLAKE2012	$R_{net} = (1-\beta)(1-\alpha_{SW})SW_{in,t-1} + \beta SW_{in,t-1} + (1-\alpha_{LW})LW_{in,t-1} - LW_{out}$
CLM4-LISSS	$R_{net} = (1-\alpha_{SW})(SW_{in,t-1} + 1/4\Delta SW_{in}) + (LW_{in,t-1} + 1/4\Delta LW_{in}) - LW_{out}$

Besides variations in the computation of LHF and SHF, also different formulations are employed by the models to determine R_{net}, as shown in Table 4.3. In particular, note that FLake and CLM4-LISSS assume $\alpha_{LW} = 0$, while LAKE and LAKEoneD assume $\alpha_{SW} = 0$ for the near-infrared fraction of SW_{in}, on average responsible for a higher energy input into the lake of 11 W m^{-2} and 5 W m^{-2}, respectively. Also, given the small time step used by LAKE, SimStrat and CLM4-LISSS, SW_{in} and LW_{in} require modification to achieve surface heat balance closure over each output time step. Finally, MINLAKE2012 employs the input radiative fluxes of the previous time step to compute hourly values. As a consequence of these differences, models predict variable radiative input into the lake: maximum discrepancies of monthly mean R_{net} values range from 13 W m^{-2} to 20 W m^{-2} (Fig. 4.6b). The radiative input into the lake peaks twice a year: once during February-March and again during August-September, in agreement with the two distinct maxima in SW_{net} and the drop in LW_{net} from May to July.

In contrast to the treatment of radiative fluxes, turbulent energy exchanges show more variation among different models. For instance, relative to other participating models, in the Hostetler model, a higher portion of the available heat is consumed by evaporation: the annual mean LHF in the control integration is 14 W m^{-2} higher relative to the multi-model mean LHF (105 W m^{-2}; Fig. 4.6c), equivalent to an enhanced total lake evaporation of 0.5 km^3

yr^{-1}. Over time, the resulting year-round reduction in net energy available to heat the lake will therefore enhance the cold bias observed for the Hostetler model (Fig. 4.6a, 4.3), even though the enhanced evaporative cooling is partly compensated by the limited energy loss through the SHF and the higher radiative input into the lake, equivalent to 6 W m^{-2} lower and 2 W m^{-2} higher compared to multi-model means, respectively (Fig. 4.6d, b). For SimStrat, in turn, on the one hand slightly higher radiative input into the lake (+7 W m^{-2} relative to the multi-model mean) and on the other hand slightly positive LHF (+4 W m^{-2}) and SHF (+3 W m^{-2}) anomalies compensate for each other and generate a close reproduction of the observed enthalpy change, hence no change of the cold bias is expected (Fig. 4.6a,c,d). By analogy, also for CLM4-LISSS the cold bias is not expected to change over time (Fig. 4.6a). In future intercomparison experiments, wherein lake models will be interactively coupled to atmospheric models, the impact of variations in the turbulent heat fluxes on lake models will require further attention.

Besides differences among the models, also intra- and inter-annual variations in the water column stratification can be attributed to meteorological variability and associated changes in the lake energy balance. Since all models report high to very high correlations between wind velocity and LHF (with correlation coefficients up to 0.95 ($p < 0.01$) in Hostetler and LAKEoneD, for instance), and because stronger winds cause enhanced mechanical mixing, variations in wind speed must certainly be considered in this case. In particular, the increasing annual mean wind velocities explain the generally reducing stratification observed throughout the integration period, as well as the sudden decrease in water temperatures observed mid 2006 (Sect. 4.3.1) and the very weak stratification during the first months of 2008 (Fig. 4.2a). However, variations in wind velocity provide no explanation for the high near-surface water temperatures and relatively strong stratification observed during the first months of 2005 (Fig. 4.2a). During this period, enhanced solar radiation reaches the lake surface, therewith increasing the amount of energy available to stratify the near-surface layers. In response to this relatively high radiative forcing (Fig. 4.7c), but normal turbulent heat fluxes (Fig. 4.7a,b) at the start of 2005, all models show similar variability in the lake's enthalpy change (Fig. 4.7d), and therewith reproduce the enhanced stratification during this period.

4.3.3 Deep water stratification

The deep simulations conducted by a subset of models (LAKEoneD, SimStrat, LAKE, MINLAKE2012) all succeed in reproducing Lake Kivu's meromictic state (Fig. 4.8). Compared to the corresponding freshwater simulation, all models display similar BSS for the top 60 m of the water column, except for

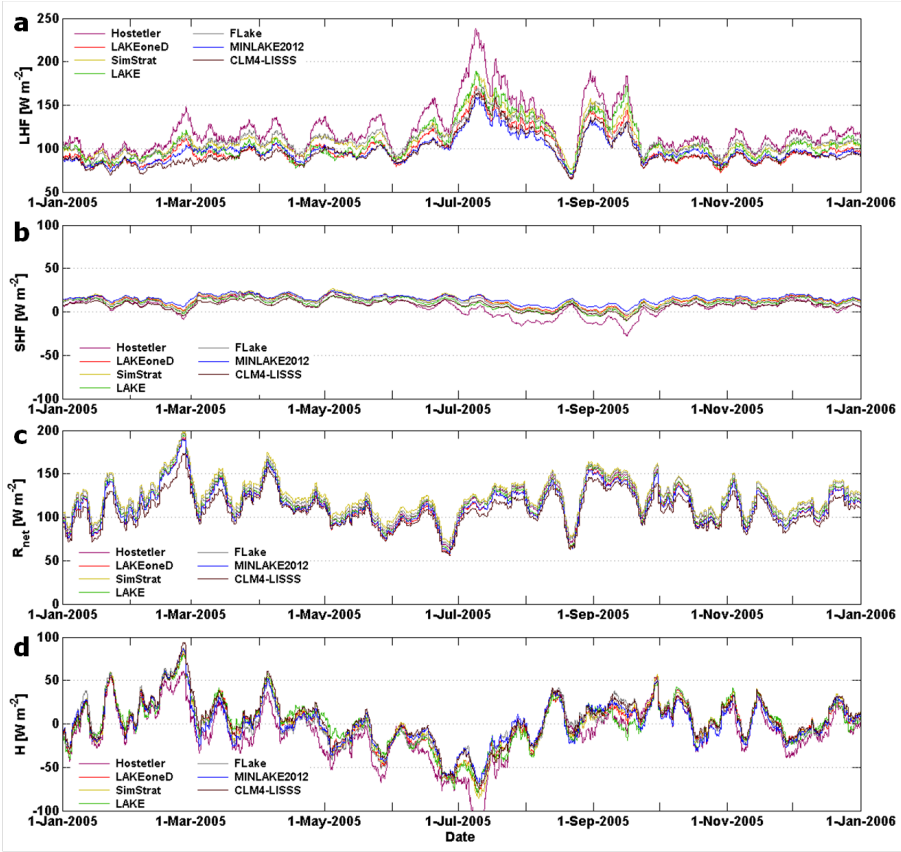

Figure 4.7: **Running mean lake energy balance components (W m^{-2}; seven days averaging window) at Ishungu (Lake Kivu), for 2005. Components are (a) latent heat flux LHF, (b) sensible heat flux SHF, (c) net radiation R_{net}, and (d) the resulting lake enthalpy change H.**

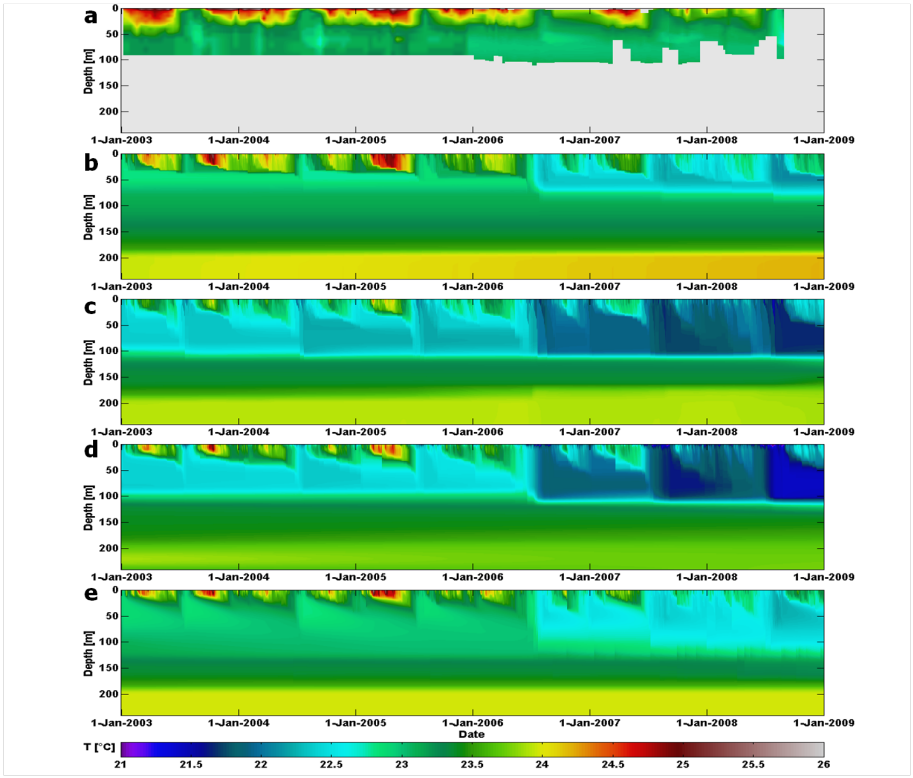

Figure 4.8: **Lake water temperatures (°C) at Ishungu (Lake Kivu), 2003 – 2008: (a) as observed, and as predicted by the models: (b) LAKEoneD, (c) SimStrat, (d), LAKE, (e) MINLAKE2012 for the 240 m deep geometry. Note that linear interpolation was applied to the observed Ishungu profiles to avoid spurious extrapolation effects, and grey areas therefore denote depths or longer time periods for which no observations are available.**

LAKE, where a cold bias decreases the BSS towards 60 m (Fig. 4.4c). Again, it is found that setting the light extinction coefficient to the highest and lowest observed values at Ishungu, or switching off the bottom sediment routine, has little to no impact upon the results of LAKEoneD, LAKE and MINLAKE2012.

Below 60 m, modelled temperature variations are only regulated by thermal diffusion. In the permanently stratified hypolimnion represented in the deep simulations (Fig. 4.8), the eddy diffusivity usually vanishes and molecular diffusivity becomes the dominant term. In Lake Kivu, both double diffusive convection (Schmid et al., 2010) and subsurface inflows (Schmid et al., 2005),

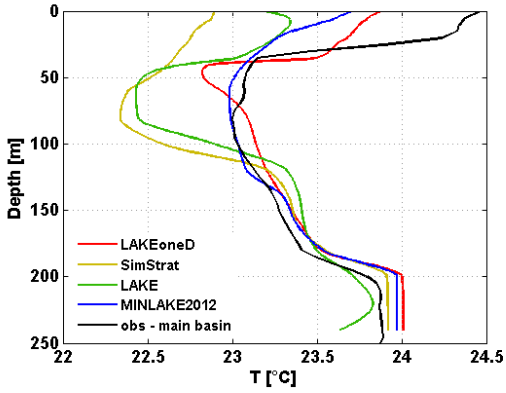

Figure 4.9: **Comparison of the observed temperature profile representative for the main basin during February 2004, as reported by Schmid et al. (2005, reproduced with permission), and corresponding modelled profiles (February 2004 average).**

associated with the slow upward motion of the whole water column by about 0.5 m yr^{-1}, additionally influence the deep water temperature structure. However, none of the models involved in this study include mechanisms to account diffusivity generated by these processes. Nevertheless, the predicted temperature profiles still correspond fairly well to the observed temperature profile in the main basin during February 2004 (Schmid et al., 2005), i.e. two years after being initialised with this profile (Fig. 4.9).

In the last ∼50 m above ground, the heat input into the deep zone starts to influence water temperatures. At the bottom of Lake Kivu, strong geothermal heating can be expected due to its location on the East African rift. In addition to the geothermal heat flow, some warm, subaquatic springs heat the bottom layers. Together, their magnitude was estimated at 0.1-0.3 W m^{-2} by Schmid et al. (2010). The excess heat is removed both by the upward motion and enhanced diffusion through the double-diffusive staircases (Schmid and Wüest, 2012). Relative to the sensitivity experiment wherein the bottom heat flux is neglected, average temperature of the lowest 50 m are 0.02 to 0.18 °C higher when including the bottom heat flux leads, while the water masses above this depth are almost not affected by the bottom heat flux. Throughout the integration period, LAKEoneD exhibits a warming trend of 0.24 °C for the lowest 50 m, while the other comprehensive model show no temperature change for this zone.

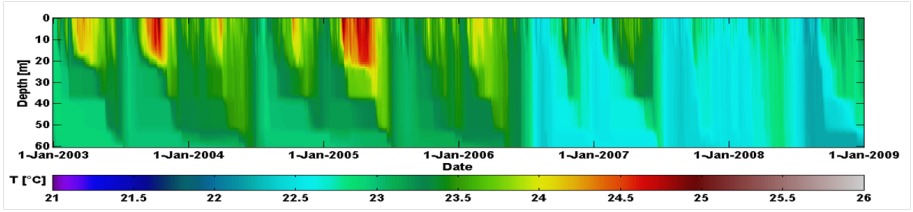

Figure 4.10: **Lake water temperatures (°C) at Ishungu (Lake Kivu), 2003 – 2008, as predicted by SimStrat, using a modified turbulent heat flux calibration parameter.**

4.4 Discussion

4.4.1 Model improvement

At this point, an interesting question is if, and in which way, the performance of individual models can be improved. For instance, for FLake, which was found sensitive both to its model configuration and forcing fields when applied to a deep, tropical lake, enhancing the robustness of the model would be beneficial. Work is currently underway to meet this need. Therewith, potentially this model will become more applicable to large, deep lakes for which no accurate forcing fields and external parameter values are available.

While for the one-dimensional lake models Hostetler, CLM4-LISSS and SimStrat, a key asset is the ability to capture the observed water temperature variability, a cold bias is observed in each case (Fig. 4.2, 4.3). However, the systematic bias can be removed through a calibration step. To illustrate the potential of a bias correction procedure, all simulations with the SimStrat model were also conducted using a modified calibration parameter for the turbulent heat fluxes. In SimStrat, the SHF and LHF are deduced from an empirical formulation which contains a parameter to calibrate the obtained result within a certain range. Through a much better reproduction of the observed lake enthalpy change, SimStrat predictions significantly improved: for instance, for the WS Kamembe driven freshwater simulation, there is now a very close agreement between modelled and observed water temperatures (Fig. 4.2, 4.10). In particular, the vertically averaged BSS increased from -23.5 to -2.9, therewith even obtaining the highest score of all models. In short, the success of the bias correction procedure illustrates the added value of a model outcome containing a systematic bias, but a correct reproduction of the observed variability, over an unbiased prediction which fails to reproduce the observed variability.

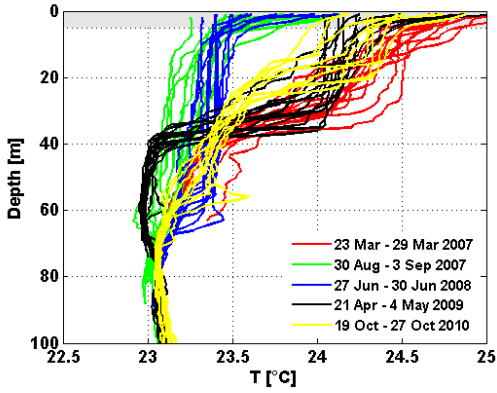

Figure 4.11: **Temperature profiles collected at 14 different locations in Lake Kivu during 5 cruises. Profiles collected at Bukavu and Kabuno bay are omitted due to their clear deviation from profiles of the main basin. Differences in the top 5 m (grey shade area) are partly due to daily variations.**

4.4.2 Validity of the horizontal homogeneity assumption

Analysis of 60 temperature profiles collected during five cruises from March 2007 to October 2010 shows that spatial differences are clearly less important than seasonal variations (Fig. 4.11). Maximum horizontal temperature variations during a single cruise range from 0.3 °C to 0.6 °C (0.5 °C on average) at 5 m depth, while maximum temporal temperature fluctuations at one location range from 0.3 to 1.5 °C (1.1 °C on average) at 5 m. Towards 60 m, vertical temperature profiles converge, both in space and time. In agreement, previous studies report very similar thermal, chemical and biological lake characteristics across all sub basins except Bukavu and Kabuno bay, and attribute horizontal homogeneity in the monimolimnion to long residence times (Sarmento et al., 2006; Pasche et al., 2009, 2011; Tassi et al., 2009; Schmid and Wüest, 2012). The assumption of horizontal homogeneity can thus be considered valid for Lake Kivu.

4.5 Conclusion

The model intercomparison experiment for Lake Kivu showed that all models succeed in reproducing the timing and magnitude of water temperatures in the mixolimnion and the observed lake enthalpy change. Moreover, during the integration period the models accounting for the effects of salinity and

dissolved gases upon the water column stratification can correctly represent the meromictic state of Lake Kivu. At the same time, this study also revealed a number of strengths and weaknesses for the different groups of models.

First, while FLake is computationally the most efficient and depicts good predictive skill in the control simulation compared to other models, water temperatures towards the bottom of Lake Kivu's mixolimnion are found sensitive to modifications in the forcing fields and model configuration. Further research is needed to address the ability of FLake to represent weakly stratified lakes. However, since near-surface temperatures, in contrast to near-bottom temperatures, are more robust, the model remains a good candidate in applications where a quick and reliable computation of lake surface temperatures is important.

Second, given their limited computational expense, the Hostetler-based models (Hostetler and CLM4-LISSS) are also attractive candidates to represent lake processes within atmospheric models. Although both models predict colder water temperatures compared to observations, they correctly reproduce the observed variability, and a model calibration can potentially correct for the small systematic bias.

Third, the more comprehensive lake models, i.e. MINLAKE2012 and the $k-\epsilon$ models SimStrat, LAKE and LAKEoneD, not only capture the variability of Lake Kivu's mixolimnion and therewith the effects of the meteorological controls on mixing, they also succeed in reproducing the effect of salinity and dissolved gases on the stratification. Sometimes, individual models react stronger to a certain forcing than other models, such as the heating in the lowest layers of LAKEoneD in response to the imposed geothermal heat flow (deep simulation), or the marked response to wind stress in LAKE. However, altogether, the considered comprehensive lake models are suited to investigate hydrodynamic processes occurring within large, deep lakes, and therewith make way for further studies of, for instance, biogeochemical cycling within these lakes.

Thanks to this and previous lake model intercomparison studies, the selection of a one-dimensional lake model most appropriate for a certain purpose can now be based on an informed choice. The aforementioned set of strengths and weaknesses may serve as a first indication in this respect. At the same time, this set calls for continuing the development of individual lake models, and for monitoring their progress in future intercomparison experiments.

4.6 Acknowledgements

We would like to thank Martin Schmid for the helpful discussions on this project. The Institut Supérieur Pédagogique in Bukavu and Meteo Rwanda are acknowledged for supplying meteorological observations, and Alberto V. Borges for providing the temperature profiles of the CAKI cruises. This work was partially funded by the Research Foundation – Flanders (FWO), the Belgian Science Policy Office (BELSPO) through the research project EAGLES, and the Fund for Scientific Research (FNRS) through the research projects CAKI and MICKI, and used resources of the National Energy Research Scientific Computing Center (NERSC).

Chapter 5

The impact of the African Great Lakes on the regional climate

This chapter is published as: Thiery, W., Davin, E.L., Panitz, H.-J., Demuzere, M., Lhermitte, S., and Van Lipzig, N., 2015. The impact of the African Great Lakes on the regional climate. *Journal of Climate* 28(10), 4061-4085. doi:10.1175/JCLI-D-14-00565.1

Although the African Great Lakes are important regulators for the East African climate, their influence on atmospheric dynamics and the regional hydrological cycle remains poorly understood. We aim to assess this impact by comparing a regional climate model simulation which resolves individual lakes and explicitly computes lake temperatures to a simulation without lakes. The Consortium for Small-scale Modeling regional climate model (COSMO-CLM), coupled to the Freshwater Lake model (FLake) and Community Land Model (CLM), is used to dynamically downscale a CORDEX-Africa (Coordinated Regional Climate Downscaling Experiment) simulation to 7 km grid spacing for the period of 1999-2008. Evaluation of the model reveals good performance compared to both in situ and satellite observations, especially for spatio-temporal variability of lake surface temperatures (0.68 K bias), and precipitation (-116 mm yr^{-1} *or 8% bias). Model integrations indicate that the four major African Great Lakes almost double the annual precipitation amounts over their surface, but hardly exert any influence on precipitation beyond their shores. Except for Lake Kivu, the largest lakes also cool the annual near-surface air by -0.6 to -0.9 K on average, this time with pronounced downwind influence. The lake-induced cooling happens during daytime, when the lakes absorb incoming solar radiation*

and inhibit upward turbulent heat transport. At night, when this heat is released, the lakes warm the near-surface air. Furthermore, Lake Victoria has a profound influence on atmospheric dynamics and stability as it induces circular airflow with over-lake convective inhibition during daytime, and the reversed pattern at night. Overall, this study shows the added value of resolving individual lakes and realistically representing lake surface temperatures for climate studies in this region.

5.1 Introduction

The African Great Lakes (AGL) represent the largest reservoir of freshwater lakes in the tropics, including the second largest freshwater lake on earth in terms of surface area (Lake Victoria, 68800 km^2) and the second largest in terms of volumetric water storage (Lake Tanganyika, 17800 km^3). The AGL provide numerous ecosystem services to local communities, such as fishing resources, drinking water, and electrical power. Lake Victoria alone directly supports 200,000 fishermen operating from its shores and sustains the livelihood of more than 30 million people living at its coasts (Semazzi, 2011).

Lakes also influence regional climate conditions, in particular in regions where they are abundant. Mediated by the fluxes of energy, moisture and momentum, they significantly alter the surface energy and water balance in a particular region, and therewith its climate. Such reciprocal relations are often studied using numerical models. At the global scale, general circulation model (GCM) studies demonstrate an average annual cooling effect of lakes, but also highlight important seasonal and regional effects (Bonan, 1995; Subin et al., 2012a; Rooney and Bornemann, 2013). Numerous studies also mention the increase in annual precipitation due to the presence of lakes (e.g. Coe and Bonan, 1997). Regional climate model (RCM) studies have been performed at higher horizontal resolution (e.g. 50 km), thereby better emphasizing the lake-atmosphere interplay at the local scale (e.g. Hostetler et al., 1994; Hostetler and Giorgi, 1995; Bates et al., 1995; Goyette et al., 2000; Anyah et al., 2006; Samuelsson et al., 2010; Gula and Peltier, 2012; Lauwaet et al., 2012; Martynov et al., 2012; Gu et al., 2013; Notaro et al., 2013; Bennington et al., 2014; Williams et al., 2014).

Although the AGL are widely recognized as an important driver of the East African regional climate system, their impact on atmospheric dynamics and the regional hydrological cycle remains poorly understood. Studies on the interplay between climate and the AGL are therefore necessary to identify, among other information, the patterns of evaporation and precipitation induced by lake presence, and the reasons behind their observed spatio-temporal variability. The need to enhance the understanding is urgent as every year, possibly more than 5000 fishermen lose their life over Lake Victoria alone, mostly due to hazardous weather conditions and associated water currents (Semazzi, 2011).

The poor understanding of African Lake-climate interactions is related to a number of challenges when applying a regional climate model to the AGL region. (i) First, a model should be applicable to tropical conditions. Amongst others, such a set-up must be able to reproduce tropical features such as deep convection or mesoscale convective systems (and associated precipitation extremes, Lauwaet

et al., 2009; Goyens et al., 2011) and must include a land surface model (LSM) capable of simulating tropical vegetation. In recent climate model studies over tropical Africa, these challenges have received particular attention (e.g. Vizy and Cook, 2012; Saeed et al., 2013; Crétat et al., 2014; Panitz et al., 2014; Dosio et al., 2014). (ii) Second, the horizontal model grid resolution should be sufficiently high to resolve individual lakes and strong orography of the region. Combined with the long integration period and high vertical extent necessary to model tropical climatic conditions, the need for computational resources rises. (iii) Third, a correct representation of lake surface temperatures within the atmospheric model is essential to investigate the two-way interactions between climate and lake processes over East Africa (Stepanenko et al., 2013). This can be particularly challenging for large, deep lakes given the role of vertical heat transport and three-dimensional water circulation within these lakes (Gu et al., 2013; Bennington et al., 2014). (iv) Finally, the limited number of observational datasets available, and issues regarding the quality of available products over highly mountainous, tropical domains (e.g. Dinku et al., 2008) complicate a comprehensive model evaluation over this region. Consequently, up to now only few RCM studies explicitly examine aspects of lake-atmosphere interactions over a specific African Great Lake (Savijärvi and Järvenoja, 2000; Song et al., 2004; Anyah and Semazzi, 2004; Anyah et al., 2006; Argent et al., 2014; Sun et al., 2014, 2015; Williams et al., 2014), while none investigates these interactions for the whole region.

Hence, the main goals of this study are to assess the regional climate impact of the AGL, and understand the physical mechanisms underlying these impacts. This is achieved by addressing the aforementioned challenges in the following way: (i) The regional climate model COSMO-CLM (COSMO model in Climate Mode; Rockel et al., 2008) is applied in its tropical set-up (configuration following Panitz et al., 2014). In their comprehensive evaluation of the COSMO-CLM evaluation simulation conducted in the framework of the African Coordinated Regional Climate Downscaling Experiment (CORDEX-Africa; Giorgi et al., 2009), Panitz et al. (2014) demonstrate the ability of COSMO-CLM to reproduce the overall features of the African climate (when downscaling ERA-Interim), and show that, relative to several gridded observational products, it even outperforms ERA-Interim in terms of the mean annual precipitation cycles and interannual variability over major parts of the domain. Among the considered regional biases, the authors point to an underestimation of the precipitation intensity by 2 mm day^{-1} in East Africa, which is ascribed to an underestimation of the latent heat flux and overestimation of the sensible heat flux. To address this issue, here we employ COSMO-CLM coupled to a state-of-the-art LSM, the Community Land Model version 3.5 (CLM3.5; Davin and Seneviratne, 2012). For various applications this version already showed improved skills compared to the standard version (see section 5.2.1). (ii) Model integrations

are performed for a period of 13 years on a horizontal resolution high enough for large to medium-sized lakes to become resolved features (0.0625°; ∼7 km). (iii) The one-dimensional fresh-water lake model (FLake), recently coupled to COSMO-CLM (Mironov et al., 2010), is used to compute lake water surface temperatures. (iv) Special attention is paid to model evaluation, in particular by using remote sensing products and comprehensive in situ observational datasets to assess the model's ability to reproduce observed spatial and temporal lake surface temperature variability, turbulent fluxes and precipitation. Adopting one or more of the above challenges may improve the representation of the regional climate, as demonstrated in many recent studies (e.g. Mironov et al., 2010; Nikulin et al., 2012; Akkermans, 2013; Laprise et al., 2013; Akkermans et al., 2014; Crétat et al., 2014; Dosio et al., 2014; Williams et al., 2014).

Within this paper, the results of the RCM control simulation are extensively evaluated. This simulation is subsequently compared to a no-lake simulation where the lakes are replaced by representative land pixels. This approach makes it possible to quantify the impact on the regional climate, in particular on near-surface temperature and precipitation. The impact of the lakes is then investigated in more detail by applying a surface energy balance decomposition technique and studying the dynamical changes induced by the lakes.

5.2 Model, data and methodology

5.2.1 COSMO-CLM^2

To investigate the influence of the AGL on the climate, we use the three-dimensional, non-hydrostatic regional climate model, COSMO-CLM (Rockel et al., 2008) version 4.8. The model development is a joint effort of the Consortium for Small-scale Modelling (COSMO) and the Climate Limited-area Modelling Community (CLM-community). Its dynamical core solves the fully compressible hydro-thermodynamical equations for three-dimensional Cartesian wind components, pressure perturbation, temperature, specific humidity, cloud water content and optionally cloud ice content, turbulent kinetic energy, and rain, snow and graupel specific water content (Doms, 2011). Physical parameterizations include a description of subgrid-scale turbulence (Raschendorfer, 2001), grid-scale clouds and precipitation (Doms et al., 2011), shallow and moist convection (Tiedtke, 1989) and δ-two-stream radiative transfer (Ritter and Geleyn, 1992). A detailed description of the model system dynamics, numerics and physical parameterizations can be found in the model documentation (e.g. Doms, 2011; Doms et al., 2011, http://www.cosmo-model.org).

Additionally, the native COSMO-CLM Multi-Layered land surface model (TERRA-ML, Grasselt et al., 2008) is replaced by the more comprehensive Community Land Model (CLM, Oleson et al., 2004, 2008) version 3.5. CLM3.5 is maintained at the National Center for Atmospheric Research (NCAR), and given its explicit treatment of the photosynthetic process and its control on the stomatal conductance ("big-leaf" approach), it can be considered a third generation LSM (Sellers et al., 1997). Moreover, an individual land pixel can be composed of multiple land units due to the nested tile approach, which allows representation of multiple soil columns and represents biomes as a combination of different plant functional types. An extensive description and evaluation of CLM3.5 in offline mode are presented in Oleson et al. (2004, 2008) and Stöckli et al. (2008).

The model system COSMO-CLM coupled to CLM3.5 (hereafter referred to as COSMO-CLM^2) is described in detail by Davin and Seneviratne (2012) and references herein. The added value of COSMO-CLM^2, relative to the standard set-up, was recently demonstrated over Europe (Davin et al., 2011; Davin and Seneviratne, 2012; Lorenz et al., 2012) and central Africa (Akkermans, 2013). A better partitioning of the turbulent fluxes and associated improvement of climate characteristics, such as near-surface temperature, precipitation and cloud cover, were found in all cases, supporting the usage of this model for studying biogeophysical impacts of altered land surface characteristics (e.g. Davin et al., 2014; Lejeune et al., 2014; Jacobs et al., 2015a). Based on an offline comparison of both LSMs at four central African flux tower sites, Akkermans et al. (2012) attributed this enhanced skill mainly to a more realistic representation of the leaf area index, surface albedo and root depth in CLM3.5 compared to TERRA-ML. Furthermore, Akkermans et al. (2014) extensively evaluated COSMO-CLM^2 over the larger central African domain and found a close correspondence between the observed and modeled near-surface temperature, column precipitable water and surface net longwave radiation. For precipitation, cloud cover, top of the atmosphere outgoing longwave radiation and various solar radiation quantities, the model adequately reproduced observed values, with some notable differences potentially ascribed to an underestimation of the optical thickness of convective clouds by COSMO-CLM^2.

5.2.2 FLake

As a one-dimensional lake model embedded in COSMO-CLM^2, FLake computes the evolution of a lake column temperature profile and the integral energy budgets of its different layers (Mironov et al., 2010). The model considers two layers in the water column: a mixed layer at the top and a thermocline down to the lake bottom. While the mixed layer is assumed to have a

uniform temperature (T_{ML}), the temperature-depth curve in the thermocline is parameterized through the concept of self-similarity, or assumed-shape (Kitaigorodskii and Miropolskii, 1970). This shape is only dependent on the temperature at its extremities and a shape factor which describes the curve through a fourth-order polynomial (Mironov, 2008). In the absence of snow and ice cover and when neglecting bottom sediments, the prognostic variables are: the mixed layer depth (h_{ML}), the bottom and water column average temperatures (T_{BOT} and T_{MW}, respectively) and the shape factor with respect to the temperature profile in the thermocline (C_T). Given their control on turbulence in the surface mixed layer (Read et al., 2012), h_{ML} is predicted taking convective and mechanical mixing into account, whereas volumetric heating is computed from the net short-wave radiation penetration through the lake surface and absorption at depth according to the Beer-Lambert law. To this end, the default downward light attenuation coefficient of 3 m^{-1} is employed. A recent global bathymetry dataset (Kourzeneva, 2010; Kourzeneva et al., 2012a) is used to specify lake depth of each lake pixel, thereby assuming a maximum lake depth of 50 m. A detailed description of FLake is provided in Mironov (2008) and Mironov et al. (2010).

Although FLake is a relatively simple model, its skill proves comparable to other, more comprehensive one-dimensional lake models, and this for various lake types and climatic conditions (e.g. Perroud and Goyette, 2009; Stepanenko et al., 2010, 2013, 2014). Moreover, FLake was extensively tested in offline mode over several AGL and judged an adequate tool to compute lake surface temperatures in comparison to other one-dimensional lake models, even though lake bottom temperatures may be sensitive to changes in certain external parameters and driving variables, such as wind speed (Thiery et al., 2014a,b). This is the first study to consider lake-atmosphere interactions over the AGL using FLake interactively coupled to an RCM. Previous RCM studies focusing on Lake Victoria either used prescribed lake surface temperatures (e.g. Anyah and Semazzi, 2004; Argent et al., 2014; Sun et al., 2015; Williams et al., 2014), the Hostetler lake model (e.g. Song et al., 2004) or the Princeton Ocean Model (POM; e.g. Song et al., 2004; Anyah and Semazzi, 2006; Sun et al., 2014).

5.2.3 Model set-up

To obtain information on small-scale variability, RCMs dynamically downscale lateral boundary conditions at a coarser resolution to a regional finer-scale model grid (Laprise et al., 2008). Here, we use the COSMO-CLM CORDEX-Africa evaluation simulation (Panitz et al., 2014) as lateral boundary conditions. The CORDEX-Africa evaluation simulation represents a dynamical downscaling to a 50 km (0.44°) horizontal grid spacing of the ERA-Interim reanalysis,

made available by the European Center for Medium-Range Weather Forecast (ECMWF; Dee et al., 2011) for 1979-2014 at 79 km (T255) resolution. Given the large difference in resolution between the latter and the target configuration, a direct downscaling of ERA-Interim is not advisable in this case.

The COSMO-CLM^2 model system is used to generate two climate simulations. First, a control simulation (hereafter referred to as CTL) is conducted where the lakes are included in the model integration. For this purpose, FLake is employed to compute the water temperatures for the AGL. The second simulation (hereafter referred to as NOL) is identical to the control experiment, except that each lake pixel is replaced by a representative land pixel selected from all land pixels within a distance of 50 km. The representative land pixel was chosen through random selection from a all land pixels within this radius. Since not all lake pixels had land within 50 km distance, this procedure was repeated until all lake pixels were eventually replaced. The external parameters and initial conditions of replaced land pixels show similar values and spatial patterns as the surrounding land; for instance, the area change of various plant functional types (PFTs) within the domain is 0.35% on average, and less than 3% for each individual PFT. Note that in the absence of spatio-temporally explicit satellite lake surface temperature observations (owing to the quasi-permanent cloud cover), forcing the model with time-explicit observed lake surface temperatures is not feasible. Only annual or multiyear monthly mean lake surface temperature observations may be used in that respect, but this option was not considered here.

Both experiments are conducted at a horizontal resolution of 0.0625° (∼7 km), which is finer than previous multiyear RCM experiments over this region (e.g. Sun et al., 1999a; Song et al., 2004; Anyah and Semazzi, 2004; Anyah et al., 2006; Williams et al., 2014, with resolutions ranging from 20 to 60 km), using 50 vertical levels and a time step of 60 s. The model domain encompasses the central part of the East African rift (Fig. 5.1) and therewith includes most of the AGL. Since enlarging the model domain by 50 grid points (3.125°) in each direction reduced the predictive skill of a one-year test simulation and more than doubled the total computation time, this option was not considered. The simulations cover the period 1996-2008 (13 years), of which the first three years are considered as spin-up time and excluded from the analysis. Inspection of predicted lake water surface temperatures shows that three years is enough to spin-up the model: lake water surface temperatures evolve to normal climatological values within the first year already. Finally, on each side 10 grid points were excluded from the analysis. Computation of the Davies relaxation function (Davies, 1983) in east-west direction showed that direct influence of lateral boundary conditions vanishes beyond this zone. The presence of two north-south oriented mountain ranges within the model domain are expected to further reduce the imprint of

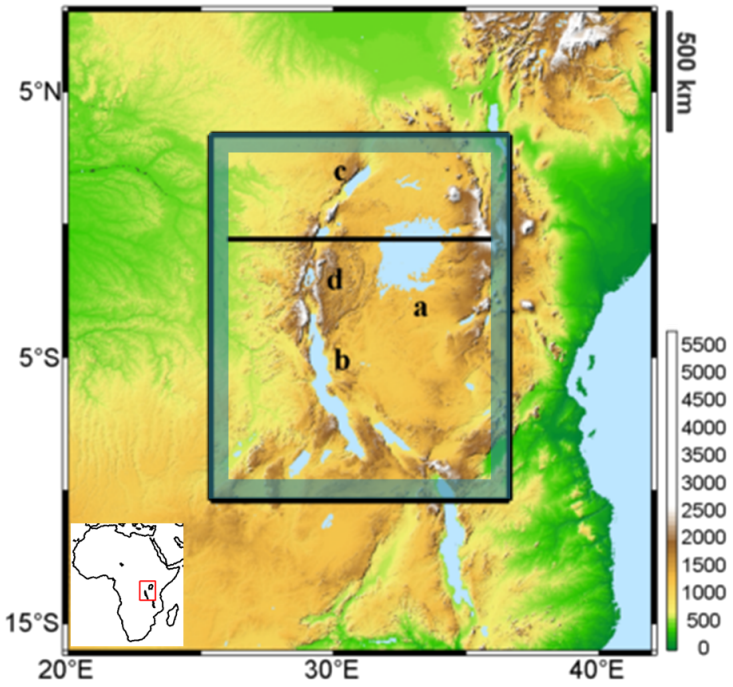

Figure 5.1: **Shuttle Radar Topography Mission (SRTM) surface height (m) over the African Great Lakes region. The model domain used in this study is denoted by the black rectangle (25.375°E to 36.625°E; 10.375°S to 3.375°N, center at 31°E, 3.5°S) and a 10 grid point wide zone excluded from the analysis by the blue band. The transect (26-36°E; 0.55°S) used for the vertical cross section in Figs. 5.13,5.14 is shown by the black line. The four largest African Great Lakes within the model domain are a) Lake Victoria, b) Lake Tanganyika, c) Lake Albert and d) Lake Kivu.**

the parent model on the COSMO-CLM^2 predictions.

The configuration used in this study is based on tropical set-up of COSMO-CLM described by Panitz et al. (2014) and used for the CORDEX-Africa simulations (Panitz et al., 2014; Dosio et al., 2014). In the tropical configuration, the model top is set to 30 km and the lower height of the damping layer is increased from 11 km to 18 km. In addition, we introduced the following modifications:(i) CLM3.5 replaces the default LSM in COSMO-CLM. (ii) Next, FLake is used, instead of the Hostetler-based lake model embedded within CLM3.5 (Bonan et al., 2002), as the latter exhibits a cold lake temperature bias over the AGL (Thiery et al., 2014b). As recommended by Thiery et al. (2014a), the lake temperature profile is initialised with stratified conditions, an approach also

adopted by Hernández-Díaz et al. (2012). (iii) Finally, certain model settings (e.g. time step, number of vertical layers, width of the relaxation layer) were adapted to be consistent with the higher horizontal grid resolution.

5.2.4 Evaluation datasets

The performance of the CTL simulation is assessed by comparing model output to observational products for various quantities (see Table 5.1 for their technical specifications). For precipitation, we use gridded datasets from the following sources: the Global Precipitation Climatology Project (GPCP; Huffman and Adler, 2001), the Global Precipitation Climatology Centre (GPCC; Rudolf et al., 2011), the University of Delaware (UDEL; Legates and Willmott, 1990), the Climate Prediction Center Morphing Technique (CMORPH; Joyce and Janowiak, 2004) and satellite derived precipitation rates from the Tropical Rainfall Measuring Mission products 3B42 and 2B31 (TRMM; Kummerow et al., 2000). The TRMM 2B31 product is a combined rainfall-profile product derived from the Precipitation Radar and TRMM Microwave Imager (Bookhagen and Strecker, 2008). Since the standard TRMM precipitation product (3B42) and CMORPH demonstrate poor performance over complex African terrain (Dinku et al., 2008), the TRMM 2B31 product is preferred over 3B42, given the higher spatial resolution and ability to reproduce orographically-induced precipitation patterns over complex terrain (Bookhagen and Burbank, 2006; Bookhagen and Strecker, 2008; Burbank et al., 2012). The high spatial resolution TRMM 2B31 1999-2008 data were re-projected from their original 4.3-5 km resolution to the 0.0625° grid using a bilinear interpolation algorithm to account for projection and resolution inhomogeneities (Bookhagen and Strecker, 2008). The precipitation rates [mm h^{-1}] from each satellite overpass ($\sim$16 day^{-1}) were subsequently rescaled to monthly mean precipitation values using the number of measurements within each grid cell, after which a convolution filter with a 5-by-5 equal weights window was applied. Note that no further calibration of the data was performed. Finally, a dataset of in situ daily accumulated precipitation measurements was compiled. A similar approach was followed for observed monthly and daily mean near-surface temperature observations, however, measurements of this type are very sparse in the region.

Particular attention is paid to the model's ability to reproduce observed lake surface water temperatures (LSWT), using both in situ and satellite measurements as a reference. To this end, the Along-track scanning radiometers Reprocessing for Climate/Lake (ARC-Lake) project provides high resolution, spatially-explicit global LSWT observations (MacCallum and Merchant, 2012). The lake temperature evaluation is complemented using 419 conductivity-temperature-depth (CTD) casts collected during daytime at three multi-year

Table 5.1: **Data products used for model evaluation (SRes.: spatial resolution; TRes.: temporal resolution).**

Variable, Symbol [units]	Dataset (Version)	Source	SRes.	TRes.	Years	References
Precipitation, P [mm/month]	TRMM (3B42)	mixed	0.25°	monthly	'99-'08	(Kummerow et al., 2000)
	TRMM (2B31)	satellite	∼0.04°	∼1.5-hourly	'99-'08	(Kummerow et al., 2000)
	GPCP (1DD)	mixed	1.00°	daily	'99-'08	(Huffman and Adler, 2001)
	GPCC (v6)	stations	0.50°	monthly	'99-'08	(Rudolf et al., 2011; Schneider et al., 2013)
	UDEL (v3.01)	stations	0.50°	monthly	'99-'08	(Legates and Willmott, 1990)
	CMORPH (ds502.0)	mixed	0.25°	3-hourly	'03-'08	(Joyce and Janowiak, 2004; Climate Prediction Center et al., 2011)
	in situ	stations	/	daily	'99-'08	(Nyeko-Ogiramoi et al., 2010, 2013)
Near-surface temperature, T_{2m} [K]	in situ	stations	/	daily	'99-'08	(Plisnier et al., 2000)
Lake surface temperature, T_S [K]	ARC-Lake (v1.1.2)	satellite	0.05°	variable	'99-'08	(MacCallum and Merchant, 2012)
Lake water temperature, $T_{0.5m}$ [°C]	in situ	stations	/	bi-monthly	'99-'08	(Plisnier et al., 2009; Darchambeau et al., 2014)
Surface net shortwave radiation, SW_{net} [W m^{-2}]	GEWEX-SRB (REL3.0)	satellite	1.0°	monthly	'99-'07	(Stackhouse et al., 2011)
Surface net longwave radiation, LW_{net} [W m^{-2}]	GEWEX-SRB (REL3.1)	satellite	1.0°	monthly	'99-'07	(Stackhouse et al., 2011)
Latent heat flux, LHF [W m^{-2}]	LandFlux-EVAL	mixed	1.0°	monthly	'99-'05	(Mueller et al., 2013)
Sensible heat flux, SHF [W m^{-2}]	FLUXNET-MTE	stations	0.50°	monthly	'99-'08	(Jung et al., 2010)
Cloud cover fraction, CCF [%]	ISCCP (D2)	satellite	1.0°	monthly	'99-'08	(Rossow and Schiffer, 1999)

monitoring sites: Ishungu (Lake Kivu), Kigoma (Lake Tanganyika's northern basin) and Mpulungu (Lake Tanganyika's southern basin) (Plisnier et al., 2009; Darchambeau et al., 2014). Vertical piecewise cubic Hermite interpolation (increment 0.1 m; De Boor, 2001) was applied to each cast, after which the near-surface water temperature (0.5 m) was extracted and used as a reference. This depth is assumed to be the depth closest to the surface with a reliable measurement from the CTD cast.

The net surface shortwave (SW_{net}) and longwave (LW_{net}) radiation, latent heat flux (LHF) and sensible heat flux (SHF) were compared to satellite-derived values available from the Global Energy and Water cycle Experiment Surface Radiation Budget (GEWEX-SRB; Stackhouse et al., 2011), the benchmark synthesis of available diagnostic evapotranspiration estimates (LandFlux-EVAL; Mueller et al., 2013) and the global upscaling of observations from eddy-covariance flux towers using the Model Tree Ensembles (Fluxnet-MTE; Jung et al., 2010), respectively. The MTE approach represents a machine learning algorithm integrating in situ flux measurements with satellite observations and surface meteorological data to produce global gridded evapotranspiration estimates and associated uncertainties (Jung et al., 2009). Finally, the cloud cover fraction (CCF) is evaluated using the International Satellite Cloud Climatology Project D2 dataset (ISCCP; Rossow and Schiffer, 1999).

All gridded datasets used are available for the entire analysis period, except for CMORPH (2003-2008), LandFlux-EVAL (1999-2005) and GEWEX-SRB (1999-2007). Aside from ARC-Lake, their horizontal resolution is usually much coarser than the *CTL* simulation (Table 5.1). No height correction, gap filling or other modifications were applied to the various datasets. The COSMO-CLM^2 rotated model grid is considered as the reference grid to which all other gridded products are remapped using bilinear interpolation. Evaluation with in situ data is performed by comparing the observed time series to the model grid box encompassing the measurement site.

5.2.5 Surface energy balance decomposition

The energy balance at the surface-atmosphere interface is given by:

$$\epsilon\sigma T_s^4 = (1-\alpha)SW_{in} + LW_{in} - LHF - SHF - G \tag{5.1}$$

where ϵ is the surface emissivity, σ is the Stefan-Boltzmann constant (5.67 x 10^{-8} W m^{-2} K^{-4}), T_s is the surface temperature, α is the surface albedo with respect to shortwave radiation, SW_{in} is the incoming shortwave radiation, LW_{in}

is the incoming longwave radiation, LHF and SHF are the turbulent fluxes of latent heat and sensible heat, and G is the subsurface energy flux.

The causes for the surface temperature response to the presence of lakes are investigated using a surface energy balance decomposition method developed by Juang et al. (2007) and further modified by Luyssaert et al. (2014) and Akkermans et al. (2014). The net impact of the AGL on surface temperature is decomposed *a posteriori* and attributed to direct contributions of modified biogeophysical processes (such as surface reflection and evapotranspiration) and indirect contributions due to atmospheric feedbacks (such as cloud-radiative feedbacks or surface layer stability changes).

The net change in outgoing longwave radiation is given by $4\epsilon\sigma T_s^3 \delta T_s$, i.e. the first order derivative of the left hand side in Eq. (5.1) with respect to T_s. Note that here, the term "surface temperature" (T_s) denotes the surface radiative temperature at which the soil-vegetation-lake complex emits longwave radiation to the atmosphere. From this, δT_s can be derived by solving the total derivative of the Eq. (5.1) and solving for δT_s:

$$\begin{aligned} \delta T_s = & \frac{1}{4\epsilon\sigma T_s^3}(-SW_{in}\delta\alpha + (1-\alpha)\delta SW_{in} + \delta LW_{in} - \delta LHF \\ & + \delta SHF - \delta G - \sigma T_s^4 \delta\epsilon) \end{aligned} \tag{5.2}$$

with δSHF encompassing the SHF changes induced by the modified aerodynamic resistance and the modified temperature gradient. Most terms in Eq. (5.2) can be calculated from the difference between mean quantities in the control and no-lakes simulation (CTL minus NOL), except for $\delta\epsilon$ which is recomputed from the model equations.

5.3 Results

5.3.1 Model evaluation

Precipitation and air temperature

Observed precipitation patterns are reasonably reproduced by COSMO-CLM^2, in terms of spatial patterns (Fig. 5.2) as well as the amplitude and phase of the annual cycle (Fig. 5.3). The model captures the enhanced precipitation in the northwestern part of the domain, associated with strong orographically-induced

convection in a region where tropical rainforest is the dominant land cover type (Fig. 5.2a-g). However, the disagreement between the various observational products regarding the magnitude of precipitation over this part of the domain is large (with differences locally exceeding 3900 mm year^{-1}; Fig. 5.2h), and the bias is either positive or negative, depending on the benchmark product considered. Generally, the limited number of rain gauges within the model domain and the numerous data gaps in the available time series call for cautious use of gridded precipitation datasets based on in situ measurements, but also satellite based or mixed source products contain important uncertainties over the mountainous regions of tropical Africa (e.g. Dinku et al., 2008; Nikulin et al., 2012; Endris et al., 2013; Sylla et al., 2013, note that, due to differences in the reliability of precipitation products over water surfaces, the observational spread was omitted over the AGL). Furthermore, COSMO-CLM^2 is able to reproduce the higher precipitation observed by TRMM 3B42 and TRMM 2B31 over some AGL especially during the wet seasons (MAM and OND, see below). In particular, the strong precipitation signal over Lake Kivu is reproduced, while the spatial pattern of precipitation over Lake Victoria is reproduced but underestimated relative to both TRMM products. The dry bias over Lake Victoria relative to TRMM 3B42 and 2B31 amounts up to -493 mm year^{-1} (-24%) and -691 mm year^{-1} (-30%), respectively, and is centred over the western half of the lake as the modeled precipitation maximum is shifted towards the northeast. Relative to GPCP and CMORPH, in contrast, COSMO-CLM^2 overestimates precipitation over Lake Victoria by 217 mm year^{-1} (16%) and 250 mm year^{-1} (19%), respectively. Again, the maximum difference amongst the gridded observational products is large (1131 mm year^{-1} averaged over Lake Victoria, Fig. 5.2h), and largely exceeds the biases between COSMO-CLM^2 and individual products. Such a large spread calls for further research to quantify the uncertainties of observed precipitation in the region. Furthermore, over the central rift valley, where the observational products agree fairly well, a dry bias is apparent. This is confirmed by the comparison to in situ precipitation records, located mostly within the rift valley (Fig. 5.4a-b). Over 75% of the domain, the absolute precipitation bias against individual products remains below 185 mm year^{-1}, corresponding to 13% of the average precipitation observed over the region (observational ensemble mean).

Seasonal precipitation variability in the AGL region is primarily governed by the north-south migration of the Intertropical Convergence Zone (ITCZ) across the region (Nicholson, 1996; Williams et al., 2014). Monthly mean precipitation subsequently indicates a bi-modal distribution with a distinct dry season during JJA and two wet seasons: MAM ("long rains"; northward ITCZ migration) and OND ("short rains"; southward ITCZ migration), separated by the slight decrease in rainfall during JF ("little dry season"; Fig. 5.3). The annual cycle of precipitation is reasonably captured by COSMO-CLM^2; averaged over the

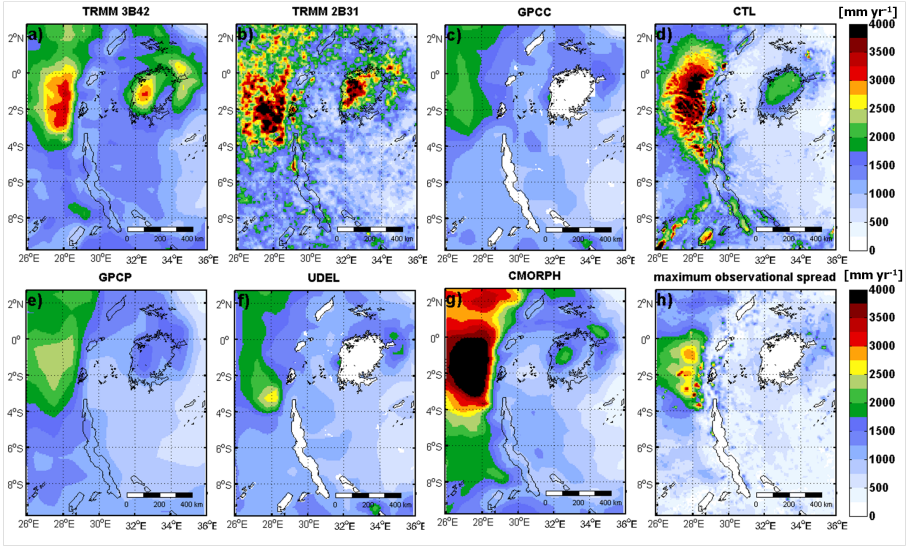

Figure 5.2: **Observed annual mean precipitation P [mm yr^{-1}] from the datasets described in Table 5.1: (a) TRMM 3B42, (b) TRMM 2B31, (c) GPCC, (e) GPCP, (f) UDEL and (g) CMORPH averaged over the period 1999-2008, except CMORPH (2003-2008). (d) 1999-2008 modeled P (CTL). (h) Maximum difference among observational products, considering only land pixels. The observational products GPCC and UDEL are masked out over the lakes since they are based solely on land station data.**

entire domain, fair correspondence exists between the observations and CTL, although precipitation is underestimated in April and during the main dry season. Multiyear monthly accumulated, domain-averaged precipitation biases against individual observational products are smaller than 90 mm month^{-1} during 90% of all months. Furthermore, monthly mean, domain-average modelled precipitation values are positively correlated with corresponding observations (significant ($p < 0.001$) Spearman rank correlation of 0.72, 0.85, 0.84, 0.80 and 0.84 with respect to TRMM 3B42, GPCC, GPCP, UDEL and CMORPH, respectively).

Although very sparse, aggregated daily and monthly mean near-surface temperature observations in the region (T_{2m}) suggest the ability of COSMO-CLM^2 to reproduce spatial differences in T_{2m} (Fig. 5.4c). In addition, their annual cycle is well captured by COSMO-CLM^2, but the magnitude of the seasonality is slightly exaggerated by the model (not shown).

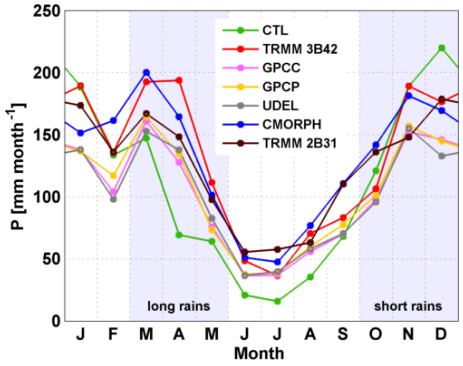

Figure 5.3: **Observed and modeled domain-averaged seasonal precipitation cycles [mm month^{-1}] over the period 1999-2008, except CMORPH (2003-2008).**

Lake temperature

COSMO-CLM^2 succeeds in reproducing the observed differences in LSWT among four major AGL, but demonstrates a slight warm bias for each of them (0.68 K on average; Fig. 5.5a-h; Table 5.2) and overestimates the amplitude of the seasonal LSWT cycle (Fig. 5.5i-l). Spatial LSWT patterns correspond to observations especially over Lake Victoria and Lake Tanganyika, with statistically significant spatial rank correlations of 0.68 and 0.61, respectively, and to a lesser extend over the other AGL. Over Lake Victoria, COSMO-CLM^2 suggest a positive temperature gradient from southwest to northeast, with a maximum temperature difference of 1 K. Although this modeled pattern is in contradiction with previous studies (e.g. Song et al., 2004; Anyah et al., 2006; Sun et al., 2014, 2015), it matches with the spatial pattern derived from remote sensing (Fig. 5.5a,e), as well as with a recent observational based on water temperature measurements at 48 locations during two cruises in February and August 2000 (MacIntyre et al., 2014). Unlike the observations, COSMO-CLM^2 furthermore predicts slightly higher lake surface temperatures in coastal zones and embayments as a result of the lower lake depths in these sectors.

The model's ability to reproduce lake surface temperatures is also apparent from the comparison between modeled and observed lake water temperatures at 0.5 m for three multi-year monitoring sites in Lake Kivu and Lake Tanganyika (Fig. 5.6). FLake reasonably predicts the annual mean 0.5 m lake temperature (with a warm bias of 1.23 °C, 0.71 °C and 0.60 °C at Ishungu, Kigoma and Mpulungu, respectively) and reproduces the phase of the annual cycle, but again exaggerates the amplitude of the seasonal temperature variations. Despite this

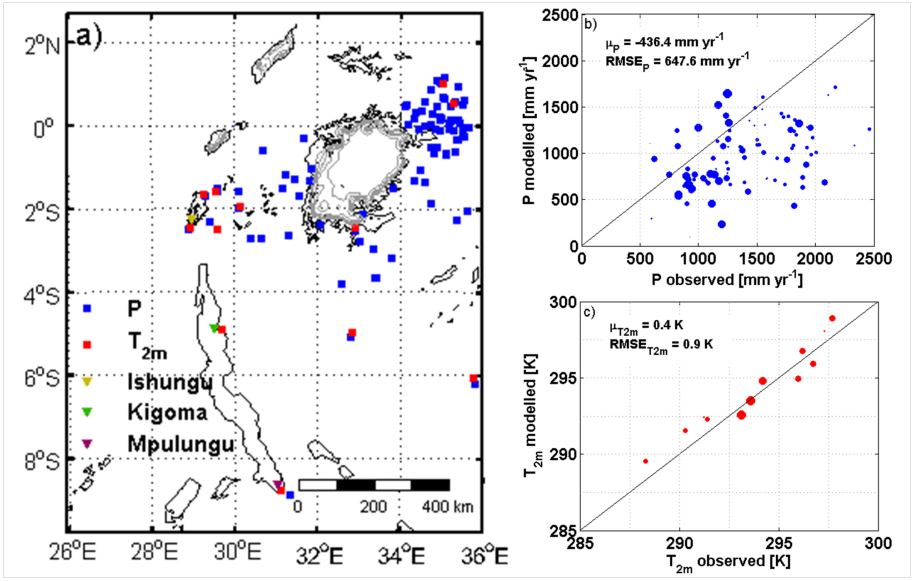

Figure 5.4: **(a) Map of in situ measurement locations of near-surface temperature T_{2m} (red squares), precipitation P (blue squares) and three lake water temperature monitoring sites (colored triangles, see Fig. 5.6). Grey lines represent the bathymetry data (Kourzeneva et al., 2012a) employed for the COSMO-CLM^2 CTL simulation (10 m equidistance and lake depths capped at 50 m, resulting in the absence of contours for several deep lakes). Scatter plots of modeled versus observed mean (b) P [mm yr^{-1}] and (c) T_{2m} [K]. μ presents the mean difference and RMSE the Root Mean Squared Error of modeled versus observed P and T_{2m}, respectively. Data gaps in the observations were removed from the corresponding modelled time series. The size of the individual points reflects the availability of data during the analysis period (1999-2008) (the larger, the more data).**

overestimation, FLake captures the increasing seasonal cycle's amplitude with distance from the equator (Fig. 5.6). As this distance grows, the dry season becomes more pronounced, leading to a stronger evaporative-driven cooling of the lakes' mixed layer (Thiery et al., 2014a). Furthermore, interannual (near-)surface lake temperature variability is present, but can be considered small compared to the seasonal cycle. Observed anomalies include the high temperatures during the 2005 long rains at Kigoma relative to the preceding months, and the low temperatures during the 2007-2008 stratified season at Ishungu (Fig. 5.6a,b). While the model reproduces the former warm anomaly at Kigoma, it does not predict the cold anomaly at Ishungu.

The overestimation of the annual LSWT cycle is primarily due to the

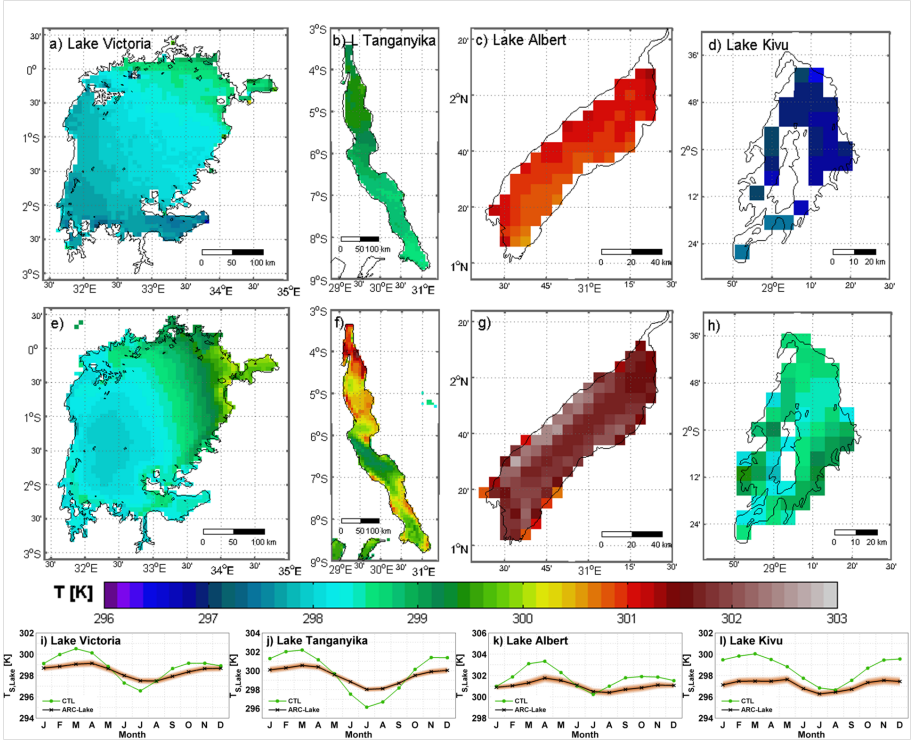

Figure 5.5: **1999-2008 observed lake surface water temperatures LSWT [K] from the ARC-Lake dataset (top panels) and modeled LSWT from the COSMO-CLM^2 *CTL* simulation (central panels) for (a,e) Lake Victoria, (b,f) Lake Tanganyika, (c,g) Lake Kivu and (d,h) Lake Albert. (i-l) Lake-averaged observed (black line) and modeled (green line) monthly mean LSWT including observational error estimate as provided with the product (red shading).**

underestimation of the mixed layer depth when stratified conditions are imposed in FLake (Thiery et al., 2014a). For a relatively shallow mixed layer, heat is concentrated in the top of the water column rather than being distributed over a larger volume. This in turn causes a stronger temperature response to seasonal changes in the lake's heat content and hence an overestimation of the annual LSWT cycle (Fig. 5.5i-l). Another potential cause for the remaining biases might be the role of three-dimensional water circulation within the larger lakes. For the relatively shallow Lake Victoria, Song et al. (2004) argue that an RCM coupled to a one-dimensional lake model reproduces first order spatial lake surface temperature patterns, but that only a three-dimensional lake model predicts a southwest to northeast heat transport within the lake. In the deep

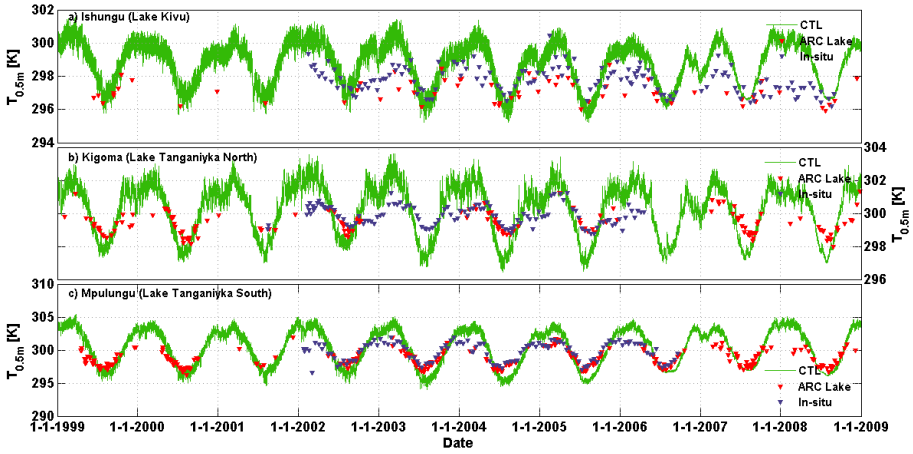

Figure 5.6: **Modeled (green lines), remotely sensed (ARC-Lake; red triangles) and bi-monthly, in situ observed (blue triangles) lake temperatures [K] at (a) Ishungu (Lake Kivu; 2.34°S, 28.98°E), (b) Kigoma (Lake Tanganyika's northern basin; 4.85°S, 29.59°E) and (c) Mpulungu (Lake Tanganyika's southern basin; 8.73°S, 31.04°E) at a depth of 0.5 m (lake surface temperatures in case of ARC-Lake).**

Lake Tanganyika, actual lake hydrodynamics are still debated (e.g. Naithani et al., 2003; Verburg et al., 2011), but also here, variable wind forcing (Naithani et al., 2002), differential cooling (Verburg and Antenucci, 2010; Verburg et al., 2011), water exchange across the thermocline (Gourgue et al., 2007) and internal Kelvin waves (Naithani and Deleersnijder, 2004) may eventually influence LSWT patterns. Further research could help to discriminate the influence of lake hydrodynamics on lake-atmosphere exchanges for this region.

Surface energy balance and clouds

The ability of COSMO-CLM^2 to represent the surface climate is investigated by evaluating the surface energy fluxes. Good agreement is noted for the surface radiative fluxes, SW_{net} and LW_{net}, both in terms of spatial patterns and the domain-averaged annual cycle, indicating, among other things, the skill of CLM3.5 to simulate spatial and temporal albedo patterns over land (Fig. 5.7a-b,f-g,k-l). Modeled over-lake variations in SW_{net} (Fig. 5.7f) are due to spatial cloud cover variability, given the constant water surface albedo employed in FLake (0.07). Furthermore, very good agreement exists between model and observations for cloud cover fraction, CCF (+4% bias; Fig. 5.7e,j,o;

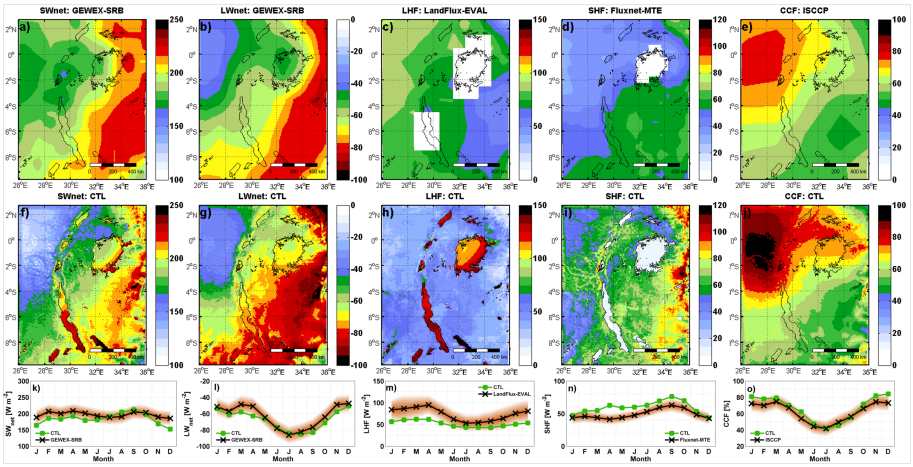

Figure 5.7: **Observed and modeled annual mean maps (top and central panels, respectively), and domain-averaged seasonal cycles (lower panels) for (a,f,k) net shortwave radiation at the surface SW_{net} [W m^{-2}], (b,g,l) net longwave radiation at the surface LW_{net} [W m^{-2}], (c,h,m) latent heat flux LHF [W m^{-2}], (d,i,n) sensible heat flux SHF [W m^{-2}] and (e,j,o) percent cloud cover CCF [%]. The various observational products are described in Table 5.1 and both observational products and model output are shown for the respective measurement periods (a,e: 1999-2008; b,c: 1999-2007; d: 1999-2005). For the white areas in (c) and (d), no data is available. The red shading around the observed annual cycle (black line) indicates the observational uncertainty as provided with the products.**

Table 5.2). The seasonal cycles of LW_{net} and CCF are strongly linked to each other and indicate more longwave radiative energy loss during the main dry season when lower cloud cover fraction reduces the amount of incoming longwave radiation. During the short rains and the little dry season, a slight overestimation of CCF by ∼8% induces a negative LW_{net} bias of -5 W m^{-2} during these months. Lower performance is noted for the turbulent fluxes, LHF and SHF (-22 W m^{-2} and +10 W m^{-2} bias, respectively; Fig. 5.7c-d,h-i,m-n; Table 5.2), with generally an underestimation of LHF and an overestimation of SHF. Possibly, this overestimation of the Bowen ratio is caused by limited soil moisture availability, but given the lack of observational evidence this is impossible to verify. Overall, domain-averaged monthly mean values for SW_{net}, LW_{net}, LHF, SHF and CCF are within the observational uncertainty range during 10, 11, 7, 4 and 11 months of the year, respectively.

Comparison to ERA-Interim and CORDEX

To put the performance of the COSMO-CLM^2 CTL simulation into perspective, the same evaluation procedure was repeated for ERA-Interim and the COSMO-CLM CORDEX-Africa evaluation simulation (Panitz et al., 2014, hereafter referred to as CORDEX), each, in turn, representative of a state-of-the-art global reanalysis product and a continental-scale RCM simulation. Results indicate that COSMO-CLM^2 largely outperforms ERA-Interim for all considered variables, except for SHF and CCF where both products depict similar skill (Table 5.2), and with the seasonal cycles of CCF mostly within the margins of observation uncertainty. Especially for precipitation and lake surface temperatures, COSMO-CLM^2 demonstrates remarkably lower biases and spatial root mean square errors (RMSE) compared to ERA-Interim. Relative to the CORDEX simulation, the enhanced skill of COSMO-CLM^2 is also evident for both P, SW_{net} and LSWT, whereas LW_{net}, LHF, SHF and CCF predictions demonstrate similar skill. Several effects are responsible for this enhanced skill. First, relatively few observations are assimilated into ERA-Interim over central Africa, leaving the model to run more freely over this region compared to other parts of the globe. Second, the use of a lake model clearly improves model performance relative to other common techniques, such as the sea surface temperature interpolation employed in ERA-Interim and CORDEX (Balsamo et al., 2012), for instance by reducing the absolute LSWT error over Lake Tanganyika by 86% and 65% relative to ERA-Interim and CORDEX, respectively (Table 5.2). Third, COSMO-CLM^2 benefits from the higher resolution relative to ERA-Interim and CORDEX (7 km versus 79 km and 50 km, respectively), allowing for more fine-scale circulation and associated precipitation patterns to develop over this complex terrain. Finally, the use of the Community Land Model improves the representation of the land surface albedo and other land surface characteristics relative to the default LSM of COSMO-CLM (Akkermans, 2013).

In addition, the evaluation procedure was repeated for the NOL simulation, wherein lakes have been replaced by representative land pixels (see section 5.2.3). The added value of the CTL simulation relative to NOL is apparent especially for precipitation and (lake) surface temperature (not shown). For precipitation, the enhanced skill of CTL can be attributed to the underestimation of the moisture input into the atmosphere in NOL (in the absence of lake evaporation), whereas an underestimation of surface thermal inertia deteriorates surface temperature variability in NOL.

In general, the evaluation results demonstrate that the near-surface climate is well represented by COSMO-CLM^2, the resolution is sufficient to capture effects of lakes and local orography on precipitation and other atmospheric variables,

Table 5.2: **Bias and spatial RMSE of COSMO-CLM^2, ERA-Interim and the CORDEX parent simulation (section 5.2.3) versus various observational products (see Table 5.1 for an overview).**

Physical quantity [Units]	COSMO-CLM^2		ERA-Interim		CORDEX	
	bias	RMSE	bias	RMSE	bias	RMSE
TRMM 3B42 Precipitation [mm yr^{-1}]	-261	683	612	881	-717	838
GPCC Precipitation [mm yr^{-1}]	68	631	941	1160	-389	508
GPCP Precipitation [mm yr^{-1}]	30	554	903	1069	-427	519
UDEL Precipitation [mm yr^{-1}]	84	604	957	1167	-373	478
CMORPH Precipitation [mm yr^{-1}]	-330	712	739	907	-771	973
TRMM 2B31 Precipitation [mm yr^{-1}]	-273	678	599	873	-730	927
ensemble Precipitation* [mm yr^{-1}]	-116	554	757	932	-573	669
GEWEX-SRB SW$_{net}$ [W m^{-2}]	-12	22	39	42	-26	33
GEWEX-SRB LW$_{net}$ [W m^{-2}]	-5	8	-21	24	1	7
LandFlux-EVAL LHF [W m^{-2}]	-22	34	32	35	-27	31
Fluxnet-MTE SHF [W m^{-2}]	10	22	-2	15	6	23
ISCCP CCF [%]	4	7	-1	6	3	6
ARC-Lake LSWT Victoria [K]	0.40	0.53	-4.16**	4.52**	-2.70	2.81
ARC-Lake LSWT Tanganyika [K]	1.09	1.16	-7.58**	7.82**	-3.07	3.35
ARC-Lake LSWT Albert [K]	0.90	0.94	/	/	-5.90	5.94
ARC-Lake LSWT Kivu [K]	1.80	1.83	/	/	-4.19	4.19

* Average of the 6 gridded precipitation products.
** Given its coarse resolution and associated limited number of lake pixels, nearest neighbour interpolation was used here instead of bilinear interpolation.

and the spatial and temporal patterns of the lake surface temperatures as well as differences between individual lakes are well represented by FLake. We therefore conclude that COSMO-CLM^2 is an appropriate tool to investigate the impact of the AGL on the regional climate.

5.3.2 Impact of the African Great Lakes on the regional climate

Temperature

Generally, the AGL clearly cool over-lake near-surface air (Table 5.3; Fig. 5.8), with average values of -0.67 K, -0.58 K and -0.86 K for Lake Victoria, Lake Tanganyika and Lake Albert, respectively. Locally, the cooling exceeds -1.5 K over each of these lakes, and -2 K over Lake Victoria. An interesting exception to this general pattern is Lake Kivu, where the lake presence induces an average warming of over-lake T$_{2m}$ by +0.75 K relative to the *NOL* simulation. In section 5.3.3, we further investigate causes of the temperature impact induced by the AGL.

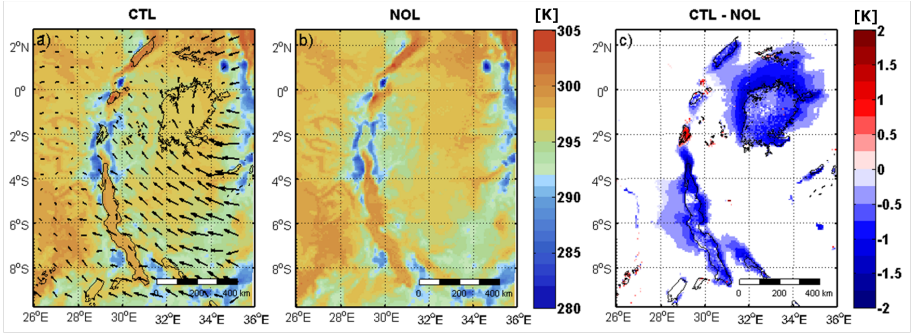

Figure 5.8: **Impact of the AGL on 2 m air temperature T_{2m}. Shown are annual mean T_{2m} [K] for the (a) control (CTL) and (b) no-lakes (NOL) simulations, and (c) statistically significant changes at the 5% significance level (CTL-NOL; two-tailed t-test) over the period 1999-2008. Temporally averaged 10 m wind vectors from the control simulation are shown in (a).**

Table 5.3: **Impact of the African Great Lakes on various climatological values (CTL minus NOL).**

Physical quantity [Units]	**all pixels**		**lake pixels**	
	ABS**	**REL****	**ABS**	**REL**
Temperature at 2 m [K]	-0.17	-1	-0.57*	-2
Precipitation [mm yr^{-1}]	59.10	5	712.77*	79
Surface temperature [K]	0.26	1	3.02*	13
Net SW radiation, surface [W m^{-2}]	3.28*	2	30.63*	17
Net LW radiation, surface [W m^{-2}]	-0.23	0	-4.95*	7
Latent heat flux [W m^{-2}]	6.97	15	73.56*	142
Sensible heat flux [W m^{-2}]	-4.34	-7	-52.36*	-85
Sea level pressure [hPa]	0.15	0	0.43*	0
Cloud cover fraction [%]	-0.05	0	-0.94	-1
evaporation [mm yr^{-1}]	87.96	15	927.9*	142

* changes significant at the 5% significance level (two-tailed t-test).
** ABS and REL: absolute and percentage change, respectively.

Besides cooling the over-lake surfaces, the AGL also have a pronounced downwind influence on T_{2m}, as the cooler temperatures are advected by the daytime lake breeze into the adjacent land. This is especially visible north of Lake Victoria and around Lake Tanganyika, and results in a domain-averaged cooling of -0.17 K. In contrast, the central part of Albertine rift mountains (e.g. Rwenzori (29.7-30.2°E; 0.0-0.8°N) and Virunga (29.1-29.7°E ; 1.3- 1.6°S) mountain ranges) block all near-surface atmospheric circulation and therewith constrain the influence of Lake Albert, Lake Edward and Lake Kivu to their direct surroundings. Likewise, the steep topography surrounding Lake Tanganyika (e.g. Itombwe (28.5- 29.1°E; 2.5-4.5°S), Kibira (29.1- 29.6°E;

2.2-3.8°S) and Mahale (29.7- 30.1°E; 6.0-6.5°S) Mountains) limits its cooling influence to the lower inland (Figs. 5.1, 5.8). The Albertine rift valley south of Lake Victoria is also not influenced by the lake presence, given the predominantly southeasterly flow in this part of the domain. These elements highlight that distance from the lake is not the only decisive factor determining the lake influence on T_{2m}, but that topography and atmospheric circulation also play a major role.

The lake influence on T_{2m} is characterized by a clear seasonal pattern, with stronger cooling in the months following the main dry season (August-October: -1.4 K over the AGL versus -0.3 K during the remaining months; Fig. 5.10a,d), caused by seasonally variable land-water temperature contrasts. Near-surface water temperature variability in the AGL is primarily governed by LHF, for which the lake induced change peaks during the main dry season (JJA; Fig. 5.10c,f) as near-surface relative humidity drops and induces the evaporative cooling of the lake surfaces (Savijärvi and Järvenoja, 2000; MacIntyre, 2012; Schmid and Wüest, 2012; Thiery et al., 2014a). Land temperatures follow a similar seasonal pattern, but increase more rapidly at the end of the dry season due to their relatively low heat capacity. Hence, the largest land-lake temperature contrast and associated lake cooling effect is found from August to October. For similar reasons, the strongest AGL cooling occurs during daytime (07-16 UTC), because at night lakes have a warming effect (18-05 UTC; Fig. 5.10g,j).

Precipitation

As a result of the lakes' presence, modeled precipitation is enhanced by 59 mm yr^{-1} (+5%) on average over the model domain, by 713 mm yr^{-1} (+79%) over all lake pixels and by 732 mm yr^{-1} (+87%) over the four major AGL (Table 5.3; Fig. 5.9). The largest increase is noted over Lake Kivu (+1373 mm yr^{-1} or +145%), whereas the three other major AGL induce similar absolute increase over their surface (+706 mm yr^{-1} (+85%), +745 mm yr^{-1} (+82%) and +647 mm yr^{-1} (+112%) over Lake Victoria, Lake Tanganyika and Lake Albert, respectively). The smaller lakes within the model domain generate similar increases, except for Lake Edward which does not produce any additional precipitation according to COSMO-CLM^2.

In contrast to the influence of the lakes on T_{2m}, the precipitation impact is very localised and mostly limited to the lake itself (Fig. 5.9c). Over Lake Victoria, lake-induced precipitation increases from southeast to northwest, demonstrating the non-uniform response of the atmospheric column to the presence of the lake, in line with Anyah and Semazzi (2004). Over Lake Tanganyika, the

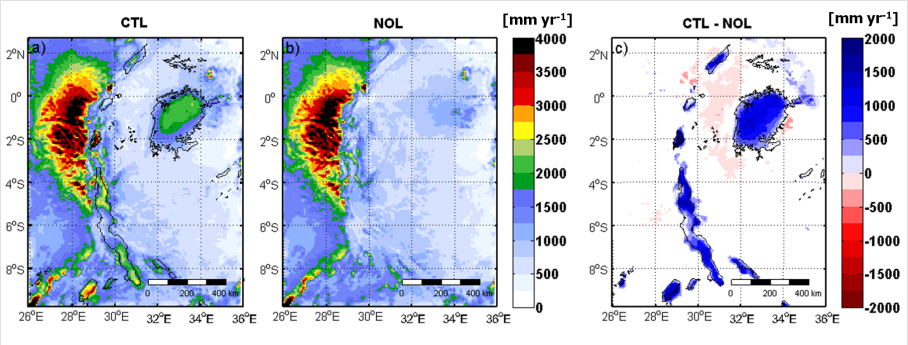

Figure 5.9: **Impact of the AGL on precipitation P. Shown are annual mean P [mm yr^{-1}] for the (a) control (CTL) and (b) no-lakes (NOL) simulations, and (c) statistically significant changes at the 5% significance level (CTL-NOL; two-tailed t-test) over the period 1999-2008.**

increase in precipitation over the central part is absent or weak compared to the northern and southern sectors. In this part of the lake, a narrow corridor induces relatively strong dry season winds (see also Savijärvi and Järvenoja, 2000) which transport over-lake air masses westward into the Congo Basin (see also Fig. 5.8a). The differential spatial impact patterns confirm that next to changes in evapotranspiration, also temporal patterns and changes in circulation induced by the AGL play a dominant role in redistributing precipitation (Datta, 1981; Savijärvi, 1997; Savijärvi and Järvenoja, 2000; Song et al., 2004; Anyah and Semazzi, 2004; Anyah et al., 2006; Anyah and Semazzi, 2007, 2009; Williams et al., 2014). Our findings furthermore suggest that onshore pluviometer measurements will never fully capture precipitation effects induced by the AGL. The dynamical response to lake presence is further investigated in section 5.3.4.

Precipitation over the AGL displays a distinct diurnal cycle, with precipitation occurring mostly at night and morning hours over the lakes (00-09 UTC). This is in general agreement with observations from a pluviometer representative of the central Lake Victoria (Datta, 1981). For the surrounding land, in contrast, the precipitation maxima occurs around local noon (07-12 UTC; Fig. 5.10h,k). The nighttime precipitation maximum is enabled by the sustained evaporation from the lakes throughout the whole day. This is not the case for the land evapotranspiration which displays a clear maximum during the local afternoon and slightly lags the precipitation peak (Fig. 5.10i,l). Overall, the AGL generate a total moisture input into the atmosphere of 222 km^3 yr^{-1}, that is 134 km^3 yr^{-1} more than the equivalent land surface (+151%). This increase is more than sufficient to explain the enhanced over-lake precipitation production (+99 km^3

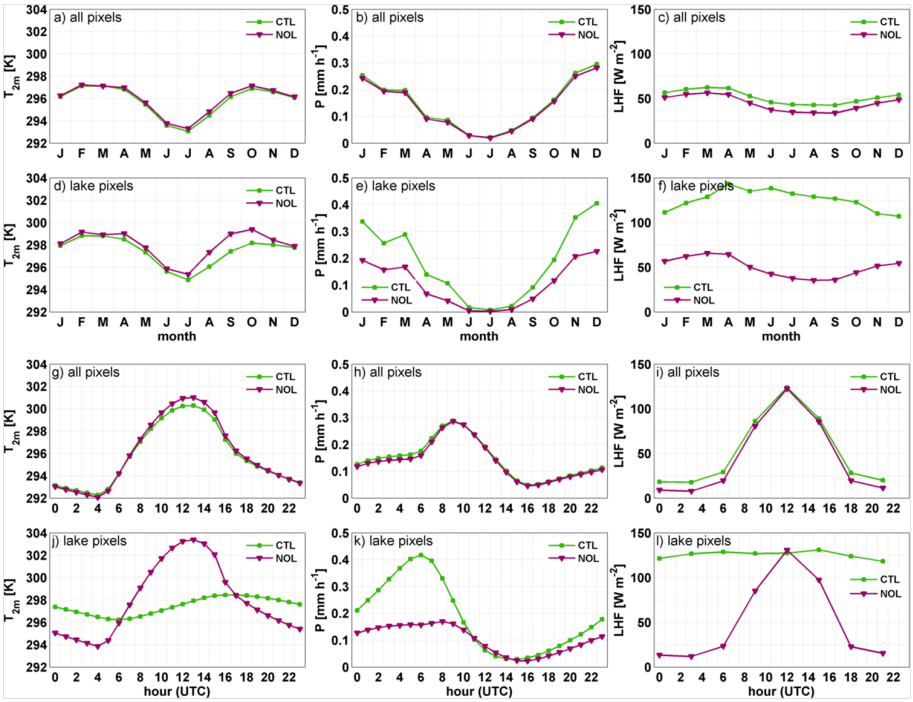

Figure 5.10: **Domain-averaged seasonal cycle over the period 1999-2008 for (a) 2 m air temperature T_{2m} [K], (b) precipitation P [mm h^{-1}] and (c) latent heat flux LHF [W m^{-2}] from the CTL and NOL simulations (green and purple lines, respectively). (d)-(f): same as (a)-(c), but considering only lake pixels in CTL and the corresponding pixels in NOL. (g)-(l): same as (a)-(f), but for the diurnal cycle.**

yr^{-1}), both on daily and subdaily time scales. On seasonal scales, the impact on precipitation is lowest during the main dry season (JJA: +7 mm $month^{-1}$ over the AGL versus +77 mm $month^{-1}$ during the remaining months). Note that, although interesting, the change in frequency and magnitude of individual precipitation events is not considered in this study. Their future change under the influence of anthropogenic greenhouse gas emissions is however analysed in detail in chapter 7.

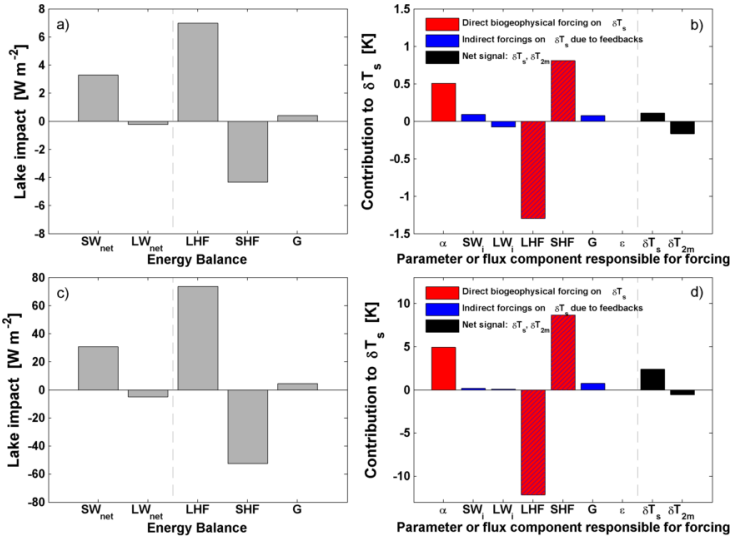

Figure 5.11: **Lake-induced change in the surface energy balance components net shortwave radiation $\mathbf{SW}_{net}$, net longwave radiation $\mathbf{LW}_{net}$, latent heat flux LHF, sensible heat flux SHF and subsurface heat flux G for (a) the whole domain and (c) lake pixels only (all units W $\mathbf{m}^{-1}$). Individual direct (red), indirect (blue) and mixed (hatched) contributions to $\delta\mathbf{T}_s$ described in Eq. (5.2) are shown for (b) the whole domain and (d) lake pixels only (all units K). Each contributing factor is indicated by its corresponding responsible parameter or flux component, with α denoting the change in $\mathbf{T}_s$ caused by a modified albedo, $\mathbf{SW}_i$ by changing incoming shortwave radiation, $\mathbf{LW}_i$ by changing incoming longwave radiation, LHF by changing evapotranspiration, SHF by changing sensible heat flux, G by changing subsurface heat flux and ϵ by changing emissivity. Finally, the AGL impact on $\mathbf{T}_{2m}$ is also shown.**

5.3.3 Decomposing the lake-induced surface temperature change

An overview of the net changes in the main components of the surface energy balance induced by the lake presence, for all pixels and lake pixels only, is provided in Fig. 5.11a and c, respectively. The increase in net shortwave radiation ($\delta\mathrm{SW}_{net}$) is caused by the lower albedo of water relative to the surrounding land (-0.12) and reduced cloud cover during daytime. Furthermore, as lakes evaporate at the potential evaporation rate, they enhance evapotranspiration (LHF) relative to the surrounding land, while SHF is reduced (Table 5.3).

The seven factors contributing to a change in surface temperature are described

in Eq. (5.2) and are expressed in Kelvin. The parameters and flux components responsible for these forcings are shown with their corresponding forcing in Figure 5.11b,d. Note that the temperature imbalance is only 0.005 K and 0.002 K for the all pixels and lake pixels case, respectively, demonstrating balance closure for the depicted components.

Lakes are darker and therefore reflect less incoming radiation, resulting in a positive contribution to δT_s from changing albedo of +0.51 K over the whole domain and +4.91 K over the lakes (Figs. 5.11b,d: α). On the other hand, the contribution to δT_s caused by the higher surface longwave emissivity of water relative to the surrounding vegetation is negligible (Fig. 5.11b,d: ϵ). A strong increase in evaporation from the lakes contributes to a lower δT_s by -1.30 K over the whole domain and up to -12.21 K over the lakes, and forms the largest individual contribution to δT_s (Fig. 5.11b,d: LHF). Note that, since the change in evapotranspiration is influenced by the latent heat of vaporization and air saturation (in turn depending on temperature), it is impossible to distinguish between direct and indirect components in the case of LHF (Akkermans et al., 2014). The lower roughness length of the lake surface relative to vegetated land increases aerodynamic resistance and therewith slows down the turbulent heat transfer from the surface to the atmosphere. The upward SHF is also modified by a changing temperature gradient within the atmospheric surface layer. Together, both processes induce a warming of the surface by +0.81 K over the whole domain, and +8.64 K over the AGL, therewith presenting the strongest positive impact of T_s (Fig. 5.11b,d: SHF). Furthermore, since daytime cloud cover over the AGL is not significantly modified (+2%), the contribution of changing incoming shortwave radiation to δT_s is negligible over the AGL (Fig. 5.11b,d: SW_{in}). The same can be said for the contribution from changing incoming longwave radiation, a feedback depending both on cloud cover and atmospheric temperature (Fig. 5.11b,d: LW_{in}). Finally, the impact of a changing subsurface heat flux represents a small positive contribution to δT_s (Figs. 5.11b,d: G).

As expected, the temperature impact of lake presence is much larger over the AGL compared to the rest of the domain (Table 5.3). However, due to the dynamical changes induced by the AGL and associated changes in near-surface temperature and moisture (see section 5.3.4 for a detailed description), some components are altered over land as well. For instance, the warming effect caused by the enhanced daytime incoming solar radiation (SW_{in}) becomes slightly more important when considering the whole domain, while the influence of a change in incoming longwave radiation (LW_{in}) switches sign (Fig. 5.11b,d).

Altogether, individual contributions to δT_s result in surface temperature increases of 0.26 and 3.02 K over the whole domain and the AGL, respectively (Fig. 5.11b,d; Table 5.3). This seems to be in contradiction with the simulated

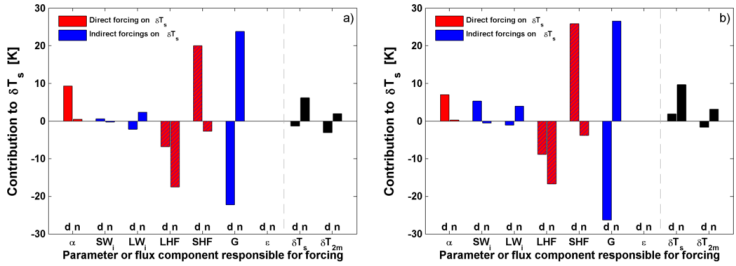

Figure 5.12: **(a) Same as Fig. 5.11d, but now separately from 09-18 UTC ("daytime", shown as d) and from 21-06 UTC ("nighttime", shown as n). (b) Same as panel (a), but for Lake Kivu only.**

change in T_{2m}, which was shown to decrease on average (Figs. 5.8,5.11b,d; Table 5.3). This apparent contradiction is however solved when comparing the forcing components separately during daytime (09, 12, 15 and 18 UTC) and nighttime (21, 00, 03 and 06 UTC; Fig. 5.12a). Note that the full surface energy balance decomposition method cannot be applied on subdaily time scales due to the lag effect of the heat storage component; hence, δG is computed from Eq. (5.2) in this case.

Although δT_s and δT_{2m} depict the same sign on subdaily time scales, their magnitudes vary. During daytime, both T_s and T_{2m} are lower in CTL relative to NOL, as a large fraction of the solar energy penetrates the lakes rather than being absorbed at the surface (Fig. 5.12a: G). At night, when this heat is released again from the mixed layer to the surface, the opposite effect is seen. Note that in this analysis, shortwave radiation penetration into the lake is not taken into account (all radiation is assumed to be absorbed at the surface), hence the large contribution of G. In case shortwave radiation penetration would be taken into account and the energy balance would be considered over a layer deep enough to absorb all radiation, the main contribution would come from the change in energy stored in that layer instead of the subsurface flux out of that layer. The contribution of G to δT_s is only partly compensated by reduced SHF during daytime and enhanced LHF during nighttime in CTL relative to NOL (Fig. 5.12a: SHF and LHF). Furthermore, the lake influence on vertical turbulent heat transport explains the differences in magnitude between δT_s and δT_{2m}: during daytime, the strong decrease in SHF over the lakes (shown by the strong positive contribution of SHF to δT_s in Fig. 5.12a) effectively inhibits heat transfer away from the surface, hence the more pronounced decrease in T_{2m} relative to T_s. At night, the relative contribution to δT_s vanishes as SHF drops over land while remaining more or less constant over lake surfaces (Fig. 5.12a), but again low SHF limits warming at 2 meter (see also Fig. 5.7i). Hence,

when considering the whole day, the nighttime warming dominates δT_s, whereas the daytime cooling dominates δT_{2m} (Figs. 5.11d,5.12a).

Lake Kivu constitutes an interesting exception, as argued in sections 5.3.2 - 5.3.2, given the positive T_{2m} anomaly and strong precipitation increase generated by its presence (Figs. 5.8-5.9). The reasons for this behaviour become apparent when applying the surface energy balance decomposition method to this lake alone. Over Lake Kivu, daytime T_s increases as SHF is strongly dampened during this time (+25.81 K contribution to δT_s; Fig. 5.12b). Furthermore, the lake presence lowers daytime cloud cover and therewith enhances solar radiation input. Both effects are only partly compensated by changes in other contributions to δT_s (Fig. 5.12b: G, α, LHF). At night, the heat release from Lake Kivu is modeled to be more effective relative to the other AGL, further strengthening the nighttime warming influence. The different response of the various surface energy balance components is likely caused by the high-altitude of Lake Kivu (1463 m a.s.l.) relative to other AGL. In our simulation, the surface layer over Lake Kivu is predicted to be very unstable, with an average 3.4 K temperature difference between the lake surface and 2m level (relative to 1.7 K, 1.7 K and 1.2 K over Lake Victoria, Lake Tanganyika and Lake Albert, respectively). Overall, the absence of daytime T_s cooling and strong nighttime T_s warming in CTL relative to NOL causes Lake Kivu to display a general warming influence upon the near-surface air. In addition, the strong nighttime warming intensifies the dynamical response to lake presence (see also section 5.3.4), leading to enhanced atmospheric column destabilisation (Fig. 5.15b) and associated precipitation production.

5.3.4 Dynamical response to lake presence

The dynamical response of the atmosphere to lake presence is further investigated using a set of vertical cross sections along a transect covering the northern sector of Lake Victoria (Fig. 5.1). Based on the diurnal variability of lake impact on T_{2m} and precipitation (Fig. 5.10g-l), we construct two composites of the 1999-2008 3-hourly mean model output, with a first composite averaging output during daytime (09, 12, 15 and 18 UTC; Fig. 5.13), and a second during nighttime (21, 00, 03 and 06 UTC; Fig. 5.14).

During daytime, the atmospheric temperature decrease induced by the lake extends well beyond its shores and up to ∼2 km height above the surface (Fig. 5.13c). At 2 km a.s.l., annual average daytime temperature still decreases by around -0.14 K over the whole model domain, and by -0.40 K over lake surfaces (both changes statistically significant at the 5% significance level). The pressure increase resulting from this cooling (in excess of +0.60 hPa; Fig.

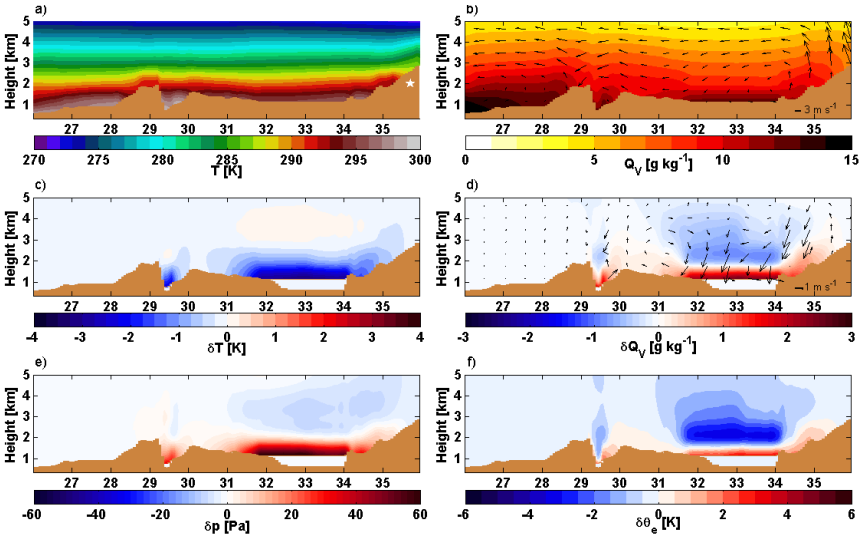

Figure 5.13: **Vertical cross sections along the transect indicated in Fig. 5.1 for the 10-year reference climatologies (*CTL*, 1999-2008) from 09-18 UTC ("daytime") of (a) air temperature T [K] and (b) specific humidity Q_V [g kg^{-1}] including longitudinal circulation climatology, and for the mean change due to lake presence (*CTL* minus *NOL*) in (c) air temperature δT [K], (d) specific humidity δQ_V [g kg^{-1}] due to heat low-induced net convergence at lower levels, as indicated by arrows, (e) pressure δp [Pa], and (f) equivalent potential temperature $\delta\theta_e$ [K]. Lake depth and vertical wind velocity were height-exaggerated by factor 10 and 200, respectively. The white star in (a) denotes the Kenyan Rift Valley mountains.**

5.13e) generates a lake breeze between ∼1-2 km a.s.l. across the lake shore into the western sector of the rift valley (Fig. 5.13d). The lake breeze is offset by updrafts over land, and with westerlies at ∼3-5 km a.s.l. and an over-lake, drying subsidence flow closing the secondary circulation cell over Lake Victoria's western sector (Fig. 5.13d). Although the moisture build-up in the persistently unstable surface layer (Verburg and Antenucci, 2010) tends to destabilize the atmospheric column, the clockwise circulation induces a stabilization of the atmospheric column especially over the western sector of the lake, as reflected by an increased equivalent potential temperature (θ_e) above ∼1.5 km a.s.l. and extending up to ∼6 km a.s.l. (Fig. 5.13f):

$$\theta_e = \left(T + \frac{L_v}{c_p} q_v\right)\left(\frac{p_0}{p}\right) \tag{5.3}$$

with L_v the latent heat of evaporation [2.50 x 10^6 J kg^{-1}], c_p the specific heat capacity of air at constant pressure [1005 J kg^{-1} K^{-1}], q_v the specific humidity [kg kg^{-1}], p_0 the standard reference pressure [1000 x 10^2 Pa] and p the surface air pressure [Pa]. θ_e at lower levels enhances as the effect of increased humidity (Fig. 5.13d) overcompensates the effect of lower temperatures and higher air pressure (Fig. 5.13c,d). The stabilization of the air results in a decrease in upward convective mass flux density (i.e. the vertical mass transport per unit area at cloud base height due to convection; Fig. 5.15a), less intense convection and consequently less rainfall during daytime over the lake. In contrast, the lake presence enhances the convective mass flux density during daytime around the lake (Fig. 5.15a) and therewith daytime precipitation.

In the eastern lake sector, the vicinity of the Kenyan Rift Valley mountains (Fig. 5.13a) modifies the classic lake-breeze circulation as observed over the western sector. Here, the primary daytime circulation is one of orographically induced convection (Fig. 5.13b), associated with an anabatic wind advecting the over-lake moisture upslope up to ∼3 km a.s.l., confirming the conclusion from Anyah et al. (2006) that the anabatic daytime circulation is enhanced by the lake breeze. The strengthening of the anabatic component induces near-surface divergence and associated downward secondary flow aloft from ∼2 to 5 km (Fig. 5.13d). Consequently, the primary upward motion is already suppressed onshore, causing less intense stabilisation over the eastern sector relative to the western part (Fig. 5.13d,f) and consequently a more limited decrease in convective mass flux density (Fig. 5.15a).

At night, the lake surface warms the boundary layer and generates a statistically significant pressure deficit of about -0.12 hPa at the surface (Fig. 5.14c,e). As a response, the circulation over the western sector is effectively reversed, with the lake breeze being replaced by a weak land breeze from the colder land to the warmer lake surface, and compensated by a counter-clockwise motion aloft (Fig. 5.14b,d). When advected over the water, the cold air is warmed and moistened by strong evaporation from the lake (LHF ∼100 W m^{-2} higher than equivalent land points; Fig. 5.10l). While the near-surface air converges and induces upward motion, the warming signal dissipates more quickly in the vertical due to adiabatic decompression, and the enhanced moisture is efficiently transported aloft (Fig. 5.14c,d). At 1 km a.s.l., annual average nighttime specific humidity still increases by around +0.30 g kg^{-1} over the whole domain, and by +1.66 g kg^{-1} over lake surfaces (both changes statistically significant at the 5% significance level). Also note that, again, this is the opposite of the daytime, when downward motion inhibits upward moisture transport building up in the boundary layer and rather transports it horizontally across the lake boundaries (Fig. 5.13d). At night, higher air temperatures, higher specific humidity and lower air pressure reinforce each other in destabilizing the first ∼1

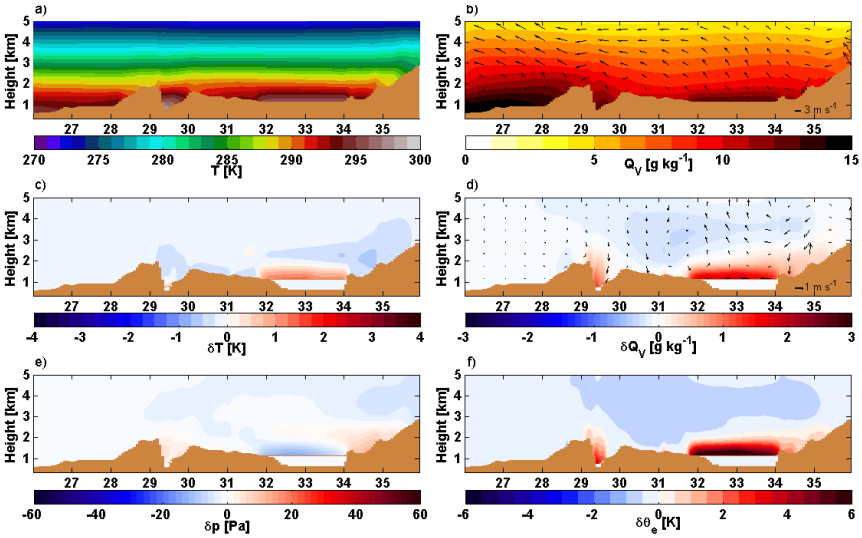

Figure 5.14: **Same as Fig. 5.13, but from 21-06 UTC ("nighttime").**

km of the atmospheric column over Lake Victoria (see Eq. (5.3)), as reflected by the strong increase in θ_e there (∼+6 K; Fig. 5.14c-f). This time, the increase of θ_e in lower levels is not accompanied by a notable decrease at higher levels caused by secondary circulation, pointing to the general destabilization of the nighttime over-lake atmospheric column. This in turn causes an increase in upward convective mass flux density (Fig. 5.15b), more intense convection and associated precipitation during nighttime over the lake. Again, the sign is reversed around the lake, where the lake presence reduces convection and therewith precipitation.

At night, the difference between the west- and eastern sectors is generally less pronounced, although some differences can be noted. Over the eastern sector, the nighttime land breeze enforces katabatic winds flowing down from the eastern mountains (Anyah et al., 2006) and inhibits upslope transport of the warm temperature anomaly (Fig. 5.14b-d). The enhanced katabatic wind generates near-surface divergence on the eastern mountain slope and associated secondary downward motion aloft from ∼2 to 4 km a.s.l., therewith displaying similar secondary circulation over land compared to daytime, although less pronounced (Fig. 5.14d).

Local evaporation and over-lake precipitation are the major contributing terms in the water balances of the African Great Lakes, more than river in- and

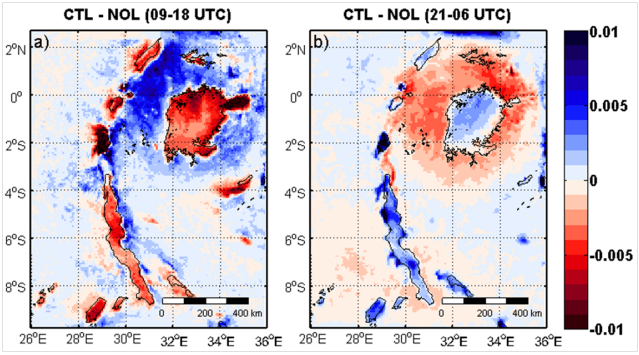

Figure 5.15: **1999-2008 mean change in convective mass flux density at cloud base height [kg m^{-2} s^{-1}] induced by lake presence, for (a) 09-18 UTC ("daytime") and (b) 21-06 UTC ("nighttime").**

outflow. For Lake Kivu, for instance, over-lake precipitation (1470 mm yr^{-1}) and evaporation (1530 mm yr^{-1}) have been estimated to account for 55% and 57% of the total input and output of water to the lake, respectively (Muvundja et al., 2014), while for the larger Lake Victoria, over-lake precipitation (1166 mm yr^{-1}) and evaporation (1784 mm yr^{-1}) account for 59% and 76% of the total input and output of water to the lake, respectively (Swenson and Wahr, 2009). In our simulations, aggregated annual average evaporation and precipitation are close to equal in the AGL region (1583 mm yr^{-1} and 1617 mm yr^{-1}, respectively). This does however not imply that over-lake precipitation is supplied by local evaporation in a closed recycling process. On the contrary, evaporated moisture is transported away from the lake along with the lake breeze during daytime, whereas at night the land breeze advects moisture to the lake.

5.4 Conclusions

The influence of the AGL on the regional climate was studied for the period of 1999-2008 with the regional climate model, COSMO-CLM^2. Efforts were made to enhance the realism of the simulations, by accounting for (i) a model set-up and land surface model suited for tropical conditions, (ii) a horizontal grid resolution effectively resolving individual lakes and complex topography, unprecedented for climate simulations in this region, and (iii) a state-of-the-art one-dimensional lake model capable of reproducing tropical LSWT.

A comprehensive evaluation of COSMO-CLM^2, nested within the ERA-Interim driven CORDEX-Africa simulation (COSMO-CLM), shows an adequate representation of precipitation and LSWT; the model reproduces the most important spatial patterns, including enhanced over-lake precipitation, absolute LSWT values and LSWT gradients within and between lakes. The phase and amplitude of the mean annual cycle are also similar to observations, although the amplitude is overestimated for LSWT and precipitation is underestimated during April and the main dry season. The remaining LSWT biases are ascribed to an underestimation of the mixed layer depth and the absence of three-dimensional circulation in the larger lakes. Furthermore, the mean annual cycles of net shortwave and longwave radiation at the surface, sensible and latent heat flux and cloud cover are mostly simulated within the margins of observational uncertainty. Finally, we show that our simulation largely outperforms a state-of-the-art reanalysis product (ERA-Interim) for most of the considered variables, especially precipitation and LSWT, whereas the added value relative to a state-of-the-art, continent-scale RCM simulation (COSMO-CLM CORDEX-Africa evaluation simulation) is evident for precipitation, LSWT and net surface shortwave radiation.

The AGL significantly reduce offshore near-surface air temperature by about -0.57 K, with maxima in excess of -1.50 K. The cooling effect is advected across the lake shores within dynamic and orographic constraints, and is found to be strongest at the end of the main dry season, when the land surface warms faster than the water surface and the lake-land temperature contrast reaches a maximum. The four major AGL also enhance precipitation by +732 mm yr^{-1} (+87%) over their surface, and even +1373 mm yr^{-1} (+145%) over Lake Kivu. All lakes together annually evaporate 222 km^3 of water into the atmosphere. In contrast to the near-surface temperature impact, the precipitation change is highly restricted to the lake areas. Both for temperature and precipitation, the mean effect masks a pronounced diurnal pattern: the temperature signal exhibits strong cooling during daytime and moderate warming during nighttime over the lakes, whereas precipitation is enhanced mostly at night and during early morning.

Decomposition of the lake-induced surface temperature increase over the AGL shows that reduced albedo has a moderate warming influence (+5.91 K), while reduced sensible heating enhances surface temperatures even more (+8.64 K). For most part, their effect is compensated by the enhanced lake evaporation, responsible for -12.21 K cooling. The apparent contradiction between surface and near-surface temperate change is cleared by considering day- and nighttime separately: daytime heat storage in the lake and reduced upward sensible heat flux dominate the near-surface air temperature change, whereas the nighttime warming determines the surface temperature signal.

Finally, analysis of the dynamical response using day- and nighttime cross sections over lake Victoria highlights the importance of circulation changes induced by the lake-land temperature contrast. During daytime, the lake breeze transports cold air across the lake borders and generates over-land updrafts and over-lake subsidence. This secondary circulation stabilizes the atmosphere above ∼1.5 km and therewith effectively suppresses convection from the unstable surface layer. At night, the thermal inertia of the lake surface generates a positive temperature anomaly and a pressure deficit, and maintains the daytime evaporation rates, inputting large amounts of moisture into the boundary layer. These three effects together cause a strong destabilization of the lower atmosphere. As the land breeze and secondary circulation subsequently induce near-surface convergence and the lifting of these highly unstable air masses, strong convection is triggered and precipitation is released over the lake. On the eastern shore, complex topography and associated gravity currents superimpose on this pattern, generating a somewhat different response especially during daytime.

5.5 Acknowledgments

We would like to thank the CLM-community (http://www.clm-community.eu), and in particular Tom Akkermans and Alessandro Dosio, for the helpful discussions on the modelling with COSMO-CLM^2. François Darchambeau, Pierre-Denis Plisnier, Meteo Rwanda and Patrick Willems are thanked for supplying observational data, Thomas Antheunis for his thoughts on the surface energy balance decomposition technique, and Sonia Seneviratne for supporting this research. Wim Thiery, Matthias Demuzere and Stef Lhermitte are research fellows at the Research Foundation Flanders (FWO). This work was further supported by the Belgian Science Policy Office (BELSPO) through the research projects EAGLES, CLIMLAKE and CLIMFISH. Part of the station data were obtained from the FRIEND/NILE project of UNESCO and the Flanders in Trust Fund of the Flemish Government of Belgium. The computational resources and services used in this work were provided by the VSC (Flemish Supercomputer Center), funded by the Hercules Foundation and the Flemish Government − department EWI.

Chapter 6

Lake Victoria, hotspot of future hazardous thunderstorm intensification

Future climate simulations project an amplification of precipitation extremes and associated weather conditions with harmful consequences for human societies (Lenderink and van Meijgaard, 2008; O'Gorman and Schneider, 2009; O'Gorman, 2012; Kharin et al., 2013; Seneviratne et al., 2012). Today, communities around Lake Victoria in East Africa are already strongly impacted by hazardous thunderstorms, as weather-related deaths among fishermen operating on its surface presumably reach up to several thousands per year (Semazzi, 2011). Here we combine new satellite data, the first high-resolution, coupled lake-land-atmosphere future climate projection for the African Great Lakes and ensemble projections to investigate the potential consequences of anthropogenic greenhouse gas emissions for these nighttime thunderstorms. Our results indicate that the future increase of the strongest precipitation extremes is amplified over Lake Victoria relative to the surrounding land. Land precipitation on the previous day moreover demonstrates a marked control on nighttime occurrence of extremes on the lake through its influence on moisture availability and the lake-land breeze system. The future increase in extremes over Lake Victoria is attributed to thermodynamic processes, that is, a higher water holding capacity of advected air masses, in contrast to the average over-lake precipitation decline caused by local circulation changes. Our results highlight a new major hazard associated with climate change over East Africa with potentially severe human impacts.

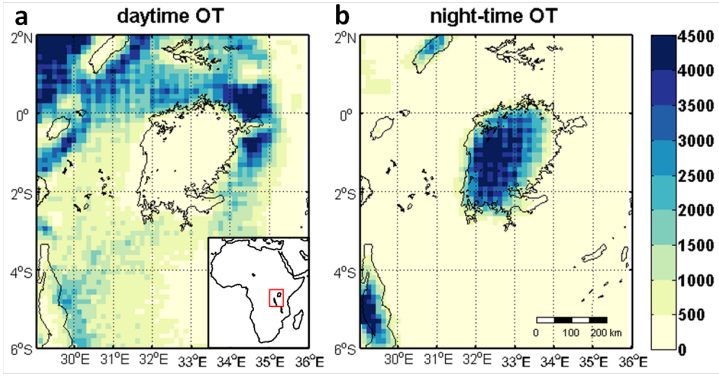

Figure 6.1: **Lake imprint on hazardous thunderstorm occurrence. a-b, Objective satellite-based OT detection during 2005-2013 from 09.00h to 14.45h UTC and 00.00h to 08.45h UTC, respectively. The improved OT detection algorithm was applied to Meteosat Second Generation (MSG) Spinning Enhanced Visible and Infrared Imager (SEVIRI) infrared data (Methods and Supplementary Information).**

Lake Victoria is long known for its notorious weather (Carpenter, 1922), yet its extreme thunderstorms received only very little scientific attention (Semazzi, 2011; Thiery et al., 2015). The impact of its severe weather on society is however undeniable. Thousands of lives are lost per year, and every perished fisherman leaves on average eight dependants behind without an income (Semazzi, 2011), highlighting the major economic consequences of these natural hazards.

Satellite observations enable the recognition of severe weather by detecting overshooting tops (OTs), or dome-like protrusions shooting out of the top of a cumulonimbus anvil (Bedka et al., 2010). OTs are tightly linked to surface severe weather reports (Bedka et al., 2010; Bedka, 2011) and thus mark the presence of strong thunderstorms. Results from an improved OT detection algorithm applied to East Africa (Methods) reveal a marked imprint of Lake Victoria on the diurnal thunderstorm cycle and confirm its status as one of the most active convective regions on Earth (Zipser et al., 2006; Anyah et al., 2006; Thiery et al., 2015) (Fig. 6.1). Notably, from 2005 to 2013, 70% of all 354 000 OTs detected over the lake occurred at night (22.15h-08.00h UTC), in contrast to the surrounding land where afternoon storms dominate (74% of all 356 000 OTs during 11.15h-17.00h UTC). Local evaporation and mesoscale circulation have been identified as key controls on present-day diurnal cycle of precipitation over Lake Victoria (Song et al., 2004; Anyah et al., 2006; Thiery et al., 2015), but so far the triggers for extreme events remain unknown. Combined analysis of satellite-based observation datasets and a multiyear, high-resolution reanalysis

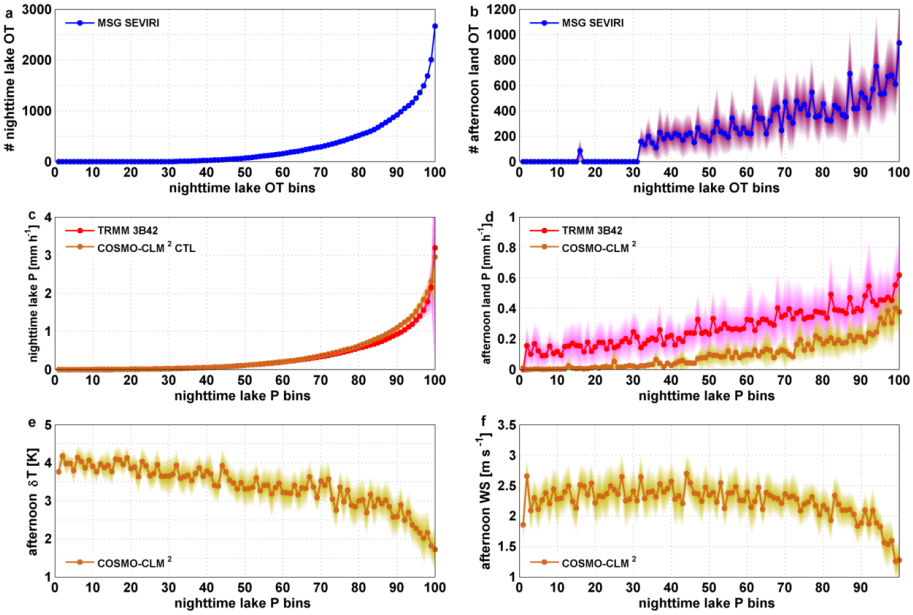

Figure 6.2: **Afternoon controls on nighttime extreme precipitation. a, inverted cumulative density functions of nighttime lake OT detections from the satellite-based SEVIRI product (2005-2013). b, afternoon land OTs surrounding Lake Victoria binned according to a. c, inverted cumulative density functions of nighttime lake precipitation from the satellite-based TRMM product (1998-2013) and corresponding modelled values from the COSMO-CLM^2 control simulation (CTL; 1999-2008). d, afternoon land precipitation surrounding Lake Victoria binned according to c. e-f, Same as d, but for lake-land near-surface air temperature contrast and lake breeze strength. Uncertainty bands indicate one standard deviation.**

downscaling simulation with a state-of-the-art regional climate model (Thiery et al., 2015) (COSMO-CLM^2; Methods) allows, for the first time, to build an explanation for the occurrence of extreme thunderstorms over Lake Victoria.

Binned multi-year OT and TRMM observations reveal that increased thunderstorm activity and precipitation amounts over Lake Victoria are preceded by intense storms and rainfall the afternoon before over land (Fig. 6.2a-d). The enhanced afternoon thunderstorm activity generates a positive moisture anomaly at the surface, therewith increasing the potential for moisture convergence the following night.

Besides enhanced moisture availability, other effects may also play a role. COSMO-CLM^2 generally underestimates precipitation amounts surrounding Lake Victoria, but clearly reproduces the observed positive relationship between

daytime land and nighttime lake precipitation (Fig. 6.2d) and outperforms a state-of-the-art climate simulation in terms of thunderstorm representation (Supplementary Information), indicating that this model may be used to further analyse controls on extreme nighttime precipitation. Afternoon lake surface temperatures binned according to nighttime lake precipitation amounts demonstrate no relationship with extreme precipitation and are therefore considered to have no influence on the occurrence of precipitation extremes. This can also be inferred from theoretical considerations: lake temperatures are among the slowest components of the climate system, whereas extreme precipitation variability is among the fastest components. In contrast to lake temperatures, near-surface land temperatures demonstrate a clear drop the day preceding an extreme event associated with the cold pools of the afternoon thunderstorms. This results in reduced afternoon near-surface air temperature gradients between land and lake (Fig. 6.2e). As a result of this reduced gradient, the afternoon lake breeze also weakens (Fig. 6.2f), therewith limiting moisture transport away from the lake. Here the lake breeze is computed as the average 10 m wind vector length normal to the Lake Victoria contour (outward defined positive, Fig. S9). In addition, since the surrounding land is cold during the day, it will cool down more strongly during the night, thus enhancing the lake-land temperature contrast and the nighttime land breeze. However, as the nighttime storm activity again modifies this pattern, it is not possible to verify this contribution.

Daytime mesoscale dynamical processes thus play a key role in determining extreme nighttime precipitation over Lake Victoria. Three local effects contribute to enhanced over-lake moisture and to the atmospheric column destabilization at night: (i) a positive moisture anomaly over land, (ii) a weaker afternoon lake breeze and associated reduced moisture divergence, and (iii) anticipated enhanced moisture convergence during the following night along a stronger land breeze. This novel understanding of antecedent controls on severe thunderstorms over Lake Victoria paves the way for an early warning system for weather hazards over this lake.

With future climate change, precipitation extremes are projected to increase in intensity almost across the globe (Seneviratne et al., 2012; Kharin et al., 2013; Fischer et al., 2013; Fischer and Knutti, 2015) and even more so over tropical land (O'Gorman, 2012; Kharin et al., 2013; O'Gorman, 2015). Results from the first high-resolution, coupled lake-land-atmosphere climate projection for the African Great Lakes region (Methods; Supplementary information) under a high-emission scenario (RCP8.5) project a contrasting change of mean and extreme precipitation over Lake Victoria. While the annual mean precipitation projected by COSMO-CLM^2 clearly declines over the lake (-135 mm yr^{-1} or -6% compared to -9 mm yr^{-1} or -0.04% over surrounding land; Fig. S3), the 99^{th}

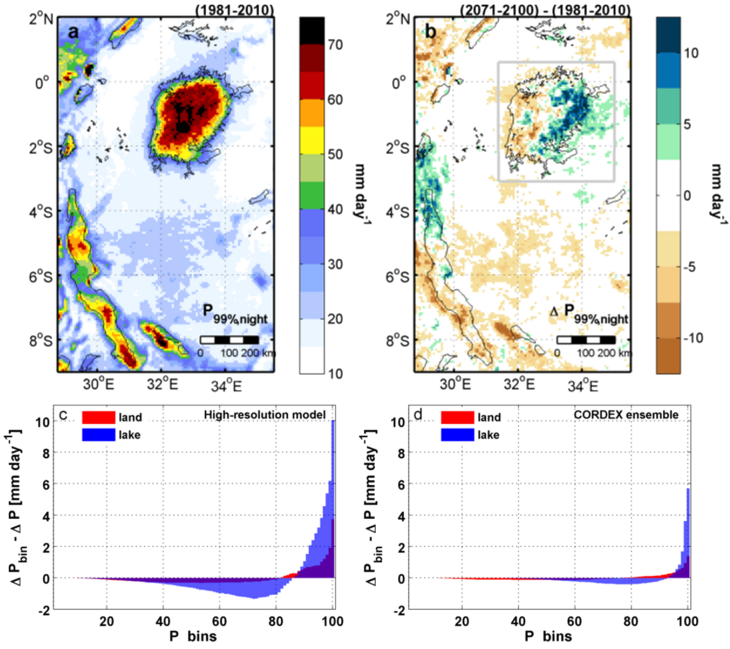

Figure 6.3: **Projected end-of-century changes in extreme precipitation over Lake Victoria. a, Nighttime 99^{th} percentile precipitation ($P_{99\%,night}$) and b, its projected future change (FUT - HIS) according to the high-resolution COSMO-CLM^2 model. The grey rectangle denotes the land pixels considered as "surrounding land". c-d, 24h Lake (blue bars) and land (red bars) binned precipitation change from COSMO-CLM^2 and the ensemble mean of nine CORDEX-Africa members employing a lake model for their simulations, respectively, after subtracting from each bin the mean percentage change $\Delta\overline{P}$. All changes are between time periods 1981-2010 and 2071-2100 under RCP8.5.**

percentile nighttime precipitation increases by 1.2 mm d^{-1} (+2.4%) on average over the lake and locally up to +16 mm d^{-1} and +32% (Fig. 6.3b). This is also evident from the daily binned precipitation changes of integrated over-lake precipitation, which show a future drying for most bins but an increase for the bins containing precipitation above the 90^{th} percentile, and up to +7.4 mm d^{-1} (+18%) for the bin containing the 1% most intense precipitation (Fig. S5). If we additionally subtract the fractional contribution to the average precipitation change from each bin (assuming equal weights), the increase in the highest bin is 2.7 times larger over Lake Victoria compared to surrounding land (Fig. 6.3c). Isolating the local impact on the precipitation distribution from other drivers thus reveals a clear lake effect which amplifies the shift of the precipitation distribution towards higher extremes. The dipole pattern of change (Fig. 6.3b) indicates an eastward shift of intense precipitation systems: convection initiates

in the east and intensifies while being advected westward along the trade winds. In the future, the intensification process is sped up considerably, leading to an earlier release of extreme precipitation.

Results from applying the same analysis to nine members from the CORDEX-Africa regional climate projection ensemble (Methods) confirms that the high-resolution projection disclosed robust features. The ensemble mean annual precipitation projection again shows a significant decline over the African Great Lakes and in particular over Lake Victoria (Fig. S4), while extremes increase faster compared to surrounding land (Fig. S5b). The possibility of an independent mean and extreme precipitation change was already advanced for other regions of the world based on continental-scale regional climate model (RCM) simulations (Fowler et al., 2007), and further in this study we explore the causes for this differential change over Lake Victoria. More importantly, when again isolating the local influence on the precipitation distribution, a pattern emerges which is qualitatively very similar to the high-resolution projection (Fig. 6.3d). According to this ensemble, the isolated 99^{th} percentile precipitation increase over Lake Victoria is 4.2 times larger compared to surrounding land. Although some differences between the CORDEX members are noted, it is clear that the lake effect on the future precipitation distribution is to a large extent independent of the driving global model (Fig. S6). Notably, the precipitation reduction in all bins below the 90^{th} percentile precipitation and the amplification effect for the increase in highest percentiles is projected by every simulation. At the same time, however, it is clear that the absolute response is smaller in the CORDEX ensemble mean (Fig. 6.3c-d). Relative to the high-resolution projection, a coarse-scale model ensemble thus demonstrates a consistent but muted response. Possibly, the muted response is related to the coarser resolution of the continental-scale ensemble. The beneficial effects of enhanced horizontal resolution for model studies in the region were recently described (Thiery et al., 2015), and although the assessment of model skill in terms of the ability to reproduce tropical climate extremes is challenging, the skill of a coarser-scale model simulation was nonetheless clearly lower than our high-resolution COSMO-CLM^2 simulation over the region (Supplementary Information).

To explain the future intensification in precipitation extremes, it needs to be verified whether these events are induced by dynamical changes, e.g. more intense updrafts or stronger near-surface convergence, or by thermodynamical contributions, that is, the enhanced moisture content of advected air masses or enhanced moisture supply through local evaporation, or a combination of these factors. According to preliminary analysis from the high-resolution model projection, in the future not so much the mesoscale dynamics associated with extreme events will change (Fig. S8c-d), but rather the positive moisture anomaly in the atmosphere during the previous day (Fig. S8a-b). This

is consistent with the sensitivity of the strong extremes to temperature changes: only over the lakes moisture availability is high enough to enable scaling according to the Clausius-Clapeyron relationship, whereas moisture is a limiting factor over the surrounding land leading to a significantly lower scaling (Supplementary Information). Further research is however needed to quantify the contributions from the different dynamic and thermodynamic drivers to the change in extremes.

The picture is different for the change in mean precipitation. The average precipitation decline over Lake Victoria is due to a decrease in moisture convergence rather than changes in evaporation over the lake, which in fact increases (Supplementary Information). By the end of the century, nighttime near-surface air temperatures will have warmed faster over land compared to the lake, thus weakening the lake-land temperature contrast responsible for the land breeze and nightttime moisture advection. In addition, during daytime the warmer land intensifies the lake breeze system and associated moisture removal from the lake (Fig. S3). With almost half of the precipitation generated over Lake Victoria depending on this mesoscale circulation (Thiery et al., 2015), this projected change in local circulation patterns can explain the average precipitation decrease over Lake Victoria.

Using a dedicated, high-resolution RCM set-up for equatorial East Africa, we project a significant future decline in annual mean precipitation over the African Great Lakes, and Lake Victoria in particular. The decrease is robust, despite large uncertainties regarding the precipitation change at the regional scale, and it is explained by means of future enhanced (reduced) lake (land) breezes associated with a faster warming land, leading to reductions in local moisture convergence over the lake. Despite this average decrease, we project a strong and robust increase in precipitation extremes over Lake Victoria and show that this increase is stronger over the lake compared to surrounding land. In contrast to the mean change, this differential change in precipitation extremes is not caused by changes in circulation but by future moisture availability: only over the lake the moisture supply through local evaporation and especially moist advection is high enough to sustain Clausius-Clapeyron scaling.

Our results underline the need to take local effects into account when assessing high-impact climate change. Local effects, for instance induced by mesoscale circulation, superimpose on large-scale climate change patterns and may yield very different responses at the local scale. This is especially relevant in the context of climate change in Sub-Saharan Africa, where limited adaptive capacities render populations more vulnerable to climate change and associated changes in climate extremes. State-of-the-art climate models face difficulties in representing precipitation extremes as they parameterize convection rather than explicitly resolving it (Ban et al., 2014; Brisson et al., 2015; Prein et al.,

2015). Rapidly increasing computing capacities may therefore soon be applied for ensemble projections for East Africa at convection-permitting scales.

6.1 Methods

6.1.1 Overshooting top detections

We improved an overshooting top detection algorithm (OTDA)(Bedka et al., 2010; Bedka, 2011) and applied it to the Meteosat Second Generation (MSG) Spinning Enhanced Visible and Infrared Imager (SEVIRI) infrared satellite data for the African Great Lakes region. The OTDA builds on the premise that OTs are composed of a small region of very cold infrared (IR) brightness temperatures (BTs) surrounded by a warmer cirrus anvil cloud (Bedka et al., 2010; Bedka, 2011). As OTs penetrate through the level of neutral buoyancy (LNB), they continue to cool at a rate of 7-9 K km^{-1} making them much colder than the anvil cloud which typically resides between the LNB and the tropopause (Wang, 2007). The OTDA first identifies candidate OT regions by selecting MSG SEVIRI pixels with an IR BT $\leq$ 217.5 K and near to or colder than the tropopause temperature defined by the Modern Era Retrospective analysis for Research and Applications (MERRA) (Rienecker et al., 2011). The cirrus anvil cloud surrounding a candidate OT region is sampled, and if the candidate is significantly ($\geq$ 6 K) colder than the anvil it is classified as an OT. Detection thresholds for the OTDA were based on analysis of a large sample of OT-producing storms depicted within 1-km spatial resolution Moderate Resolution Imaging Spectroradiometer (MODIS) and Advanced Very High Resolution Radiometer (AVHRR) imagery.

6.1.2 Climate simulations

All simulations are performed with COSMO-CLM^2, which couples the non-hydrostatic regional climate model COSMO-CLM version 4.8 to the Community Land Model version 3.5 (CLM3.5) and the Freshwater Lake model (FLake)(Davin et al., 2011; Davin and Seneviratne, 2012). Detailed descriptions of the model system and its subcomponents are provided in earlier studies (Davin et al., 2011; Davin and Seneviratne, 2012; Oleson et al., 2008; Rockel et al., 2008; Mironov et al., 2010; Doms, 2011; Doms et al., 2011; Panitz et al., 2014; Thiery et al., 2015).

The COSMO-CLM^2 model is applied in its tropical configuration(Panitz et al., 2014; Thiery et al., 2015) to generate three climate simulations. First, a control simulation (CTL) is conducted with ERA-Interim reanalysis as lateral boundary conditions for the period 1996-2008 and using the 0.44° COSMO-CLM CORDEX-Africa evaluation simulation (Panitz et al., 2014) as intermediate nesting step. The CTL simulation may thus be considered an

ideal boundary experiment. But while this simulation may serve to analyse the processes governing precipitation extremes, it is not suitable for climate change assessments. The same nesting strategy is therefore employed to dynamically downscale a global climate model (GCM) simulation from the Coupled Model Intercomparison Project phase 5 (CMIP5). The Max Plank institute MPI-ESM-LR GCM was selected based on its ability to well represent observed seasonal and annual precipitation variability over East Africa (Otieno and Anyah, 2012). GCM downscalings are performed for the historical reference period 1979-2010 (HIS) and the future projection 2068-2100 under a high emission scenario RCP8.5 (FUT).

All experiments are conducted at a horizontal resolution of 0.0625° (∼7 km), using 50 vertical levels and a time step of 60 s. The model domain encompasses the central part of the East African rift (Fig. S1) and therewith includes most of the African Great Lakes. A recent global bathymetry dataset (Kourzeneva et al., 2012a) is used as a basis for the lake depth specification in FLake. The first 3 years of each simulation are considered as spin-up and excluded from the analysis.

The COSMO-CLM^2 model system demonstrates excellent performance for the present-day climate of this region (Thiery et al., 2015) and FLake was judged suitable for application to the African Great Lakes (Thiery et al., 2014a,b). A comparison of modelled and observed OT detections moreover demonstrates the ability of COSMO-CLM^2 to well represent the diurnal cycle of OT over Lake Victoria (Supplementary Information). The enhanced skill relative to the parent simulation is mainly due to the inclusion of a lake model and the high horizontal grid resolution, effectively resolving individual lakes and complex topography and unprecedented for climate simulations in this region.

6.1.3 CORDEX ensemble analysis

The public domain CORDEX Africa RCP8.5 ensemble currently consists of 17 members, from which we select the 9 members that compute the two-way lake-atmosphere exchange interactively with a lake model (in casu FLake). Daily precipitation sums of these 9 members are available from 1951 to 2100 and were remapped to the COSMO-CLM^2 grid using bilinear interpolation. From these fields we computed the 99.9^{th} percentile precipitation per model and per decade. Their arithmetic averages over Lake Victoria and surrounding land (4.01°S - 2.01°N and 29.98°E - 35.95°E) are subsequently binned according to the corresponding decadal mean 2-meter air temperatures over lake and land using a bin width of 1 K. Medians, first and third quartiles are computed for each bin and visualised in Fig. S7. Clausius-Clapeyron scaling factors over

the whole 150-year simulation period are obtained through a linear fit to the natural logarithm of the spatially averaged decadal mean 99.9^{th} percentiles of daily lake and land precipitation, respectively. The same approach is applied to compute the Clausius-Clapeyron scaling factors from the COSMO-CLM^2 HIS (1981-2010) and FUT (2071-2100) simulations, and to test the sensitivity of the scaling to the precipitation percentile and choice of RCP. Note that in the considered dataset, only a subset of the CMIP5 ensemble is downscaled using one RCM and one RCP, thus reducing the spread relative to a downscaling of the full ensemble.

6.2 Acknowledgements

We acknowledge the CLM-community (http://www.clm-community.eu) for developing COSMO-CLM^2 and making the model code available, and Hans-Jürgen Panitz for providing the lateral boundary conditions. Wim Thiery and Stef Lhermitte are research fellows of the Research Foundation Flanders (FWO). This work was further supported by the Belgian Science Policy Office (BELSPO) through the research project EAGLES. Computational resources and services used for the regional climate modelling were provided by the VSC (Flemish Supercomputer Center), funded by the Hercules Foundation and the Flemish Government − department EWI.

Author contributions

Wim Thiery (W.T.), Nicole van Lipzig (N.V.L.), Edouard Davin (E.L.D.) and Sonia Seneviratne (S.I.S.) designed the study. W.T. conducted the RCM simulations, performed all model analyses and wrote the manuscript. Kristopher Bedka (K.B.) developed the OT detection algorithm and retrieved the Lake Victoria time series. Stef Lhermitte (S.L.), W.T. and K.B. analysed this data. All authors commented on the manuscript.

Additional information

The model output encompasses 9.6 TBytes and is available upon request. Correspondence and requests for materials should be addressed to W.T. (wim.thiery@ees.kuleuven.be).

6.3 Supplementary Information

6.3.1 Evaluation of COSMO-CLM^2 for extremes

The skill of the COSMO-CLM^2 model system has been assessed in several recent regional climate modelling studies (Davin et al., 2011; Davin and Seneviratne, 2012; Lorenz et al., 2012; Akkermans, 2013; Akkermans et al., 2014; Lejeune et al., 2014; Thiery et al., 2015). The added value of COSMO-CLM^2 relative to the standard COSMO-CLM set-up was demonstrated both over Europe (Davin et al., 2011; Davin and Seneviratne, 2012; Lorenz et al., 2012) and Central Africa (Akkermans, 2013), and appeared through a better partitioning of the turbulent fluxes and associated improved representation of climate characteristics, such as near-surface temperature, precipitation and cloud cover. Based on the comparison of offline simulations with TERRA-ML and CLM3.5 (the land surface models of COSMO-CLM and COSMO-CLM^2, respectively) at four central African flux tower sites, this enhanced skill was attributed to a more realistic representation of the leaf area index, surface albedo and root depth in CLM3.5 (Akkermans et al., 2012). In a multiyear 25 km resolution COSMO-CLM^2 simulation over Central Africa, a close correspondence was obtained between the observed and modeled near-surface temperature, column precipitable water and surface net longwave radiation, whereas the seasonal cycles of precipitation, cloud cover, top of the atmosphere outgoing longwave radiation and various solar radiation quantities were mostly reproduced within the margins of observational uncertainty, albeit some regional deficiencies (Akkermans et al., 2014).

An extensive evaluation (Thiery et al., 2015) of the COSMO-CLM^2 CTL simulation over the African Great Lakes region (Fig. S1) demonstrated the ability of the model system to represent the mean climate of the region considered in this study. In particular, the resolution was deemed sufficient to capture effects of lakes and local orography on precipitation and other atmospheric variables, and the spatial and temporal patterns of the lake surface temperatures as well as differences between individual lakes were found well represented by the lake model embedded within COSMO-CLM^2 (FLake), confirming earlier findings from offline FLake simulations (Thiery et al., 2014a,b). The mean annual cycles of net shortwave and longwave radiation at the surface, sensible and latent heat flux and cloud cover were also simulated mostly within the margins of observational uncertainty. Moreover, it was shown that the CTL simulation largely outperforms ERA-Interim for most of the considered variables, and the COSMO-CLM CORDEX-Africa evaluation simulation for precipitation, lake surface temperature and net surface shortwave radiation. Relative to these two other model products available for the African Great Lakes region, the CTL

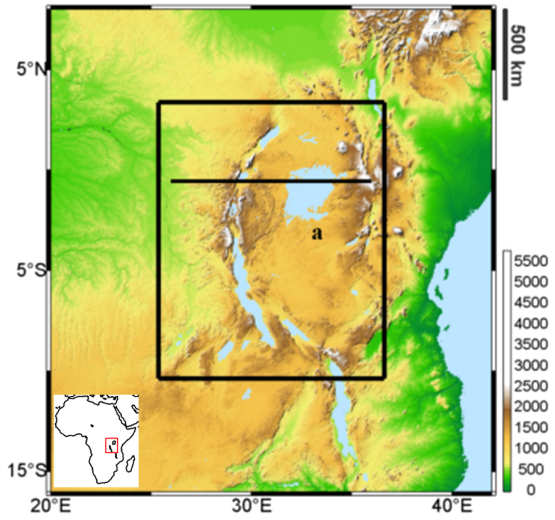

Figure S1: **COSMO-CLM^2 domain description. Shuttle Radar Topography Mission (SRTM) surface height (m) over the African Great Lakes region. The black rectangle denotes the COSMO-CLM^2 model domain (25.375°E to 36.625°E; 10.375°S to 3.375°N, center at 31°E, 3.5°S). The black line shows the transect (26-36°E; 0.55°S) used for the vertical cross sections in Fig. S8. Lake Victoria (a) is the largest of the African Great Lakes.**

simulation benefits from the coupling to state-of-the-art land surface and lake models, as well as from the enhanced model resolution which allows for more fine-scale circulation and associated precipitation patterns to develop over this complex terrain.

Compared to evaluating the simulated mean climate over the African Great Lakes region, a model evaluation for precipitation extremes presents itself as more challenging. Observational precipitation products are highly uncertain for extremes in the tropics (Kharin et al., 2013), hence they cannot be readily used to assess the model's ability to reproduce extreme precipitation. The OT dataset, in contrast, provides a spatio-temporally explicit detection of local convective cloud top cold temperature anomalies at the level of neutral buoyancy, and constitutes a reliable proxy for a vigorous convective cell causing severe weather at the surface(Bedka et al., 2010; Bedka, 2011; Bedka et al., 2012). However, since convective cloud top temperatures are not provided by the model, a direct comparison between modelled and observed OT is not possible. We therefore construct a time series of modeled OT by selecting the model pixels with convective cloud top height above the tropopause height, set at 15 km. This height threshold is regionally dependent and was chosen such that the

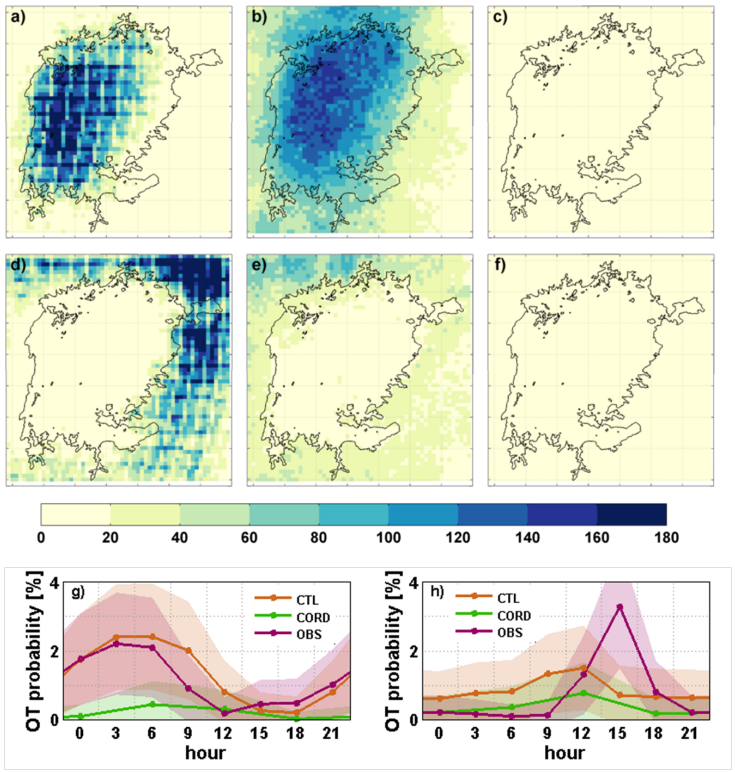

Figure S2: **Evaluating COSMO-CLM^2 and CORDEX for Overshooting Top (OT) occurrence. a,d 2005-2008 Observed OT detections during daytime (10-15 UTC) and nighttime (01-06 UTC), respectively. b,e Corresponding COSMO-CLM^2 and d,f CORDEX modelled OT detections, with a modelled OT defined as a convective cloud top height pixel exceeding 15 km altitude. g-h OT diurnal cycle over Lake Victoria and the surrounding land, respectively.**

total number of hits in the COSMO-CLM^2 CTL simulation and OT dataset differ less than factor 2 for the Lake Victoria region. Consequently, although we cannot evaluate the model's ability to reproduce hazardous storms of a predefined intensity, we can compare spatial and temporal patterns of events defined as extreme for both datasets.

COSMO-CLM^2 captures the strong lake imprint on nighttime OT occurrence, although the lake-land contrast is less pronounced than observed (Fig. S2a-b). During daytime, COSMO-CLM^2 underestimates OT occurrence over land, especially east of the lake where interactions between the synoptic and mesoscale circulation generate enhanced thunderstorm activity (Lauwaet et al., 2012) (Fig. S2d-e). The COSMO-CLM CORDEX-Africa evaluation simulation (Panitz

et al., 2014) (hereafter referred to as CORDEX) fails to reproduce the observed signal as the convective cloud top height almost never exceeds the 15 km altitude level in this coarser-scale simulation (Fig. S2c,f). Furthermore, COSMO-CLM^2 succeeds well in reproducing the daily cycle of OT occurrence probability over Lake Victoria, except for an underestimation OT probability at 9 and 12 UTC, while the CORDEX simulation again fails to reproduce an appropriate diurnal OT cycle (Fig. S2g). In contrast, the diurnal convection cycle over land is ill represented both in CTL and CORDEX, with the OT probability peak predicted too wide and too early in the afternoon (Fig. S2h). This is a well known issue in RCM simulations with parameterized convection (Ban et al., 2014). Conducting our simulations at 1 km resolution would allow major cloud systems to be resolved (Palmer, 2014), and would probably lead to improved representation of hourly precipitation extremes and the diurnal cycle of convection (Lauwaet et al., 2010; Ban et al., 2014; Prein et al., 2015).

6.3.2 Projected climate change for the African Great Lakes region

This study presents the first high-resolution, dedicated climate projection for the African Great Lakes region (Fig. S1). Under a high-emission scenario, near-surface air temperatures is projected to rise by +4.16 K on average over the model domain towards 2071-2100 (relative to 1981-2010), and by +3.74 K over the lake surfaces (Fig. S3c). The projected temperature change is consistent with the ensemble mean 2-meter temperature projection of +4.0 K (+2.4 to +5.6 K) under RCP8.5 by the CMIP5 ensemble for the larger East Africa (11.3°S to 15°N, 25°E to 52°E).

Precipitation decreases by -7.95% on average over the model domain and by -7.46% over the lake surfaces. The average precipitation decline is for most part due to the decreases over the western part of the rift valley mountains and over the African Great Lakes (Fig. S3f). The distinct decrease in precipitation over the African Great Lakes is consistent with the ensemble mean projection of 15 CORDEX members currently available in the public domain (Fig. S4). Precipitation projections between COSMO-CLM^2 and CORDEX generally agree also in terms of binned precipitation change, although the precipitation increase of the land surrounding lake Victoria is more pronounced (Fig. S5). Also the amplification effect on the intensification of extremes is consistent in COSMO-CLM^2 and the individual CORDEX members (Fig. S6).

Change in evapotranspiration are small over land (+31 mm yr^{-1}) but a large increase is projected over the lake surfaces (+142 mm yr^{-1}; Fig. S4i). The vertically integrated moisture convergence flux, calculated here as the

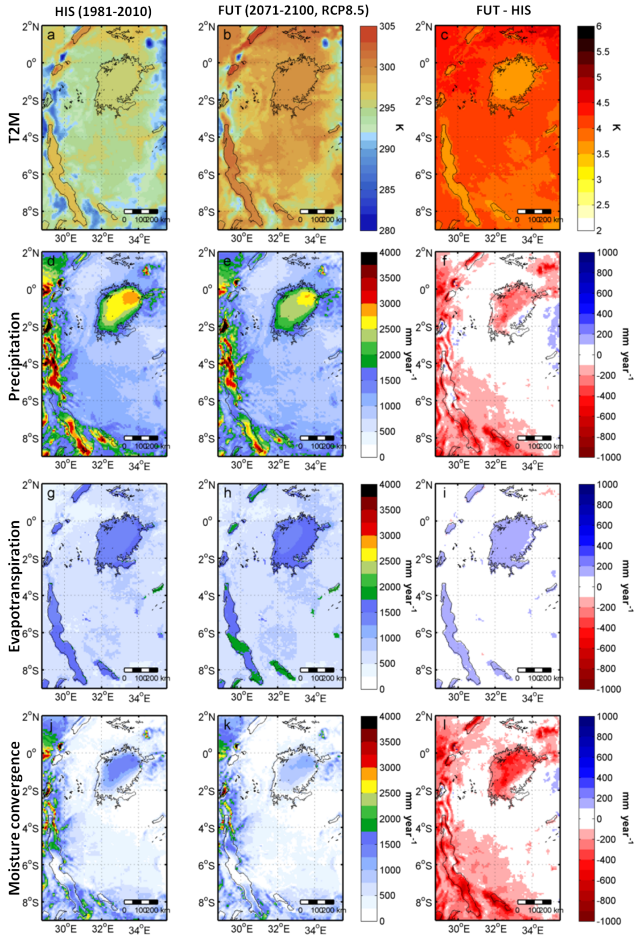

Figure S3: **Projected climate change for the African Great Lakes region. Shown are annual mean 2 m air temperature T_{2m} [K], precipitation P [mm year^{-1}], Evapotranspiration ET [mm year^{-1}] and vertically integrated moisture convergence P-ET [mm year^{-1}] for the (a,d,g,j) historical (HIS) and (b,e,h,k) end-of-the-century (FUT) simulations, and (c,f,i,l) change between the periods 1981-2010 and 2071-2100 (FUT-HIS).**

residual of the precipitation and local evapotranspiration (P-E) is a measure for future changes in horizontal moisture transport. Reduction in moisture convergence over Lake Victoria overcompensates the future increase in local evapotranspiration and is also main cause for the precipitation reduction (Fig. S4l).

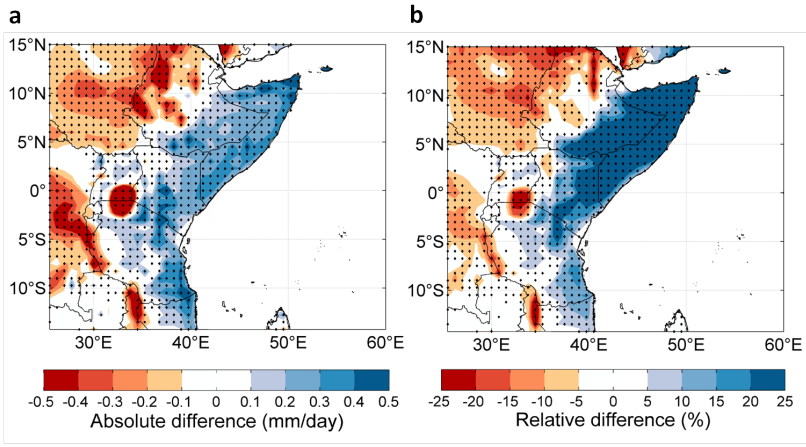

Figure S4: **CORDEX Projected precipitation change in East Africa. Absolute and relative precipitation change between 1981-2010 and 2071-2100 (RCP8.5; 15 member ensemble mean). Statistically significant changes at the 1% level are shown by the black diamonds (Kolmogorov-Smirnov test against null hypothesis of both samples being drawn from the same distribution; Courtesy of Niels Souverijns).**

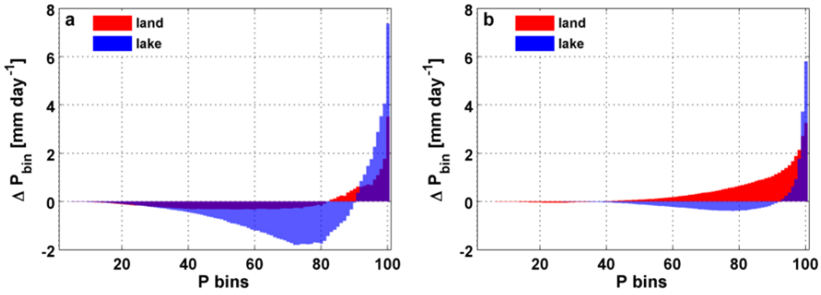

Figure S5: **Projected end-of-century precipitation percentile changes over Lake Victoria. a, 24h Lake (blue bars) and land (red bars) binned precipitation change from COSMO-CLM^2 and b, the ensemble mean of nine CORDEX-Africa members employing a lake model for their simulations. All changes are between time periods 1981-2010 and 2071-2100 under RCP8.5.**

6.3.3 Clausius-Clapeyron scaling

Many studies have related the increase of precipitation extremes with global warming to the Clausius-Clapeyron relation (Allen and Ingram, 2002; O'Gorman, 2012; Kharin et al., 2013; Ban et al., 2015), which expresses the increase of the water-holding capacity of the atmosphere with warmer temperatures and sets

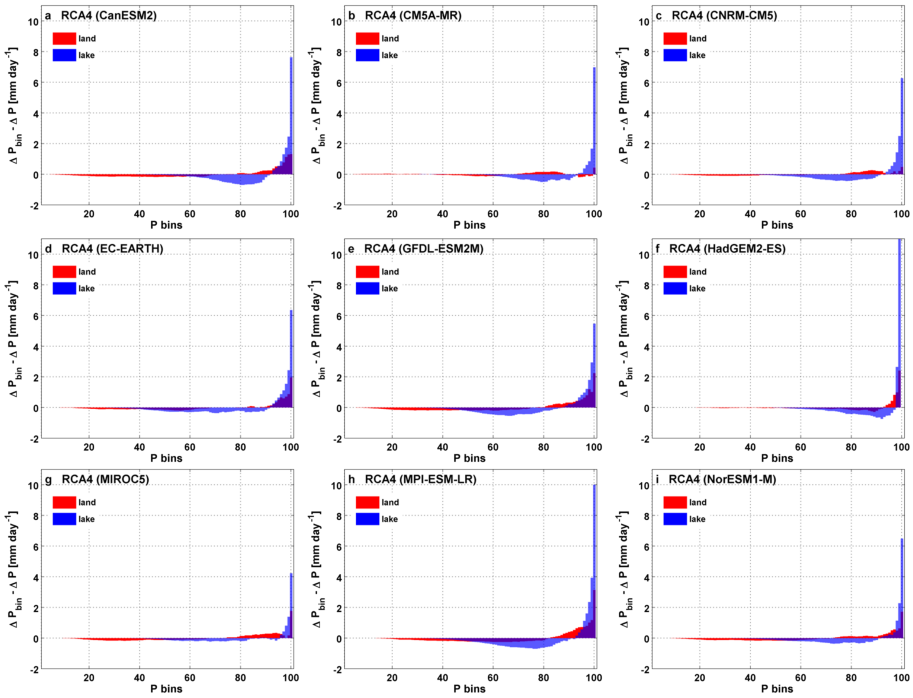

Figure S6: **CORDEX member dependence on lateral boundary conditions. 24h lake (blue bars) and land (red bars) precipitation percentile change from the nine CORDEX-Africa members employing a lake model for their simulations, after subtracting from each bin the mean percentage change. All changes are between time periods 1981-2010 and 2071-2100 for RCP8.5. The ensemble mean is visualised in Fig. 6.3d.**

the sensitivity to 6-7% K^{-1} for typical surface temperatures (O'Gorman, 2015). Others have advanced the potential of subdaily precipitation extremes to exceed expectations from the Clausius-Clapeyron relation (super-Clausius-Clapeyron scaling) from the analysis of rain gauge data (Lenderink and van Meijgaard, 2008; Berg et al., 2013; Loriaux et al., 2013; Ban et al., 2014) and historical (Lenderink and van Meijgaard, 2008; Ban et al., 2014) and future (Lenderink and van Meijgaard, 2008; Kendon et al., 2014) climate simulations. Here we assess the expected Clausius-Clapeyron scaling for daily, moderate extreme precipitation (Fischer and Knutti, 2015) (exceeding the 99.9^{th} percentile - that is, expected once in about three years) over this large tropical lake (Methods). For the selected CORDEX members (1950-2000 and 2010-2100), the ensemble mean scaling for the 99.9^{th} daily precipitation percentile is 7.9% K^{-1} over Lake Victoria and significantly higher compared to the surrounding land (5.8% K^{-1}; Fig. S7a). In the high-resolution COSMO-CLM^2 output (1981-2010 and

2071-2100), 99.9^{th} daily precipitation extremes scale by 6.5% K^{-1} over Lake Victoria and 3.9% K^{-1} over the surrounding land, corresponding to about 1 and 0.6 times the Clausius-Clapeyron scaling, respectively. Although sensitive to the choice of the RCP and extreme precipitation index (Fig. S7b-d), super-Clasius-Clapeyron scaling is found in none of the cases, while over land the scaling remains below 1 time Clausius-Clapeyron even for the strongest extremes.

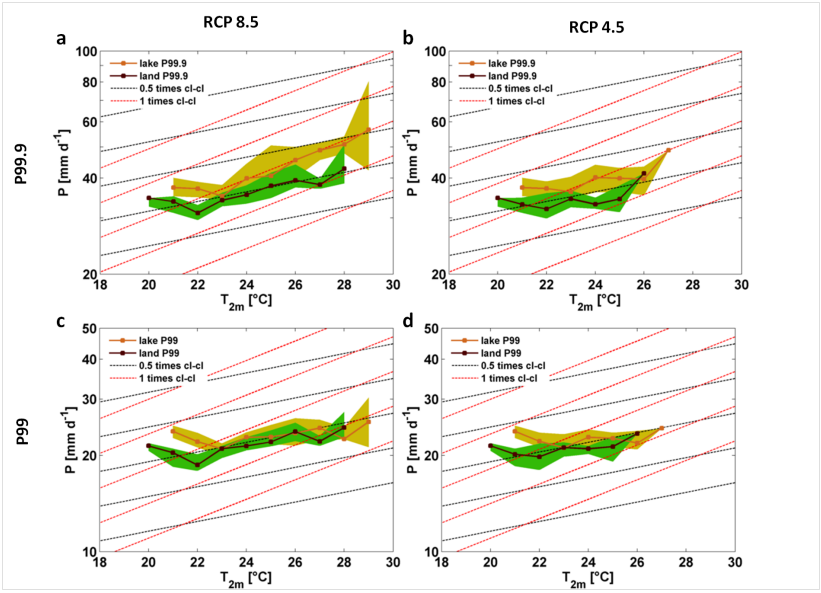

Figure S7: **Sensitivity of Clausius-Clapeyron scaling to percentile and scenario choice. Brown and purple lines indicate the ensemble mean CORDEX daily a,b 99.9^{th} percentile precipitation intensity (only members having a lake model) a function of temperature for RCP8.5 and RCP4.5, respectively, with the coloured bands denoting the interquartile range. c,d Same as a,b, but for the 99^{th} percentile precipitation intensity. Dashed lines are the exponential relations given by 0.5 (black) and 1 (red) times the Clausius-Clapeyron relation. Note the logarithmic y-axis and different y-axis ranges.**

The distinct scaling pattern for moderate extreme precipitation is remarkable, considering the fact that scaling patterns in the extra-tropics generally display little geographical structure, even in the presence of strong orography (Ban et al., 2015). It highlights the key role of Lake Victoria as a regulator of future extremes. Only over the lake, enough moisture will be available in the future to sustain the thermodynamic rate. Over land, moisture availability constrains future extreme precipitation increases expected from thermodynamic considerations. This is in agreement with an analysis of the CMIP5 projections for the region suggesting an increased deficit in local moisture supply (Otieno and Anyah,

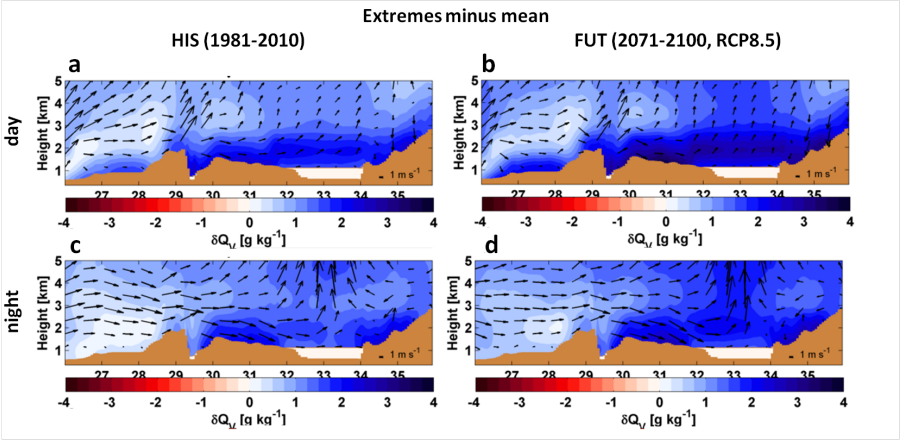

Figure S8: **Anomalous moisture and wind conditions preceding extreme precipitation. Vertical cross sections of specific humidity anomalies δQ_V [g kg^{-1}] and longitudinal circulation anomalies (indicated by wind vectors) between the conditions preceding rainfall events above the 99th precipitation percentile and the 30-year mean along the transect indicated in Fig. S1. Panels indicate the anomalies from 12-15 UTC ("daytime") for a, the historical global climate model (GCM) downscaling (HIS, 1981-2010) and b, the future scenario under RCP8.5 (FUT, 2071-2100). b,d Same as a,c but for 03-09 UTC ("nighttime"). Lake depth and vertical wind velocity were height-exaggerated by factor 10 and 200, respectively.**

2013) and associated increased dependence of regional precipitation to moisture influx from the Indian Ocean (Shongwe et al., 2011). In addition, it has already been suggested that the thermodynamic constraint may not be a good predictor in tropical regions experiencing circulation changes (Seneviratne et al., 2012). In previous studies, changes in the moist-adiabatic temperature lapse rate, tropospheric temperatures and vertical velocity during extremes (O'Gorman and Schneider, 2009) have been advanced next to increased atmospheric moisture content (Lenderink and van Meijgaard, 2008) as explanations for intenser precipitation extremes (Seneviratne et al., 2012). However, while the thermodynamic argument for extreme precipitation sensitivity to temperature changes is well known, other, dynamical factors have been much less studied (O'Gorman, 2015).

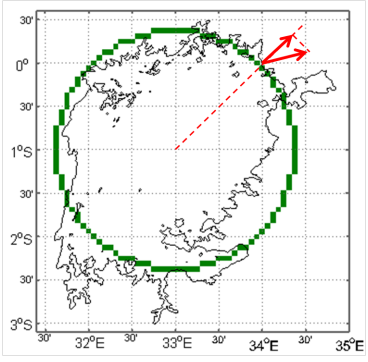

Figure S9: **Illustration of lake breeze calculation. For each pixel on the green circle, the 10 m wind vector is projected onto the radiant direction, after which vector lengths are averaged along the circle (outward defined positive).**

Chapter 7

Conclusions

7.1 Concluding summary

Weather hazards in the African Great Lakes region have a detrimental impact on local societies. The major impact of these vast inland waters on the hydrological cycle urges for an improved understanding of tropical lake-climate interactions and for future projections assessing the consequences of increased greenhouse gas concentrations on the regional climate. Previous efforts put the first steps in this direction. On the one hand, process studies focusing mainly on Lake Victoria allowed for the identification of the most important controlling factors. However, these studies generally lack (i) knowledge on the skill and behaviour of lake models over the African Great Lakes, (ii) an in-depth quality control of the regional climate model output, and (iii) isolation of regional lake effects in long-term, high-resolution climate simulations. On the other hand, international efforts have recently converged into the production of continental-scale, ensemble future climate projections using coarse-scale regional climate models. However, the complex interplay between lakes, orography and synoptic flow in the African Great Lakes region highlights the need to account for lake-atmosphere interactions at high resolution to project the future change in precipitation for the region.

This study addresses the above-mentioned challenges and generates the first high-resolution assessment of the present and future imprint of the African Great Lakes on the regional climate system. The choice and configuration of the coupled lake-land-atmosphere climate model is informed by two detailed studies of the behaviour of one-dimensional lake models over the African Great Lakes

(Chapters 3 and 4). The 10-year climate simulation conducted with optimized configuration is subsequently cross-checked against 15 different observational products, with particular attention to the model's ability to reproduce observed precipitation, lake surface temperatures and surface-atmosphere fluxes. The established model framework then allows to isolate the lake effect from other climatic drivers, in particular by comparing the control simulation to a climate integration with lakes replaced by representative land. It also allows to assess the climatic influence of lake-atmosphere interactions from a surface energy balance perspective and identify changes in atmospheric dynamics and stability induced by the lakes (Chapter 5). Finally, the framework is applied to generate the first dedicated high-resolution, coupled lake-land-atmosphere climate projection for the African Great Lakes region (Chapter 6).

A well-functioning lake surface temperature parameterization scheme is key to impact modelling studies focused on lake-atmosphere interactions. Two preparatory studies therefore precede the actual climate impact assessments. We first conduct an in-depth study of the skill and behaviour of the one-dimensional lake model FLake for the African Great Lakes (Chapter 3). FLake is a rather simple lake model, but thanks to its excellent compromise between physical realism and computational efficiency, it has recently evolved to the standard for lake parameterizations in state-of-the-art climate and weather predictions models. Careful forcing data correction and model configuration enables the reproduction of observed mixed layer depths and water temperatures at three multiyear monitoring sites in equatorial East Africa. Furthermore, a process study establishes the predominant control of dry-season evaporative-driven cooling on seasonal mixed layer dynamics. At the same time, deep-water temperature predictions are identified as being very sensitive to small perturbations in meteorological forcing and model constants. The inability of FLake to robustly simulate deep-water temperatures entails that this model is not suitable to study climate change influences on lake hydrodynamics. Near-surface temperature predictions, in contrast, are judged robust irrespective of the modelled mixing regime, demonstrating the applicability of FLake for lake surface parameterizations in climate models.

In a second study, the skill of the FLake model is benchmarked against other lake models (Chapter 4). This time, a set of seven one-dimensional lake models are evaluated in their ability to reproduce the mixing dynamics within the freshwater layer of Lake Kivu and the salinity-induced permanent stratification of the hypolimnion thereunder. FLake demonstrates good predictive skill relative to the other lake models for the control simulation in terms of mixolimnion temperatures and lake enthalpy change, but sensitivity experiments confirm the strong sensitivity of its bottom temperatures to forcing fields and model configuration. In addition, comparison of CPU times needed to conduct a single

simulation indicates that FLake is 4 to 132 times faster than the other tested lake models. In the multi-model framework, differences between the models are ascribed to variations in the treatment of stratification, radiative forcing and turbulent heat fluxes. Our results therewith indicate possible ways for future improvements of FLake and other lake models (see also sect. 7.2.3).

Besides the skill of standalone lake models, we also assess the performance of the regional climate model (RCM) interactively coupled to a land surface and lake model (Chapter 5). A fully coupled climate simulation with optimized configuration is therefore thoroughly evaluated over a period of 10 years (1999-2008). The COSMO-CLM^2 simulation reproduces observed features such as the seasonal precipitation cycle and its augmentation over the lakes, as well as annual average lake surface temperatures and their gradients within and between lakes. The amplitude of the seasonal cycle of lake surface temperature is, however, overestimated. Benchmarking the skill of this COSMO-CLM^2 integration against the parent simulation and a state-of-the-art reanalysis product demonstrates its added value for most of the considered variables, above all for precipitation and lake surface temperatures.

Essential ingredients for successful precipitation predictions in the region are both a realistic lake surface temperature representation and high resolution, effectively resolving complex topography, surface processes and mesoscale circulation. These insights are particularly useful for ongoing efforts to produce climate assessments and projections at the regional scale, and especially for the Coordinated Regional Downscaling Experiment (CORDEX, see also sections 5.3.1 and 7.3.2).

Moreover, analysis of the spatially-explicit model output allows to assess the validity of the upward wind velocity correction applied in chapter 3 (but not in chapter 4). Average observed wind speed at the Bukavu and Kamembe weather stations are 1.9 m s^{-1} (2003-2011) and 2.7 m s^{-1} (2003-2008), respectively. In Chapter 3, the wind speed measurements of AWS Bukavu were raised by 1 m s^{-1} before using them as forcing for FLake over Ishungu. In Chapter 4, unaltered measurements from AWS Kamembe were used as forcing. In our control RCM simulation, the average modeled wind speed is 1.61 m s^{-1}, 1.79 m s^{-1} and 2.12 m s^{-1} in Bukavu, Kamembe and Ishungu, respectively (1999-2008). The average wind velocity over all lake pixels within the model domain is 1.82 m s^{-1}, or 0.51 m s^{-1} higher compared to the corresponding pixels in the no-lakes simulation (+39%). Comparison of the modeled and observed wind velocities thus suggests that, although COSMO-CLM^2 generally underestimates wind velocity, an upward correction of wind measurements at AWS Bukavu can be justified, but that the applied correction (+1 m s^{-1}) might be higher than the actual wind speed difference between the onshore station and the offshore monitoring site (+0.51 m s^{-1} in the model). The lower wind speed velocities in

COSMO-CLM^2 relative to observed values can furthermore explain differences in modelled lake surface temperature variability noted between the offline and online model simulations (compare Figs 3.4, 3.6, 3.8 and 4.3 to Fig. 5.6). Too low wind speeds in COSMO-CLM^2 as well as in the Ishungu and Kigoma raw and ERA-Interim simulations result in permanently stratified conditions (Fig. 3.11) and consequently the overestimation of the observed seasonal lake surface temperature cycle at Ishungu and Kigoma (Fig. 3.4, 3.6 and 5.6). On the other hand, a correct representation of the mixing seasonality in the control simulations (presumably thanks to an adequate representation of wind velocities) removes this overestimation of the annual cycle, although introducing a small cold bias in some cases (Fig. 3.4, 3.6 and 4.3).

Comparison of 10-year climate simulations with and without lakes reveals a marked imprint of the African Great Lakes on the surface-atmosphere exchange of water and energy. First, lakes are darker and therefore absorb more incoming radiation, while reduced sensible heat loss holds even more energy in the lake. For most part, their combined effect is offset by enhanced lake evaporation. Yet the largest difference compared to the surface energy balance (SEB) over land is the subsurface heat storage during daytime, heat which is released again to the surface at night.

The subsurface heat storage also dominates the lakes influence on near-surface air temperature and results in a cooling effect during daytime (down to -5.60 K at 12 UTC) and a warming influence at night (up to +2.63 K at 4 UTC). Averaged over 24h, the African Great Lakes reduce the temperature of their own surface air by -0.57 K while cooling the entire model domain by -0.17 K. Furthermore, the enhanced evaporation, which is sustained throughout the whole day at an almost constant rate, determines the lake's influence on the hydrological cycle. According to our results, the African Great Lakes annually evaporate 222 km^3 of water into the atmosphere, or 1.5 times more compared to the equivalent land surface.

The lake signature on the surface-atmosphere exchange of water and energy translates into secondary patterns of atmospheric circulation and stability which interact with the synoptic conditions. Our results for Lake Victoria show how the lake breeze transports cold air across the lake borders during daytime, generating over-land updrafts and over-lake subsidence. Consequences of this secondary circulation are the stabilization of the atmosphere above $\sim$1.5 km and the effective suppression of convection. At night, the lower atmosphere is highly destabilised due to the thermal inertia of the lake surface and the large amounts of moisture evaporated into the boundary layer. As the land breeze subsequently induces near-surface convergence and the lifting of these highly unstable air masses, strong convection is triggered and precipitation released over the lake. Our model results indicate that these processes together increase

precipitation production over the African Great Lakes by 713 mm yr^{-1} (+79%). They moreover highlight that the moisture precipitating over the lake is only partly supplied by direct local evaporation, as moisture is transported away from the lake during daytime while being advected from over land at night.

The quantification of the lake effect and its study through the SEB and dynamical framework improves the scientific understanding of climate processes in East Africa. The strong imprint of the lakes on the hydrological cycle additionally highlights the need to implement regional numerical weather prediction (NWP) systems to forecast lake-induced precipitation and storm activity (sect. 7.3). Insights from our analyses may thereby provide useful information for improving the skill of these predictions systems.

Our model projections for the end-of-the-century underline the major role for Lake Victoria in modulating precipitation changes (Chapter 6). Under a high-emission scenario (RCP8.5), over-lake 99^{th} percentile precipitation may intensify by 18% towards 2071-2100 relative to 1981-2010, that is 2.7 times faster compared to the projected change over the surrounding land after isolation from the mean change. The expected Clausius-Clapeyron scaling of precipitation extremes to temperature increases holds over Lake Victoria but not over the surrounding land, confirming the lake imprint on future precipitation change patterns. Interestingly, this is in contrast to the change in average over-lake precipitation, which is projected to decrease by -6% for the same period. By further analysing the high-resolution output we were able to explain this different response. On the one hand, average over-lake moisture availability and associated precipitation reduces towards the future due to a strengthening of the lake breeze and weakening of the land breeze caused by a faster warming of the land. The projected increased water-holding capacity of over-lake and advected air is, on the other hand, responsible for the increase in extremes. Hence, while mesoscale circulation changes cause the average precipitation decline, the response of extremes is essentially thermodynamic.

The results of our high-resolution projection are qualitatively confirmed by the analysis of an ensemble of continental-scale climate projections, but coarse-resolution RCMs fail to grasp the present-day variability of extreme thunderstorms over the lake. Moreover, the potential amplifying influence of lakes on future changes in precipitation extremes is not addressed in previous studies (O'Gorman, 2015) and consequently not mentioned in the recently published fifth assessment report (AR5) of the Intergovernmental Panel on Climate Change (IPCC). So not only will Lake Victoria possibly amplify projected future increases in wet extremes, this is also an effect which is not accounted for by current climate change assessments.

This has important implications for upcoming assessments reports. Our findings

stress the need for high-resolution information on climate change effects on extremes to find its way to mainstream scenarios. Although perhaps less relevant on the global scale, the local effects identified by high-resolution projections of climate extremes may turn out to have a strong impact on local societies (Fowler et al., 2007; Wehner et al., 2011). This calls for a framework wherein information from both RCMs and global climate models (GCMs) are merged to obtain climate change projections at the regional scale.

7.2 Ongoing work

The results described in this thesis shed new light on the role of the African Great Lakes in the regional climate system. Our findings also identified a number of constraints in the current ability to observe, model and adapt to the harmful consequences of tropical lake-atmosphere interactions. In response to these challenges, three new research lines were set up, for which the analysis is currently ongoing. A short overview of their current status is provided hereafter.

7.2.1 Measuring lake-atmosphere interactions

Adequately forcing lake models and evaluating modeled lake-atmosphere interactions is a challenge, especially in the absence of trustworthy direct observations (Sections 3.2.4, 4.2.2 and 5.2.4). Important uncertainties remain present in several of the reference products used nowadays (Dinku et al., 2008; Sylla et al., 2013; Awange et al., 2015), hence the need for high-quality, in-situ meteorological measurements over the African Great Lakes cannot be stressed enough (Anyah and Semazzi, 2004; Anyah et al., 2006; Anyah and Semazzi, 2009). To address this issue, it was decided to install a state-of-the-art automatic weather station (AWS) over the surface of Lake Kivu to measure near-surface meteorological variables and radiation fluxes. During a first field campaign to Lake Kivu, an optimal location for the station was selected and local contacts were established. Then, observational sensors and technical equipment were ordered and extensively tested at KU Leuven in collaboration with technical experts from the Department of Earth and Environmental Sciences. After this successful testing phase, a second field campaign was undertaken during which the AWS was installed on the research platform of the Rwanda Energy Company, ∼3 km offshore of the cities of Gisenyi (Rwanda) and Goma (D.R. Congo; Fig. 7.1).

The measurement set-up consists of sensors for air temperature (T, K), relative humidity (RH, %), air pressure (p, Pa), precipitation (P, mm), wind speed

Figure 7.1: **Automatic weather station on Lake Kivu after its installation, 8 October 2012 (©Wim Thiery).**

(u, m s^{-1}) and direction (WD, °) and the four radiation components (SW_{in}, SW_{out}, LW_{in}, LW_{out}, all in W m^{-2}). The station is powered by a solar panel, and all sensors are placed at a height of 4.40 m above the water surface (a in Fig. 7.1), except for u and WD which are measured at 7.20 m above the lake (b in Fig. 7.1). Variables are sampled every 3 minutes after which 30 minute averages are calculated and stored. Moreover, short periods of high-frequency radiation measurements enable an assessment of the potential effect of platform movements. Through a GPRS communication line, the KU Leuven regional climate studies group directly receives the observations from the station, allowing for a quick and remote detection of potential problems.

Since 9 October 2012, the AWS provides continuous, high-quality observations of near-surface meteorology and four-component radiation. The continuous time series obtained so far from AWS Kivu is unique of its kind in the tropics. The station is also well located to study the influence of the lake-land breeze system on lake-atmosphere interactions (Fig. 7.2). The ongoing data analysis follows two tracks. First, observations are used to conduct an in-depth study of the lake's water and surface energy balance (see also Thiery et al., 2012; Gorodetskaya et al., 2015). Turbulent fluxes of heat and moisture were calculated following Verburg and Antenucci (2010) and demonstrate a marked dependency on both wind speed and direction (Fig. 7.2b). Second, AWS Kivu will be used to evaluate the output from NWP systems and RCM output. In particular, the effect of model resolution on the ability to capture the diurnal pattern of the observed lake/land breeze system (Fig. 7.2) will be assessed.

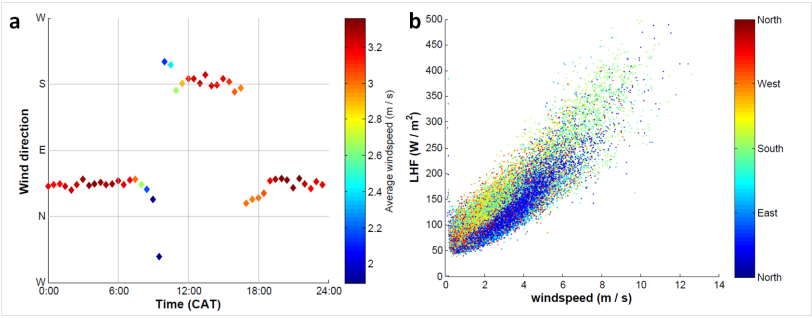

Figure 7.2: **(a) Diurnal cycle of wind speed and direction observed at AWS Kivu; (b) Dependency of calculated Latent Heat Flux (LHF) on wind speed and direction (Courtesy of Stijn Bruggen).**

7.2.2 Towards an early warning system for hazardous thunderstorms over Lake Victoria

The presentation of a new, satellite-derived dataset of extreme thunderstorm counts in chapter 6 demonstrated the strong imprint of Lake Victoria on their occurrence. The consequences of nighttime thunderstorms over Lake Victoria for the livelihood and economy of local communities are enormous (chapter 6). An important cause for this unacceptable human cost is the current absence of a well-functioning early warning system, which would prevent fishermen from sailing off when a severe thunderstorm is about to develop. Recent efforts have been aiming at reducing accidents by issuing storm warnings derived from operational, high-resolution NWP systems. Notably, the meteorological service of the United Kingdom (Met Office) is currently in the process of establishing a 4 km limited area NWP system for the larger Lake Victoria region and a first evaluation indicates an added values relative to a persistence forecast (Chamberlain et al., 2014; Eagle et al., 2015). In parallel, a "Mobile Weather Alert" pilot was launched in 2011 by the World Meteorological Organization (WMO), providing local fishermen with free forecast and warning information via their cell phone (Semazzi, 2011; Chamberlain et al., 2014).

Our study of the controlling factors of extreme nighttime thunderstorms over Lake Victoria revealed a strong dependency of the nighttime over-lake storm intensity on the antecedent daytime land storm activity (Chapter 6). Physically, intense daytime land storms induce a moist anomaly in the lower layers of the atmosphere, and cool the land surface. The cold anomaly limits moisture divergence from the lake (weak lake breeze) while favouring nighttime near-surface convergence (strong land breeze). Satellite-based observations

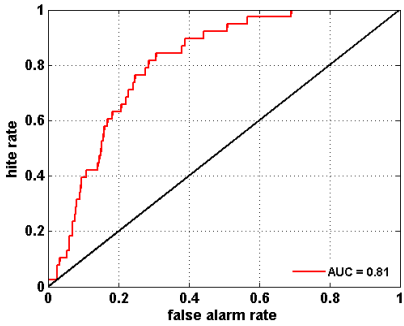

Figure 7.3: **Example Receiver Operating Characteristic (ROC) curve for logistic regression applied to 16 years of TRMM 3B42 precipitation observations over lake Victoria (1998-2013), using daytime land precipitation as predictor and the probability for nighttime precipitation over Lake Victoria to exceed 25 mm as predicted value. The dimensionless Area-Under-the-Curve (AUC) is a measure for the skill of the regression model and is 0.81 in this case.**

of precipitation intensity or thunderstorm activity may therefore potentially serve as a risk indicator for storm intensity over Lake Victoria the following night. Preliminary results of a logistic regression model applied to multiyear observations from the Tropical Rainfall Measuring Mission (TRMM) over and around Lake Victoria (Fig. 7.3) indeed suggest that observed antecedent land precipitation may act as a predictor for hazardous thunderstorms over Lake Victoria.

7.2.3 Improving the stratification treatment in FLake

As described in sections 3.3 and 4.3.1, FLake predictions for water temperatures within the thermocline are very sensitive to perturbation in e.g. the model's external parameters and forcing fields. Possibly, this model deficiency may be attributed to the stratification treatment, in particular the time-rate-of-change of the shape factor with respect to the thermocline dC_T/dt, treated in FLake through eq. 2.3 (see section 4.3.1). Preliminary steps have been taken to improve the stratification treatment in FLake. In particular, an alternative formulation for eq. 2.3 is proposed based upon theoretical considerations, and verified against observational data from a variety of lakes across the globe. This work is conducted in close collaboration with Dr. Georgiy Kirillin, who originally proposed the idea and developed the alternative formulation for dC_T/dt.

The idea builds on the reflection that if the temperature-depth curve within the thermocline has a characteristic, 'self-similar' shape, its time evolution should satisfy the same idea. The proposed alternative relaxation formula is given by:

$$\frac{dC_T}{dt} \propto \frac{dh_{ML}}{dt} \frac{C_T^{max} - C_T^{min}}{h_{BOT} - h_{ML}} \tag{7.1}$$

with a proportionality coefficient subject to quantification. In eq. 7.1, h_{BOT} and h_{ML} represent the lake and mixed layer depth, respectively, while C_T^{min} and C_T^{max} stand for the minimum and maximum values of the shape factor C_T. When merging all constants, eq. 7.1 reduces to

$$\frac{dC_T}{dt} = \frac{dh_{ML}}{dt} \frac{\beta}{h_{BOT} - h_{ML}} \tag{7.2}$$

with β now the sole unknown constant. An advantage of this new approach is that it removes the dependency of dC_T/dt on the characteristic relaxation time scale, t_{rc}, and therewith the dependency on a constant which was determined based on observational data from one lake. A constant which, in fact, turns out to vary with lake depth rather than being universally valid.

The validity of the proposed relationship can be verified by computing all terms from eq. 7.2 from in-situ temperature measurements. To this end, multiyear thermistor chain data from six lakes were employed: Lake Mendota (USA), Lake Kinneret (Israel), Arendsee (Germany), Lake Sparklin (USA), Lake Kivu (Rwanda, D.R. Congo), and Stechlinsee (Germany). The lakes are located in different climates and stretch a wide range of potential mixing regimes. Results indicate a very clear relationship for all considered lakes (Fig. 7.4). In fact, comparison of the slopes of the least squares fit to the respective data clouds even suggests a universal value for β ($\sim$0.37 s^{-1}) irrespective of the lake's depth, climate and mixing regime. This empirical corroboration highlights the potential to improve FLake by replacing eq. 2.3 with eq. 7.2. This improvement may possibly reduce the strong sensitivity of FLake described in chapters 3 and 4.

7.3 Recommendations for further research

In its fifth assessment report (AR5), the Intergovernmental Panel on Climate Change (IPCC) presents the reference projections of future climate change

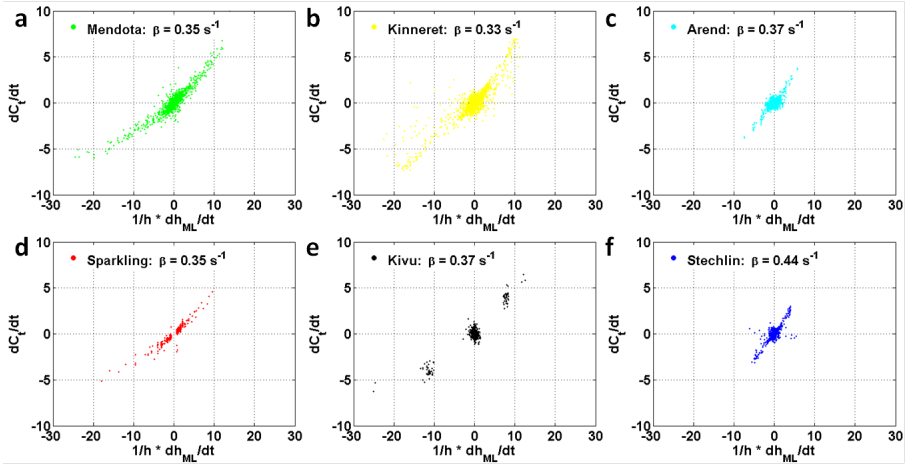

Figure 7.4: **Empirical evidence for the equation proposed in replacement of eq. 2.3. The value mentioned in each panel is the slope of the least squares fit to the data cloud and hence corresponds to β.**

using state-of-the-art global climate models (GCMs; Christensen et al., 2013). Yet their coarse resolution may hamper their ability to capture some of the important climate effects at the local scale (Nyeko-Ogiramoi et al., 2010). Our study clearly demonstrates the added value of high-resolution, coupled lake-land-atmosphere model simulations for present and future climate assessments in a region where complex orography and surface processes are major drivers of climate processes. This has important implications for the future potential of regional climate studies. Conversely, although the present study was conducted with a state-of-the-art regional modelling system and with greatest care for achieving realism, several possible developments may be identified which would - likely - further improve climate research in the African Great Lakes region, both in terms of climate modelling and regional climate assessments.

7.3.1 Climate modelling over the African Great Lakes

Even at 7 km grid spacing, some features of the local climate are still not sufficiently well represented by our model simulations. These remaining deficiencies are to a large extent linked to the parameterization of convection, still required at this resolution. Next-generation computer architectures will allow for long-term climate simulations at even finer grid spacings. At horizontal resolutions below ∼3 km, moist convection can be explicitly resolved, removing

the need for grid-scale parameterization (e.g. Tiedtke, 1989) employed in most model studies. Although never applied to tropical Africa, convection-permitting climate models have been shown to substantially improve the representation of extreme weather events, meso-scale circulation and complex surface-atmosphere interactions, especially over regions characterized by strong orography (Goyette, 2008; Wang et al., 2012; Wouters et al., 2013; Ban et al., 2014; Prein et al., 2015). Given the key role of these processes for regional precipitation production, explicitly resolved moist convection would most likely enhance the physical realism of climate simulations over the African Great Lakes.

Second, while FLake was proven to be an adequate tool for lake surface temperature parameterization in RCMs, it cannot be used to study climate influences on complex within-lake processes. To investigate interactions between e.g. climate variability and lake circulation or ecosystem dynamics, coupling to more comprehensive lake models will be required. For instance, an atmospheric model coupled to a three-dimensional lake model may be used to study the complex hydrodynamics of Lake Tanganyika (Naithani et al., 2003; Verburg et al., 2011), as has been done for Lake Victoria (Song et al., 2004; Anyah and Semazzi, 2009). Future studies within the Lake Model Intercomparison Project (LakeMIP; chapter 4) could potentially contribute to this development by comparing and evaluating lake parameterizations of variable complexity as they are interactively coupled to climate models.

Apart from rising greenhouse gas concentrations, land use changes also shape the future of the Great Lakes region. While historical deforestation has already removed most of the natural vegetation in the region, the remaining patches are under ever increasing pressure, and multiple scenarios project their degradation over the coming decades (Justice et al., 2001; Hansen et al., 2013). Previous studies have shown that accounting for realistic deforestation scenarios in future climate simulations may significantly enhance the projected warming signal for Sub-Saharan Africa (Paeth and Thamm, 2007; Akkermans et al., 2014). Besides direct human-induced changes in vegetation cover, also vegetation dynamics responding to anthropogenic future climate change need to be taken into account to improve the realism of climate projections for this region. Ongoing efforts to improve current land surface models will soon enable inclusion of these processes.

In addition, urban sprawl is likely to become a major contributor to the region's changing land cover. An area covering the Northern shores of Lake Victoria extending into Rwanda and Burundi has been identified as one of the four hot-spots of future urbanization in the world (Seto et al., 2012). In the absence of intervention, urban expansion in the region is likely to result in vast "horizontal cities" dominated by one-story-buildings surrounded by green areas used for urban farming (Vermeiren et al., 2012; Vermeiren; et al., 2015). Climatic

impacts of urbanisation have been well documented for other parts of the world (e.g. Shepherd, 2005; Han et al., 2014; Zhao et al., 2014; Demuzere et al., 2013, 2014; Wouters et al., 2013, 2015), but are highly unknown for East Africa. But since our study showed that convection highly depends on subtle differences in surface temperatures, future urban sprawl is likely to have an important impact on the hydrological cycle. Finally, accounting for land-use changes in climate change projections is also necessary to comply with the assumptions made to construct the radiative concentration pathways (RCPs; Hurtt et al., 2011; DiVittorio et al., 2014). In short, implementation of realistic land-use change scenarios in future projections is expected to further enhance the realism of climatic assessments for the region.

Besides their direct biogeophysical and biogeochemical influence on the regional climate, land use changes exert another, indirect influence on lake-atmosphere interactions. When they lead to a reduction of vegetation cover or wetland area, land use changes enhance the sediment yield of river catchments and therewith also the sediment influx into the African Great Lakes (Alin et al., 1999; Hecky et al., 2003; Vanmaercke et al., 2014; Ryken et al., 2015). Once transported into the lake, suspended sediments reduce the water clarity and therewith the shortwave radiation penetration into the lake (Davies-Colley and Smith, 2001). Likewise, human-induced changes in nutrient loading affect the ecosystem functioning and therewith the water transparency of the African Great Lakes (Hecky et al., 2003). As shown in this thesis, a correct representation of light attenuation turns out to be of great importance for modelling the stratification of the water column (chapters 3, 4). Enhanced understanding of anthropogenic influences on water transparency would therefore contribute to improved regional climate projections in the African Great Lakes region.

The scarcity of high-quality benchmark products finally highlights strong need for ambitious measurement programs in the region. Model developers ultimately rely on preceding efforts from observational studies, and the skill of their model systems can only be assessed as far as qualitative benchmark products are available. As regularly done for mid-latitude lakes (e.g. Le Moigne et al., 2013; Salgado et al., 2014), intensive observation periods may be combined with long term monitoring programs to obtain an in-depth understanding of the processes governing short- and long-term variability. Ideally, efforts in this direction would also go together with capacity building and lead to the coordination of the monitoring programs by local meteorological agencies. The development of a high-qualitative, long-term observational database in central Africa would eventually result in better forecasts and climate assessments. A major step forward in this respect is the recent recognition of the Lake Victoria basin as one of the Regional Hydroclimate Projects by the Global Energy and Water Cycle Experiment (GEWEX).

7.3.2 Regional climate assessments

Two major lines have dominated the progress of regional climate modelling in recent years (Rockel, 2015). One has been been the evolution of regional atmospheric models to regional earth system models: thanks to their coupling to new components, RCMs today increasingly account for atmospheric interactions with, for instance, regional oceanic circulation, comprehensive biogeophysical and biogeochemical land surface processes, cryospheric phenomena and terrestrial hydrology. Particular attention is thereby paid to the interactions between human activities and the climate system (Yang, 2015). On the other hand, regional climate modellers have also used the ever increasing available computational power to increase the spatial resolution of their simulations, eventually obtaining climate projections at convection resolving scales (Ban et al., 2015).

The unique characteristics of equatorial East Africa, with its complex orography, large collection of lakes and tropical meteorological features incited us to follow both pathways to a maximal extent rather than allocating all resources to one track. Hence the model resolution was increased to a maximum extent while accounting for complex lake and land surface processes as much as possible. Our results demonstrate the clear added value of our approach, it enabled us to establish the present-day climatic impact of the African Great Lakes and to project a robust increase in hazardous thunderstorm intensity over Lake Victoria. We also note the potential of further progress in both directions. Provided that the coupling to more complex, three-dimensional lake models would yield equal or improved skill, model simulations would enable the assessment of climate change and their two-way interactions with lake processes: water column stratification, nutrient cycling and ultimately ecosystem responses. On the other hand, convection permitting climate simulations would further improve the representation of regional precipitation dynamics.

To comply with the rapid evolution of climate science, crystallized in regular IPCC assessments, the next phase of the CORDEX effort will ultimately have to push both tracks to their limit. Regional high-resolution ensemble climate projections will be performed for selected regions where complex orography and surface processes have an important influence on the regional climate. The African Great Lakes region is a primary example of such a region, and might just be the perfect test case for such a project.

Bibliography

Akkermans, T., 2013. Modeling land-atmosphere interactions in tropical Africa: the climatic impact of deforestation in the Congo Basin. Ph.D. thesis, 160 pp. pages 27, 97, 98, 113, 140

Akkermans, T., Lauwaet, D., Demuzere, M., Vogel, G., Nouvellon, Y., Ardö, J., Caquet, B., De Grandcourt, A., Merbold, L., Kutsch, W., Van Lipzig, N., 2012. Validation and comparison of two soil-vegetation-atmosphere transfer models for tropical Africa. Journal of Geophysical Research 117, G02013. pages 22, 98, 140

Akkermans, T., Thiery, W., Van Lipzig, N. P. M., 2014. The Regional Climate Impact of a Realistic Future Deforestation Scenario in the Congo Basin. Journal of Climate 27 (7), 2714–2734. pages 5, 27, 50, 65, 97, 98, 105, 120, 140, 162

Akurut, M., Willems, P., Niwagaba, C., 2014. Potential Impacts of Climate Change on Precipitation over Lake Victoria, East Africa, in the 21st Century. Water 6 (9), 2634–2659. pages 10

Alin, S. R., Cohen, A. S., Bills, R., Gashagaza, M. M., Michel, E., Tiercelin, J. J., Martens, K., Coveliers, P., Mboko, S. K., West, K., Soreghan, M., Kimbadi, S., Ntakimazi, G., 1999. Effects of landscape disturbance on animal communities in Lake Tanganyika, East Africa. Conservation Biology 13 (5), 1017–1033. pages 163

Alleman, L. Y., Cardinal, D., Cocquyt, C., Plisnier, P.-D., Descy, J.-P., Kimirei, I., Sinyinza, D., André, L., 2005. Silicon Isotopic Fractionation in Lake Tanganyika and Its Main Tributaries. Journal of Great Lakes Research 31 (4), 509–519. pages 32

Allen, M. R., Ingram, W. J., 2002. Constraints on future changes in climate and the hydrologic cycle. Nature 419 (6903), 224–232. pages 145

Anyah, R. O., Qiu, W., 2012. Characteristic 20th and 21st century precipitation and temperature patterns and changes over the Greater Horn of Africa. International Journal of Climatology 32 (3), 347–363. pages 8

Anyah, R. O., Semazzi, F., 2009. Idealized simulation of hydrodynamic characteristics of Lake Victoria that potentially modulate regional climate. International Journal of Climatology 29, 971–981. pages 13, 14, 117, 156, 162

Anyah, R. O., Semazzi, F. H. M., 2004. Simulation of the sensitivity of Lake Victoria basin climate to lake surface temperatures. Theoretical and Applied Climatology 79 (1-2), 55–69. pages 13, 14, 96, 99, 100, 116, 117, 156

Anyah, R. O., Semazzi, F. H. M., 2006. Climate variability over the Greater Horn of Africa based on NCAR AGCM ensemble. Theoretical and Applied Climatology 86 (1-4), 39–62. pages 5, 8, 99

Anyah, R. O., Semazzi, F. H. M., 2007. Variability of East African rainfall based on multiyear RegCM3 simulations. International Journal of Climatology 27, 357–371. pages 5, 117

Anyah, R. O., Semazzi, F. H. M., Xie, L., 2006. Simulated Physical Mechanisms Associated with Climate Variability over Lake Victoria Basin in East Africa. Monthly Weather Review 134, 3588–3609. pages 4, 5, 13, 14, 31, 95, 96, 100, 108, 117, 124, 125, 130, 156

Argent, R., Sun, X., Semazzi, F. H. M., Xie, L., Liu, B., 2014. The Development of a Customization Framework for the WRF Model over the Lake Victoria Basin, Eastern Africa on Seasonal Timescales. Advances in Meteorology, 653473. pages 13, 14, 96, 99

ASTM, 2012. Standard tables for reference solar irradiance: direct normal and hemispherical on 37° tilted surface.
URL http://www.astm.org/Standards/G173.htm pages 72

Awange, J., Ferreira, V., Forootan, E., Khandu, Andam-Akorful, S., Agutu, N., He, X., 2015. Uncertainties in remotely sensed precipitation data over Africa. International Journal of Climatology. pages 156

Ba, M., Nicholson, S., 1998. Analysis of convective activity and its relationship to the rainfall over the Rift Valley lakes of East Africa during 1983-90 using the Meteosat infrared channel. Journal of Applied Meteorology. pages 5

Balsamo, G., Albergel, C., Beljaars, a., Boussetta, S., Brun, E., Cloke, H., Dee, D., Dutra, E., Muñoz Sabater, J., Pappenberger, F., de Rosnay, P., Stockdale, T., Vitart, F., 2015. ERA-Interim/Land: a global land surface reanalysis data set. Hydrology and Earth System Sciences, 389–407. pages 11

Balsamo, G., Salgado, R., Dutra, E., Boussetta, S., Stockdale, T., Potes, M., 2012. On the contribution of lakes in predicting near-surface temperature in a global weather forecasting model. Tellus A 64, 15829. pages 11, 51, 65, 113

Ban, N., Schmidli, J., Schär, C., 2014. Evaluation of the convection-resolving regional climate modeling approach in decade-long simulations. Journal of Geophysical Research: Atmospheres 119, 7889–7907. pages 135, 143, 146, 162

Ban, N., Schmidli, J., Schär, C., 2015. Heavy precipitation in a changing climate : Does short-term summer precipitation increase faster? Geophysical Research Letters 42, 1165–1172. pages 145, 147, 164

Bates, G., Hostetler, S., Giorgi, F., 1995. Two-year simulation of the Great Lakes region with a coupled modeling system. Monthly Weather Review 123, 1505–1522. pages 12, 23, 95

Beadle, L. C., 1981. The inland waters of Tropical Africa, An introduction to tropical limnology. Longman, London, United Kingdom, 475 pp. pages 33

Bedka, K., Brunner, J., Dworak, R., Feltz, W., Otkin, J., Greenwald, T., 2010. Objective Satellite-Based Detection of Overshooting Tops Using Infrared Window Channel Brightness Temperature Gradients. Journal of Applied Meteorology and Climatology 49 (2), 181–202. pages 130, 137, 141

Bedka, K. M., 2011. Overshooting cloud top detections using MSG SEVIRI Infrared brightness temperatures and their relationship to severe weather over Europe. Atmospheric Research 99 (2), 175–189. pages 130, 137, 141

Bedka, K. M., Dworak, R., Brunner, J., Feltz, W., 2012. Validation of Satellite-Based Objective Overshooting Cloud-Top Detection Methods Using CloudSat Cloud Profiling Radar Observations. Journal of Applied Meteorology and Climatology 51 (10), 1811–1822. pages 141

Behera, S. K., Luo, J.-J., Masson, S., Delecluse, P., Gualdi, S., Navarra, A., Yamagata, T., 2005. Paramount Impact of the Indian Ocean Dipole on the East African Short Rains : A CGCM Study. Journal of Climate 18 (21), 4514–4530. pages 7, 8

Bennington, V., Notaro, M., Holman, K. D., 2014. Improving Climate Sensitivity of Deep Lakes within a Regional Climate Model and Its Impact on Simulated Climate. Journal of Climate 27 (8), 2886–2911. pages 12, 23, 95, 96

Berg, P., Moseley, C., Haerter, J. O., 2013. Strong increase in convective precipitation in response to higher temperatures. Nature Geoscience 6 (March), 181–185. pages 146

Black, E., Slingo, J., Sperber, K. R., 2003. An Observational Study of the Relationship between Excessively Strong Short Rains in Coastal East Africa and Indian Ocean SST. Monthly Weather Review 131, 74–94. pages 7, 8

Bonan, G., 1995. Sensitivity of a GCM simulation to inclusion of inland water surfaces. Journal of Climate 8, 2691–2704. pages 31, 65, 95

Bonan, G. B., Oleson, K. W., Vertenstein, M., Levis, S., Zeng, X., Dai, Y., Dickinson, R. E., Yang, Z.-L., 2002. The land surface climatology of the Community Land Model coupled to the NCAR Community Climate Model. Journal of Climate 94, 3123–3149. pages 67, 101

Bookhagen, B., Burbank, D. W., 2006. Topography, relief, and TRMM-derived rainfall variations along the Himalaya. Geophysical Research Letters 33 (8), L08405. pages 102

Bookhagen, B., Strecker, M. R., 2008. Orographic barriers, high-resolution TRMM rainfall, and relief variations along the eastern Andes. Geophysical Research Letters 35 (6), L06403. pages 102

Borges, a. V., Abril, G., Delille, B., Descy, J.-P., Darchambeau, F., 2011. Diffusive methane emissions to the atmosphere from Lake Kivu (Eastern Africa). Journal of Geophysical Research 116, G03032. pages 32, 69

Brisson, E., Demuzere, M., Willems, P., van Lipzig, N. P. M., 2014. Assessment of natural climate variability using a weather generator. Climate Dynamics, 1–14. pages 15

Brisson, E., Weverberg, K. V., Demuzere, M., Devis, A., Saeed, S., Stengel, M., 2015. How well can a convection-permitting climate model reproduce decadal statistics of precipitation, temperature and cloud characteristics? Climate Dynamics in review. pages 135

Bultot, F., 1971. Atlas climatique du bassin Congolais, vol 2: Les composantes du bilan d'eau. Publications de l'Institut National pour l'Étude Agronomique du Congo, Brussels, Belgium. pages 50

Burbank, D. W., Bookhagen, B., Gabet, E. J., Putkonen, J., 2012. Modern climate and erosion in the Himalaya. Comptes Rendus Geoscience 344 (11-12), 610–626. pages 102

Burnett, A. P., Soreghan, M. J., Scholz, C. a., Brown, E. T., 2011. Tropical East African climate change and its relation to global climate: A record from Lake Tanganyika, Tropical East Africa, over the past 90+kyr. Palaeogeography, Palaeoclimatology, Palaeoecology 303 (1-4), 155–167. pages 7

Cai, W., Santoso, A., Wang, G., Weller, E., Wu, L., Ashok, K., Masumoto, Y., Yamagata, T., 2014. Increased frequency of extreme Indian Ocean Dipole events due to greenhouse warming. Nature 510 (7504), 254–8. pages 7, 10

Capart, A., 1952. Le milieu géographique et géophysique. Résultats scientifiques de l'exploration hydrobiologique du Lac Tanganika (1946-1947), 1st Edition. Inst. R. Sci. Nat. Belg., Brussels, Belgium, pp. 3–27. pages 59

Carpenter, H., 1922. Waterspouts on Lake Victoria. Nature 110 (2760), 414. pages 130

Chamberlain, J. M., Bain, C. L., Boyd, D. F. a., McCourt, K., Butcher, T., Palmer, S., 2014. Forecasting storms over Lake Victoria using a high resolution model. Meteorological Applications 21 (2), 419–430. pages 3, 13, 14, 158

Christensen, J., Kumar, K. K., Aldria, E., An, S.-I., Cavalcanti, I., Castro, M. D., Dong, W., Goswami, P., Hall, A., Kanyanga, J., Kitoh, A., Kossin, J., Lau, N.-C., Renwick, J., Stephenson, D., Xie, S.-P., Zhou, T., 2013. Climate Phenomena and their Relevance for Future Regional Climate Change. In: Stocker, T., Qin, D., Plattner, G.-K., Tignor, M., Allen, S., Boschung, J., Nauels, A., Xia, Y., Bex, V., Midgley, P. (Eds.), Climate Change 2013: The Physical Science Basis. Contribution of Working Group I to the Fifth Assessment Report of the Intergovernmental Panel on Climate Change. Cambridge University Press, Cambridge, United Kingdom and New York, NY, USA, pp. 1217–1308. pages 4, 8, 9, 10, 161

Climate Prediction Center, National Centers for Environmental Prediction, National Weather Service, NOAA, U.S. Department of Commerce, 2011. NOAA CPC Morphing Technique (CMORPH) Global Precipitation Analyses. pages 103

Coe, M., Bonan, G., 1997. Feedbacks between climate and surface water in northern Africa during the middle Holocene. Journal of Geophysical Research 102 (D10), 11087–11101. pages 95

Conway, D., Hanson, C. E., Doherty, R., Persechino, a., 2007. GCM simulations of the Indian Ocean dipole influence on East African rainfall: Present and future. Geophysical Research Letters 34 (3), 1–6. pages 7, 10

Cook, K. H., Vizy, E. K., 2012. Impact of climate change on mid-twenty-first century growing seasons in Africa. Climate Dynamics 39 (12), 2937–2955. pages 10

Cook, K. H., Vizy, E. K., 2013. Projected Changes in East African Rainy Seasons. Journal of Climate 26 (16), 5931–5948. pages 10

Coulter, 1991. Lake Tanganyika and its life. Oxford University Press, London, United Kingdom, 354 pp. pages 32

Crétat, J., Vizy, E. K., Cook, K. H., 2014. How well are daily intense rainfall events captured by current climate models over Africa? Climate Dynamics 42 (9-10), 2691–2711. pages 4, 96, 97

Darchambeau, F., Sarmento, H., Descy, J.-P., 2014. Primary production in a tropical large lake: the role of phytoplankton composition. Science of the Total Environment 473, 178–188. pages 16, 37, 103, 104

Datta, R. K., 1981. Certain aspects of monssonal precipitation dynamics over Lake Victoria. In: Lighthill, J., Pearce, R. P. (Eds.), Monsoon Dynamics. Cambridge University Press, Cambridge, United Kingdom, Ch. 22, pp. 333–349. pages 117

Davies, H., 1983. Limitations of some common lateral boundary schemes used in regional NWP models. Monthly Weather Review 111, 1002–1012. pages 100

Davies-Colley, R., Smith, D., 2001. Turbidity, Suspended Sediment, and Water Clarity: a Review. Journal of the American Water Resources Association 37 (5), 1085–1101. pages 163

Davin, E. L., Seneviratne, S. I., 2012. Role of land surface processes and diffuse/direct radiation partitioning in simulating the European climate. Biogeosciences 9 (5), 1695–1707. pages 27, 96, 98, 137, 140

Davin, E. L., Seneviratne, S. I., Ciais, P., Olioso, A., Wang, T., 2014. Preferential cooling of hot extremes from cropland albedo management. Proceedings of the National Academy of Sciences of the United States of America 111 (27), 9757–9761. pages 11, 27, 98

Davin, E. L., Stöckli, R., Jaeger, E. B., Levis, S., Seneviratne, S. I., 2011. COSMO-CLM2: a new version of the COSMO-CLM model coupled to the Community Land Model. Climate Dynamics 37 (9-10), 1889–1907. pages 27, 98, 137, 140

Davis, N., Bowden, J., Semazzi, F., Xie, L., Önol, B., 2009. Customization of RegCM3 Regional Climate Model for Eastern Africa and a Tropical Indian Ocean Domain. Journal of Climate 22 (13), 3595–3616. pages 4

De Boor, C., 2001. A practical guide to splines, applied ma Edition. 27. Springer-Verlag, Berlin, Germany, 348 pp. pages 38, 71, 75, 104

Dee, D. P., Uppala, S. M., Simmons, a. J., Berrisford, P., Poli, P., Kobayashi, S., Andrae, U., Balmaseda, M. a., Balsamo, G., Bauer, P., Bechtold, P., Beljaars, a. C. M., van de Berg, L., Bidlot, J., Bormann, N., Delsol, C., Dragani, R., Fuentes, M., Geer, a. J., Haimberger, L., Healy, S. B., Hersbach, H., Hólm, E. V., Isaksen, L., Kå llberg, P., Köhler, M., Matricardi, M., McNally, a. P., Monge-Sanz, B. M., Morcrette, J.-J., Park, B.-K., Peubey, C., de Rosnay, P., Tavolato, C., Thépaut, J.-N., Vitart, F., 2011. The ERA-Interim reanalysis: configuration and performance of the data assimilation system. Quarterly Journal of the Royal Meteorological Society 137 (656), 553–597. pages 45, 100

Degens, E., Von Herzen, R., Wong, H.-K., Deuser, W., Jannash, H., 1973. Lake Kivu: Structure, chemistry and biology of an East African rift lake. Geologische Rundschau 62, 245–277. pages 32, 69

Demuzere, M., Oleson, K., Coutts, A. M., Pigeon, G., van Lipzig, N. P. M., 2013. Simulating the surface energy balance over two contrasting urban environments using the Community Land Model Urban. International Journal of Climatology 33 (15), 3182–3205. pages 163

Demuzere, M., Orru, K., Heidrich, O., Olazabal, E., Geneletti, D., Orru, H., 2014. Mitigating and adapting to climate change : Multi-functional and multi-scale assessment of green urban infrastructure. Journal of Environmental Management 146, 107–115. pages 163

Descy, J.-P., Darchambeau, F., Schmid, M., 2012. Lake Kivu: Past and Present. In: Descy, J.-P., Darchambeau, F., Schmid, M. (Eds.), Lake Kivu: Limnology and Biogeochemistry of a Tropical Great Lake. Springer, Dordrecht, Netherlands, pp. 1–11. pages 32, 66, 69

Dinku, T., Chidzambwa, S., Ceccato, P., Connor, S. J., Ropelewski, C. F., 2008. Validation of high-resolution satellite rainfall products over complex terrain. International Journal of Remote Sensing 29 (14), 4097–4110. pages 96, 102, 106, 156

DiVittorio, A. V., Chini, L. P., Bond-Lamberty, B., Mao, J., Shi, X., Truesdale, J., Craig, A., Calvin, K., Jones, A., Collins, W. D., Edmonds, J., Hurtt, G. C., Thornton, P., Thomson, A., 2014. From land use to land cover: restoring the afforestation signal in a coupled integrated assessment – earth system model and the implications for CMIP5 RCP simulations. Biogeosciences 11 (5), 6435–6450. pages 163

Doms, G., 2011. A Description of the Nonhydrostatic Regional COSMO-Model, Part I: Dynamics and Numerics. German Weather Service, Offenbach am Main, Germany, 153 pp. pages 22, 24, 97, 137

Doms, G., Orstner, J., Heise, E., Herzog, H.-J., Mironov, D., Raschendorfer, M., Reinhardt, T., Ritter, B., Schrodin, R., Schulz, J.-P., Vogel, G., 2011. A Description of the Nonhydrostatic Regional COSMO Model Part II: Physical Parameterization. German Weather Service, Offenbach am Main, Germany, 161 pp. pages 22, 24, 97, 137

Dosio, A., Panitz, H.-J., Schubert-Frisius, M., Lüthi, D., 2014. Dynamical downscaling of CMIP5 global circulation models over CORDEX-Africa with COSMO-CLM: evaluation over the present climate and analysis of the added value. Climate Dynamics. pages 16, 96, 97, 101

Dutra, E., Stepanenko, V. M., Balsamo, G., Viterbo, P., Miranda, P., Mironov, D., Schär, C., 2010. An offline study of the impact of lakes on the performance of the ECMWF surface scheme. Boreal Environment Research 15 (2), 100–112. pages 31

Eagle, C., Lean, H., Webster, S., 2015. Convective Scale NWP Model configurations for the Lake Victoria Region.pdf. Met Office, Exeter, United Kingdom, 28 pp. pages 3, 14, 158

Endris, H. S., Omondi, P., Jain, S., Lennard, C., Hewitson, B., Chang'a, L., Awange, J. L., Dosio, A., Ketiem, P., Nikulin, G., Panitz, H.-J., Büchner, M., Stordal, F., Tazalika, L., 2013. Assessment of the Performance of CORDEX Regional Climate Models in Simulating East African Rainfall. Journal of Climate 26 (21), 8453–8475. pages 16, 106

Fang, X., Stefan, H., 1996. Long-term lake water temperature and ice cover simulations/measurements. Cold Regions Science and Technology 24, 289–304. pages 68

Fischer, E. M., Beyerle, U., Knutti, R., 2013. Robust spatially aggregated projections of climate extremes. Nature Climate Change 3 (12), 1033–1038. pages 132

Fischer, E. M., Knutti, R., 2015. Anthropogenic contribution to global occurrence of heavy-precipitation and high-temperature extremes. Nature Climate Change 5, 560–565. pages 132, 146

Fowler, H. J., Ekström, M., Blenkinsop, S., Smith, A. P., 2007. Estimating change in extreme European precipitation using a multimodel ensemble. Journal of Geophysical Research: Atmospheres 112, D18104. pages 134, 156

Giannini, A., Biasutti, M., Held, I. M., Sobel, A. H., 2008. A global perspective on African climate. Climatic Change 90 (4), 359–383. pages 7

Giorgi, F., Jones, C., Asrar, G., 2009. Addressing climate information needs at the regional level: the CORDEX framework. WMO Bulletin 58 (3), 175–183. pages 15, 31, 96

Gorodetskaya, I. V., Kneifel, S., Schween, J. H., Crewell, S., Van Lipzig, N. P. M., 2015. Cloud and precipitation properties from ground-based remote sensing instruments in East Antarctica. The Cryosphere 9, 285–304. pages 157

Goudsmit, G.-H., 2002. Application of k-ϵ turbulence models to enclosed basins: The role of internal seiches. Journal of Geophysical Research 107, 3230–3243. pages 68

Gourgue, O., Deleersnijder, E., Legat, V., Marchal, E., White, L., 2011. Free and forced thermocline oscillations in Lake Tanganyika. In: Alpert, P., Sholokhman, T. (Eds.), Factor separation in the atmosphere: applications and future prospects. Cambridge University Press, Cambridge, United Kingdom, pp. 146–162. pages 31

Gourgue, O., Deleersnijder, E., White, L., 2007. Toward a generic method for studying water renewal, with application to the epilimnion of Lake Tanganyika. Estuarine, Coastal and Shelf Science 74 (4), 628–640. pages 111

Goyens, C., Lauwaet, D., Schröder, M., Demuzere, M., Van Lipzig, N. P. M., 2011. Tracking mesoscale convective systems in the Sahel: relation between cloud parameters and precipitation. International Journal of Climatology 32 (12), 1921–1934. pages 5, 96

Goyette, S., 2008. Development of a model-based high-resolution extreme surface wind climatology for Switzerland. Natural Hazards 44 (3), 329–339. pages 162

Goyette, S., McFarlane, N., Flato, G. M., 2000. Application of the Canadian regional climate model to the Laurentian great lakes region: Implementation of a lake model. Atmosphere-Ocean 38 (3), 481–503. pages 12, 95

Goyette, S., Perroud, M., 2012. Interfacing a one-dimensional lake model with a single-column atmospheric model: Application to the deep Lake Geneva, Switzerland. Water Resources Research 48 (4), W04507. pages 65

Grasselt, R., Schüttemeyer, D., Warrach-Sagi, K., Ament, F., Simmer, C., 2008. Validation of TERRA-ML with discharge measurements. Meteorologische Zeitschrift 17 (6), 763–773. pages 25, 98

Gu, H., Jin, J., Wu, Y., Ek, M. B., Subin, Z. M., 2013. Calibration and validation of lake surface temperature simulations with the coupled WRF-lake model. Climatic Change. pages 12, 23, 95, 96

Guillod, B. P., Orlowsky, B., Miralles, D. G., Teuling, A. J., Seneviratne, S. I., 2015. Reconciling spatial and temporal soil moisture effects on afternoon rainfall. Nature Communications 6, 6443. pages 5

Gula, J., Peltier, W. R., 2012. Dynamical Downscaling over the Great Lakes Basin of North America Using the WRF Regional Climate Model: The Impact of the Great Lakes System on Regional Greenhouse Warming. Journal of Climate 25 (21), 7723–7742. pages 12, 95

Hamblin, P., Bootsma, H., Hecky, R., 2003. Surface meteorological observations over Lake Malawi/Nyasa. Journal of Great Lakes Research 29, 19–33. pages 15

Han, J. Y., Baik, J. J., Lee, H., 2014. Urban impacts on precipitation. Asia-Pacific Journal of Atmospheric Sciences 50 (1), 17–30. pages 163

Hansen, M. C., Potapov, P. V., Moore, R., Hancher, M., Turubanova, S. A., Tyukavina, A., Thau, D., Stehman, S. V., Goetz, S. J., Loveland, T. R., Kommareddy, A., Egorov, A., Chini, L., Justice, C. O., Townshend, J. R. G., 2013. High-resolution global maps of 21st-century forest cover change. Science 342 (6160), 850–853. pages 162

Hastenrath, S., 2001. Variations of East African climate during the past two centuries. Climatic change, 209–217. pages 7

Hastenrath, S., Polzin, D., Mutai, C., 2007. Diagnosing the 2005 drought in equatorial East Africa. Journal of Climate 20, 4628–4637. pages 8

Hecky, R. E., Bootsma, H. a., Kingdon, M. L., 2003. Impact of Land Use on Sediment and Nutrient Yields to Lake Malawi/Nyasa (Africa). Journal of Great Lakes Research 29, 139–158. pages 163

Hecky, R. E., Mugidde, R., Ramlal, P. S., Talbot, M. R., Kling, G. W., 2010. Multiple stressors cause rapid ecosystem change in Lake Victoria. Freshwater Biology 55, 19–42. pages 10

Hernández-Díaz, L., Laprise, R., Sushama, L., Martynov, A., Winger, K., Dugas, B., 2012. Climate simulation over CORDEX Africa domain using the fifth-generation Canadian Regional Climate Model (CRCM5). Climate Dynamics 40 (5-6), 1415–1433. pages 15, 51, 56, 57, 102

Hostetler, S., Giorgi, F., 1995. Effects of a 2× CO2 climate on two large lake systems: Pyramid Lake, Nevada, and Yellowstone Lake, Wyoming. Global and Planetary Change 10, 43–54. pages 12, 23, 95

Hostetler, S. W., Bates, G. T., Giorgi, F., 1993. Interactive coupling of a lake thermal model with a regional climate model. Journal of Geophysical Research 98, 5045–5057. pages 23, 67

Hostetler, S. W., Giorgi, F., Bates, G. T., Bartlein, P. J., 1994. Lake-Atmosphere Feedbacks Associated with Paleolakes Bonneville and Lahontan. Science 263 (5147), 665–668. pages 12, 23, 65, 95

Huffman, G., Adler, R., 2001. Global precipitation at one-degree daily resolution from multisatellite observations. Journal of Hydrometeorology, 36–50. pages 16, 102, 103

Hurtt, G. C., Chini, L. P., Frolking, S., Betts, R. A., Feddema, J., Fischer, G., Fisk, J. P., Hibbard, K., Houghton, R. A., Janetos, A., Jones, C. D., Kindermann, G., Kinoshita, T., Klein Goldewijk, K., Riahi, K., Shevliakova, E., Smith, S., Stehfest, E., Thomson, A., Thornton, P., van Vuuren, D. P., Wang, Y. P., 2011. Harmonization of land-use scenarios for the period 1500-2100: 600 years of global gridded annual land-use transitions, wood harvest, and resulting secondary lands. Climatic Change 109 (1), 117–161. pages 163

Indeje, M., Semazzi, F., Xie, L., Ogallo, L., 2001. Mechanistic model simulations of the East African climate using NCAR regional climate model: Influence of large-scale orography on the Turkana low-level jet. Journal of climate 14, 2710–2724. pages 4

Indeje, M., Semazzi, F. H., Ogallo, L. J., 2000. ENSO signals in East African rainfall seasons. International Journal of Climatology 20 (1), 19–46. pages 7

Jacobs, L., Dewitte, O., Poesen, J., Delvaux, D., Thiery, W., Kervyn, M., 2015a. The Rwenzori Mountians, a landslide-prone region? Landslides. pages 27, 98

Jacobs, L., Maes, J., Mertens, K., Sekajugo, J., Thiery, W., Van Lipzig, N., Poesen, J., Kervyn, M., Dewitte, O., 2015b. A recipe for disaster: The May 2013 Kilembe flash flood, Rwenzori Mountains, Uganda. Journal of Hydrology in review. pages 10, 27

Jöhnk, K., 2013. Limnophysics - Turbulenz, Meromixis, Sauerstoff. Institute of Limnophysics, Cottbus, Germany. pages 68

Jöhnk, K., Umlauf, L., 2001. Modelling the metalimnetic oxygen minimum in a medium sized alpine lake. Ecological Modelling 136 (1), 67–80. pages 68, 75

Joyce, R., Janowiak, J., 2004. CMORPH: A method that produces global precipitation estimates from passive microwave and infrared data at high spatial and temporal resolution. Journal of Hydrometeorology 5, 487–503. pages 16, 102, 103

Juang, J.-Y., Katul, G., Siqueira, M., Stoy, P., Novick, K., 2007. Separating the effects of albedo from eco-physiological changes on surface temperature along a successional chronosequence in the southeastern United States. Geophysical Research Letters 34 (21), L21408. pages 105

Jung, M., Reichstein, M., Bondeau, A., 2009. Towards global empirical upscaling of FLUXNET eddy covariance observations: validation of a model tree ensemble approach using a biosphere model. Biogeosciences 6 (10), 2001–2013. pages 104

Jung, M., Reichstein, M., Ciais, P., Seneviratne, S. I., Sheffield, J., Goulden, M. L., Bonan, G., Cescatti, A., Chen, J., de Jeu, R., Dolman, a. J., Eugster, W., Gerten, D., Gianelle, D., Gobron, N., Heinke, J., Kimball, J., Law, B. E., Montagnani, L., Mu, Q., Mueller, B., Oleson, K., Papale, D., Richardson, A. D., Roupsard, O., Running, S., Tomelleri, E., Viovy, N., Weber, U., Williams, C., Wood, E., Zaehle, S., Zhang, K., 2010. Recent decline in the global land evapotranspiration trend due to limited moisture supply. Nature 467 (7318), 951–4. pages 16, 103, 104

Justice, C., Wilkie, D., Zhang, Q., Brunner, J., Donoghue, C., 2001. Central African forests, carbon and climate change. Climate Research 17 (2), 229–246. pages 162

Katsev, S., Aaberg, A. a., Crowe, S. a., Hecky, R. E., 2014. Recent warming of lake Kivu. PloS one 9 (10), e109084. pages 10

Kendon, E., Roberts, N., Fowler, H., 2014. Heavier summer downpours with climate change revealed by weather forecast resolution model. Nature Climate Change 4 (June), 570–576. pages 146

Kharin, V. V., Zwiers, F. W., Zhang, X., Wehner, M., 2013. Changes in temperature and precipitation extremes in the CMIP5 ensemble. Climatic Change 119 (2), 345–357. pages 129, 132, 141, 145

Kijazi, a. L., Reason, C. J. C., 2009. Analysis of the 2006 floods over northern Tanzania. International Journal of Climatology 29, 955–970. pages 8

Kirillin, G., 2010. Modeling the impact of global warming on water temperature and seasonal mixing regimes in small temperate lakes. Boreal environment research 15, 279–293. pages 60, 81

Kirillin, G., Hochschild, J., Mironov, D., Terzhevik, A., Golosov, S., Nützmann, G., 2011. FLake-Global: Online lake model with worldwide coverage. Environmental Modelling & Software 26 (5), 683–684. pages 81

Kitaigorodskii, S. A., Miropolskii, Y. Z., 1970. On the theory of the open ocean active layer. Izv. Atmos. Oceanic Phys. 6, 97–102. pages 20, 36, 99

Kizza, M., Rodhe, A., Xu, C.-Y., Ntale, H. K., Halldin, S., 2009. Temporal rainfall variability in the Lake Victoria Basin in East Africa during the twentieth century. Theoretical and Applied Climatology 98 (1-2), 119–135. pages 7

Knutti, R., Sedláček, J., 2012. Robustness and uncertainties in the new CMIP5 climate model projections. Nature Climate Change 3 (4), 369–373. pages 8

Kothe, S., Panitz, H.-j., Ahrens, B., Aug. 2014. Analysis of the radiation budget in regional climate simulations with COSMO-CLM for Africa. Meteorologische Zeitschrift 23 (2), 123–141. pages 4

Kourzeneva, E., 2010. External data for lake parameterization in Numerical Weather Prediction and climate modeling. Boreal Environment Research 15, 165–177. pages 51, 99

Kourzeneva, E., Asensio, H., Martin, E., Faroux, S., 2012a. Global gridded dataset of lake coverage and lake depth for use in numerical weather prediction and climate modelling. Tellus A 64, 15640. pages 51, 99, 109, 138

Kourzeneva, E., Martin, E., Batrak, Y., Le Moigne, P., 2012b. Climate data for parameterisation of lakes in Numerical Weather Prediction models. Tellus A 64, 17226. pages 38, 60

Kourzeneva, E., Samuelsson, P., Ganbat, G., Mironov, D., 2008. Implementation of Lake Model FLake into HIRLAM. Russian State Hydrometeorological University, pp. 54–61. pages 31, 51, 65

Krähenmann, S., Kothe, S., Panitz, H. J., Ahrens, B., 2013. Evaluation of daily maximum and minimum 2-m temperatures as simulated with the regional climate model COSMO-CLM over Africa. Meteorologische Zeitschrift 22 (3), 297–316. pages 4

Kummerow, C., Simpson, J., Thiele, O., Barnes, W., Chang, A., Stocker, E., Adler, R., Hou, A., Kakar, R., Wentz, F., Ashcroft, P., Kozu, T., Hong, Y., Okamoto, K., Iguchi, T., Kuroiwa, H., Im, E., Haddad, Z., Huffman, G., Ferrier, B., Olson, W. S., Zipser, E., Smith, E., Wilheit, T., North, G., Krishnamurti, T., Nakamura, K., 2000. The status of the Tropical Rainfall Measuring Mission (TRMM) after two years in orbit. Journal of Applied Meteorology 39, 1965–1982. pages 2, 16, 102, 103

Lahmeyer, Osae, 1998. Bathymetric survey of Lake Kivu - Final report. Republic of Rwanda, Ministry of Public Work, Directory of Energy and Hydrocarbons, Kigali, Rwanda, 18 pp. pages 73

Laing, A. G., Carbone, R. E., Levizzani, V., 2011. Cycles and Propagation of Deep Convection over Equatorial Africa. Monthly Weather Review 139 (9), 2832–2853. pages 5, 7

Lanckriet, S., Frankl, A., Adgo, E., Termonia, P., Nyss, 2014. Droughts related to quasi-global oscillations: a diagnostic teleconnection analysis in North Ethiopia. International Journal of climatology. pages 7

Laprise, R., de Elía, R., Caya, D., Biner, S., Lucas-Picher, P., Diaconescu, E., Leduc, M., Alexandru, A., Separovic, L., 2008. Challenging some tenets of Regional Climate Modelling. Meteorology and Atmospheric Physics 100 (1-4), 3–22. pages 4, 99

Laprise, R., Hernández-Díaz, L., Tete, K., Sushama, L., Šeparović, L., Martynov, A., Winger, K., Valin, M., 2013. Climate projections over CORDEX Africa domain using the fifth-generation Canadian Regional Climate Model (CRCM5). Climate Dynamics 41 (11-12), 3219–3246. pages 16, 97

Lauwaet, D., 2009. The influence of land use changes on precipitation in the Sahel. Ph.D. thesis, 149 pp. pages 4

Lauwaet, D., Lipzig, N. P. M., Ridder, K., 2009. The effect of vegetation changes on precipitation and Mesoscale Convective Systems in the Sahel. Climate Dynamics 33 (4), 521–534. pages 5, 95

Lauwaet, D., van Lipzig, N. P. M., Kalthoff, N., De Ridder, K., 2010. Impact of vegetation changes on a mesoscale convective system in West Africa. Meteorology and Atmospheric Physics 107 (3-4), 109–122. pages 5, 143

Lauwaet, D., van Lipzig, N. P. M., Van Weverberg, K., De Ridder, K., Goyens, C., 2012. The precipitation response to the desiccation of Lake Chad. Quarterly Journal of the Royal Meteorological Society 138 (664), 707–719. pages 5, 12, 31, 65, 95, 142

Le Moigne, P., Legain, D., Lagarde, F., Potes, M., Tzanos, D., Moulin, E., Barrié, J., Salgado, R., Messiaen, G., Fiandrino, A., Donier, S., Traullé, O., Costa, M. J., 2013. Evaluation of the lake model FLake over a coastal lagoon during the THAUMEX field campaign. Tellus A 65, 20951. pages 11, 163

Legates, D., Willmott, C., 1990. Mean seasonal and spatial variability in gauge-corrected, global precipitation. International Journal of Climatology 10, 111–127. pages 16, 102, 103

Lejeune, Q., Davin, E., Guillod, B., Seneviratne, S., 2014. Influence of Amazonian deforestation on the future evolution of regional surface fluxes, circulation, surface temperature and precipitation. Climate Dynamics. pages 27, 98, 140

Lekvam, K., Bishnoi, P., 1997. Dissolution of methane in water at low temperatures and intermediate pressures. Fluid Phase Equilibria 131, 297–309. pages 75

Lenderink, G., van Meijgaard, E., 2008. Increase in hourly precipitation extremes beyond expectations from temperature changes. Nature Geoscience 1 (8), 511–514. pages 129, 146, 148

Lorenz, R., Davin, E. L., Lawrence, D. M., Stökli, R., Seneviratne, S. I., 2013. How important is vegetation phenology for european climate and heat waves? Journal of Climate 26 (24), 10077–10100. pages 27

Lorenz, R., Davin, E. L., Seneviratne, S. I., 2012. Modeling land-climate coupling in Europe: Impact of land surface representation on climate variability and extremes. Journal of Geophysical Research 117, D20109. pages 27, 98, 140

Loriaux, J. M., Lenderink, G., De Roode, S. R., Siebesma, P. A., 2013. Understanding Convective Extreme Precipitation Scaling Using Observations and an Entraining Plume Model. Journal of Atmospherical Science 70, 3641–3655. pages 146

Lorke, A., Tietze, K., Halbwachs, M., Wüest, A., 2004. Response of Lake Kivu stratification to lava inflow and climate warming. Limnology and oceanography 49 (3), 778–783. pages 66

Luyssaert, S., Jammet, M., Stoy, P. C., Estel, S., Pongratz, J., Ceschia, E., Churkina, G., Don, A., Erb, K., Ferlicoq, M., Gielen, B., Grünwald, T., Houghton, R. A., Klumpp, K., Knohl, A., Kolb, T., Kuemmerle, T., Laurila, T., Lohila, A., Loustau, D., McGrath, M. J., Meyfroidt, P., Moors, E. J., Naudts, K., Novick, K., Otto, J., Pilegaard, K., Pio, C. A., Rambal, S., Rebmann, C., Ryder, J., Suyker, A. E., Varlagin, A., Wattenbach, M., Dolman, A. J., 2014. Land management and land-cover change have impacts of similar magnitude on surface temperature. Nature Climate Change 4 (5), 389–393. pages 105

Lyon, B., DeWitt, D. G., 2012. A recent and abrupt decline in the East African long rains. Geophysical Research Letters 39, L02702. pages 8

MacCallum, S., Merchant, C., 2012. Surface water temperature observations of large lakes by optimal estimation. Canadian Journal of Remote Sensing 44 (1). pages 16, 102, 103

MacIntyre, S., 2012. Climatic variability, mixing dynamics, and ecological consequences in the African Great Lakes. In: Goldman, C. R., Kumagai, M., Robarts, R. D. (Eds.), Climatic Change and Global Warming of Inland Waters: Impacts and Mitigation for Ecosystems and Societies. John Wiley & Sons, Inc., Chichester, United Kingdom, pp. 311–337. pages 2, 10, 116

MacIntyre, S., Romero, J. R., Silsbe, G. M., Emery, B. M., 2014. Stratification and horizontal exchange in Lake Victoria, East Africa. Limnology and Oceanography 59 (6), 1805–1838. pages 108

Mallard, M., Nolte, C., Bullock, O. R., Spero, T. L., Gula, J., 2014. Using a Coupled Lake Model with WRF for Dynamical Downscaling. Journal of Geophysical Research: Atmospheres 119, 7193–7208. pages 12

Mallard, M. S., Nolte, C. G., Spero, T. L., Bullock, O. R., Alapaty, K., Herwehe, J. a., Gula, J., Bowden, J. H., 2015. Technical challenges and solutions in representing lakes when using WRF in downscaling applications. Geoscientific Model Development 8, 1085–1096. pages 12, 13

Marchant, R., Mumbi, C., Behera, S., Yamagata, T., 2007. The Indian Ocean dipole - The unsung driver of climatic variability in East Africa. African Journal of Ecology 45 (1), 4–16. pages 7

Martynov, A., Sushama, L., Laprise, R., 2010. Simulation of temperate freezing lakes by one-dimensional lake models: performance assessment for interactive coupling with regional climate models. Boreal environment research 15, 143–164. pages 11, 12, 51, 81

Martynov, A., Sushama, L., Laprise, R., Winger, K., Dugas, B., 2012. Interactive lakes in the Canadian Regional Climate Model, version 5: the role of lakes in the regional climate of North America. Tellus A 64, 16226. pages 12, 23, 31, 56, 57, 65, 75, 95

Mbungu, W., Ntegeka, V., Kahimba, F., Taye, M., Willems, P., 2012. Temporal and spatial variations in hydro-climatic extremes in the Lake Victoria basin. Physics and Chemistry of the Earth 50-52, 24–33. pages 7

Mironov, D., 2008. Parameterization of lakes in numerical weather prediction. Part 1: Description of a lake model. German Weather Service, Offenbach am Main, Germany, 44 pp. pages 20, 21, 31, 35, 36, 38, 68, 81, 99

Mironov, D. V., Heise, E., Kourzeneva, E., Ritter, B., Schneider, N., Terzhevik, A., 2010. Implementation of the lake parameterisation scheme Flake into the numerical weather prediction model cosmo. Boreal Environment Research 15, 218–230. pages 11, 20, 31, 35, 36, 41, 51, 60, 65, 97, 98, 99, 137

Moufouma-Okia, W., Jones, R., 2014. Resolution dependence in simulating the African hydroclimate with the HadGEM3-RA regional climate model. Climate Dynamics. pages 4

Mueller, B., Hirschi, M., Jimenez, C., Ciais, P., Dirmeyer, P. a., Dolman, a. J., Fisher, J. B., Jung, M., Ludwig, F., Maignan, F., Miralles, D. G., McCabe,

M. F., Reichstein, M., Sheffield, J., Wang, K., Wood, E. F., Zhang, Y., Seneviratne, S. I., 2013. Benchmark products for land evapotranspiration: LandFlux-EVAL multi-data set synthesis. Hydrology and Earth System Sciences 17 (10), 3707–3720. pages 16, 103, 104

Munk, W., Anderson, E., 1948. Notes on a theory of the thermocline. Journal of Marine Research 7, 276–295. pages 20, 36

Muvundja, F. a., Wüest, A., Isumbisho, M., Kaningini, M. B., Pasche, N., Rinta, P., Schmid, M., May 2014. Modelling Lake Kivu water level variations over the last seven decades. Limnologica - Ecology and Management of Inland Waters 47, 21–33. pages 126

Naithani, J., Darchambeau, F., Deleersnijder, E., Descy, J., Wolanski, E., 2007a. Study of the nutrient and plankton dynamics in Lake Tanganyika using a reduced-gravity model. Ecological Modelling 200 (1-2), 225–233. pages 31

Naithani, J., Darchambeau, F., Deleersnijder, E., Descy, J.-P., Wolanski, E., 2007b. Study of the nutrient and plankton dynamics in Lake Tanganyika using a reduced-gravity model. Ecological Modelling 200 (1-2), 225–233. pages 32, 37

Naithani, J., Deleersnijder, E., 2004. Are there internal Kelvin waves in Lake Tanganyika? Geophysical Research Letters 31 (6), L06303. pages 111

Naithani, J., Deleersnijder, E., Plisnier, P., 2003. Analysis of wind-induced thermocline oscillations of Lake Tanganyika. Environmental Fluid Mechanics 3, 23–39. pages 48, 111, 162

Naithani, J., Deleersnijder, E., Plisnier, P.-D., 2002. Origin of intraseasonal variability in Lake Tanganyika. Geophysical Research Letters 29 (23), 2093. pages 111

Naithani, J., Plisnier, P.-D., Deleersnijder, E., 2011. Possible effects of global climate change on the ecosystem of Lake Tanganyika. Hydrobiologia 671 (1), 147–163. pages 10

Nash, J., Sutcliffe, J., 1970. River flow forecasting through conceptual models part I—A discussion of principles. Journal of hydrology 10, 282–290. pages 41, 71

Niang, I., Ruppel, O., Abdrabo, M., Essel, A., Lennard, C., Padgham, J., P. Urquhart, 2014. Africa. In: Barros, V., Field, C., Dokken, D., Mastrandrea, M., Mach, K., Bilir, T., Chatterjee, M., Ebi, K., Estrada, Y., Genova, R., Girma, B., Kissel, E., Levy, A., MacCracken, S., Mastrandrea, P., White, L. (Eds.), Climate Change 2014: Impacts, Adaptation, and Vulnerability. Part B:

Regional Aspects. Contribution of Working Group II to the Fifth Assessment Report of the Intergovernmental Panel on Climate Change. Cambridge University Press, Cambridge, United Kingdom and New York, NY, USA, pp. 1199–1265. pages 10

Nicholson, S., 1996. A review of climate dynamics and climate variability in Eastern Africa. In: Johnson, T., Odada, E. (Eds.), The limnology, climatology and paleoclimatology of the East African lakes. Gordon and Breach, Amsterdam, pp. 25–56. pages 33, 106

Nikulin, G., Jones, C., 2011. Simulated precipitation in an ensemble of 10 RCMs over Africa. Weather, 158. pages 15

Nikulin, G., Jones, C., Giorgi, F., Asrar, G., Büchner, M., Cerezo-Mota, R., Christensen, O. B. s., Déqué, M., Fernandez, J., Hänsler, A., van Meijgaard, E., Samuelsson, P., Sylla, M. B., Sushama, L., 2012. Precipitation Climatology in an Ensemble of CORDEX-Africa Regional Climate Simulations. Journal of Climate 25 (18), 6057–6078. pages 97, 106

Notaro, M., Holman, K., Zarrin, A., Fluck, E., Vavrus, S., Bennington, V., 2013. Influence of the Laurentian Great Lakes on Regional Climate. Journal of Climate 26 (3), 789–804. pages 12, 13, 23, 95

Nyeko-Ogiramoi, P., Ngirane-Katashaya, G., Willems, P., Ntegeka, V., 2010. Evaluation and inter-comparison of Global Climate Models' performance over Katonga and Ruizi catchments in Lake Victoria basin. Physics and Chemistry of the Earth 35 (13-14), 618–633. pages 4, 103, 161

Nyeko-Ogiramoi, P., Willems, P., Ngirane-Katashaya, G., 2013. Trend and variability in observed hydrometeorological extremes in the Lake Victoria basin. Journal of Hydrology 489, 56–73. pages 103

O'Gorman, P. a., 2012. Sensitivity of tropical precipitation extremes to climate change. Nature Geoscience 5 (10), 697–700. pages 129, 132, 145

O'Gorman, P. a., 2015. Precipitation Extremes Under Climate Change. Current Climate Change Reports 1, 49–59. pages 132, 146, 148, 155

O'Gorman, P. A., Schneider, T., 2009. The physical basis for increases in precipitation extremes in simulations of 21st-century climate change. Proceedings of the National Academy of Sciences of the United States of America 106 (35), 14773–14777. pages 129, 148

Ohsumi, T., Nakashiki, N., Shitashima, K., Hirama, K., 1992. Density change of water due to dissolution of carbon dioxide and near-field behavior of CO2 from a source on deep-sea floor. Energy Conversion and management 33 (5), 685–690. pages 75

Oleson, K., Dai, Y., Bonan, G., Bosilovich, M., Dickinson, R., Dirmeyer, P., Hoffman, F., Houser, P., Levis, S., Niu, G.-Y., Thornton, P., Vertenstein, M., Yang, Z.-L., Zeng, 2004. Technical description of the community land model (CLM). National Center for Atmospheric Research, Boulder, Colorado, 186 pp. pages 25, 98

Oleson, K. W., Niu, G.-Y., Yang, Z.-L., Lawrence, D. M., Thornton, P. E., Lawrence, P. J., Stöckli, R., Dickinson, R. E., Bonan, G. B., Levis, S., Dai, A., Qian, T., 2008. Improvements to the Community Land Model and their impact on the hydrological cycle. Journal of Geophysical Research 113 (G1), G01021. pages 25, 98, 137

Omondi, P., Ogallo, L. a., Anyah, R., Muthama, J. M., Ininda, J., Jun. 2013. Linkages between global sea surface temperatures and decadal rainfall variability over Eastern Africa region. International Journal of Climatology 33 (8), 2082–2104. pages 7

O'Reilly, C. M., Alin, S. R., Plisnier, P.-D., Cohen, A. S., McKee, B. a., 2003. Climate change decreases aquatic ecosystem productivity of Lake Tanganyika, Africa. Nature 424 (6950), 766–768. pages 2, 10, 31

Otieno, V. O., Anyah, R. O., 2012. CMIP5 simulated climate conditions of the Greater Horn of Africa (GHA). Part 1: contemporary climate. Climate Dynamics 41 (7-8), 2081–2097. pages 8, 138

Otieno, V. O., Anyah, R. O., 2013. CMIP5 simulated climate conditions of the Greater Horn of Africa (GHA). Part II: projected climate. Climate Dynamics 41 (7-8), 2099–2113. pages 8, 10, 147

Paeth, H., Thamm, H. P., 2007. Regional modelling of future African climate north of 15°S including greenhouse warming and land degradation. Climatic Change 83 (3), 401–427. pages 10, 162

Palmer, T., 2014. Build high-resolution global climate models. Nature 515, 338–339. pages 143

Panitz, H.-J., Dosio, A., Büchner, M., Lüthi, D., Keuler, K., 2014. COSMO-CLM (CCLM) climate simulations over CORDEX-Africa domain: analysis of the ERA-Interim driven simulations at 0.44° and 0.22° resolution. Climate Dynamics 42 (11-12), 3015–3038. pages 16, 24, 96, 99, 101, 113, 137, 142

Pasche, N., Dinkel, C., Müller, B., Schmid, M., Wüest, A., Wehrli, B., 2009. Physical and bio-geochemical limits to internal nutrient loading of meromictic Lake Kivu. Limnology and Oceanography 54 (6), 1863–1873. pages 89

Pasche, N., Schmid, M., Vazquez, F., Schubert, C. J., Wüest, A., Kessler, J. D., Pack, M. A., Reeburgh, W. S., Bürgmann, H., 2011. Methane sources and sinks in Lake Kivu. Journal of Geophysical Research 116, G03006. pages 89

Perroud, M., Goyette, S., 2009. Simulation of multiannual thermal profiles in deep Lake Geneva: A comparison of one-dimensional lake models. Limnology and Oceanography 54 (5), 1574–1594. pages 65, 67, 99

Philippon, N., Camberlin, P., Moron, V., Boyard-Micheau, J., 2015. Anomalously wet and dry rainy seasons in Equatorial East Africa and associated differences in intra-seasonal characteristics. Climate Dynamics, 1–22. pages 5

Plisnier, P., Chitamwebwa, D., 1999. Limnological annual cycle inferred from physical-chemical fluctuations at three stations of Lake Tanganyika. Hydrobiologia 407, 45–58. pages 37, 46

Plisnier, P.-D., 2007. Climate change impact on the sustainable use of lake tanganyika fisheries (CLIMFISH). Royal Museum for Central Africa, Tervuren, Belgium, 155 pp. pages 50

Plisnier, P.-D., Mgana, H., Kimirei, I., Chande, A., Makasa, L., Chimanga, J., Zulu, F., Cocquyt, C., Horion, S., Bergamino, N., Naithani, J., Deleersnijder, E., André, L., Descy, J.-P., Cornet, Y., 2009. Limnological variability and pelagic fish abundance (Stolothrissa tanganicae and Lates stappersii) in Lake Tanganyika. Hydrobiologia 625 (1), 117–134. pages 16, 103, 104

Plisnier, P.-D., Serneels, S., Lambin, E., 2000. Impact of ENSO on East African ecosystems: a multivariate analysis based on climate and remote sensing data. Global Ecology and Biogeography 9 (6), 481–497. pages 7, 50, 103

Podsetchine, V., Huttula, T., Savijärvi, H., 1999. A three dimensional-circulation model of Lake Tanganyika. Hydrobiologia 407, 25–35. pages 15

Poole, H., Atkins, W., 1929. Photo-electric measurements of submarine illumination throughout the year. Journal of the Marine Biological Association of the United Kingdom 16, 297–324. pages 72

Potes, M., Costa, M., Salgado, R., Bortoli, D., 2013. Spectral measurements of underwater downwelling radiance of inland water bodies. Tellus A 65, 20774. pages 11

Potes, M., Costa, M. J., Salgado, R., 2012. Satellite remote sensing of water turbidity in Alqueva reservoir and implications on lake modelling. Hydrology and Earth System Sciences 16 (6), 1623–1633. pages 11

Prein, A. F., Langhans, W., Fosser, G., Ferrone, A., Ban, N., Goergen, K., Keller, M., Tölle, M., Gutjahr, O., Feser, F., Brisson, E., Kollet, S., Schmidli, J., van Lipzig, N. P. M., Leung, R., 2015. A review on convection permitting climate modelling: Demonstrations, prospects and challenges. Reviews of Geophysics, in press. pages 135, 143, 162

Raschendorfer, M., 2001. The new turbulence parameterization of LM. German Weather Service, Offenbach am Main, Germany, pp. 89–97. pages 22, 97

Read, J. S., Hamilton, D. P., Desai, A. R., Rose, K. C., MacIntyre, S., Lenters, J. D., Smyth, R. L., Hanson, P. C., Cole, J. J., Staehr, P. a., Rusak, J. a., Pierson, D. C., Brookes, J. D., Laas, A., Wu, C. H., 2012. Lake-size dependency of wind shear and convection as controls on gas exchange. Geophysical Research Letters 39, L09405. pages 21, 99

Rienecker, M. M., Suarez, M. J., Gelaro, R., Todling, R., Bacmeister, J., Liu, E., Bosilovich, M. G., Schubert, S. D., Takacs, L., Kim, G. K., Bloom, S., Chen, J., Collins, D., Conaty, A., Da Silva, A., Gu, W., Joiner, J., Koster, R. D., Lucchesi, R., Molod, A., Owens, T., Pawson, S., Pegion, P., Redder, C. R., Reichle, R., Robertson, F. R., Ruddick, A. G., Sienkiewicz, M., Woollen, J., 2011. MERRA: NASA's modern-era retrospective analysis for research and applications. Journal of Climate 24, 3624–3648. pages 137

Ritter, B., Geleyn, J., 1992. A comprehensive radiation scheme for numerical weather prediction models with potential applications in climate simulations. Monthly Weather Review 120, 303–325. pages 97

Rockel, B., 2015. The Regional Downscaling Approach: a Brief History and Recent Advances. Current Climate Change Reports 1 (1), 22–29. pages 164

Rockel, B., Will, A., Hense, A., 2008. The Regional Climate Model COSMO-CLM (CCLM). Meteorologische Zeitschrift 17 (4), 347–348. pages 96, 97, 137

Rontu, L., Eerola, K., Kourzeneva, E., Vehviläinen, B., 2012. Data assimilation and parametrisation of lakes in HIRLAM. Tellus A 64, 17611. pages 51, 60

Rooney, G., Bornemann, F., 2013. The performance of FLake in the Met Office Unified Model. Tellus A 1, 21363. pages 95

Rossow, W. B., Schiffer, R. a., 1999. Advances in Understanding Clouds from ISCCP. Bulletin of the American Meteorological Society 80 (11), 2261–2287. pages 103, 104

Rouse, W. R., Oswald, C. M., Binyamin, J., Blanken, P. D., Schertzer, W. M., Spence, C., 2003. Interannual and Seasonal Variability of the Surface Energy Balance and Temperature of Central Great Slave Lake. pages 11

Rowell, D. P., 2013. Simulating SST Teleconnections to Africa: What is the State of the Art? Journal of Climate 26 (15), 5397–5418. pages 7

Rudolf, B., Becker, A., Schneider, U., 2011. New GPCC full data reanalysis version 5 provides high-quality gridded monthly precipitation data. GEWEX News 21 (2), 4–5. pages 16, 102, 103

Ryken, N., Vanmaercke, M., Wanyama, J., Isabirye, M., Vanonckelen, S., Deckers, J., Poesen, J., 2015. Impact of papyrus wetland encroachment on spatial and temporal variabilities of stream flow and sediment export from wet tropical catchments. Science of The Total Environment 511, 756–766. pages 163

Saeed, F., Haensler, A., Weber, T., Hagemann, S., Jacob, D., 2013. Representation of Extreme Precipitation Events Leading to Opposite Climate Change Signals over the Congo Basin. Atmosphere 4 (3), 254–271. pages 4, 96

Saji, N. H., Goswami, B. N., Vinayachandran, P. N., Yamagata, T., 1999. A dipole mode in the tropical Indian Ocean. Nature 401, 360–363. pages 7

Salgado, R., Le Moigne, P., 2010. Coupling of the FLake model to the Surfex externalized surface model. Boreal Environment Research 15, 231–244. pages 31

Salgado, R., Potes, M., Albino, A., Rodrigues, C. M., 2014. Eddy covariance flux measurements over a man made lake during the ALEX 2014 field campaign in South Portugal. American Geophysical Union, Fall Meeting 2014, abstract #B13D-0217. pages 163

Samuelsson, P., Kourzeneva, E., Mironov, D., 2010. The impact of lakes on the European climate as simulated by a regional climate model. Boreal Environment Research 15, 113–129. pages 12, 31, 95

Sarmento, H., Darchambeau, F., Descy, J., 2012. Phytoplankton of Lake Kivu. In: Descy, J.-p., Darchambeau, F., Schmid, M. (Eds.), Lake Kivu: Limnology and Biogeochemistry of a Tropical Great Lake. Springer, Dordrecht, Netherlands, pp. 67–83. pages 37

Sarmento, H., Ishumbishu, M., Descy, J.-P., 2006. Phytoplankton ecology of Lake Kivu (eastern Africa). Journal of Plankton Research 28 (9), 815–829. pages 33, 89

Saulnier-Talbot, E., Gregory-Eaves, I., Simpson, K. G., Efitre, J., Nowlan, T. E., Taranu, Z. E., Chapman, L. J., 2014. Small changes in climate can profoundly alter the dynamics and ecosystem services of tropical crater lakes. PLoS ONE 9 (1), 1–8. pages 10

Savijärvi, H., 1997. Diurnal winds around Lake Tanganyika. Quarterly Journal of the Royal Meteorological Society 123, 901–918. pages 15, 32, 65, 117

Savijärvi, H., Järvenoja, S., 2000. Aspects of the fine-scale climatology over Lake Tanganyika as resolved by a mesoscale model. Meteorology and Atmospheric Physics 73 (1-2), 77–88. pages 15, 31, 96, 116, 117

Schaettler, U., 2014. A Description of the Nonhydrostatic Regional COSMO-Model Part V: Preprocessing: Initial and Boundary Data for the COSMO-Model. German Weather Service, Offenbach am Main, Germany, 78 pp. pages 24

Schmid, M., Busbridge, M., Wüest, A., 2010. Double-diffusive convection in Lake Kivu. Limnology and oceanography 55 (1), 225–238. pages 32, 74, 86, 87

Schmid, M., Halbwachs, M., Wehrli, B., Wüest, A., 2005. Weak mixing in Lake Kivu: New insights indicate increasing risk of uncontrolled gas eruption. Geochemistry, Geophysics, Geosystems 6, Q07009. pages 31, 32, 34, 69, 74, 86, 87

Schmid, M., Tietze, K., Halbwachs, M., Lorke, A., McGinnis, D., Wüest, A., 2003. How hazardous is the gas accumulation in Lake Kivu? Arguments for a risk assessment in light of the Nyiragongo Volcano eruption of 2002. Acta Volcanologica 14 (1-2), 115–122. pages 74

Schmid, M., Wüest, A., 2012. Stratification, mixing and transport processes in Lake Kivu. In: Descy, J.-P., Darchambeau, F., Schmid, M. (Eds.), Lake Kivu: Limnology and Biogeochemistry of a Tropical Great Lake. Springer, Dordrecht, Netherlands, pp. 13–29. pages 32, 42, 50, 74, 87, 89, 116

Schneider, T., Bischoff, T., Haug, G. H., 2014. Migrations and dynamics of the Intertropical Convergence Zone. Nature 513 (7516), 45–53. pages 5

Schneider, U., Becker, A., Finger, P., Meyer-Christoffer, A., Ziese, M., Rudolf, B., 2013. GPCC's new land surface precipitation climatology based on quality-controlled in situ data and its role in quantifying the global water cycle. Theoretical and Applied Climatology 115 (1-2), 15–40. pages 103

Scholz, C. a., Johnson, T. C., Cohen, A. S., King, J. W., Peck, J. a., Overpeck, J. T., Talbot, M. R., Brown, E. T., Kalindekafe, L., Amoako, P. Y. O., Lyons, R. P., Shanahan, T. M., Castañeda, I. S., Heil, C. W., Forman, S. L., McHargue, L. R., Beuning, K. R., Gomez, J., Pierson, J., 2007. East African megadroughts between 135 and 75 thousand years ago and bearing on early-modern human origins. Proceedings of the National Academy of Sciences of the United States of America 104 (42), 16416–21. pages 7

Schreck, C. J., Semazzi, F. H. M., 2004. Variability of the recent climate of eastern Africa. International Journal of Climatology 24 (6), 681–701. pages 7

Segele, Z., Lamb, P., Leslie, L., 2009a. Large-scale atmospheric circulation and global sea surface temperature associations with Horn of Africa June-September rainfall. International Journal of Climatology 29, 1075–1100. pages 7

Segele, Z., Leslie, L., Lamb, P., 2009b. Evaluation and adaptation of a regional climate model for the Horn of Africa: rainfall climatology and interannual variability. International Journal of Climatology 29, 47–65. pages 4, 8

Sellers, P., Dickinson, R., Randall, D., Betts, A., Hall, F., Berry, J., Collatz, G., Denning, A., Mooney, H., Nobre, C., Sato, N., Field, C., Henderson-Sellers, A., 1997. Modeling the Exchanges of Energy, Water, and Carbon Between Continents and the Atmosphere. Science 275 (5299), 502–509. pages 98

Semazzi, F. H. M., 2011. Enhancing Safety of Navigation and Efficient Exploitation of Natural Resources over Lake Victoria and Its Basin by Strengthening Meteorological Services on the Lake. North Carolina State University, 104 pp. pages 2, 3, 95, 129, 130, 158

Seneviratne, S., Nicholls, N., Easterling, D., Goodess, C. M., Kanae, S., Kossin, J., Luo, Y., Marengo, J., McInnes, K., Rahimi, M., Reichstein, M., Sorteberg, A., Vera, C., Zhang, X., 2012. Changes in climate extremes and their impacts on the natural physical environment. In: Field, C., Barros, V., Stocker, T., Qin, D., Dokken, D., Ebi, K., Mastrandrea, M., Mach, K., Plattner, G.-K., Allen, S., Tignor, M., Midgley, P. (Eds.), Managing the Risks of Extreme Events and Disasters to Advance Climate Change Adaptation, a special Edition. Cambridge University Press, Cambridge, UK, and New York, NY, USA, pp. 109–230. pages 10, 129, 132, 148

Seneviratne, S. I., Corti, T., Davin, E. L., Hirschi, M., Jaeger, E. B., Lehner, I., Orlowsky, B., Teuling, A. J., 2010. Investigating soil moisture-climate interactions in a changing climate: A review. Earth-Science Reviews 99 (3-4), 125–161. pages 11

Seto, K. C., Güneralp, B., Hutyra, L. R., 2012. Global forecasts of urban expansion to 2030 and direct impacts on biodiversity and carbon pools. Proceedings of the National Academy of Sciences of the United States of America 109 (40), 16083–8. pages 162

Shepherd, J. M., 2005. A review of current investigations of urban-induced rainfall and recommendations for the future. Earth Interactions 9 (12). pages 163

Shongwe, M., van Oldenborgh, G. J., van der Hurk, B., van Aalst, M., 2011. Projected Changes in Mean and Extreme Precipitation in Africa under Global Warming. Part II: East Africa. Journal of Climate 24, 3718–3733. pages 7, 10, 148

Simmons, A., Uppala, S., Dee, D., Kobayashi, S., 2007. ERA-Interim: New ECMWF reanalysis products from 1989 onwards. European Centre for Medium-Range Weather Forecasts, Reading, United Kingdom, pp. 25–35. pages 32, 40

Smiatek, G., Rockel, B., Schättler, U., 2008. Time invariant data preprocessor for the climate version of the COSMO model (COSMO-CLM). Meteorologische Zeitschrift 17 (4), 395–405. pages 24

Smith, K. A., Semazzi, F. H. M., 2014. The Role of the Dominant Modes of Precipitation Variability over Eastern Africa in Modulating the Hydrology of Lake Victoria. Advances in Meteorology 2014, 1–11. pages 7

Song, Y., Semazzi, F. H. M., Xie, L., Ogallo, L. J., Jan. 2004. A coupled regional climate model for the Lake Victoria basin of East Africa. International Journal of Climatology 24 (1), 57–75. pages 11, 13, 14, 23, 65, 96, 99, 100, 108, 110, 117, 130, 162

Spigel, R., Coulter, G., 1996. Comparison of Hydorology and physical limnology of the East African Great LakesLakes: Tanganyika, Malawi, Victoria, Kivu and Turkana (with references to some North American Great Lakes). In: Johnson, T., Odada, E. (Eds.), The Limnology, Climatology and Paleoclimatology of the East African lakes. Gordon and Breach Publishers, Amsterdam, The Netherlands, pp. 103–140. pages 32, 33, 69

Spracklen, D. V., Arnold, S. R., Taylor, C. M., 2012. Observations of increased tropical rainfall preceded by air passage over forests. Nature 489 (7415), 282–5. pages 5

Stackhouse, P. W., Gupta, S. K., Cox, S. J., Zhang, T., Mikovitz, J. C., Hinkelman, L. M., 2011. 24.5-year SRB data set released. GEWEX News 21 (1), 10–12. pages 16, 103, 104

Stenuite, S., Pirlot, S., Hardy, M.-A., Sarmento, H., Tarbe, A.-L., Leporcq, B., Descy, J.-P., 2007. Phytoplankton production and growth rate in Lake Tanganyika: evidence of a decline in primary productivity in recent decades. Freshwater Biology 52 (11), 2226–2239. pages 37

Stepanenko, V., Goyette, S., Martynov, A., Perroud, M., Fang, X., Mironov, D., 2010. First steps of a Lake Model Intercomparison Project: LakeMIP. Boreal Environment Research 15, 191–202. pages 65, 99

Stepanenko, V., Jöhnk, K., Machulskaya, E., 2014. Simulation of surface energy fluxes and stratification of a small boreal lake by a set of one-dimensional models. Tellus A 66, 21389. pages 65, 67, 99

Stepanenko, V. M., Lykosov, V., 2005. Numerical simulation of heat and moisture transport in the lake-soil system. Russian Journal of Meteorology and Hydrology 3, 95–104. pages 68

Stepanenko, V. M., Martynov, A., Jöhnk, K. D., Subin, Z. M., Perroud, M., Fang, X., Beyrich, F., Mironov, D., Goyette, S., 2013. A one-dimensional model intercomparison study of thermal regime of a shallow, turbid midlatitude lake. Geoscientific Model Development 6 (4), 1337–1352. pages 23, 31, 65, 68, 73, 96, 99

Stöckli, R., Lawrence, D. M., Niu, G.-Y., Oleson, K. W., Thornton, P. E., Yang, Z.-L., Bonan, G. B., Denning, a. S., Running, S. W., 2008. Use of FLUXNET in the Community Land Model development. Journal of Geophysical Research 113 (G1), G01025. pages 98

Subin, Z. M., Murphy, L. N., Li, F., Bonfils, C., Riley, W. J., 2012a. Boreal lakes moderate seasonal and diurnal temperature variation and perturb atmospheric circulation: analyses in the Community Earth System Model 1 (CESM1). Tellus A 64, 15639. pages 12, 23, 65, 95

Subin, Z. M., Riley, W. J., Mironov, D., 2012b. An improved lake model for climate simulations: Model structure, evaluation, and sensitivity analyses in CESM1. Journal of Advances in Modeling Earth Systems 4, M02001. pages 11, 23, 67, 81

Sun, L., Semazzi, F., Giorgi, F., Ogallo, L., 1999a. Application of the NCAR regional climate model to eastern Africa: 1. Simulation of the short rains of 1988. Journal of Geophysical Research 104 (D6), 6529–6548. pages 4, 100

Sun, L., Semazzi, F., Giorgi, F., Ogallo, L., 1999b. Application of the NCAR regional climate model to eastern Africa: 2. Simulation of interannual variability of short rains. Journal of Geophysical research 104 (D6), 6549–6562. pages 7

Sun, X., Xie, L., Semazzi, F., Liu, B., 2015. Effect of Lake Surface Temperature on the Spatial Distribution and Intensity of the Precipitation over Lake Victoria Basin. Monthly Weather Review 143, 1179–1192. pages 13, 14, 96, 99, 108

Sun, X., Xie, L., Semazzi, F. H. M., Liu, B., 2014. A Numerical Investigation of the Precipitation over Lake Victoria Basin Using a Coupled Atmosphere-Lake Limited-Area Model. Advances in Meteorology, 960924. pages 13, 14, 96, 99, 108

Swenson, S., Wahr, J., May 2009. Monitoring the water balance of Lake Victoria, East Africa, from space. Journal of Hydrology 370 (1-4), 163–176. pages 126

Sylla, M. B., Coppola, E., Mariotti, L., Giorgi, F., Ruti, P. M., Dell'Aquila, A., Bi, X., 2009. Multiyear simulation of the African climate using a regional climate model (RegCM3) with the high resolution ERA-interim reanalysis. Climate Dynamics 35 (1), 231–247. pages 4

Sylla, M. B., Giorgi, F., Coppola, E., Mariotti, L., 2013. Uncertainties in daily rainfall over Africa: assessment of gridded observation products and evaluation of a regional climate model simulation. International Journal of Climatology 33 (7), 1805–1817. pages 106, 156

Tassi, F., Vaselli, O., Tedesco, D., Montegrossi, G., Darrah, T., Cuoco, E., Mapendano, M. Y., Poreda, R., Delgado Huertas, A., 2009. Water and gas chemistry at Lake Kivu (DRC): Geochemical evidence of vertical and horizontal heterogeneities in a multibasin structure. Geochemistry, Geophysics, Geosystems 10 (2), Q02005. pages 89

Taylor, C. M., de Jeu, R. a. M., Guichard, F., Harris, P. P., Dorigo, W. a., 2012a. Afternoon rain more likely over drier soils. Nature 489 (7416), 423–6. pages 5

Taylor, K., 2001. Summarizing multiple aspects of model performance in a single diagram. Journal of Geophysical Research: Atmospheres 106, 7183–7192. pages 41, 71, 72

Taylor, R. G., Todd, M. C., Kongola, L., Maurice, L., Nahozya, E., Sanga, H., MacDonald, A. M., 2012b. Evidence of the dependence of groundwater resources on extreme rainfall in East Africa. Nature Climate Change 3 (4), 374–378. pages 10

Tebaldi, C., Hayhoe, K., Arblaster, J. M., Meehl, G. A., 2006. Going to the extremes: An intercomparison of model-simulated historical and future changes in extreme events. Climatic Change 79 (3-4), 185–211. pages 10

Thiery, W., Davin, E., Panitz, H.-J., Demuzere, M., Lhermitte, S., van Lipzig, N., 2015. The Impact of the African Great Lakes on the Regional Climate. Journal of Climate 28 (10), 4061–4085. pages 27, 130, 131, 134, 135, 137, 138, 140

Thiery, W., Gorodetskaya, I. V., Bintanja, R., Van Lipzig, N. P. M., Van den Broeke, M. R., Reijmer, C. H., Kuipers Munneke, P., 2012. Surface and snowdrift sublimation at Princess Elisabeth station, East Antarctica. The Cryosphere 6 (4), 841–857. pages 53, 157

Thiery, W., Martynov, A., Darchambeau, F., Descy, J.-P., Plisnier, P.-D., Sushama, L., van Lipzig, N. P. M., 2014a. Understanding the performance of the FLake model over two African Great Lakes. Geoscientific Model Development 7 (1), 317–337. pages 70, 76, 81, 99, 101, 109, 110, 116, 138, 140

Thiery, W., Stepanenko, V. M., Fang, X., Jöhnk, K. D., Li, Z., Martynov, A., Perroud, M., Subin, Z. M., Darchambeau, F., Mironov, D., 2014b. LakeMIP Kivu: Evaluating the representation of a large, deep tropical lake by a set of 1-dimensional lake models. Tellus A 66, 21390. pages 31, 36, 37, 99, 101, 138, 140

Tiedtke, M., 1989. A comprehensive mass flux scheme for cumulus parameterization in large-scale models. Monthly Weather Review. pages 97, 162

Tierney, J., Mayes, M., Meyer, N., 2010. Late-twentieth-century warming in Lake Tanganyika unprecedented since AD 500. Nature Geoscience 3, 422–425. pages 10

van Oldenbrogh, G. J., Collins, M., Arblaster, J., Christensen, J. H., Marotzke, J., Power, S. B., Rummukainen, M., Zhou, T., 2013. Annex I: Atlas of Global and Regional Climate Projections. In: Stocker, T., Qin, D., Plattner, G.-K., Tignor, M., Allen, S., Boschung, J., Nauels, A., Xia, Y., Bex, V., Midgley, P. (Eds.), Climate Change 2013: The Physical Science Basis. Contribution of Working Group I to the Fifth Assessment Report of the Intergovernmental Panel on Climate Change. Cambridge University Press, Cambridge, United Kingdom and New York, NY, USA, pp. 1311–1394. pages 8, 9, 10

Vanden Broucke, S., Luyssaert, S., Davin, E., Janssens, I., Van Lipzig, N., 2015. Temperature decomposition of paired site observations reveals new insights in climate models' capability to simulate the impact of LUC. Journal of Geophysical Research: Atmospheres in press, 1–45. pages 27

Vanmaercke, M., Poesen, J., Broeckx, J., Nyssen, J., Sep. 2014. Sediment yield in Africa. Earth-Science Reviews 136, 350–368. pages 163

Verburg, P., Antenucci, J. P., 2010. Persistent unstable atmospheric boundary layer enhances sensible and latent heat loss in a tropical great lake: Lake Tanganyika. Journal of Geophysical Research 115, D11109. pages 4, 15, 50, 65, 111, 123, 157

Verburg, P., Antenucci, J. P., Hecky, R. E., 2011. Differential cooling drives large-scale convective circulation in Lake Tanganyika. Limnology and Oceanography 56 (3), 910–926. pages 4, 15, 31, 111, 162

Verburg, P., Hecky, R., 2003. Wind patterns, evaporation, and related physical variables in Lake Tanganyika, East Africa. Journal of Great Lakes Research 29, 48–61. pages 15, 33, 46, 65

Verburg, P., Hecky, R., 2009. The physics of the warming of Lake Tanganyika by climate change. Limnology and Oceanography 54, 2418–2430. pages 2, 10, 31, 32

Verburg, P., Hecky, R. E., Kling, H., 2003. Ecological consequences of a century of warming in Lake Tanganyika. Science 301 (5632), 505–507. pages 2, 10, 31

Vermeiren, K., Van Rompaey, A., Loopmans, M., Serwajja, E., Mukwaya, P., 2012. Urban growth of Kampala, Uganda: Pattern analysis and scenario development. Landscape and Urban Planning 106 (2), 199–206. pages 162

Vermeiren;, K., Vanmaercke, M., Van Rompaey, A., 2015. ASSURE: a model for the simulation of urban expansion and intra-urban social segregation. Computers, Environment and Urban Systems, in press. pages 162

Verschuren, D., 2003. The heat on Lake Tanganyika. Nature 424, 731–732. pages 10

Verschuren, D., Laird, K. R., Cumming, B. F., 2000. Rainfall and drought in equatorial east Africa during the past 1,100 years. Nature 403 (6768), 410–4. pages 7

Vizy, E. K., Cook, K. H., 2012. Mid-Twenty-First-Century Changes in Extreme Events over Northern and Tropical Africa. Journal of Climate 25 (17), 5748–5767. pages 4, 10, 96

Vollmer, M., Bootsma, H., 2005. Deep-water warming trend in Lake Malawi, East Africa. Limnology and . . . 50 (2), 727–732. pages 10

Wang, J., Feng, J., Yan, Z., Hu, Y., Jia, G., 2012. Nested high-resolution modeling of the impact of urbanization on regional climate in three vast urban agglomerations in China. Journal of Geophysical Research: Atmospheres 117 (21), 1–18. pages 162

Wang, P. K., 2007. The thermodynamic structure atop a penetrating convective thunderstorm. Atmospheric Research 83, 254–262. pages 137

Wehner, M., Easterling, D. R., Lawrimore, J. H., Heim, R. R., Vose, R. S., Santer, B. D., 2011. Projections of Future Drought in the Continental United States and Mexico. Journal of Hydrometeorology 12 (6), 1359–1377. pages 156

Wen, L., Lv, S., Li, Z., Zhao, L., Nagabhatla, N., 2014. Impacts of the Two Biggest Lakes on Local Temperature and Precipitation in the Yellow River Source Region of the Tibetan Plateau. Advances in Meteorology, 248031. pages 23

Wilks, D. S., 2005. Statistical methods in atmospheric sciences. 100. Academic Press, Oxford, United Kingdom, 676 pp. pages 41, 71

Williams, A. P., Funk, C., 2011. A westward extension of the warm pool leads to a westward extension of the Walker circulation, drying eastern Africa. Climate Dynamics 37 (11-12), 2417–2435. pages 7

Williams, K., Chamberlain, J., Buontempo, C., Bain, C., 2014. Regional climate model performance in the Lake Victoria basin. Climate Dynamics. pages 13, 14, 16, 95, 96, 97, 99, 100, 106, 117

Wouters, H., De Ridder, K., Demuzere, M., Lauwaet, D., Van Lipzig, N. P. M., 2013. The diurnal evolution of the urban heat island of Paris: A model-based case study during Summer 2006. Atmospheric Chemistry and Physics 13 (17), 8525–8541. pages 162, 163

Wouters, H., Demuzere, M., De Ridder, K., van Lipzig, N. P. M., 2015. The impact of water-storage parametrization on urban climate modelling. Urban Climate 11, 24–50. pages 163

Wüest, A., Jarc, L., Bürgmann, H., Pasche, N., Schmid, M., 2012. Methane Formation and Future Extraction in Lake Kivu. In: Descy, J.-p., Darchambeau, F., Schmid, M. (Eds.), Lake Kivu: Limnology and Biogeochemistry of a Tropical Great Lake. Springer, Dordrecht, Netherlands, pp. 165–180. pages 66

Wüest, A., Piepke, G., Johnson, T., 1996. Combined effects of dissolved solids and temperature on the density stratification of Lake Malawi. In: Johnson, T., Odada, E. (Eds.), The Limnology, Climatology and Paleoclimatology of the East-African Lakes. Gordon and Breach, Toronto, Canada, pp. 183–202. pages 75

Yang, W., Seager, R., Cane, M. a., Lyon, B., 2015. The Annual Cycle of East African Precipitation. Journal of Climate 28, 2385–2404. pages 5, 13

Yang, Z.-L., 2015. Foreword to the special issue: regional earth system modeling. Climatic Change 129 (3-4), 365–368. pages 164

Zaroug, M. a. H., Giorgi, F., Coppola, E., Abdo, G. M., Eltahir, E. a. B., 2014. Simulating the connections of ENSO and the rainfall regime of East Africa and the upper Blue Nile region using a climate model of the Tropics. Hydrology and Earth System Sciences 18 (11), 4311–4323. pages 7

Zeleke, T., Giorgi, F., Mengistu Tsidu, G., Diro, G. T., 2012. Spatial and temporal variability of summer rainfall over Ethiopia from observations and a regional climate model experiment. Theoretical and Applied Climatology 111 (3-4), 665–681. pages 8

Zhao, L., Lee, X., Smith, R. B., Oleson, K., 2014. Strong contributions of local background climate to urban heat islands. Nature 511 (7508), 216–219. pages 163

Zipser, E. J., Cecil, D. J., Liu, C., Nesbitt, S. W., Yorty, D. P., 2006. Where are the most: Intense thunderstorms on Earth? Bulletin of the American Meteorological Society 87 (8), 1057–1071. pages 130

List of publications

Akkermans, T., Thiery, W., van Lipzig, N.P.M., 2014. The regional climate impact of realistic future deforestation in the Congo Basin. Journal of Climate 27(7), 2714-2734.

Gorodetskaya, I.V., Kneifel, S., Maahn, M., Van Tricht, K., Thiery, W., Schween, J.H., Crewell, S., van Lipzig, N.P.M., 2015. Cloud and precipitation properties from ground-based remote sensing instruments in East Antarctica. The Cryosphere 9, 285-304.

Jacobs, L., Dewitte, O., Poesen, J., Delvaux, D., Thiery, W., Kervyn, M., 2015. The Rwenzori Mountains, a landslide-prone region? Landslides.

Jacobs, L., Maes, J., Mertens, K., Sekajugo, J., Thiery, W., van lipzig, N.P.M, Poesen, J., Kervyn, M., Dewitte, O. 2015. A recipe for desaster: the May 2013 Kilembe flash flood, Rwenzori Mountains, Uganda. Journal of Hydrology, in review.

Thiery, W., Gorodetskaya, I.V., Bintanja, R., van Lipzig, N.P.M., van den Broeke, M.R., Reijmer, C., Kuipers Munneke, P., 2012. Surface and snowdrift sublimation at Princess Elisabeth station, East Antarctica. The Cryosphere 6(2), 841-857.

Thiery, W., Martynov, A., Darchambeau, F., Descy, J.-P., Plisnier, P.-D., Sushama, L., van Lipzig, N.P.M., 2014a. Understanding the performance of the FLake model over two African Great Lakes. Geoscientific Model Development 7, 317-337.

Thiery, W., Stepanenko, V.M., Darchambeau, F., Fang, X., Jöhnk, K.D., Li, Z., Martynov, A., Mironov, D., Perroud, M., Subin, Z.M., van Lipzig, N.P.M., 2014b. LakeMIP Kivu: Evaluating the representation of a large, deep tropical lake by a set of one-dimensional lake models. Tellus A 66, 21390.

Thiery, W., Davin, E.L., Panitz, H.-J., Demuzere, M., Lhermitte, S., van Lipzig,

N.P.M., 2015. The impact of the African Great Lakes on the regional climate. J. Climate 28(10), 4061-4085.

FACULTY OF SCIENCE
DEPARTMENT OF EARTH AND ENVIRONMENTAL SCIENCES
REGIONAL CLIMATE STUDIES
Celestijnenlaan 200E
B-3001 Leuven
wim.thiery@ees.kuleuven.be
http://www.ees.kuleuven.be/geography/rcs/